Performance of Thermoluminescent Dosimeters Under As-Deployed Conditions

by

John A. Harvey

A dissertation submitted in partial fulfillment
of the requirements for the degree of
Doctor of Philosophy
(Nuclear Engineering and Radiological Sciences)
in the University of Michigan
2011

Doctoral Committee:

Professor Kimberlee J. Kearfott, Chair
Professor Zhong He
Professor Andrew E. Yagle
Coordinator/Senior Health Physicist Joseph A. Miklos

To my mentor, for understanding and patience

Acknowledgements

I was once asked to estimate how many TLD readouts I had examined during the course of my studies. At the time, about a year before finishing, I said it was in the tens of thousands. Thanks to my former lab assistants Zachery Beauvais, D. Emerson Cooper, James Laird, Jennifer Schlicht, Heather Wittaniemi, Tomasz Zak, Elizabeth Thomas, Benjamin Wu, Sean Carney, Robert Bergen, Caroline Lupini, Andreea Moscinat, Mark Roberts, Gabriel-Jason Fernandez, Samba Danfa, and Douglas Kripke, and former fellow graduate students Andrew Kalchik and Kaylie Thompson, for their invaluable experimental and statistical analysis work. Collecting and analyzing all that data would have been a much more daunting task without their help.

Thanks to Benjamin Hammargren, Matthew Studenski, and Zachary Whetstone for the design and construction of the ^{137}Cs irradiation facility I used extensively throughout my research. Thanks as well as to Dr. Joseph Miklos for Radiation Safety Service support with the irradiator, for answering numerous questions, and for his invaluable encouragement.

Thanks to fellow graduate students Miesher Rodrigues and Nathan Haverland for their initial work on the MATLAB computerized glow curve analysis code and determination of the parameters required to fit several TLD types.

Thanks to Nuclear Engineering and Radiological Sciences Professors Ronald Fleming, John Foster, Zhong He and Kimberlee Kearfott for allowing me to assist them in their teaching duties as a Graduate Student Instructor for six terms. Thanks to all the students in those classes, for keeping me on my toes.

Thanks to my committee members, especially my advisor, Professor Kimberlee Kearfott, for pointing me back in the right direction when I would wander off intellectually, even if in some cases it took me a while to get around to doing everything she wanted. Her constant availability and generosity was invaluable in keeping me on track. Thanks to Professor Michael Hartman for agreeing to substitute for Dr. Miklos when he unexpectedly became unavailable for my defense.

Thanks to our irreplaceable NERS Graduate Program Coordinator Peggy Jo Gramer for always sticking up for me, calming my usually overblown fears about academic requirements, and just being a great person to talk to about anything.

Thanks to my family for sticking with me through this long and winding road.

Special thanks to Adrienne Lehnert, Sonal and Willy Kaye, and Crystal Thrall for always being there for me to bounce ideas off of and blow off steam with.

This work was partially supported by the Lawrence Livermore National Laboratory, Glenn T. Seaborg Institute, Nuclear Science for National Security graduate research fellowship, as well as the Robert S. Landauer, Sr. Fellowship sponsored by Landauer Incorporated and administrated by the Health Physics Society. All opinions expressed in this paper are the author's and do not necessarily reflect the policies and views of LLNL, Landauer Incorporated, or HPS.

Table of Contents

List of Figures

List of Tables

Abstract

This dissertation examines the properties of long-term, passive radiation dosimetry systems incorporating thermoluminescent dosimeters (TLDs) for use in diverse interior and exterior settings. In so doing, a multitude of factors affecting thermoluminescence calibrations and measurements were examined.

TLD calibration precision was studied, including the time variability of TLD reader measurements, irradiation inhomogeneity, and the optimal number of calibrations. It was also determined that the visible physical quality of TLDs, such as the presence of small fractures, scratches and discolorations, does not significantly affect sensitivity. A process for identifying useful TLDs from otherwise poor batches was formulated.

Post-annealing TLD sensitivity changes, commonly referred to as pre-irradiation fading, and post-irradiation signal fading were examined for six common TL materials. To assist in data analysis, a generally useful glow curve analysis computer program was written using a common mathematics parser. Ratios of glow curve peaks, commonly used as self-normalizing quantities in TL dosimetry, were found for fading durations up to 30 d. Pre- and post-irradiation fading were individually fit to empirical functions of exponential form. For groups of LiF:Mg,Ti TLDs, it was found that a single fading function adequately described group behavior. For some deployments, the effects of high ambient temperature on fading must be known. LiF:Mg,Ti TLDs were subjected to controlled temperatures of 30°C to 50°C for up to 30 to 60 d. The sum of the areas of the two most stable glow curve peaks was found to be constant up to 50°C where it fades slightly over long periods.

The effects of high ambient radon on TLDs had not previously been well characterized. Radon was found to have a significant effect on bare TLDs and

TLDs encapsulated in dosimetry cards, but no measureable effect on cards in environmental badges for ~1 MBq m^{-3} h.

The minimum detectable dose for a TLD system was analyzed based upon a dose-response linearity experiment and other results elsewhere in the dissertation. To conclude, a prototype system based upon integrating dosimetric materials is proposed as future work.

Chapter I

Introduction

With the resurgence of the American nuclear power industry after an over 30 year slumber, and the increasing usage of radiation for medical and national security purposes, the demand for accurate radiation detection and dose assessment has never been higher. Thermoluminescence dosimetry (TLD), the study of materials that emit light when heated after exposure to ionizing radiation, has been a mainstay of health physics professionals for over 50 years. During that time, TLDs have been extremely valuable in monitoring the safety of radiation workers and performing environmental dose control.

Although extremely accurate active radiation detectors are now available, TLDs are small, inexpensive, and if the correct material is chosen, tissue equivalent. They can be used to detect photons, beta particles, and slow neutrons, and with appropriate filters, can be used to determine shallow and deep dose. Their biggest advantage is long-term deployability, possible due to a power source being unnecessary until readout. This allows time-efficient monitoring of typically uninhabited areas. In order to ensure accurate results from long deployments in diverse interior and exterior environments, however, various aspects of their performance must be examined. This work serves to improve the effectiveness of TLD systems by analyzing several factors which may affect the sensitivity and precision of TLD measurements, as well as determining a practical minimum detectable dose incorporating those factors.

TLDs must be individually calibrated, meaning that the amount of signal response to a known dose must be measured before use. The light response to doses generally between 0.1 mGy and 10 Gy, but varying by material, has a

linear relationship with dose. This makes calibration at only one dose necessary if staying within the linear range. Chapter II aims to separate and analyze several common factors that can influence the precision of TLD calibrations, analyzing their robustness against physical damage, differences in source-detector distance, history and batch dependence, and reader-induced variability. Although many of these effects have been mentioned in the literature, they had never before been defined with an in-depth quantitative analysis.

TLDs lose signal with increasing time of deployment, which is commonly called fading. Signal loss can occur due to sensitivity changes in the material between annealing and irradiation, called pre-irradiation fading, or due to loss of trapped charge carriers between irradiation and readout, called post-irradiation fading. Chapter III contains a detailed study of fading in six different TLD materials, and characterizes each different TLD type's glow curve characteristics. Fading is measured by using peak ratios, as a sort of self-normalization, fit to exponential decay functions when possible.

Fading is typically ignored by using slow-fading peaks for dosimetry measurements, or corrected for by calculating the fading occurring individually for each TLD, a painstaking process. In order to retain the useful temporal information afforded by fading while maximizing time efficiency, Chapter IV studies the reproducibility of glow peak fading characteristics. If a large batch of TLDs can be characterized using only a single fading function, only minimal corrections are required to make TLD calibrations and measurements many times more accurate, especially for long deployments in which fading is non-negligible even for the slowest-fading peaks. This work tests the concept for LiF:Mg,Ti, commonly called TLD-100, the most common type of thermoluminescent dosimeter which demonstrates near tissue equivalence.

As temperature is of utmost importance in thermoluminescent dosimetry, the ambient temperature of the environment in which the TLD is deployed has a profound effect on its response, with higher temperatures resulting in higher pre- and post-irradiation fading rates. In Chapter V, fading is characterized with respect to ambient temperatures of 30°C, 40°C, and 50°C for TLD-100. The stark

differences between pre- and post-irradiation fading are studied in detail, as their contrasting characteristics are much enhanced at higher temperatures. The effects of higher temperatures on signal are studied here for the determination of the suitability of TLD measurements in diverse exterior environments.

In interior environments, especially subterranean enclosures and areas with low ventilation, radon can be a serious problem. This radioactive noble gas can enter even the smallest of cracks and fissures and can build up to significant levels, especially in commonly unchecked workplace areas that are not frequented by personnel. Chapter VI examines the effect of radon on TLDs, which was extensively studied previously. TLDs unknowingly affected by radon can cause higher doses on reference dosimeters, which could lead to a nontrivial underestimate of personnel or environmental dose.

The light signal arising from a TLD heated slowly over 30 s or more is called a glow curve, and its constituent peaks arise from progressively higher energy electron traps being freed as temperature increases. In order to separate the signal arising from the various traps present in thermoluminescent materials, which bear different fading rates, the fairly complicated glow curve must be deconstructed into its constituent peaks. This is done with a computerized glow curve analysis program, described in Chapter VII. Written in MATLAB to handle comma-separated variable data output from TLD readers, the program can process glow curves from five different dosimeters with a figure of merit of 1.3% or less, and from $CaSO_4$:Dy with a figure of merit of 2.2% or less. Output is conveniently provided in graph and raw data formats. This program was used to generate data for chapters III, IV, V, VI, and VIII.

Chapter VIII examines the minimum detectable dose of a TLD system. Dose response linearity, light sensor dark current, the effects of using a computerized glow curve analysis program, and statistical influences including accumulation of radiation background over time are examined. High ambient radon is incorporated into background for minimum detectable dose calculations as well.

Chapter IX looks forward to future work by proposing a simple autonomous TLD system, which could be deployed for long periods and operate independently of human intervention. A similar system is also proposed for optically stimulated luminescent dosimeters. Power requirements are calculated and compared for the two systems. Such a system could benefit greatly from additional experiments using this research as a starting point.

Chapter II

Quantification of Various Factors Influencing the Precision of Thermoluminescent Detector Calibrations for New and Used Chip Sets

ABSTRACT

Factors affecting the random and systematic error in calibrating three sets of 100 LiF:Mg,Ti thermoluminescent detector chips were investigated. The chips were held in a polymethyl methacrylate plate with 0.3 cm deep wells covered with a thin top plate, affixed to a polymethyl methacrylate phantom 150 cm from a 3.2×10^{10} GBq ^{137}Cs source, used to irradiate the chips to 4.52 mGy. Three sets of chips were used: one new, one heavily used, and one having relatively high degrees of visible physical damage. Variations in the exposure rate across the plate were measured with an ion chamber. Experimental drift was judged by performing successive calibrations on subsequent days, while always reading the chips in the same order. The chips were also subject to manual examination to determine variations in mass and physical quality. This study indicates that more accurate calibrations can be obtained by accounting for the error caused by nonuniformity in the delivered dose, which was in this study as high as 4.4% from the center to the edges of the target. Making use of more than three calibrations only reduces the standard deviation as a percentage of the mean of a set by less than 1%. Desirable dosimeters in commercially rejected sets were identified by comparing each dosimeter's standard deviation of response across all calibrations to a commercially acceptable control set. Up to 50% variations in mass and visual quality, including opacity, fracture, and surface scratches to chips, showed little to no correlation with their response.

INTRODUCTION

The purpose of this study was to determine the magnitudes of error in measured dose introduced by several factors in the course of a typical irradiation and readout of thermoluminescent detector (TLD) chips. Multiple sources of error introduced by the dosimeter itself, the reader, the evaluation procedure and thermal treatment have been identified, and are present in both calibration readouts and deployment readouts. Some of these factors include variability of the mass of the thermoluminescent material in the detector, changes in the optical properties of the reader, and non-reproducibility of the thermal treatment during read-out (Busuoli 1981). The irradiation source also introduces some error, including non-uniformity of the radiation field and uncertainty in source exposure time. Other sources of error unrelated to irradiation have been previously described (German and Weinstein 2002) and include those related to the change in TLD reader performance over time, called reader drift. This effect can be influenced by (1) the quality of thermal contact between the detector and heater when a planchet is used (Samei et al. 1994); (2) the performance of the reader's reference light source; and (3) cleanliness of the reading chamber, which may cause the combustion of dust and other contaminants when the chip is heated, causing abnormally high light signals (Furetta and Weng 1998).

Typically, a TLD calibration procedure includes a certain number of irradiations performed on a set of TLDs, as multiple measurements of a distribution are required to adequately measure the mean. In a calibration, the mean and standard deviation of the response of a single chip over several irradiations are compared to those of other chips in the same readout (Plato and Miklos 1985). Although each successive measurement increases precision, diminishing returns will eventually render the benefits of additional measurements trivial. An optimal calibration provides a balance between precision and time required. Three calibrations have been shown in the literature (Simpkins and Kearfott 1997) to be sufficient for most personnel dosimetry. However, that work was restricted to multi-element TLD cards and a limited set of

reference dosimeters for comparison. This work used single TLD chips, as well as all dosimeters in a set for comparison.

Studying various effects and determining correction factors for them can be used to improve the TLD calibration. Correcting for these factors may also provide the additional benefit of achieving the precision required in a calibration with fewer irradiations, after which more irradiations will only result in marginal statistical improvement. Although previous literature has identified many possible sources of error in TLD measurements, this work serves to quantify these factors in terms of their actual effects on determining delivered dose.

Many of the sources of error found in a TLD system can be avoided by following appropriate handling procedures in a highly reproducible manner. For example, an in-reader annealing procedure, while inefficient in that only one chip may be annealed at a time without operator assistance, is highly reproducible, which is essential in order to minimize errors inherent to the dosimeters themselves (Furetta and Weng 1998). However, only low doses can be applied to the TLDs in order for an in-reader annealing procedure, which at approximately two minutes per chip is relatively short compared to an oven procedure of three to 24 hours or more, to remove all stored signal for each chip. If the dose applied to the TLDs is higher than hundreds of mGy, much higher than that typically found in personnel dosimetry, in-reader annealing will require many repetitions to clear out the stored signal and will be ineffective compared to an oven procedure.

Three previously characterized sources of error have been identified (Furetta and Weng 1998). These include factors due to the dosimeters themselves, including variation in their transparency and other optical properties, their mass and size variations, and damage to the TL material either through physical or radiological means. In this study, all of these factors with the exception of radiological damage are tested using a physical analysis of the chips to determine what effect, if any, these have on TL sensitivity, using a set of TLDs that was commercially rejected by quality control due to visible physical damage. This work also determines the effect of radiological damage on

sensitivity with a heavily used set of TLDs with an unknown history. Although optical and radiological background can cause additional sources of error in a TLD, these effects were not studied in this work and the background sources were kept under strict control by using low light, low radiation background storage.

Each chip's response can be compared to that of other chips as well as its own response over time. This process can provide a measure of reliability for a given chip compared to other chips in a set, allowing chips that show a consistent response comparable to that of chips from a commercially acceptable set to be isolated and removed from otherwise commercially unacceptable sets, and chips showing inconsistent response with a high standard deviation compared to the group's mean to be identified as outliers and removed from otherwise consistent sets, increasing the precision of the group. The sensitivity as determined by statistical analysis can then be compared to possible sources of error present in a chip, to determine what impact, if any, the conjectured sources of error may have on chip performance.

MATERIALS AND METHODS

TLD profiles

This experiment utilized three sets of one hundred crystalline chips of LiF:Mg,Ti (TLD-100, BICRON/Harshaw, 6801 Cochran Road, Solon, OH 44139, USA) with dimensions of 0.32 × 0.32 × 0.09 cm^3. Two sets, sample A and sample B, were obtained as commercially undesirable lots. Sample A, containing 100 TLDs, were considered to be undesirable for deployment in response to visual imperfections noted during a physical inspection. Sample B, containing 98 TLDs, was formerly commercially viable, but had since undergone heavy deployment and use. Sample C, the control set of 100, was purchased commercially with a manufacturer guarantee of all chips having a standard deviation of 5% of the mean. Each chip was individually weighed with a balance (Analytical Plus AP250D, Ohaus Corporation, Pine Brook, NJ 07058, USA) in order to determine if any correlation existed between chip mass and response. Without regard to

any other measurements, a Student's t-test was applied to all three sample sets to determine if the data sets were statistically significantly different.

TLD irradiation facility and method

Each of the three sets of one hundred TLDs was placed in a 40 × 40 × 0.6 cm^3 polymethyl methacrylate (PMMA) plate with one hundred wells 0.3 cm deep, covered by a 40 × 40 × 0.25 cm^3 PMMA sheet attached by four acrylic screws and four large black binder clamps placed at the edges for additional security. The TLDs were annealed (i.e., heated so as to remove the background radiation signal that may have accumulated) by running them through a readout cycle as described below. Next, the plate of TLDs was placed on a 40 × 40 × 15 cm^3 PMMA phantom, 60 cm above floor level and 150 cm from a ^{137}Cs source (Model 28-8A Irradiator, J.L. Shepherd and Associates, 1010 Arroyo Avenue, San Fernando, CA 91340-8122) with an activity of 3.2 × 10^{11} Bq at the time of the first irradiation. Both plate and phantom were custom manufactured in-house (Parker and Kearfott 2009). The phantom and source were contained in a facility designed specifically for this purpose (Studenski et al. 2007) room measuring 2.9 × 3.2 m^2 with two plaster walls against soil and two solid 39.4 × 19.1 × 9.21 cm^3 cinderblock walls against open air. The room's 18 cm thick concrete ceiling is 2.5 m from the floor, which is the lowest floor in the building and below which is soil. The TLDs were irradiated to 4.52 mGy at the center of the phantom at a rate of 0.00393 mGy s^{-1}, high enough to avoid concerns about the lower limit of detectability (LLD) of the chips, which is beyond the scope of this work. After irradiation, the plate holding the TLDs stayed attached to the phantom for approximately one to three minutes before removal. A measurement of the dose rate with the source shielded was taken at the phantom to determine if this produced any significant increase in dose delivered to the TLDs.

TLD readout

Approximately thirty minutes after the completion of irradiation, the TLDs were read out with a standard reader with hot gas and hot planchet capabilities

(Model 4500 TLD Reader, BICRON/Harshaw, 6801 Cochran Road, Solon, OH 44139, USA) and commercial reader control software (WinREMS version PL-26732.8.0.0.0, BICRON/Harshaw, 6801 Cochran Road, Solon, OH 44139, USA) under the manufacturer-recommended time-temperature profile in hot planchet mode. At the start of each readout, homemade vacuum tweezers were used to place the TLD on the planchet, which was then heated at a rate of 10 °C s^{-1} until it reached 300°C, and held at that temperature until 33.3 s after the start of the readout. The planchet was then allowed to cool to 50 °C, at which point the chip could be replaced and the next readout initiated. Pre-purified nitrogen gas (Prepurified compressed nitrogen cylinder 300, Metro Welding Supply Corporation, 12620 Southfield Road, Detroit, MI 48223), containing no more than 5 ppm of oxygen and 5 ppm of water, was used to limit undesirable signals occurring in the high temperature range, typically while the planchet was being held at 300°C. These included chemiluminescence and the combustion of dust or other contaminants on or in the vicinity of the TLD. Each TLD in sample A and sample B were irradiated and read out in this manner five and six times respectively; sample C was irradiated and read out ten times.

Signal integration and analysis

Each TLD readout resulted in the collection of the photomultiplier tube current as a function of heating time, called the glow curve. A region of interest (ROI) from each glow curve, shown in Fig. 1, was chosen to begin with the first channel at the start of the readout to the point of intersection between the tangent of the fall of the last glow curve peak and the time axis. This tangent was visually approximated for each curve and the area under the curve was found in arbitrary units. An ROI method integrating only under the approximate areas of peaks 4 and 5 has been shown to be accurate within 2% of a glow curve analysis method for those two peaks with a post-irradiation fading time of less than eight weeks (Weinstein et al. 2003) For this experiment, an ROI encompassing nearly the entire glow curve will be accurate as long as the post-irradiation fading time is short compared to that of the fading rates for peaks 2 and 3 as well. As the fixed

post-irradiation time of 30 minutes is short compared to the fading time for peak 2, with the literature estimating its effectiveness in dosimetry to be from 100 h to 1 week (Moscovitch 1986; Weinstein et al. 2003), its reproducibility was assured.

Correction for spatial non-uniformity of delivered dose to TLDs

A calibrated, NIST-traceable air-filled spherical ion chamber (Exradin Shonka-Wyckoff Spherical Ion Chamber Model A3, Standard Imaging, 3120 Deming Way, Middleton, WI 53562, USA) with collecting volume 3.6 cm^3 was used in conjunction with a calibrated, NIST traceable electrometer (Model 6517A Electrometer/High-Resistance Meter, Keithley Instruments, 28775 Aurora Road, Cleveland, OH 44139, USA) to determine the non-uniformity of the radiation field. The ion chamber was placed next to an empty TLD plate on the phantom. The ion chamber was centered at a TLD position and three measurements taken with the source shielded in order to measure leakage current and background radiation. Then, another measurement was taken with the source raised. This was repeated for all 100 TLD positions. A position correction factor, PCF_i for each location was defined using the following expression:

$$PCF_i = \frac{X_i}{X_c} \tag{2.1}$$

where X_i is the exposure at the position of the TLD numbered i and X_c is the exposure measured at the center of the phantom. Separate background and leakage current measurements were made with the source shielded, and these were subtracted from the measurement made with the source exposed in order to determine the charge resulting only from source exposure. The exposure to the ion chamber is then given by:

$$X_i = \left(\frac{\bar{q}_{irradiation}}{t_{irradiation}} - \frac{\bar{q}_{background}}{t_{background}} - \frac{\bar{q}_{leakage}}{t_{leakage}}\right) \times CF \tag{2.2}$$

where $\bar{q}$ is the mean of the charge measured at position *i*, *t* is the measurement time, and *CF* is the calibration factor specific to the electrometer and ion chamber. No corrections for environmental factors were applied as they would cancel when the position correction factor was determined, as all experiments were completed during the same time period over which the room temperature varied by less than 5% and pressure varied by less than 3%. After conversion of exposure to air kerma, the air kerma delivered to each TLD was determined by multiplying the air kerma delivered at the center by its position correction shown in Equation (2.1). The region of interest data for each TLD readout were then divided by the position corrected air kerma delivered to the TLD to determine the charge detected as a function of air kerma delivered, referred to as PMT current per delivered air kerma.

Identification of outliers

Spurious data points, defined as TLD chips having a glow curve that bore no resemblance to that of TLD-100 chips in general and other glow curves produced by the same two TLDs in question, were discarded. Outliers in this set were determined using Chauvenet's criterion (Chauvenet 1871), stating that, when assuming a Gaussian distribution, any value with a probability of occurrence less than $(2n)^{-1}$, where *n* is the number of data points, is considered an outlier and may be discarded (Taylor 1997). It can be identically stated that Chauvenet's criterion is satisfied when the product of the probability of obtaining a data point z_i standard deviations from the mean and the number of measurements is less than 0.5, namely:

$$0.5 > \ [2 \times \varphi(z_i) - 1] \tag{2.3}$$

where φ is the Gaussian distribution function,

$$\frac{1}{\sigma\sqrt{2\pi}} \int_{-\infty}^{x} exp\left[\frac{(x-\bar{x})^2}{2\sigma^2}\right] dx. \tag{2.4}$$

Equation 3 may then be solved for z_i to obtain:

$$z_i = \varphi^{-1}\left(\frac{1}{2} + \frac{1}{4n}\right). \quad (2.5)$$

The number of standard deviations z_i of the data point from the mean is determined by:

$$z_i = \frac{|x_i - \bar{x}|}{\sigma} \quad (2.6)$$

where x_i is the data point in question, $\bar{x}$ is the mean of that set of data points and σ is the standard deviation of the set.

In order to explain possible statistical outliers, all TLDs were visually analyzed for fractures, scratches, and discoloration using a qualitative 10-point scale, with 10 corresponding to no damage and highest visual quality. For fractures, 5 would represent one or two corners missing, and 1 a TLD that is nearly broken. For scratches, 5 would represent multiple scratches on both sides, with possibly some material missing, and 1 would represent deep cuts or one or more holes. For discoloration, 5 would represent the entire TLD being tinged dark enough to be completely opaque, as LiF is typically partially translucent, and 1 would be a completely brown or black TLD. After these determinations were made of each chip, its average response and each damage rating were graphed together in order and a linear trend line fit to the data to determine if any correlation existed between visual damage and chip response.

Experimental drift

The mean PMT current per delivered air kerma for each calibration in each TLD set was measured as a function of time since that set of TLDs were first annealed before any irradiations took place. Each set of data was numerically fit using commercial spreadsheet software (Microsoft Excel 2007, Microsoft Corporation, One Microsoft Way, Redmond, WA 98052) to a least squares linear regression line which was used to determine the normalization factor N_i, defined as:

$$N_i = \frac{P_i}{P_1} \quad (2.7)$$

where P_i, the predicted air kerma for trial *i,* was determined from the linear regression line and P_1 is the measured air kerma of a single TLD for a single trial.

Number of experimental trials to determine individual TLD calibration factors

The mean of all normalized data points for a TLD was set as the expected PMT current per delivered air kerma value for that TLD. This value was compared to the normalized PMT current per delivered air kerma for each TLD obtained for the first trial to determine a percent deviation, *D,* of the first calibration from the expected value (the mean of all trials), using the equation:

$$D_{i,j} = \frac{\overline{x}_{i,j} - \overline{x}_{i,j_{tot}}}{\overline{x}_{i,j_{tot}}} \times 100 \quad (2.8)$$

where *i* is the individual TLD number, *j* is the number of trials averaged, and j_{tot} is the total number of trials: five for set A, six for set B, ten for set C. The quantity $\overline{x}_{i,j}$ is produced using the following equation:

$$\overline{x}_{i,j} = \frac{\sum_{m=1}^{j} x_{i,m}}{j} \quad (2.9)$$

.

RESULTS AND DISCUSSION

Outliers and chip damage

Four single TLD trials were removed using Chauvenet's criterion before any other data were analyzed, as their average measured dose was too far from the mean, more than three standard deviations either too high or too low. No TLDs had multiple measurements so far from the sample means that all trials were excluded. These sporadic exclusions may have been due to factors unrelated to the specific TLD. For example, a high reading may have been due to the combustion of dust present on the planchet. A low reading may have been due to improper positioning of the TLD on the planchet, causing the TLD to not be heated as much as necessary to produce a full signal.

A visual inspection of the TLDs from samples A and B determined that many chips had visible physical damage, especially in sample A, the

commercially rejected set. Several chips were missing corners, had deep scratches, or were so discolored as to be completely opaque, typically a light brown or yellow-brown color. A total of 61% of TLDs in sample A were determined to be damaged. A total of 6% of TLDs in that set were determined to have damage classifications of 5 or lower on the ten-point scale in any category, though no chips had any classifications of lower than 4. A total of 16% of TLDs in sample B were determined to have damage, with no chips receiving lower than a score of 7 in any category.

The fractures, scratches, and discolorations identified, however, had little to no correlation with TLD sensitivity for either sample set as given by a linear trend line fit to the data. Several chips classified as heavily damaged, rated 6 or lower in any category, gave a response with less than 10% deviation from the mean of that set, whereas other chips with no discernable physical damage ranged from less than 1% deviation to over 50% deviation, with all but one chip in sample B showing less than 40% deviation from the mean.

If visible physical damage had a direct effect upon TLD sensitivity, it would be expected that deviation from the sample mean would increase as physical damage increases, however, from Figs. 6.2 and 6.3, this is shown not to be the case. Figs. 6.3a and 6.3b show that the squares of the Pearson product-moment correlation coefficient are $R^2 = 0.0077$ for sample A and $R^2 = 0.0073$ for sample B, showing little to no correlation between visible damage and sensitivity.

Despite this lack of correlation, the student's t-test performed showed that the three sample sets can be considered significantly different statistically. When comparing samples A and C, a p-value of 0.056 was obtained, very close to the threshold value of 0.05 which would reject the null hypothesis assuming no significant statistical difference between the sample sets. Sample B is much more likely to be statistically different than the control sample set C, with a p-value of 0.018. All three data sets were fit to Gaussian distributions in order to be valid for this type of comparison, quantified later in this section.

Mass corrections

Mass was another measured source of potential error found to have no correlation to uncorrected TLD response, as the relationship between ROI per dose and chip mass showed no correlation for any of the three sample sets, shown in Fig. 4. Though several of the chips in samples A and B were missing one or more corners, it is apparent from these data that this difference in weight, in addition to any other individual weight differences, had no measurable effect on TLD sensitivity. The squares of the Pearson product-moment correlation coefficient for the three sets were $R^2 = 0.023$, $R^2 = 0.0003$, and $R^2 = 0.084$ for samples A, B, and C respectively, indicating no or very little correlation between mass and sensitivity within this range of masses. The range in masses was small, as over 90% of chips in all sample sets were within 10% of the sample mean. It is possible that much larger differences in mass would begin to show corresponding differences in sensitivity.

Position corrections

Fig. 5a shows individual position corrections determined for all 100 TLD irradiation locations. The NIST-traceable air-filled spherical ion chamber used to calculate these corrections showed the standard deviation of the three measurements at each location ranged from 0.014% to 0.62% of the mean measurement at each location, a negligible impact on measured dose to TLDs. However, a non-trivial decrease in relative source strength from the center of the phantom to the corners, 3.7% on the right side corners and 4.3% on the left side corners, was observed. Though symmetry was observed vertically across the phantom, the “bulls-eye” geometry expected from an ideal point source, shown in Fig. 5b, was not observed due to horizontal asymmetry.

The point source approximation can be removed from the measured values to give a clearer picture of the variation not due to the difference in distance from the center of the source to the plate edges. The TLDs at the four corners of the plate were 2.1% more distant from the source than the TLDs at the center of the plate. If this variation is removed, shown in Fig. 5c, it can be seen

that the source strength on the right side of the phantom as seen from the source was higher than on the left, most likely due to the phantom's right side being tilted slightly closer to the source axis, though the areas directly above and below the source now show the most variation, 2.9%, from the center with the corners showing 2.4%. Were the source center line perfectly normal to the phantom surface, this anomaly may not have been observed. Scattering from the floor, ceiling and walls may also account for the discrepancy.

Background corrections

With the source shielded, a background radiation measurement was taken with the ion chamber in order to determine if the TLDs being left on the phantom for several minutes after irradiation contributed significantly to delivered dose. This was measured to be 3.05×10^{-3} mGy h^{-1} and did not vary significantly across the phantom. This is only 0.022% of the average dose rate of 14.1 mGy h^{-1} with the source raised, and as such, the trivial dose contribution of the shielded source was neglected in further calculations.

Drift corrections

As shown in Fig. 6, when the average responses of all chips in a sample set were plotted against the time since the first anneal of that set, a measurable temporal change in response was found for all three sample sets that could not be accounted for by any other source of error. The squares of the correlation coefficients for the three sample sets ranged from $R^2 = 0.56$ for sample C to $R^2 = 0.91$ for sample A, indicating that at least some correlation is present in all sets. With drift corrections of -0.056 nC mGy^{-1} h^{-1} for sample A, 0.007 nC mGy^{-1} h^{-1} for sample B, and -0.026 nC mGy^{-1} h^{-1} for sample C applied in addition to position corrections, the distributions of chip ROI values contain less outliers and much more closely resemble normal distributions, as seen in Fig. 7. All three samples were fit to a Gaussian distribution and the Kolmogorov-Smirnov test used to determine goodness of fit (Massey 1951). All three tests returned values of D

greater than 0.05, meaning that the data sets fit a Gaussian distribution well. These distributions are shown in Fig. 8.

More irradiations can further decrease the deviation of the mean of single chip responses compared to the cumulative mean of all chips, shown in Fig. 9, and the deviation of the cumulative mean of all chips across all irradiations, shown in Fig. 10. It should be noted that Figs. 6.9 and 6.10 show deviation from the cumulative mean and not the true mean, which is unknown. As a result, the graphs show zero deviation after the final irradiation. This is not the actual amount, and further irradiations would reveal deviations in previous trials. Once a reader drift correction is made, these data show a drop-off of the efficacy of further irradiations, as shown by the relative decrease in standard deviation from approximately 2% of the cumulative mean after the first irradiation to approximately 0.3% of the cumulative mean after the third irradiation for sample C. After three irradiations in all samples, the standard deviation fluctuates around zero but comes no closer to it, indicating that further trials do little to improve the precision of measured dose values.

Determination of commercially viable chips from rejected sets

In the commercially rejected sample sets A and B, a much wider distribution of TLD chip ROI values was determined than for the commercially purchased set C, shown in Fig. 7. From these data, those chips from A and B which would fall within the distribution of the acceptable group C can be isolated for more general use, shown in Table 2.1. Out of the 100 sample C chips, 94 were within a 10% deviation from that group's mean, with all 100 chips falling within 11.1%. Samples A and B had 52 and 42 chips within 10% deviation of the mean of sample C, respectively, with the other chips having as high as 51% deviation. In this case, nearly half of 200 chips which may have otherwise been discarded may be salvaged and distributed, only requiring a control set of commercially acceptable chips for comparison and three calibration irradiations of each set. The chips from an unacceptable set that then fall within 10%

deviation of the mean of the acceptable set can then be set aside as those still retaining high quality.

CONCLUSIONS

Visible physical damage, coloration, and mass of LiF:Mg,Ti dosimeter chips did not correlate with their observed measured individual sensitivities. The spatial non-uniformity of source irradiation, causing a variation of as much as 4.4% in this work, and temporal changes in reader response or average group dosimeter sensitivity for dosimeters with identical exposure histories were also not significant relative to individual variations in dosimeter sensitivity.

However, as the spread of values is much wider when comparing sample A, which showed considerable physical damage on average, and the control sample C, it cannot be said that physical damage has no effect upon sensitivity. It is more likely that the damage which causes a decrease in sensitivity merely cannot be seen with the unaided eye. Therefore, a true measurement of a TLD's desirability for deployment is much more effectively done with a calibration rather than with visible inspection. Quality assurance programs that rely solely or heavily on mass variations or physical inspection may result in the unnecessary discarding of many commercially viable dosimeters.

With corrections made for TLD position and reader drift to a commercially viable set of 100 TLDs, analysis showed that only three calibrations were required for the standard deviation of the mean percent deviations of each chip with respect to the mean of the group to be less than 1%. Though the non-commercially viable sets' standard deviations did not get any closer to zero with more irradiations, the precision of that value sharpened considerably after each calibration. After one calibration, the precision of sample B's measured standard deviation, approximately 1%, ranged from -17% to +12%. This range was reduced to -1% to +1% after three calibrations. Similarly, sample A improved from -8% to +6% after one trial to -2% to +2% after three trials. Although a set of three calibrations was already a well-known standard for optimal TLD precision versus efficiency, this finding serves to reinforce the previous work.

Members of non-commercially viable sets can be compared to a known acceptable set to determine which, if any, can be restored to a commercially viable set. A total of 94 out of the 100 chips in the commercially viable set displayed a standard deviation within 10% of the mean for that set, whereas 94 of the 200 chips non-commercially viable chips tested were determined to have sensitivity comparable to the commercially viable set, within 10% of the mean of the commercially viable control set. These could then subsequently be restored to the commercially viable set.

These results are most applicable to dosimetry quality control programs or nuclear facilities for which the cost of new TLDs exceeds the cost of labor. Individual LiF chips can cost anywhere from $20 USD for single chips purchased in bulk to $100 USD for badges purchased with analysis service provided by the supplier. Though commercially acceptable TLDs can be identified from an otherwise unacceptable set, this process requires additional labor in the form of calibrations. If the time and labor cost required to perform calibrations exceeds the cost of obtaining new TLDs, or the quality control program or nuclear facility has a large quantity of replacement TLDs already available, groups of questionable TLDs can be cost-effectively discarded without further analysis, However, for areas in which new TLD material exceeds the cost of labor, it is more cost-effective to perform the additional testing described in this study to determine which TLDs can be salvaged before discarding the rest of the set. It should be noted that the results of this work may not apply as well to other thermoluminescent materials, though a similar error analysis could be done with other materials. Also, lower applied doses would also most likely produce different results due to the additional uncertainty arising in determining the difference between the signal and background, especially when nearing the lower limit of detection of the dosimeter.

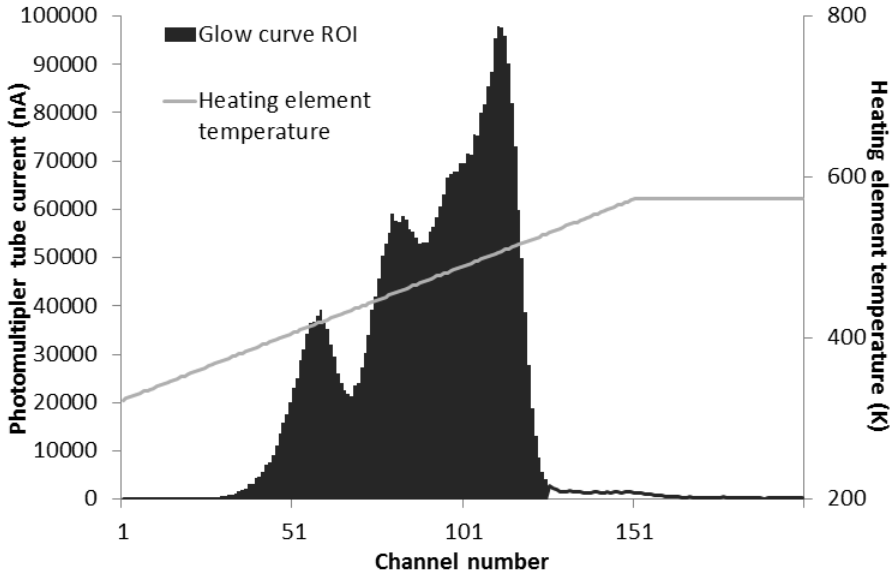

Fig 2.1. Example glow curve from thermoluminescent dosimeter after 4.52 mGy irradiation. Glow curve's region of interest is shaded.

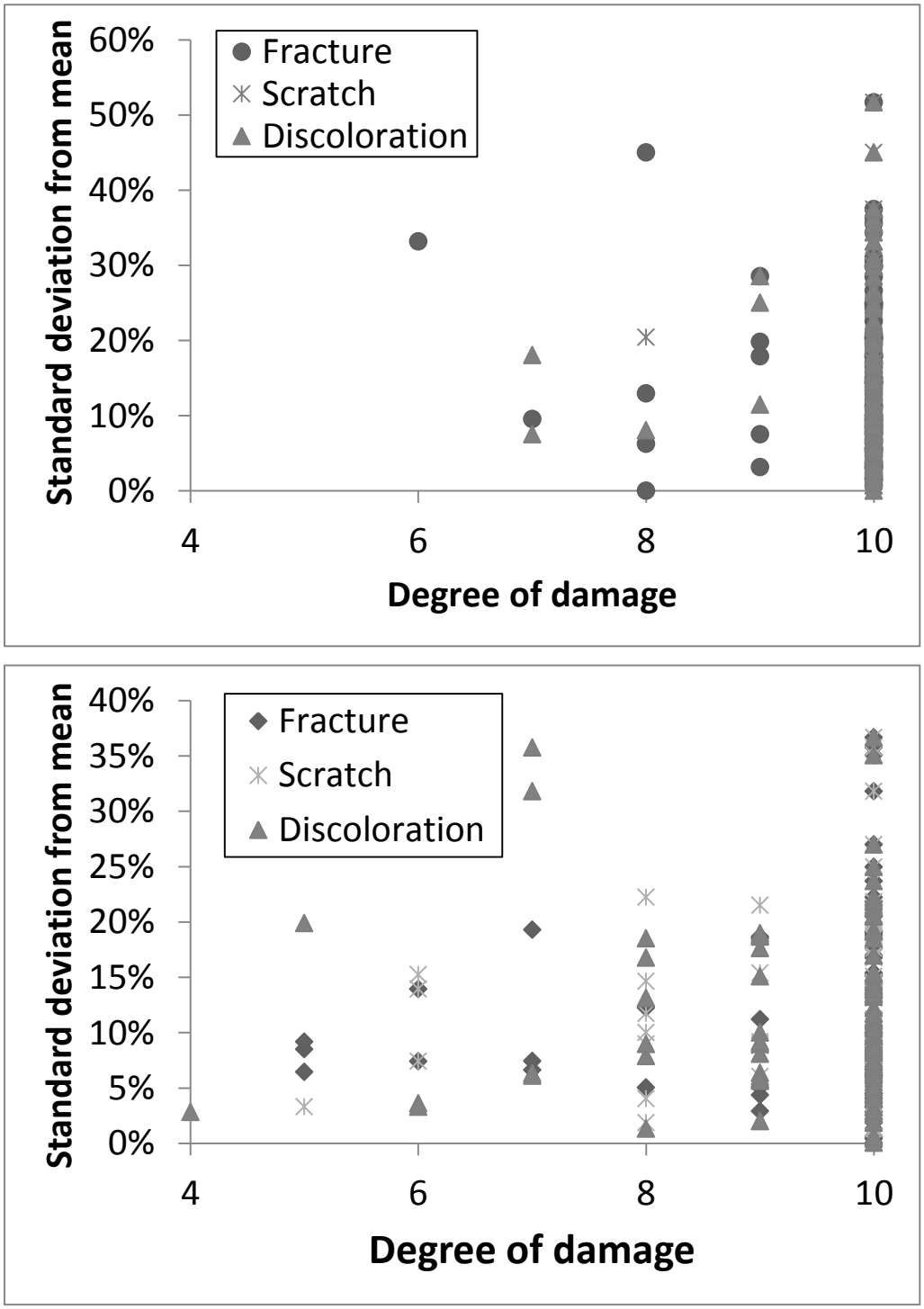

Fig 2.2. Measured physical damage to thermoluminescent detector chips where 10 is minimal damage and 1 is extreme damage in three categories, for (a) sample A, (b) sample B.

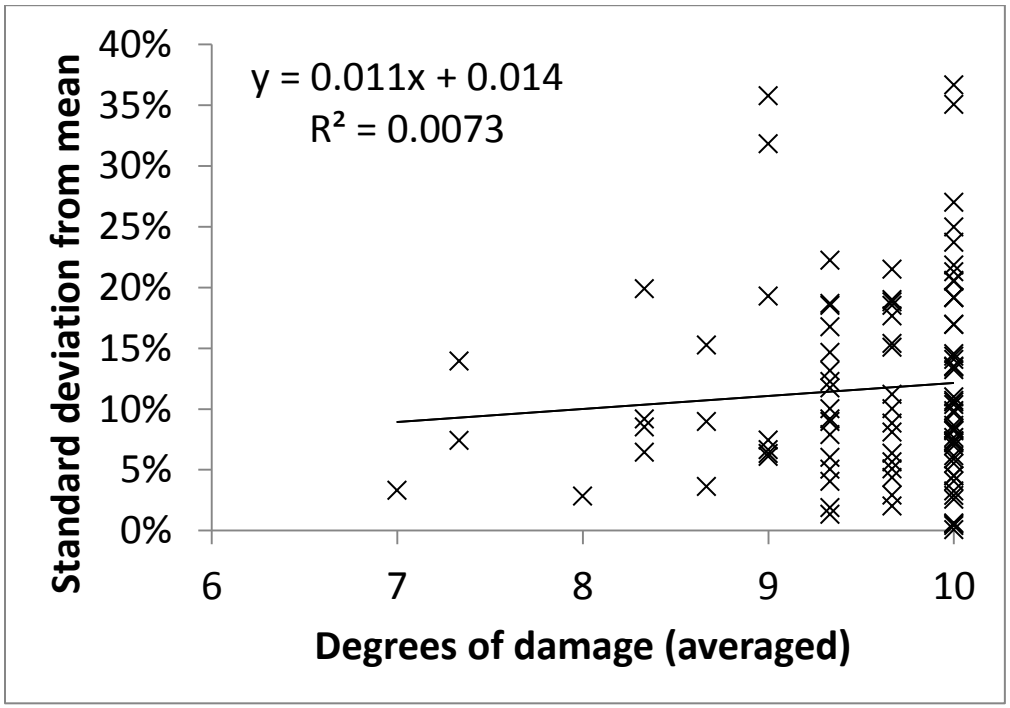

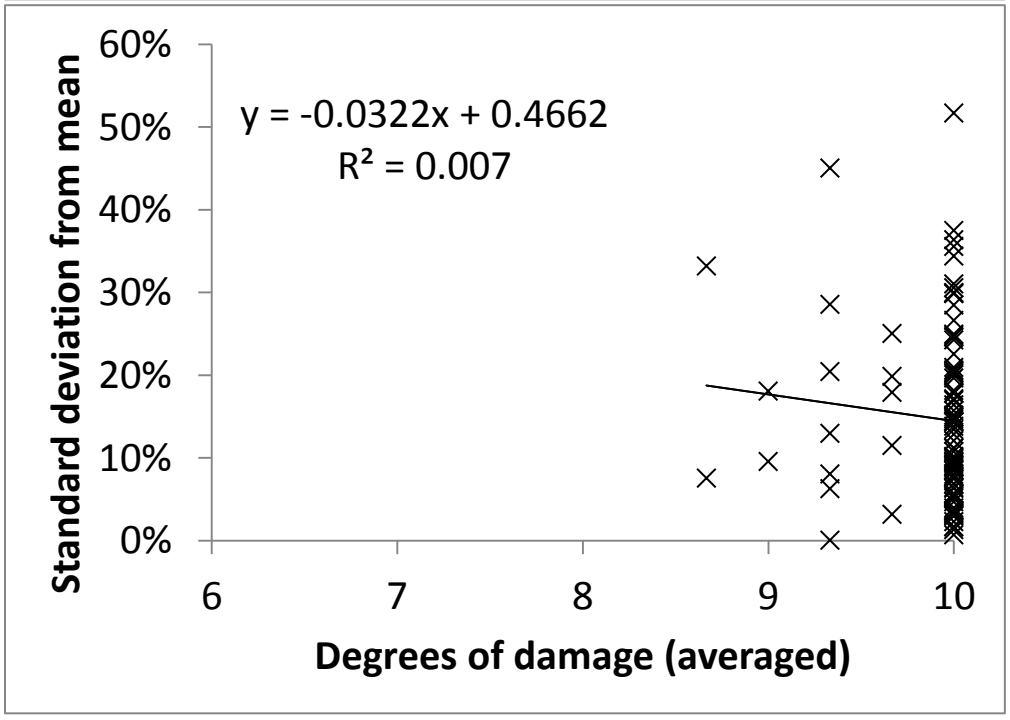

Fig 2.3. Measured physical damage to thermoluminescent detector chips where 10 is minimal damage and 1 is extreme damage in three categories averaged together, for (a) sample A, (b) sample B.

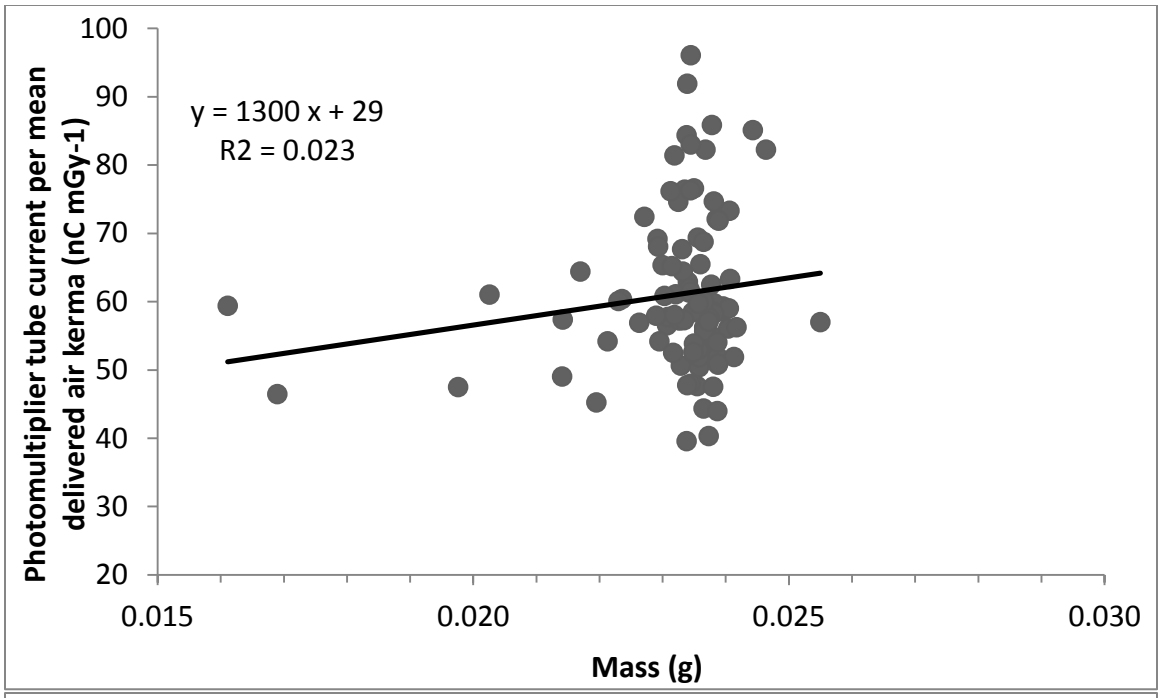
y = 1300 x + 29
R2 = 0.023
Photomultiplier tube current per mean delivered air kerma (nC mGy-1)
Mass (g)
100
90
80
70
60
50
40
30
20
0.015
0.020
0.025
0.030

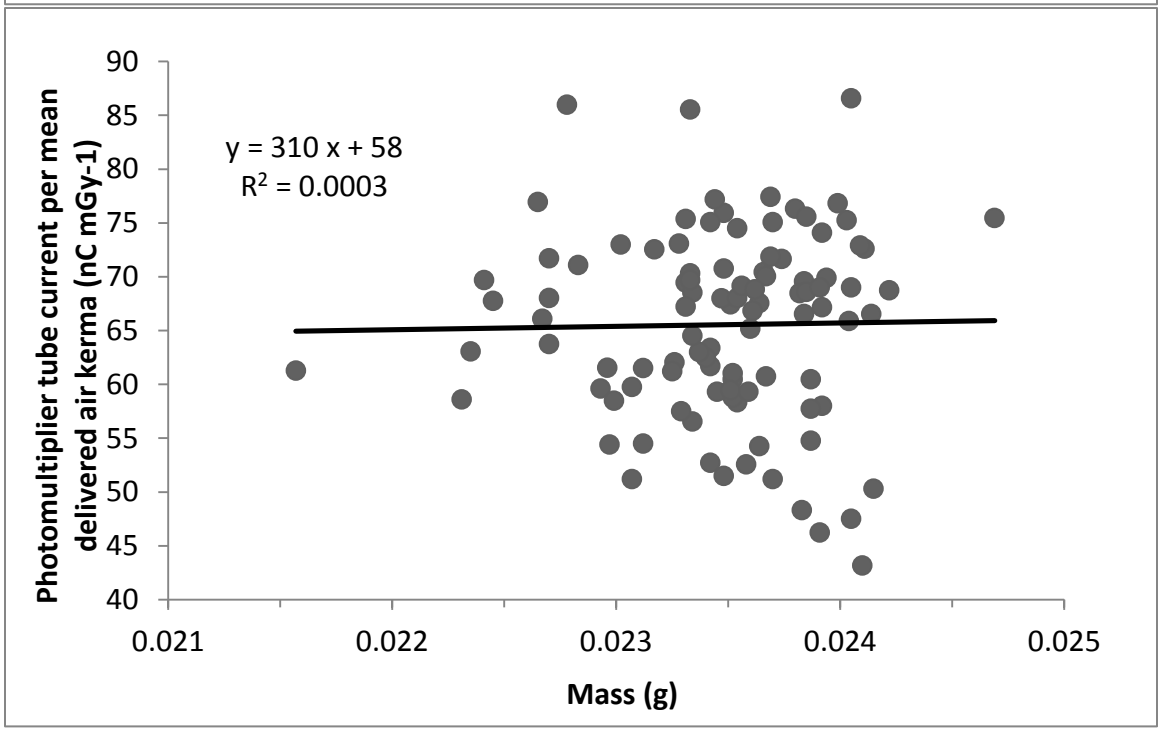
y = 310 x + 58
R2 = 0.0003
Photomultiplier tube current per mean delivered air kerma (nC mGy-1)
Mass (g)
90
85
80
75
70
65
60
55
50
45
40
0.021
0.022
0.023
0.024
0.025

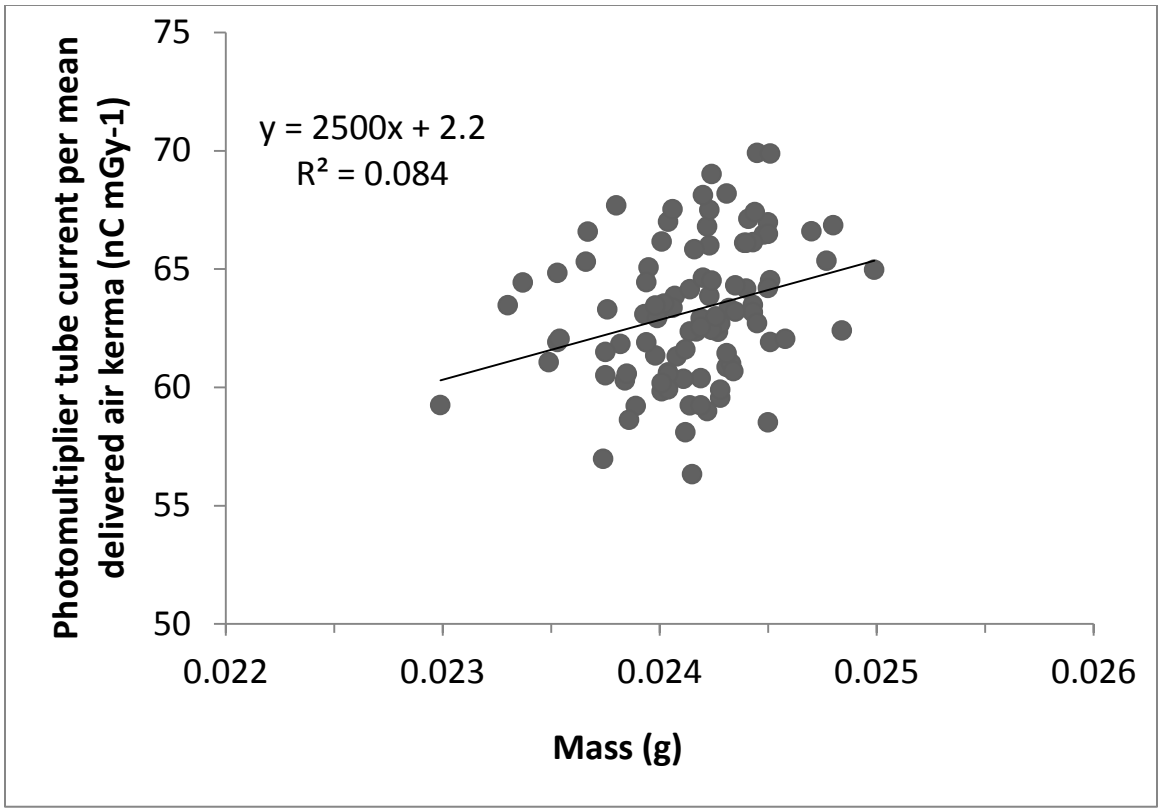

Fig 2.4. Correlation between region of interest per unit dose and chip mass for (a) sample A, (b) sample B, (c) sample C.

0.956	0.959	0.966	0.963	0.963	0.963	0.963	0.971	0.966	0.963
0.959	0.963	0.966	0.963	0.963	0.963	0.963	0.971	0.969	0.966
0.963	0.969	0.969	0.966	0.963	0.963	0.970	0.978	0.978	0.969
0.966	0.969	0.969	0.984	0.981	0.981	0.989	0.978	0.978	0.969
0.969	0.969	0.969	0.992	1.000	1.000	0.994	0.978	0.978	0.972
0.969	0.969	0.969	0.992	1.000	1.000	0.994	0.978	0.978	0.972
0.966	0.969	0.969	0.984	0.981	0.981	0.989	0.978	0.978	0.969
0.963	0.969	0.969	0.966	0.963	0.963	0.971	0.978	0.978	0.969
0.959	0.963	0.966	0.963	0.963	0.963	0.963	0.971	0.969	0.966
0.956	0.959	0.966	0.963	0.963	0.963	0.963	0.971	0.966	0.963

0.979	0.982	0.983	0.985	0.985	0.985	0.985	0.983	0.982	0.979
0.982	0.984	0.986	0.988	0.988	0.988	0.988	0.986	0.984	0.982
0.983	0.986	0.988	0.990	0.992	0.992	0.990	0.988	0.986	0.983
0.985	0.988	0.990	0.993	0.995	0.995	0.993	0.990	0.988	0.985
0.985	0.988	0.992	0.995	1.000	1.000	0.995	0.992	0.988	0.985
0.985	0.988	0.992	0.995	1.000	1.000	0.995	0.992	0.988	0.985
0.985	0.988	0.990	0.993	0.995	0.995	0.993	0.990	0.988	0.985
0.983	0.986	0.988	0.990	0.992	0.992	0.990	0.988	0.986	0.983
0.982	0.984	0.986	0.988	0.988	0.988	0.988	0.986	0.984	0.982
0.979	0.982	0.983	0.985	0.985	0.985	0.985	0.983	0.982	0.979

Fig 2.5. Position corrections for each detector chip normalized to center-line source exposure (a) as measured, (b) with a theoretical point-source geometry, (c) as measured with point-source geometry approximation removed.

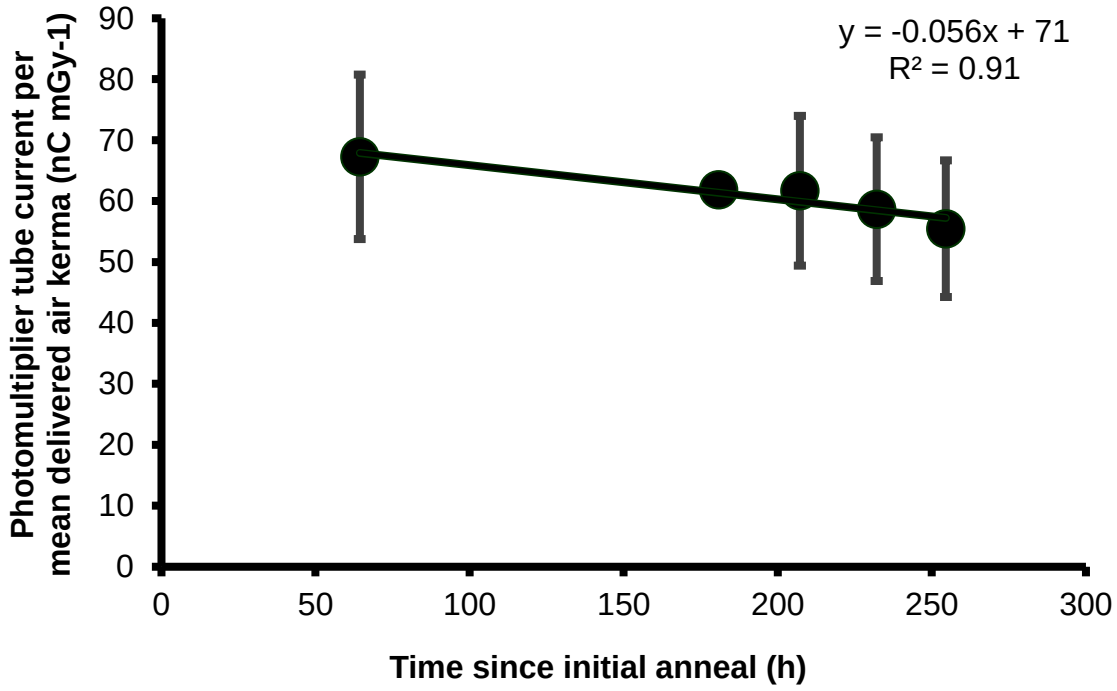
y = -0.056x + 71
R² = 0.91
Photomultiplier tube current per mean delivered air kerma (nC mGy-1)
90
80
70
60
50
40
30
20
10
0
0
50
100
150
200
250
300
Time since initial anneal (h)

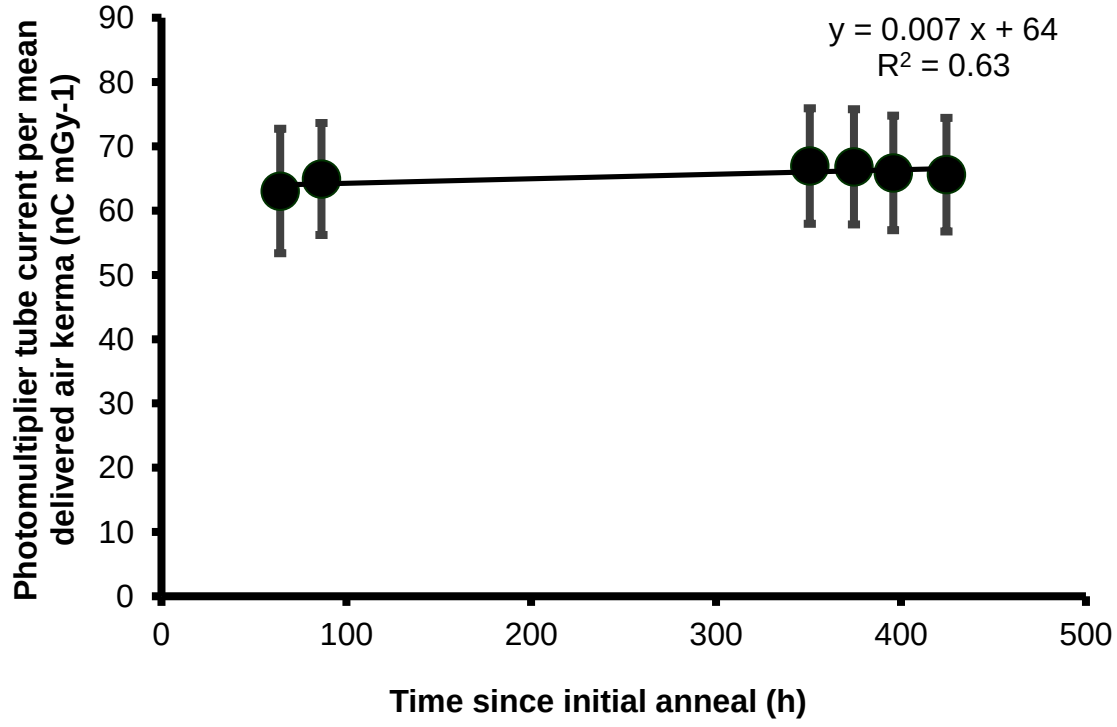
y = 0.007 x + 64
R² = 0.63
Photomultiplier tube current per mean delivered air kerma (nC mGy-1)
90
80
70
60
50
40
30
20
10
0
0
100
200
300
400
500
Time since initial anneal (h)

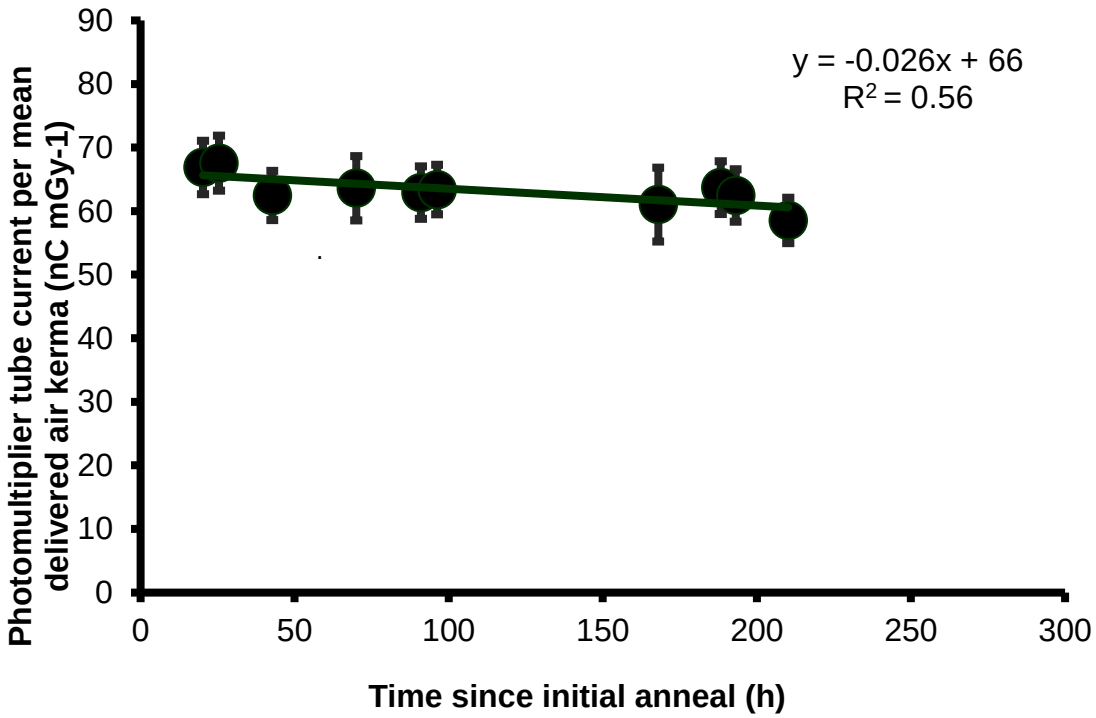

Fig 2.6. Time change in photomultiplier tube current per mean delivered air kerma for (a) sample A, (b) sample B, (c) sample C.

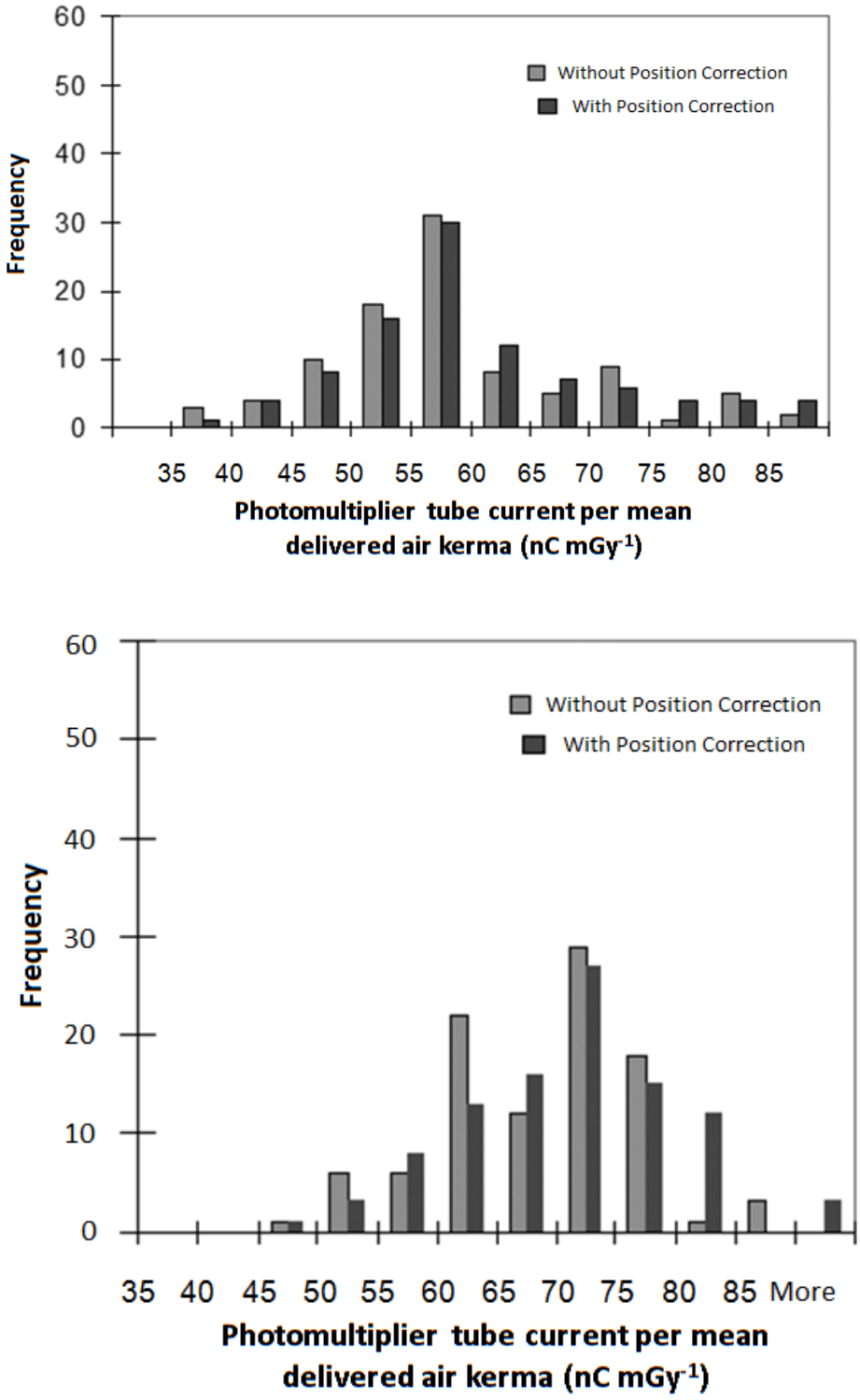

Fig 2.7. Histograms of chip ROI values with and without position corrections applied for (a) sample A, (b) sample B, (c) sample C.

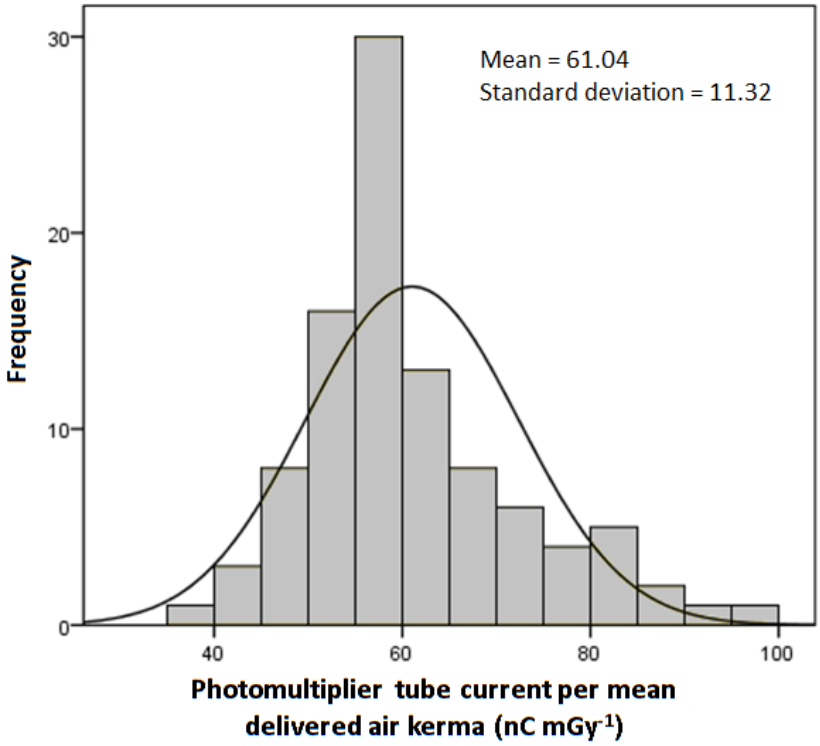
Mean = 61.04
Standard deviation = 11.32
Frequency
30
20
10
0
40
60
80
100
Photomultiplier tube current per mean delivered air kerma (nC mGy-1)

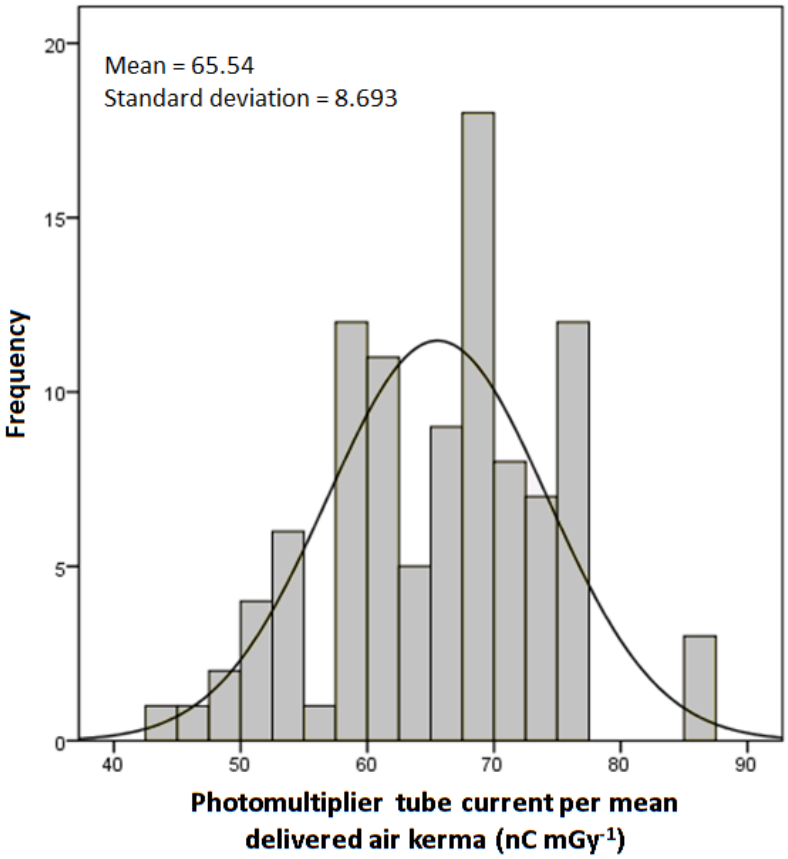
Mean = 65.54
Standard deviation = 8.693
Frequency
20
15
10
5
0
40
50
60
70
80
90
Photomultiplier tube current per mean delivered air kerma (nC mGy-1)

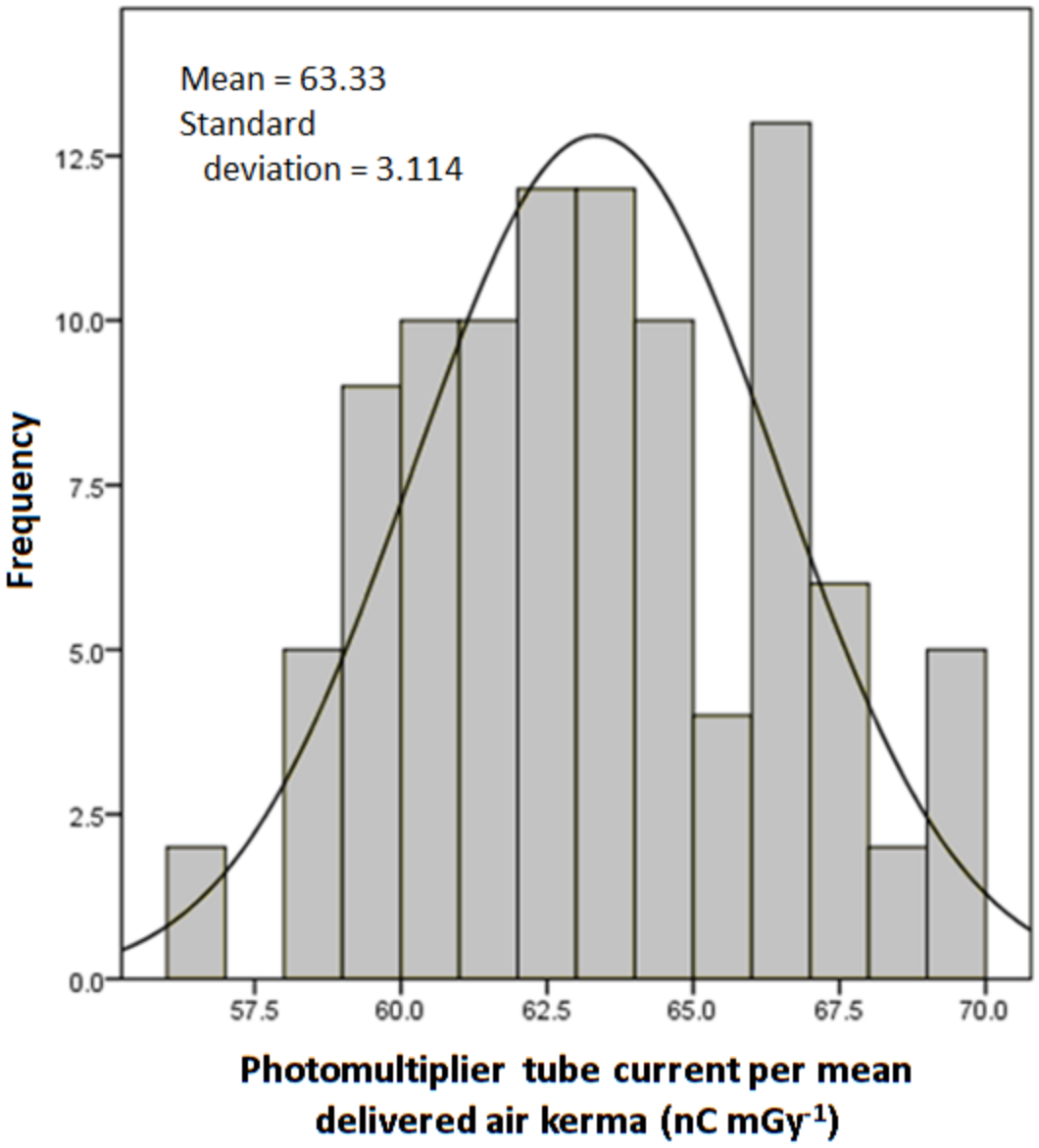

Fig 2.8. Histograms of position-corrected chip ROI values, with superimposed Gaussian distributions, for (a) sample A, (b) sample B, (c) sample C.

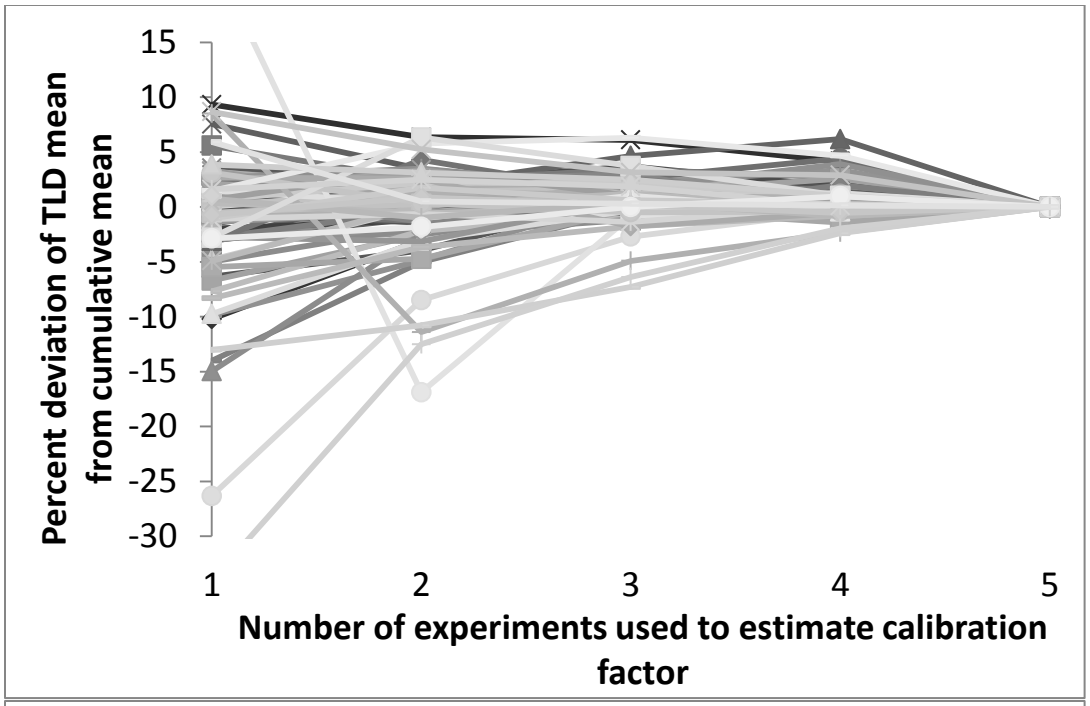
Percent deviation of TLD mean from cumulative mean
15
10
5
0
-5
-10
-15
-20
-25
-30
1
2
3
4
5
Number of experiments used to estimate calibration factor

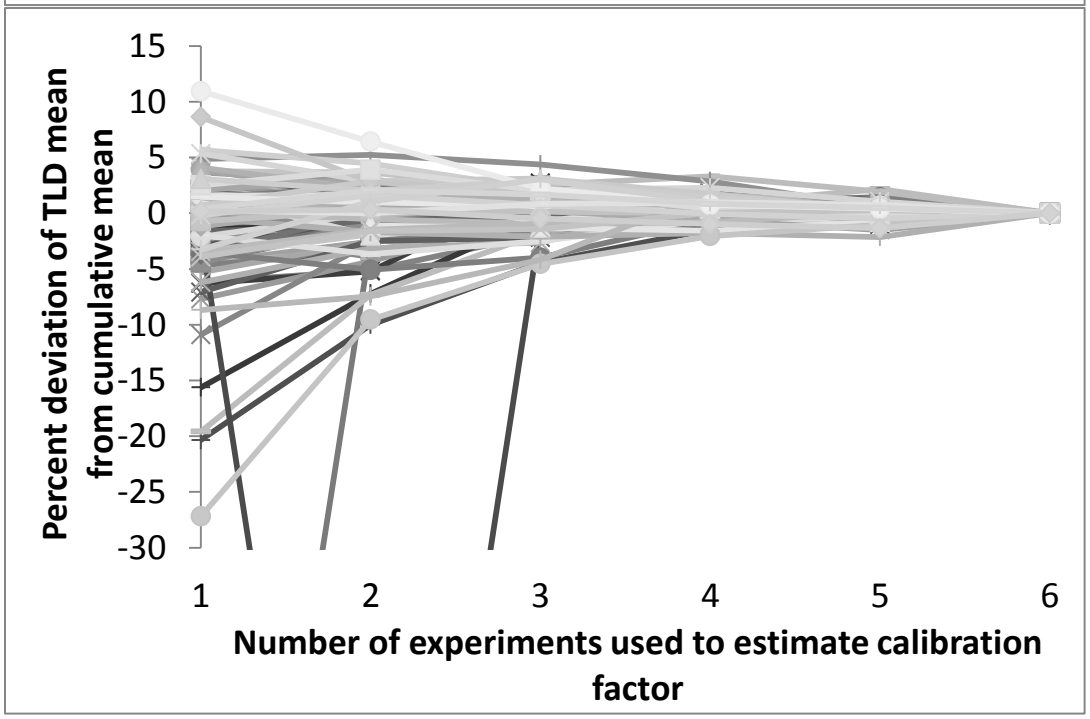
Percent deviation of TLD mean from cumulative mean
15
10
5
0
-5
-10
-15
-20
-25
-30
1
2
3
4
5
6
Number of experiments used to estimate calibration factor

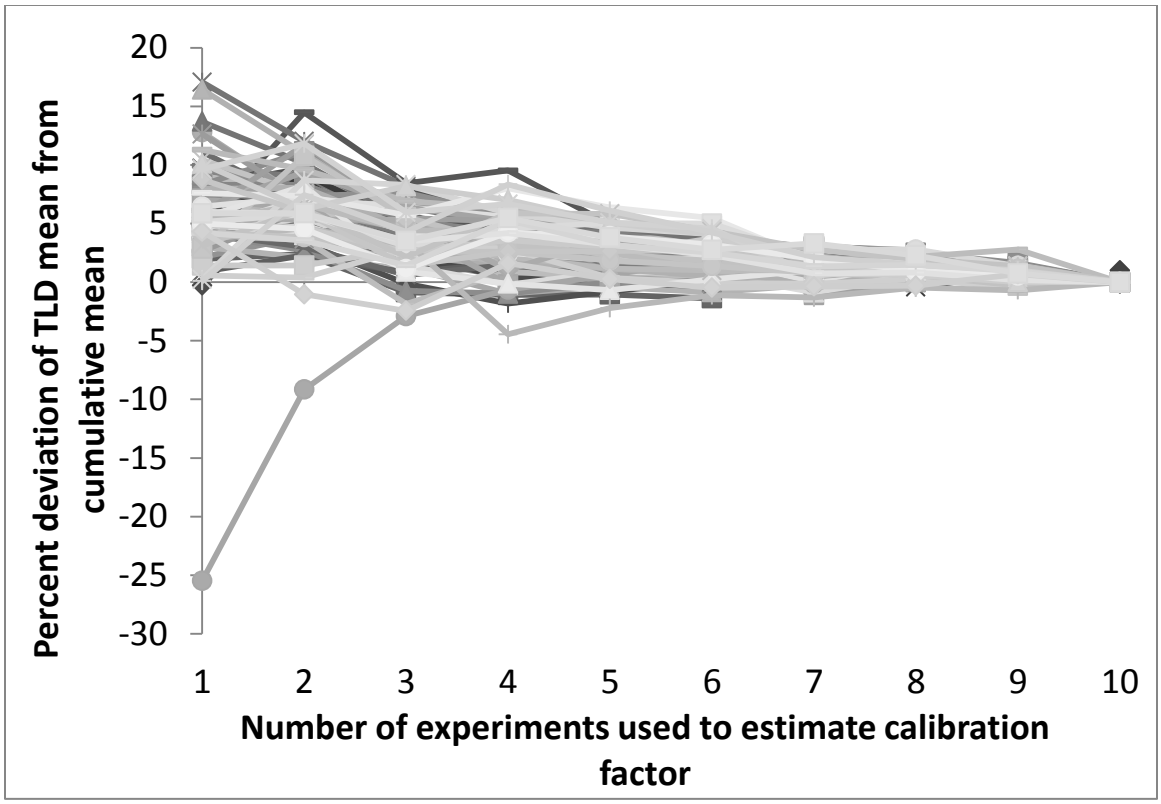

Fig 2.9. Deviation of single chips from cumulative mean of entire sample for (a) sample A, (b) sample B, (c) sample C.

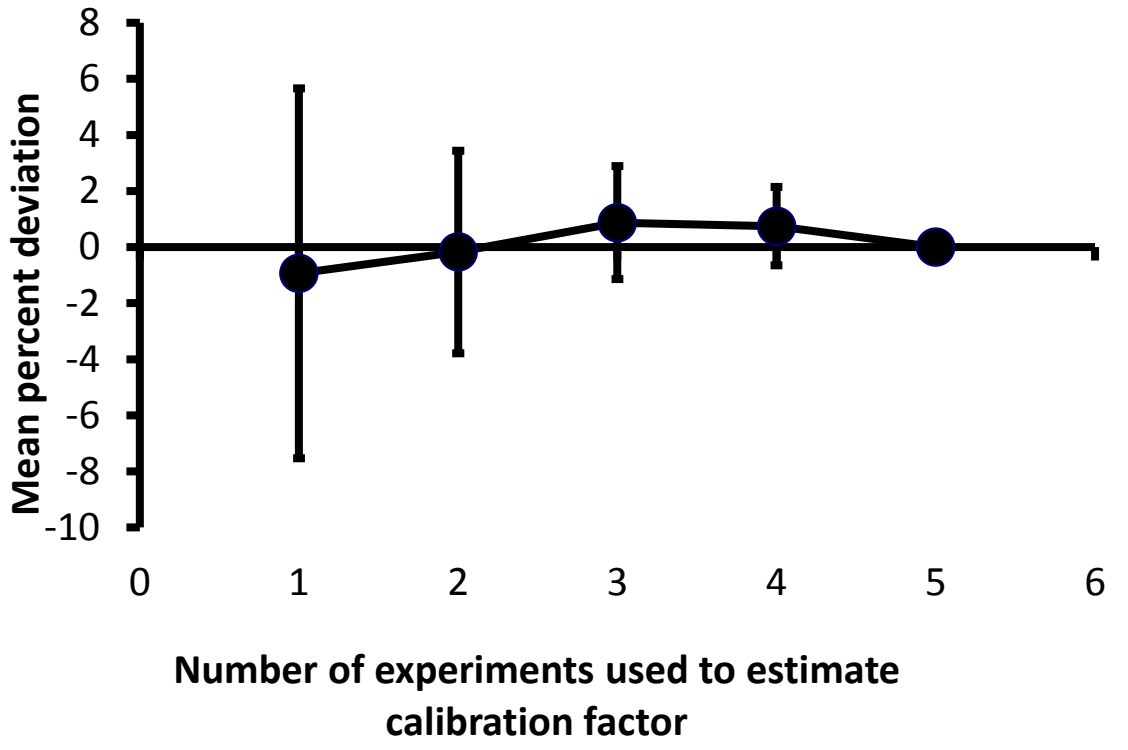
Mean percent deviation
8
6
4
2
0
-2
-4
-6
-8
-10
0
1
2
3
4
5
6
Number of experiments used to estimate calibration factor

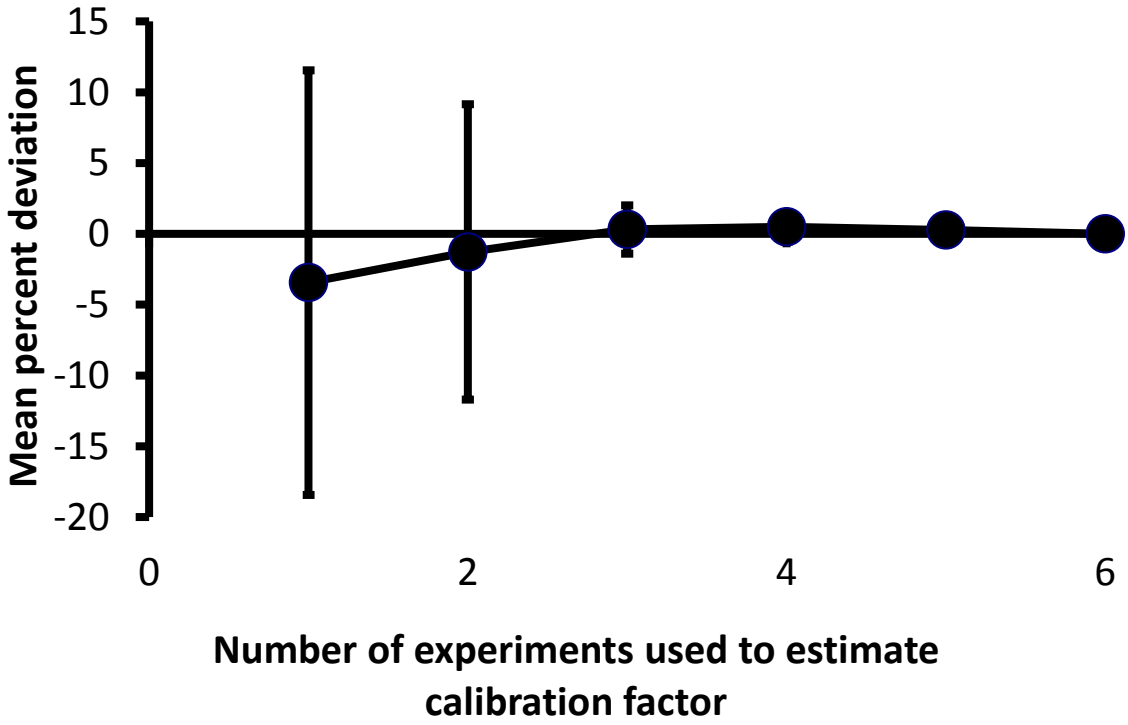
Mean percent deviation
15
10
5
0
-5
-10
-15
-20
0
2
4
6
Number of experiments used to estimate calibration factor

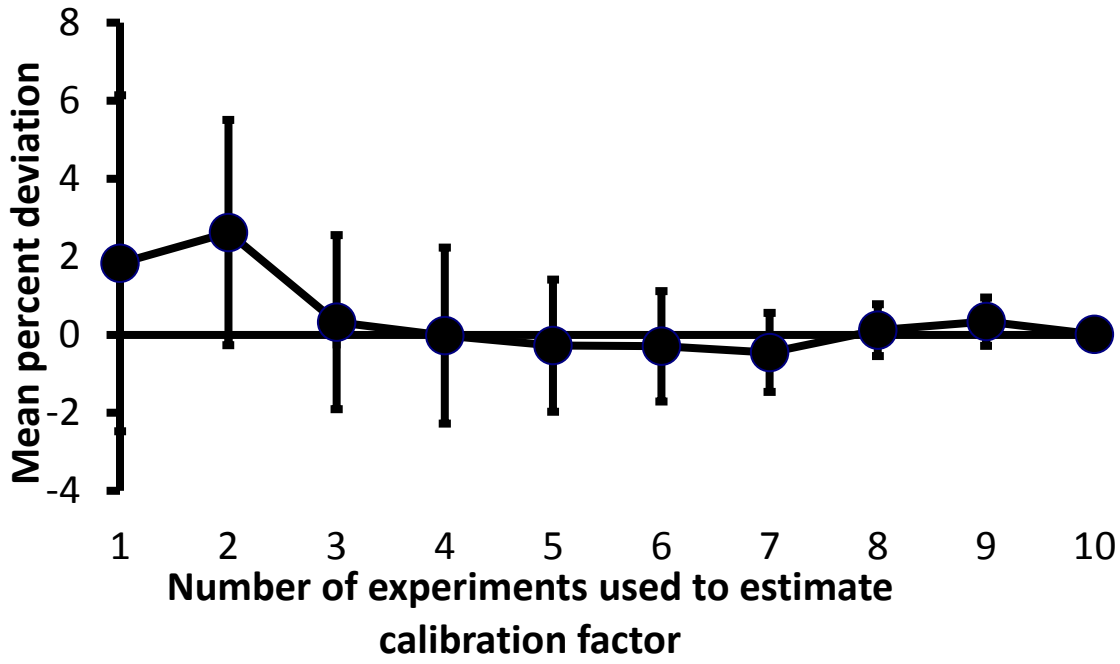

Fig 2.10. Deviation of cumulative mean of each irradiation and all previous irradiations from cumulative mean of all irradiations combined for (a) sample A, (b) sample B, (c) sample C.

Table 2.1. Deviation in values of position corrected photomultiplier tube current per dose with respect to the mean of the commercially viable group, sample C.

	Sample A	Sample B	Sample C
Deviation from mean	*Frequency*	*Frequency*	*Frequency*
0-5%	19	15	66
5-10%	33	27	28
10-15%	18	17	6
15-20%	17	12	0
>20%	13	27	0
Total	100	98	100

REFERENCES

Busuoli G., 1981. Precision and accuracy of TLD measurements. In: Oberhofer M, Scharmann A, eds. Applied Thermoluminescence Dosimetry. Bristol: Adam Hilger Ltd.;143-150.

Chauvenet W., 1871. A manual of spherical and practical astronomy, Volume II. Philadelphia: J.B. Lippincott Company.

Furetta C., Weng P., 1998. Operational Thermoluminescence Dosimetry. Singapore: World Scientific Publishing Co..

German U., Weinstein M., 2002. Non-radiation induced signals in TL dosimetry. Radiat. Prot. Dosim. 101:81-84.

Massey F., 1951. The Kolmogorov-Smirnov test for goodness of fit. J. Amer. Statistical Assoc. 46:68-78.

Moscovitch M., 1986. Automatic method for evaluating elapsed time between irradiation and readout in LiF-TLD. Radiat. Prot. Dosim. 17:165-169.

Parker L. W., Harvey J. A., Kearfott K. J., 2011. An integrated system for the beta, gamma and neutron calibration and storage of thermoluminescent dosimeters for a research laboratory. Health Phys. 100(2):S43-S49.

Plato P., Miklos J., 1985. Production of element correction factors for thermoluminescent dosimeters. Health Phys. 49:873-881.

Samei E., Kearfott K.J., Wang C.-K., Han S, 1994. Impact of variations in physical parameters on glow curves for planchet heating of TL dosimeters. Nucl. Instrum. Meth. A 353:415-419.

Simpkins R.W., Kearfott K.J., 1997. The minimum number of observations necessary to develop an average thermoluminescent dosimeter element correction factor. Radiation Protection Management 13:55-61.

Studenski M.T., Haverland N.P., Kearfott K.J., 2007. Simulation, design, and construction of a 137Cs Irradiation Facility. Health Phys. 92:S78-S86.

Taylor J.R., 1997. An Introduction to Error Analysis: The Study of Uncertainties in Physical Measurements, 2nd ed. Sausalito, CA: University Science Books.

Weinstein M., Dubinsky S., Izak-Biran T., Leichter Y., German U., Alfassi Z.B., 2003. A simple method for avoiding fading correction of absorbed dose from glow curves of TLD-100. Radiat. Meas. 37:81-86.

Weinstein M., German U., Dubinsky S., Alfassi Z.B., 2003. On the determination of the post-irradiation time from the glow curve of TLD-100. Radiat. Prot. Dosim. 106:121-130.

Chapter III

Characterization of the Glow Peak Fading Properties of Six Common Thermoluminescent Materials

ABSTRACT

The pre-irradiation and post-irradiation fading rates of the thermoluminescent glow peaks of six commonly used thermoluminescent dosimeters under controlled environmental conditions over approximately 30 d are examined. Glow peaks were fit to the first-order kinetics model using a computerized glow curve analysis program. Dosimeters studied were LiF:Mg,Ti, CaF_2:Dy, CaF_2:Tm, CaF_2:Mn, LiF:Mg,Cu,P, and $CaSO_4$:Dy. LiF:Mg,Ti and LiF:Mg,Cu,P experienced significant pre-irradiation fading. All types except CaF_2:Mn experienced post-irradiation fading. Ratios of glow peak areas were fit to exponential decay functions when possible.

INTRODUCTION

The fading of the thermoluminescent (TL) output signal is a bothersome property of thermoluminescent dosimeters (TLDs) that is important to characterize in order to accurately relate TL output with amount of radiation exposure. Researchers often apply post-irradiation treatments to empty the low temperature TL traps and remove the low temperature glow peaks before readout to reduce or eliminate this fading. Another approach is to perform a glow curve analysis and only use glow peaks that do not fade appreciably, or to integrate glow curves across regions that do not exhibit strong fading. Often overlooked is the possibility of pre-irradiation fading, which is a change in the sensitivity of the TLD prior to the delivery of the radiation dose of interest.

This study was designed to characterize the pre-irradiation and post-irradiation fading of the individual peaks of glow curves to better understand the fading of the integrated TL response and also to provide valuable information that will be used in future studies. To eliminate the need to measure and retain absolute calibration information for each individual TLD for the purposes of this experiment, the ratios between glow peak areas were investigated and provided a type of self-calibration. Six types of TLDs were chosen for studied based upon number of glow peaks, corresponding glow peak temperatures, and TLD availability. These TLD types were: LiF:Mg,Ti, CaF_2:Dy, CaF_2:Tm, CaF_2:Mn, LiF:Mg,Cu,P, and $CaSO_4$:Dy. Various means of handling, reading, storing, and glow-peak separation method have caused wide variations in the published fading properties of these materials. For this reason and because of the well-known fact that the fading is highly dependent on storage temperature, the environmental conditions during the experiment were controlled and monitored.

Glow Curve Structure and Fading Properties

LiF:Mg,Ti (TLD-100)

Glow curve structure

LiF:Mg,Ti has a glow curve typically treated as the superposition of four first-order kinetics peaks (P_2-P_5) following low dose, low ionization density irradiation (Horowitz et al., 2006). At higher doses and ionization densities, as

many as 9-10 glow peaks have been reported between room temperature and 675 K (Fairchild et al., 1978; Shachar and Horowitz, 1991). Most recently, the glow curve has been reported to have 15 glow peaks between 320 and 650 K with much of the interest being in the two satellite peaks surrounding the main dosimetric peak (Y. Horowitz et al., 2002a, 2002b, 2006; Biderman et al., 2002, 2006; Brandan et al., 2006).

Fading characteristics

Wide variation in fading characteristics measured for LiF:Mg,Ti demonstrates the complexity involved in characterizing a fading rate (Horowitz, 1990b; Moscovitch et al., 1990; Shachar and Horowitz, 1993). Variations in annealing procedures, TLD handling, and in the type of radiation used has caused the reported fading rates to vary from as little as 1% per year to 7% in two weeks (Horowitz 1990b). Applying a post-irradiation preheat procedure significantly decreases fading because of the removal of the lower temperature peaks (Izak-Biran et al. 1996).

CaF_2:Dy (TLD-200)

Glow curve structure

The number of peaks reported in the glow curve of CaF_2:Dy has increased with the evolution of the literature. Hasan and Charalambous reported seeing five major peaks in their 1983 experiment (Hasan and Charalambous, 1983). A few years later in 1986, another laboratory reported a total of six peaks, with the most evident ones being P_2 at 140^{o}C, P_3 at 200 ^{o}C, and P_4 at 250 ^{o}C (Wang et al., 1986). That group also used the ratio between peak heights to determine the type of radiation field the in which TLD was placed. Recently, Yazici et al. conducted the most thorough experiment to date to determine the number of peaks in the glow curve of CaF_2:Dy (Yazici et al., 2002). They used beta irradiation and a T_m-T_{stop} procedure, in which an irradiated sample is heated at a constant rate until reaching a point on the leading tail of the first peak, known as T_{stop}. Then, the sample is cooled to ambient temperature and heated at the same rate again to read the entire glow curve, with the maximum temperature recorded as T_m. Using this method, they found a total of nine peaks with P_1-P_7 and P_8

being of the first-order kinetics and P_6, P_7, and P_9 possibly being of general-order kinetics (Yazici et al., 2002).

Fading characteristics

Little has been reported about the overall glow curve and individual peak fading of CaF_2:Dy. One experiment reported the fading to be approximately 25% in one month without any post-irradiation treatments (Binder and Cameron, 1969). Applying a post-irradiation annealing of 80^oC for 10 min removed the lower temperature peaks, reducing the fading to 13% in the first month. When the glow curve for CaF_2:Dy was treated as being comprised of two main peaks, 45% and 12% fading in the peak areas in 35 d at room temperature was reported (Bacci et al., 1988).

CaF_2:Tm (TLD-300)

Glow curve structure

Since the introduction of CaF_2:Tm nearly three decades ago, its glow curve is most commonly treated as comprised of six glow peaks (Furetta and Lee, 1983; Shachar and Horowitz, 1988; Bos and Dielhof, 1991; Hsu and Weng, 1995). An early study on the effect of storage temperature on the material treated the glow curve as being three peaks (Bacci et al., 1988). However, a more extensive study conducted by Bos et al. a few years clearly concluded that the glow curve is best described as the superposition of six first-order kinetic peaks (Bos et al., 1991). Jafarizadeh et al. introduced the possibility a third low temperature peak based on a general-order model raising the total number of peaks to seven (Jafarizadeh et al., 1999). Most recently, Skopec et al. concluded that the glow curve featured a total of eight first-order kinetic peaks with the introduction of an additional peak located between the two main dosimetric peaks (Skopec et al., 2006).

Fading characteristics

Because part of the glow curve of CaF_2:Tm consists of low temperature peaks, it is expected that the untreated CaF_2:Tm will have a significant decrease in total TL response over a short period of time. Furetta and Lee first reported a maximum total post-irradiation fade in the TL output as 40% in 25 d (Furetta and

Lee, 1983). Applying a simple low temperature post-irradiation annealing reduces the fading caused by these lower temperature peaks (McKeever et al., 1995). Hsu and Weng reported that for storage times beyond 10 h at room temperature, the fading rate of the total TL output, the height of P_3, and the ratio of P_5 to P_3 remain constant (Hsu and Weng, 1995). P_3 has also been reported to fade at ~10% in the first day with 2% thereafter (Shachar and Horowitz, 1988). That same study reported that the sum of the areas of P_5 and P_6 remains completely stable over 2.5 months.

CaF_2:Mn (TLD-400)

Glow curve structure

CaF_2:Mn is the least studied TL material examined in this experiment, with one glow peak located at ~575 K. However, experimental evidence suggests that it is comprised of several traps closely spaced in energy, or the result of charge released from a continuous distribution of traps (McKeever et al., 1995). Phototransferred TL data obtained by Allen and McKeever suggest that the glow curve is comprised of at least two closely overlapping but discrete TL peaks (Allen and McKeever, 1990). This material's response appears to be extremely sensitive to the presence of small quantities of impurities (McMasters et al., 1987).

Fading characteristics

It has been reported that most CaF_2:Mn fading occurs within the first 24 h at a 5% loss in total TL, and then a stabilization occurs after two days at a total loss of 8% (McKeever et al., 1995).

LiF:Mg,Cu,P (TLD-700H)

Glow curve structure

LiF:Mg,Cu,P is a nearly perfect dosimetric material (Velbeck et al., 2006) and its glow curve has three main glow peaks (P_2 - P_4) with the largest, P_4, located at approximately 545 K (Horowitz, 1993). P_1 is a small, low temperature peak that fades in a matter of hours and is ignored or removed using a pre-read annealing (Cassata et al., 2002). A high temperature glow peak structure located past P_4 appeared in the glow curve of LiF:Mg,Cu,P when it was in its early stages

of development (DeWerd et al., 1984; Horowitz et al., 1990, 1993; Horowitz, 1993). Horowitz et al. observed up to six peaks in the glow curve of LiF:Cu,Mg,P with the high temperature glow peak structure (Horowitz et al., 1993). They later reported a method of eliminating the high temperature glow peak in order to reduce a residual signal directly attributed to it (Y. Horowitz, 1990a; A. Horowitz, A. and Y. Horowitz, 1993). As the material and its production became more refined, reliable, and commercially available, the high temperature glow peak structure became insignificant, if it is present at all (Moscovitch, 1999; Hosseini-Pooya and Jafarizadef, 2004; Velbeck et al., 2006).

Fading characteristics

In the last decade, several well-conducted studies (Alves et al., 1999; Budzanowski et al., 1999; Duggan and Kron, 1999; Vergara et al., 1999; Cassata et al., 2002; Hosseini-Pooya and Jafarizadef, 2004; Jones and Stokes, 2006) have investigated the pre-irradiation and post-irradiation fading rates of LiF:Cu,Mg,P. These studies have reported the exponential decay of P_3 both before and after an irradiation and an increase in the total area of P_4 during pre- and post-irradiation fading (Alves et al., 1999; Duggan and Kron, 1999). P_4 has been shown to have a high thermal stability and fades independently of the thermal temperature whereas the low temperature peaks decay exponentially and are strongly dependent on temperature (Alves et al., 1999; Vergara et al., 1999).

The total TL output has been reported to post-irradiation fade up to 26% (Hosseini-Pooya and Jafarizadef, 2004) and as little as “unchanged within experimental uncertainty” (Duggan and Kron, 1999) over a post-irradiation storage of 6 months. Another study observed and reproduced a 2% increase in the total sensitivity, pre-irradiation fade, for the first 60-70 d and then a steady decrease in the total sensitivity (Cassata et al., 2002). Most recently, Jones et al. reported seeing no significant change in the sensitivity of LiF:Cu,Mg,P at ambient temperatures (Jones et al., 2006).

$CaSO_4$:Dy (TLD-900)

Glow curve structure

The treatment of the glow curve of $CaSO_4$:Dy has varied greatly among researchers. The glow curve was first described as being comprised of as many as twelve closely overlapping glow peaks, based upon a partial bleaching technique (Nambi et al., 1974). Souza et al. later conducted a more intensive study, concluding that there must be at least ten elementary peaks of first-order kinetics to describe how the glow curve evolves with increasing doses (Souza et al., 1993). However, at doses below approximately 0.10 Gy, some of the higher temperature peaks are not present therefore making it acceptable to treat the glow curve as being comprised of two or three main peaks (Drazic and Trontelj, 1983; Bacci et al., 1988; Wang et al., 1987; Li and Hsu, 1990).

Fading characteristics

Guelev et al. reported a post-irradiation fading in the total TL response of 5% in six months at room temperature (Gueley et al., 1994). A more recent study on the fading of $CaSO_4$:Dy reported a 3.7% loss over 30 d in the total TL response from 150 to 350^oC (Al-Ghorabie, 2005). Wang et al. reported a significant increase in the P_2 to P_1 height ratio in the first 8-10 d after an exposure and then a leveling off upon considering the glow curve as being comprised of two main peaks (Wang et al., 1987). This trend was also observed by Bacci et al., who reported that for TLDs stored at 40^oC an increase in the total TL response over 20 d was observed before a normal signal decay began (Bacci et al., 1988). The fading of $CaSO_4$:Dy signal is highly dependent upon light exposure, with a reported loss of more than 50% of the TL response in a 3 h exposure to the visible part of the sunlight spectrum (Pradhan, 1993). Although many studies have shown the complexity of the glow curve of $CaSO_4$:Dy, no systematic study has been conducted to observe how these multiple glow peaks evolve with time before and after an irradiation.

Study goal

The primary goal of this study is to analyze pre-irradiation and post-irradiation fading properties of six common materials at room temperature, and compare them to previous results if available. In particular, the literature

contains a relative lack of pre-irradiation fading studies, and little in-depth analysis of fading data for CaF_2:Dy, CaF_2:Mn and $CaSO_4$:Dy. Fading functions are analyzed with exponential functions, either those previously used in the literature or formulated specifically for this study.

MATERIALS AND METHODS

TLD types and storage

One hundred new LiF:Mg,Ti, CaF_2:Dy, CaF_2:Tm, CaF_2:Mn, LiF:Mg,Cu,P, and $CaSO_4$:Dy TLDs (BICRON/Harshaw, 6801 Cochran Road, Solon, OH 44139, USA) were employed in this experiment with a guaranteed response variability of less than 5%. Their type, size, and manufacturer recommended time temperature profiles (TTP) can be found in Table 3.1. When not being read or irradiated, the TLDs were stored in a water-jacketed incubator (NuAire Model NU2700 Dual Chamber CO_2 Incubator, NuAire Inc., 2100 Fernbrook Lane N, Plymouth, MN 55447) to control environmental conditions. The temperature was kept at 21.4 $\pm$ 0.6 ^{o}C and ambient light was minimal when the incubator door was closed. Approximately 500 mL of anhydrous calcium sulfate, a desiccant, was placed inside the incubator to stabilize the humidity, which was maintained at 12.4 $\pm$ 6.4% relative humidity for the duration of the experiment.

TLD irradiation and readout

Glow curves were obtained using a standard TLD reader with hot gas and hot planchet capabilities (Model 4500 TLD Reader, BICRON/Harshaw, 6801 Cochran Road, Solon, OH 44139, USA) used in planchet heating mode with nitrogen gas (Prepurified compressed nitrogen cylinder 300, Metro Welding Supply Corporation, 12620 Southfield Road, Detroit, MI 48223) flowing to reduce oxygen induced light effects. Irradiations were performed using a 370 GBq ^{137}Cs source (Model 28-8A Irradiator, J.L. Shepherd and Associates, 1010 Arroyo Avenue, San Fernando, CA 91340-8122), in a specially designed facility (Studenski et al., 2007).

Each group of 100 TLDs was split into two subgroups, with one designated to study pre-irradiation fading and the other designated to study

post-irradiation fading. The set of 50 TLDs in each group were split into 10 batches of five TLDs. Each batch of five TLDs were irradiated, stored, and read together and their results averaged. For irradiation, the TLDs were placed in a 40 × 40 × 0.6 cm^3 polymethyl methacrylate (PMMA) plate with one hundred wells 0.3 cm deep, covered by a 40 × 40 × 0.25 cm^3 PMMA sheet attached by four acrylic screws. This was then mounted to a 40 × 40 × 15 cm^3 PMMA phantom, 60 cm above the floor and 150 cm from the source. The plate and phantom were custom manufactured in-house.

To optimize the amount of data that could be obtained from the TLDs over the 30 d of the experiment, all but one batch, five TLDs, of each set, 50 TLDs, were used twice during the experiment as is shown in Fig 3.1. For example, a batch of TLDs used to study fading after five days for example were reused immediately after being read to study the effects of fading over 25 d therefore allowing two pieces of data to be obtained from one batch of TLDs. The one batch of TLDs of each TLD type not used twice during the experiment was used to study fading over the entire length of the experiment and these TLDs were thus only read once.

After all the TLDs were annealed in the reader, the set of TLDs designated to study post-irradiation fading were given a dose of 4.4 mGy over an exposure time of approximately 18 min and then stored in the incubator until readout. Readout of post-irradiation fading TLDs consisted of reading a batch of faded using the manufacturer recommended time temperature profiles (TTPs) found in Table 3.1, exposing them to 4.4 mGy again, and then returning them to the incubator until the end of the experiment when all of the TLDs would be read at once. This process allowed for the optimization of total data obtainable in a given time period, as explained previously. The total elapsed time to complete a readout of a batch of TLDs was approximately 45 min with most of the time due to the irradiation and transit time to and from the irradiator. Fading times studied were 0.5, 1, 1.5, 2, 3, 4, 8, 15, and 30 d.

A similar process was followed with the pre-irradiation fading TLDs. A typical readout consisted of first irradiating, immediately reading/annealing, and

then returning to the incubator as is shown in Fig 3.1. At no point were any of the TLDs oven annealed; annealing was done by running them through a readout cycle.

Data analysis

Computerized glow curve analysis (GCA) into individual glow peaks was completed using a program written for a standard commercially available mathematics software package (MATLAB R2007a, The MathWorks Inc., 3 Apple Hill Drive, Natick, MA 01760) which used the first-order kinetics model for the shape of the peaks and a non-linear least-squares method to fit the peaks. An exponential high temperature background signal was fit to the glow curves when possible, accounting for handling, contamination, chemiluminescence, triboluminescence, and infrared background. The number of glow peaks extracted from the glow curves for a given TLD type was generally based upon published literature, but in a few instances additional glow peaks were added to produce a reasonable fit.

The quality of each GCA fit was judged by eye and by the figure-of-merit (FOM) calculated using (Souza et al., 1993; Weinstein et al., 2003):

$$FOM = \sum_{j_{start}}^{j_{stop}} \frac{100\left|y - y\left(x_i\right)\right|}{A} \tag{3.1}$$

where j_{start} is the initial temperature in the fit region, j_{stop} is the final temperature in the fit region, y_j is the experimental TL intensity at temperature j, $y(x_j)$ is the value of the fit found at temperature j, and A is the integral of the fitted glow curve between j_{start} and j_{stop}. The fits were considered adequate when the FOM values were below 2%, with most actually being below 1%.

The fit parameters E, activation energy, and T_{max}, the temperature at which the peak maximum appears, were allowed to vary for each peak over a small range determined through trial and error. These ranges are given in Table 3.2.

RESULTS AND DISCUSSION

The experimentally determined averages of the peak parameters *E* and T_{max} are given for all tested materials in Table 3.2. Standard deviations are not provided as at least one value of each data set was equal to one of the range limits imposed on each parameter. As many factors influence the parameters determined for each peak, including applied dose, post-irradiation annealing time, and determination method (Yazici et al., 2002), no reference values are provided for comparison.

LiF:Mg,Ti (TLD-100)

Due to the relatively low exposure to the TLDs, the glow curve of LiF:Mg,Ti was best treated as the sum of four first-order kinetics glow peaks with an exponential high-temperature background signal, as shown in Fig 3.2. The evolution of the glow curve as a result of both pre- and post-irradiation fading, shown in Fig 3.3, clearly demonstrates more rapid loss of signal as time progresses.

The pre- and post-irradiation fading of the peak area ratio of P_2 to P_4 followed an exponential decay trend. Both pre- and post-irradiation data were initially fit to the exponential decay equation

$$y = Ae^{-Bt} + C \tag{3.2}$$

but generating a fit to this equation using the P_2 to P_4 post-irradiation fading data resulted in a poor correlation for fading times of less than 15 d. It was then fit to a sum of two exponentials,

$$y = Ae^{-Bt} + C + De^{-Et} \tag{3.3}$$

and a much better fit of the initial values was obtained. This sum of two exponentials may be due to the decaying of some of the small peaks located near P_2 (Y. Horowitz et al., 2002a) but were not extracted from the glow curve. The results from generating a fit to the pre- and post-irradiation fading of the peak area ratio of P_2 to P_4 can be found in Table 3.3 and plotted in Fig 3.4.

As previously reported (Shachar and Horowitz, 1993; Delgado et al., 1993), the fading of the peak area ratios of P_4 to P_5 and P_3 to P_5 were found to be quite complex. This can be seen in Figs. 3.4a and 3.4b. The electrons in each trap may fade either back to the ground state, or into a lower energy trap. Assuming that each fading rate is a simple exponential decay equation, and that the sum of the probability of fading to the ground state or fading to a lower energy trap state is one, differential equations may be constructed for a generic higher energy and lower energy trap. Solving and taking the ratio of these equations gives

$$y = Ae^{-Bt} - Ae^{-Ct} + De^{-Et}. \tag{3.4}$$

Values for these parameters for peak area ratios P_3 to P_5 and P_4 to P_5 are given in Table 3.4.

The total TL pre- and post-irradiation fading was 35% and 37% respectively over 33 d. The pre- and post-irradiation fade of P_2 to P_4 was 88% and 100% respectively while the pre- and post-irradiation fade of P_3 to P_4 was 37% and 63% respectively, over this same time period. Although qualitatively similar, these results are higher on average than the previously published results (Horowitz, 1990b; Izak-Biran et al., 1996).

CaF_2:Dy (TLD-200)

A typical CaF_2:Dy glow curve separated into individual peaks, showing nine peaks similar to those reported by Yazici et al. (Yazici et al., 2002) can be found in Fig 3.5. Due to the use of a different TTP, however, the peaks observed for this study were located at different temperatures than previously reported. A significant difference arose with P_7 whose height was found to be on the order of P_3 and P_4 where Yzaici et al. had P_7 being smaller than P_1. P_9 also showed a significant variability in intensity among individual chips, something not mentioned by Yzaici et al.

Generating a fit for the nine peaks in this glow curve was particularly difficult due to the closeness of the peaks to each other. Generating a fit to P_5 posed the most difficulty, as it is a relatively high temperature peak and should not have faded appreciably during the experiment. Its fit parameters were strictly

limited during the use of the GCA program to stabilize the fit. The entire glow curve became significantly more difficult to fit as the time after irradiation increased.

Fig 3.6 shows an increase in the TL response, in particular the P_3-P_4 complex, over the first week followed by stabilization in the TL response for both the pre- and post-irradiation fading. The data plotted in Fig 3.7 show that the area of P_3 increased and the area of P_4 decreased during this time, as reported in the literature (Bacci et al., 1988).

The peak area ratios for the pre-irradiation fading data plotted in Fig 3.7a show no significant changes in the sensitivity of the peak ratios as a function of time. The post-irradiation fading data plotted in Fig 3.7b show that the peak area ratios of P_1 to P_4 and P_2 to P_4 fade quickly to zero after approximately three days. The peak area ratio of P_4 to P_7 remains relatively constant after the first three days. The peak area ratio of P_3 to P_4 had a loss of approximately 50% over the entire experiment. These data were fit to Eq. 2 and the parameters can be found in Table 3.5. The total post-irradiation fade in the TL response was 19% over 28 d. This is slightly less than the 25% loss over 30 d reported for CaF_2:Dy when a post-irradiation treatment is not applied (Binder and Cameron, 1969).

CaF_2:Tm (TLD-300)

A total of eight peaks shown in Fig 3.8 were extracted from the glow curve of CaF_2:Tm. Because of the lack of defining features, a traditional one peak was fit in between the two main peaks (P_5 and P_7) instead of two reported previously (Skopec et al., 2006). In addition, the low temperature region was best fit by four low temperature glow peaks instead of three. P_6 was the most difficult peak to fit, with its fit parameters strictly limited to stabilize the fit. P_8 was also difficult to fit due to the lack of complete information caused by the TTP that was used.

The peak area ratios plotted in Fig 3.9a and Fig 3.10a show no significant pre-fading of CaF_2:Tm. The sensitivity of the individual peaks of CaF_2:Tm did not significantly change for the least 30 d between annealing and irradiation.

P_1 completely faded after approximately one hour after an irradiation. Skopec et al. waited three to seven days before reading the TLDs, thereby

missing this first peak (Skopec et al., 2006). P_2 faded completely in less than one day after an irradiation, but was still reported by Skopec et al. after their three to seven day waiting period (Skopec et al., 2006).

The data plotted in Fig 3.10b show that the peak area ratio of P_3 to P_5 reduces to near zero after 14 d with small standard deviations. Difficulty in generating a fit to the peaks in the glow curve can be seen in the post-irradiation fading of the peak area ratio of P_4 to P_5. When fading time was short, other low temperature peaks were present and the fading trend was varied. After the lower temperature peaks had faded, it became easier to fit P_4, causing the remaining fading data to show the expected exponential decay. Because the data that remained after the low temperature peaks had faded are more likely to fully represent the fading of the peak area ratio of P_4 to P_5, these data were chosen to be fit to Eq. 2. The fit parameters from generating a fit to the data and the peak area ratio of P_3 to P_5 can be found in Table 3.6 and Fig 3.10b. The fits had high R^2 values and show that the post-irradiation fading of these peak area ratios follows the expected exponential decay trend. It must also be noted that a slight post-irradiation fading occurred for the ratio of $P_5/(P_7 + P_8)$ after the first three days with a total drop in TL intensity of 8% over 28 d.

The total loss in TL response was 25% over the 28 d of the experiment, less than the previously reported maximum fade of 40% in 25 d (Furetta and Lee, 1983). A stabilization did not appear as previously reported (Hsu and Weng, 1995), due to the lack of a post-irradiation annealing treatment for this work.

CaF_2:Mn (TLD-400)

In this work the CaF_2:Mn glow curve was poorly fit to two first-order peaks that had been previously reported (Allen and McKeever, 1990). The best fit was obtained by the three closely overlapping but distinct peaks, as shown in Fig 3.11.

The pre-irradiation fading of the glow curve of CaF_2:Mn shown in Fig 3.12a reveals no significant changes in the structure of the glow curve after 28 d, but shows a sizeable 24% loss in the TL response. This sensitivity loss could not be attributed to a certain peak as shown by the data in Fig 3.13a. The spread in data

and large standard deviations in Figs. 3.12a and 3.12b show the difficulty in generating the fit to the three closely overlapping peaks.

The evolution of the glow curve of CaF_2:Mn shown in Fig 3.12b shows that the glow curve remains fairly constant after a significant loss in the total TL response of 60% after the first day. Although much more dramatic in this case, this trend was previously reported with a total loss in the total TL of 8% (McMasters et al., 1987). Due to the large standard deviations and the spread in the data, no conclusive patterns in the fading of the peak area ratios could be made although it initially appears that the ratio of P_1 to P_3 decays exponentially.

LiF:Mg,Cu,P (TLD-700H)

The TTP used for the LiF:Mg,Cu,P in this experiment, although completely annealing the TLD, did not allow for the full glow curve to be observed and was designed to be used on a thicker LiF:Mg,Cu,P TLD. Generating a fit to the glow curve to the three standard glow curves (P_2-P_4) produced a poor fit suggesting the presence of a higher temperature glow peak similar to what was present in the early development of the material (DeWerd et al., 1984; A. and Y. Horowitz, 1990, 1993; Y. Horowitz, 1993). To adequately fit the glow curve, a fourth peak had to be added at a higher temperature than the main dosimetric peak, as can be seen in Fig 3.14. The fit parameters were limited to stabilize the fit.

Fig 3.15a and Fig 3.16a show a noticeable pre-irradiation fading of the peak area ratio of P_2 to P_4 with a total loss of 33%. The first three data points do not agree with what was expected due to unusually small P_2 areas which appear to have arisen from an undesired and not understood fading of P_2. The peak area ratio of P_3 to P_4 decreased in sensitivity by 8% during this time. A total TL loss in sensitivity over 32 d was 25%, which is significantly larger than sensitivity losses previously reported in the literature (Duggan and Kron, 1999; Cassata et al., 2002). These peak area ratios were fit to Eq. 2 and the fit parameters can be found in Table 3.7.

The post-irradiation fading of the peak area ratios of P_2 to P_4 and P_3 to P_4 decayed exponentially as expected (Budzanowski et al., 1999; Duggan and Kron, 1999; Hosseini-Pooya and Jafarizadeh, 2004) with the peak area ratio P_2 to P_4

approximately zero after 14 d. Large R^2 values were obtained when these data were fit to Eq. 2. These values and the fit parameters can also be found in Table 3.7.

The total post-irradiation fade of the glow curve over 32 d was 21%, which is comparable to the previously published values for six months of post-irradiation storage (Duggan and Kron, 1999; Hosseini-Pooya and Jafarizadeh, 2004).

$CaSO_4$:Dy (TLD-900)

The glow curve of $CaSO_4$:Dy was the most difficult to fit of the six TLDs used in this experiment because of the complexity in the glow curve structure in both the low and high temperature regions. An observable darkening in the color of the TLDs occurred with the recommended TTP for unknown reasons, possibly releasing blackbody radiation in the process. This is believed to be the reason for the high temperature tail in the glow curve. Because of the complexity caused by this and the little fading that is expected in this high temperature region, a fit was completed only in the region between 300 and 575 K which includes all of the peaks up to and including the main dosimetric peak, P_7. Strict limitations were placed on the fit parameters of P_6 in an effort to stabilize the fit.

Nambi et al. hypothesized a total of three low temperature peaks (Nambi et al., 1974) while Souza et al. hypothesized a total of four low temperature peaks (Souza et al., 1993) located before the main dosimetric peak but they may have allowed significant time to pass between irradiation and readout. A poor fit was obtained for the pre-irradiation fading curves when only three or four low temperature peaks were extracted. It was found that an additional two low temperature peaks along with the traditional four low temperature peaks hypothesized by Souza et al. (Souza et al., 1993) were needed to best describe the low temperature region. Thus, it was concluded that a minimum of seven peaks had to be used to describe the completely unfaded glow curve of $CaSO_4$:Dy as can be seen in Fig 3.17.

No significant pre-irradiation fading was found as can be seen in Figs. 3.18a and 3.19a. P_1 and P_2 post-irradiation faded within one day and P_3 decayed

completely within one week after an irradiation. The peak area ratios of P_3 to P_7 and P_4 to P_7 shown in Fig 3.19b were fit to the exponential decay equation of Equation 3.2 and the results can be found in Table 3.8. These results combined with the fits plotted in Fig 3.19b indicate that further data would need to be obtained to better fit the peak area ratio of P_3 to P_7 over its short decay period while a longer study would need to be conducted to better fit the slowly decaying peak area ratio of P_4 to P_7 for decays longer than one month.

A total loss in the TL response over 29 d was 30% with half of the loss occurring within the first three days due to the decay of the first three low temperature peaks. This far exceeds the 5% in six months (Gueley et al. 1994) and 3.7% in 30 d (Al-Ghorabie, 2005) reported previously due to the consideration of the low temperature peaks in this study. The previously observed (Bacci et al., 1988) initial increase in the total TL response followed by a normal decay was not observed in this case.

CONCLUSIONS

Pre-irradiation fading was found in the two lithium fluoride thermoluminescent detectors, LiF:Mg,Ti and LiF:Mg,Cu,P, with the total loss in sensitivity being 35% and 25% respectively over a one month period. The peak area ratios involving lower temperature peaks were found to decrease more quickly than those involving higher temperature peaks. These results indicate that pre-irradiation fading represents a true TLD sensitivity change in sensitivity before irradiation, which occurs independent of any background radiation dose that may be present during storage before irradiation.

Post-irradiation fading of peak area ratios were found for all of the TLD types studied with the exception of CaF_2:Mn, which only showed a post-irradiation fade of 60% in the first day. The peak area ratios of P_2 to P_4 of LiF:Mg,Ti, P_3 to P_5 of CaF_2:Tm, and P_2 to P_4 of LiF:Mg,Cu,P decayed completely after approximately 14 d whereas the peak area ratios of P_3 to P_4 of LiF:Mg,Ti, P_3 to P_4 of Ca F_2:Dy, P_4 to P_5 of CaF_2:Tm, and P_3 to P_4 of LiF:Mg,Cu,P displayed slower fading rates due to the higher temperature peaks. These peak area ratios generally stabilized after approximately 30 d. Differences between these and

previously published results may be due to differing experimental conditions, including different TLD sets and their irradiation histories, irradiation sources, readers, TTPs, storage conditions, and environmental factors, with a much more comprehensive list available in the literature (Furetta and Weng, 1998).

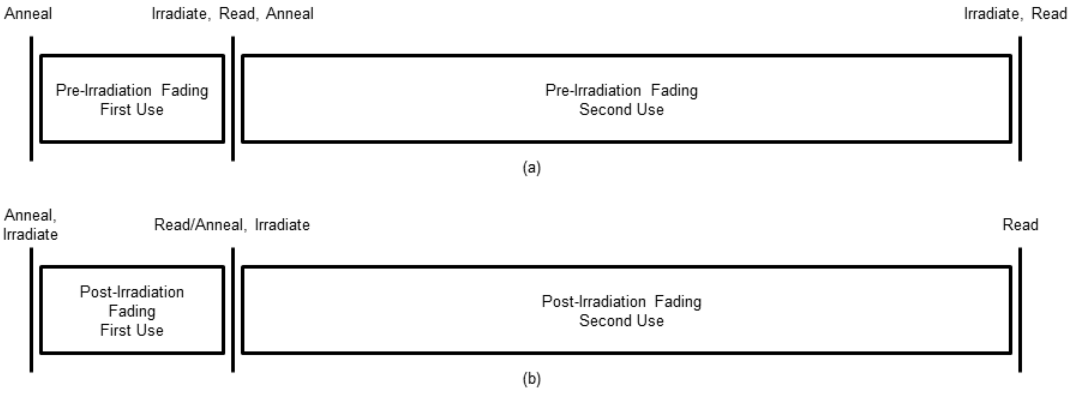

Fig 3.1. Typical use cycle for a (a) pre-irradiation fading and (b) post-irradiation fading TLD.

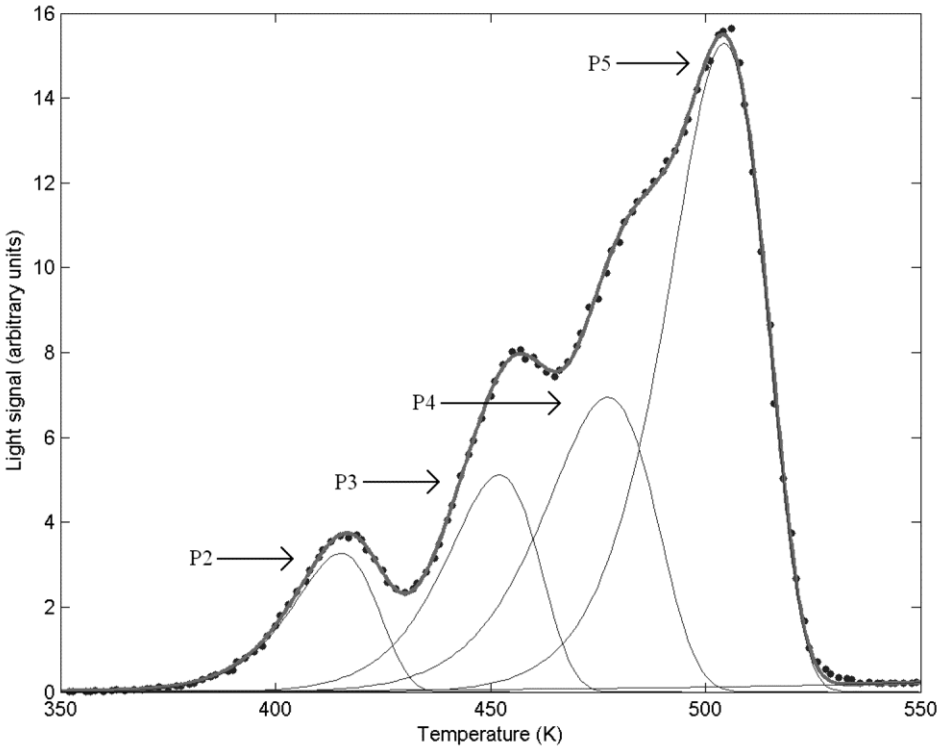

Fig 3.2. A typical glow curve of LiF:Mg,Ti and its separation into four glow peaks.

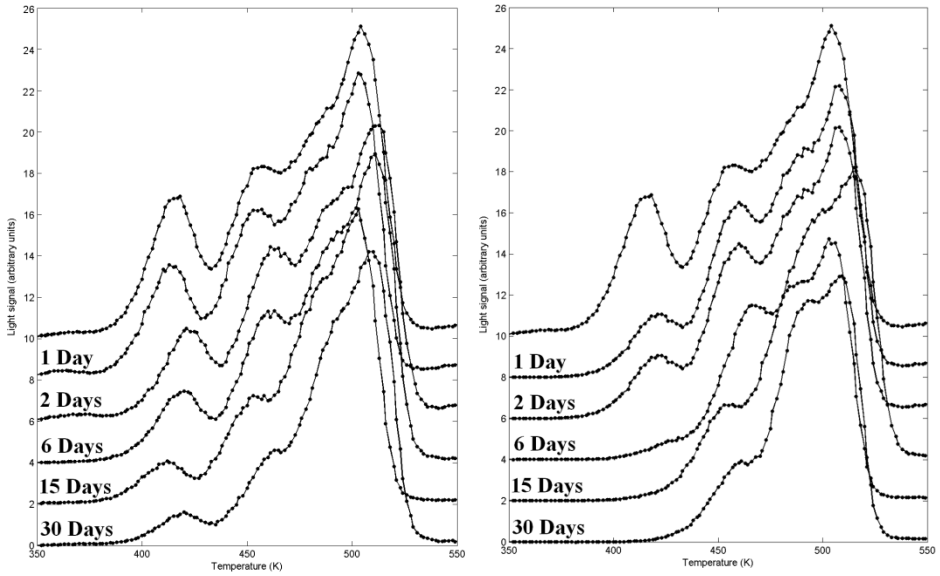

Fig 3.3. (a) Pre-irradiation and (b) post-irradiation fading of the glow curve of LiF:Mg,Ti. Each curve is displaced by 2 arbitrary units for clarity.

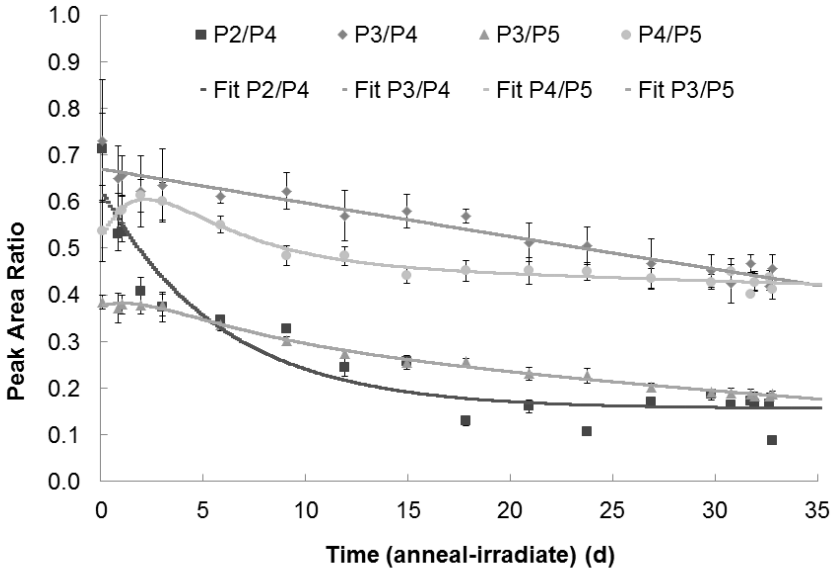

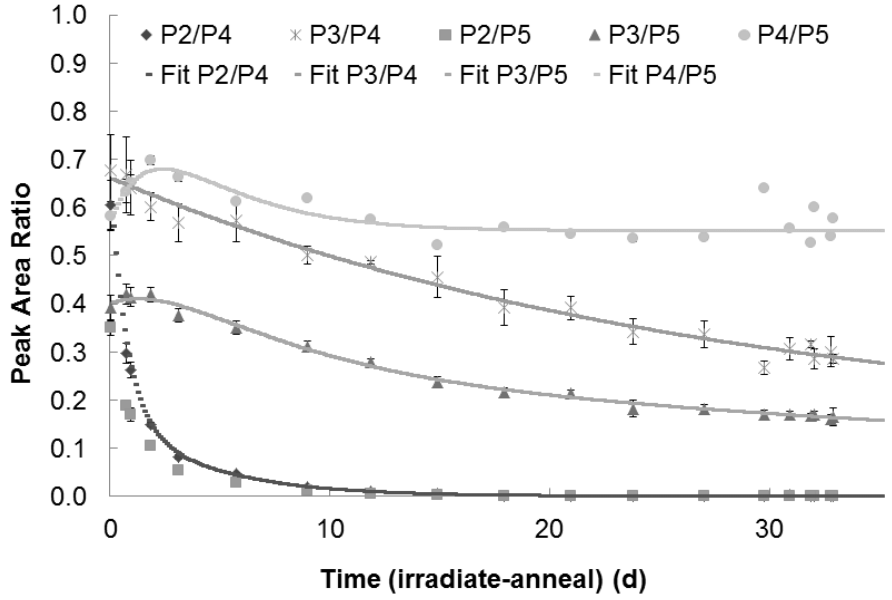

Fig 3.4. (a) Pre-irradiation and (b) post-irradiation fading of the peak area ratios of LiF:Mg,Ti. Error bars represent one standard deviation.

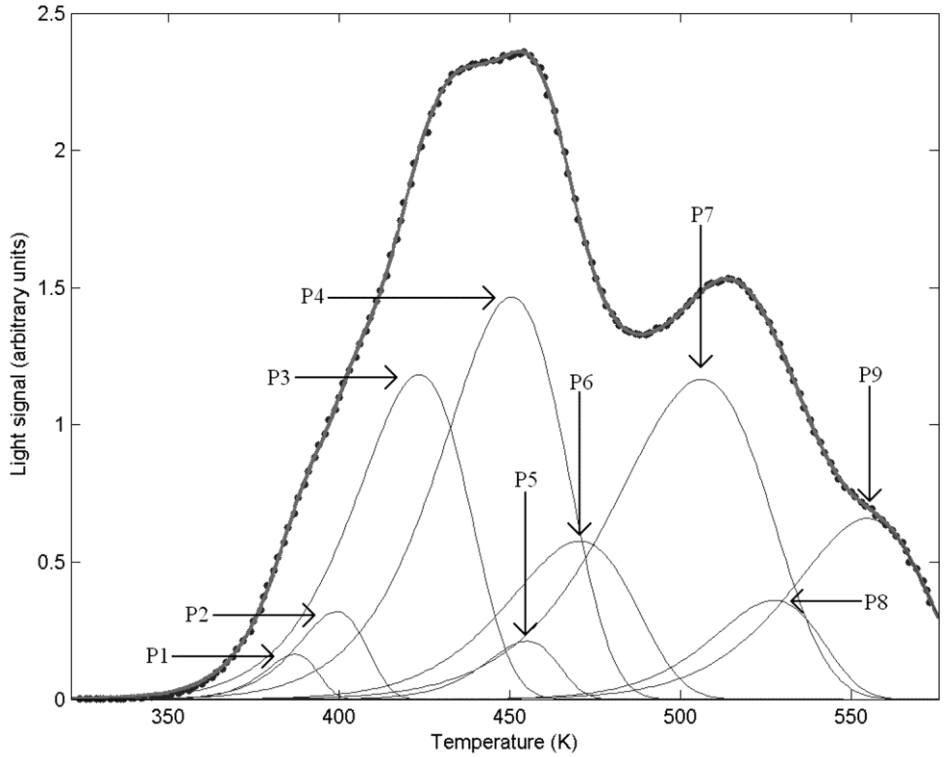

Fig 3.5. A typical glow curve of CaF_2:Dy and its separation into nine glow peaks.

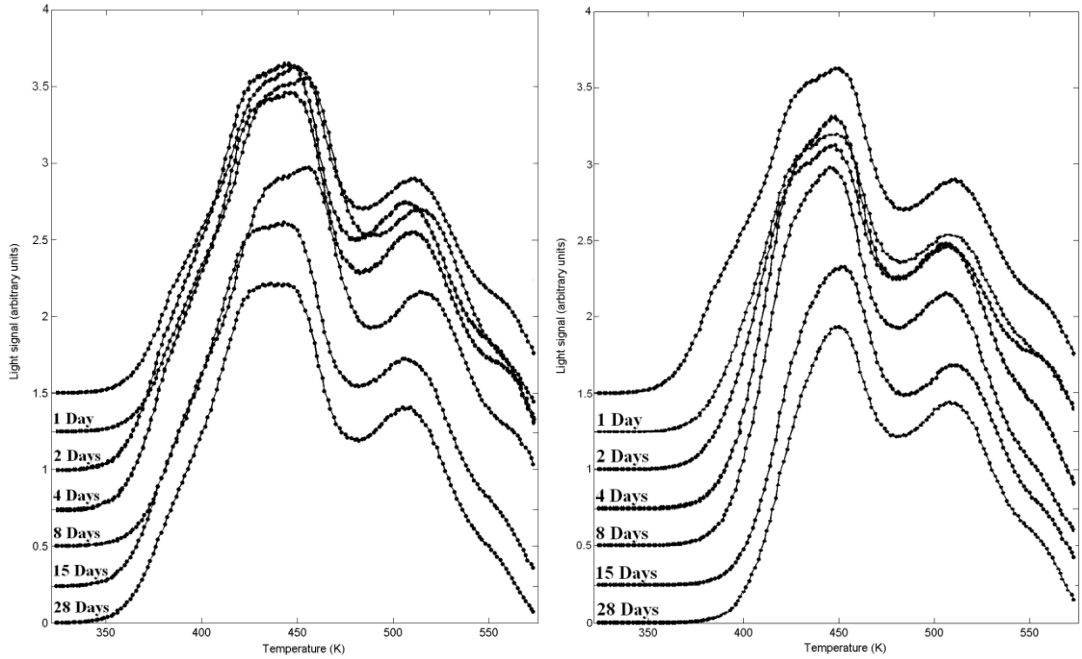

Fig 3.6. (a) Pre-irradiation fading and (b) post-irradiation fading of the glow curve of CaF_2:Dy. Each curve is displaced by 0.25 arbitrary units for clarity.

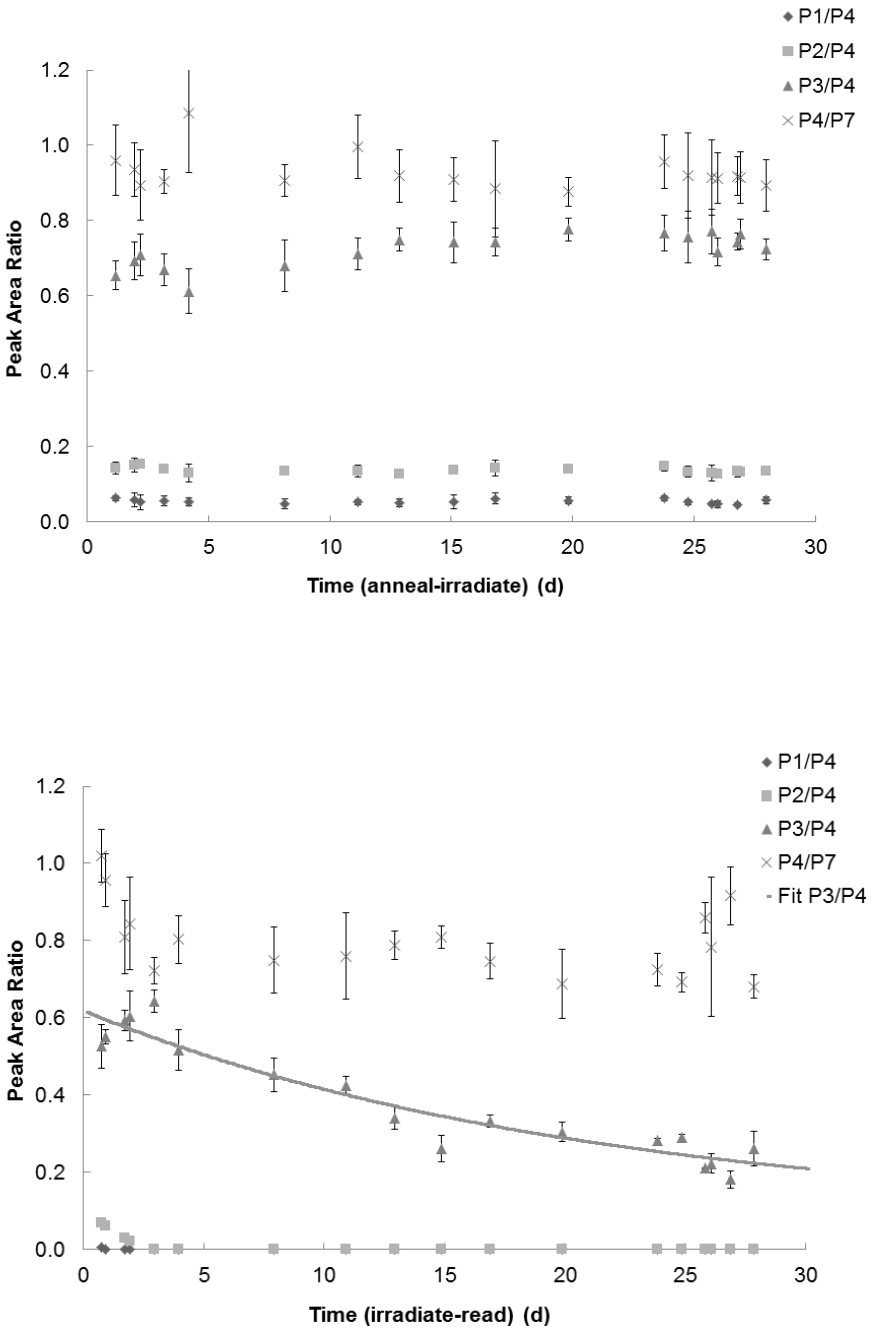

Fig 3.7. (a) Pre-irradiation and (b) post-irradiation fading of the peak area ratios of CaF_2:Dy. Error bars represent one standard deviation.

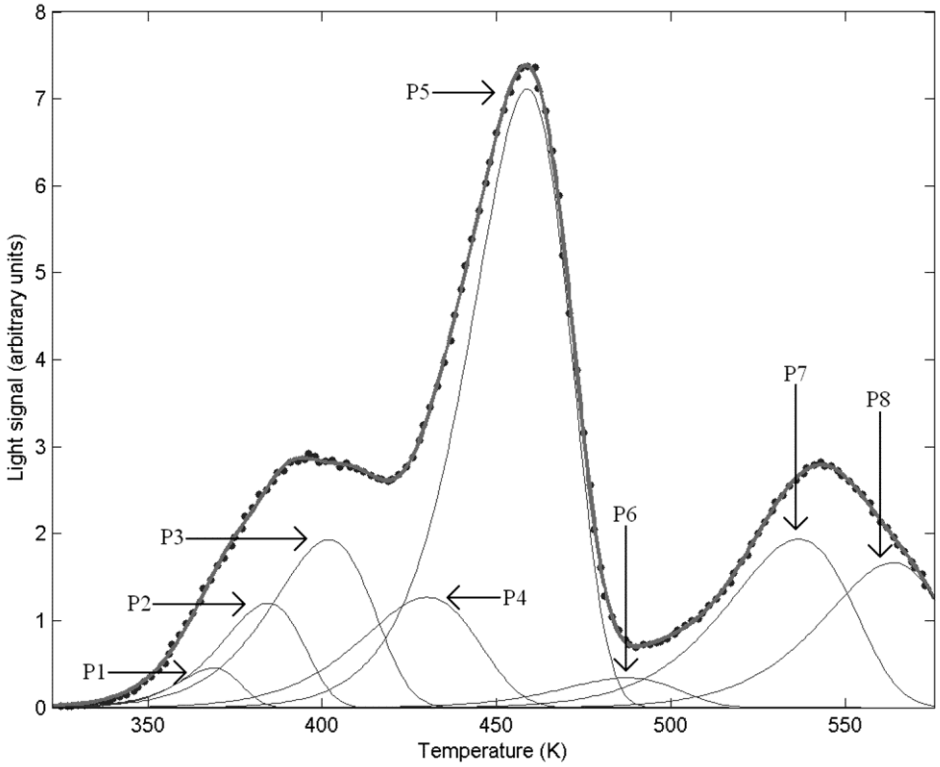

Fig 3.8. A typical glow curve of CaF_2:Tm and its separation into eight glow peaks.

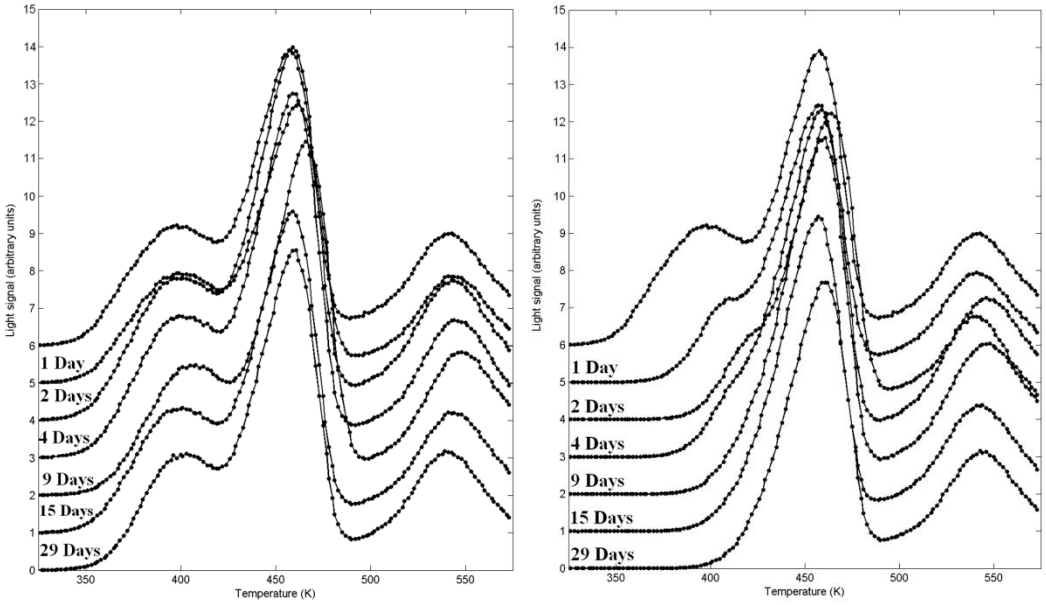

Fig 3.9. (a) Pre-irradiation fading and (b) post-irradiation fading of CaF_2:Tm. Each curve is displaced by 1 arbitrary unit for clarity.

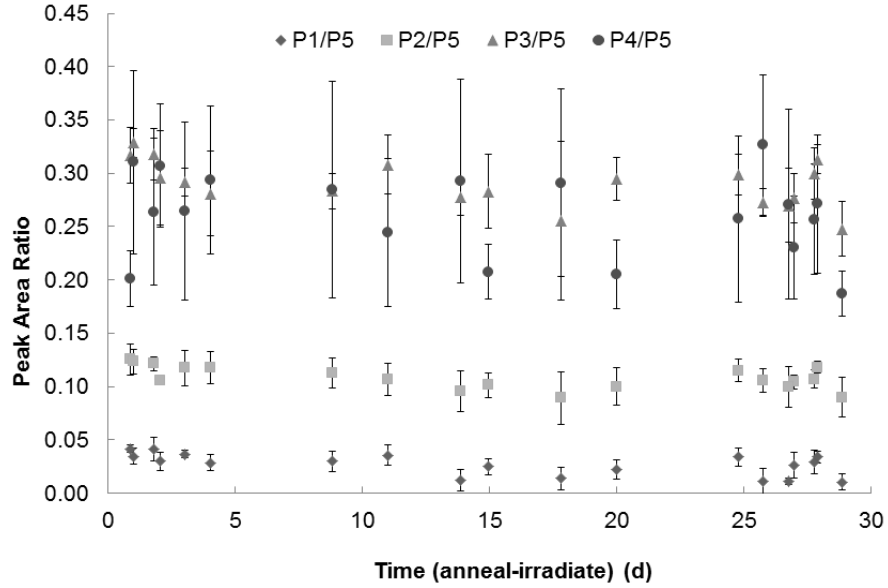

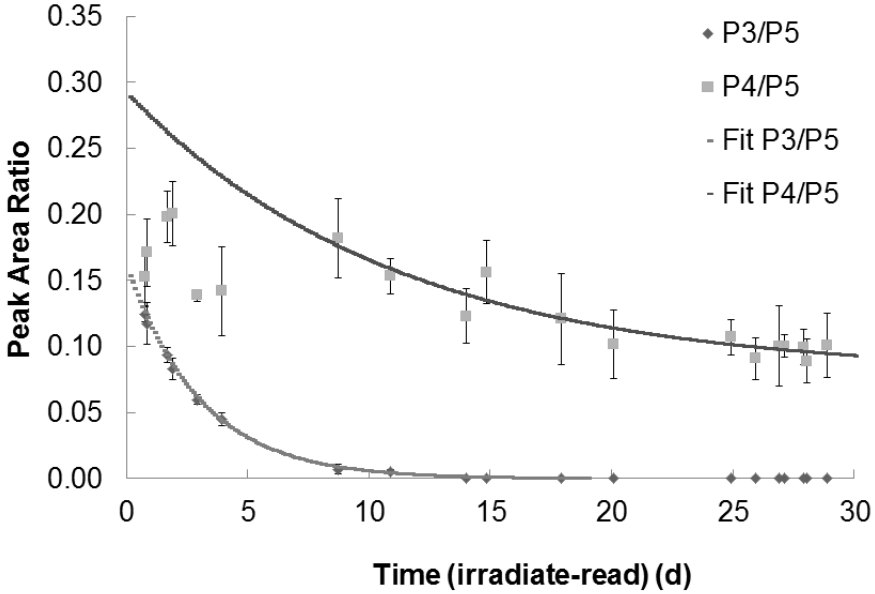

Fig 3.10. (a) Pre-irradiation and (b) post-irradiation fading of the peak area ratios of CaF_2:Tm. Error bars represent one standard deviation.

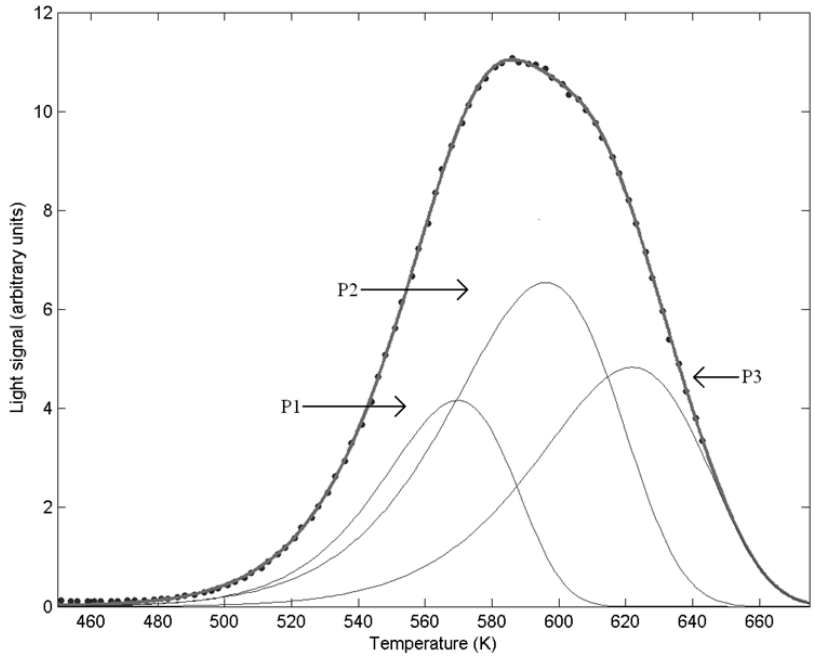

Fig 3.11. A typical glow curve of CaF_2:Mn and its separation into three glow peaks.

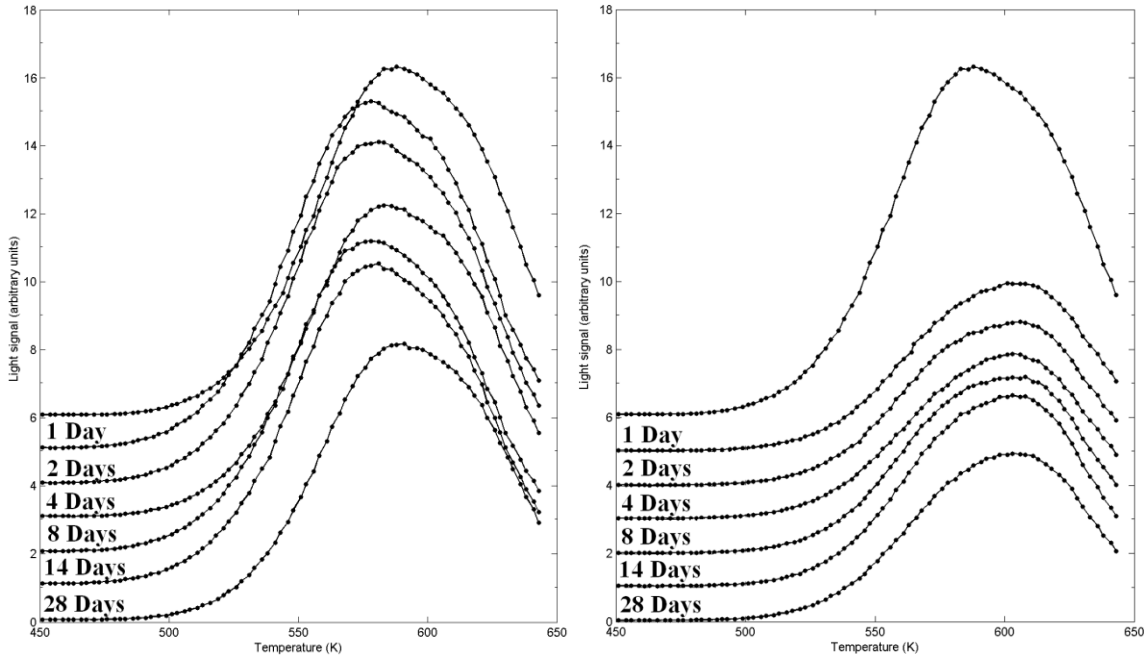

Fig 3.12. (a) Pre-irradiation fading and (b) post-irradiation fading of CaF_2:Mn. Each curve is displaced by 1 arbitrary unit for clarity.

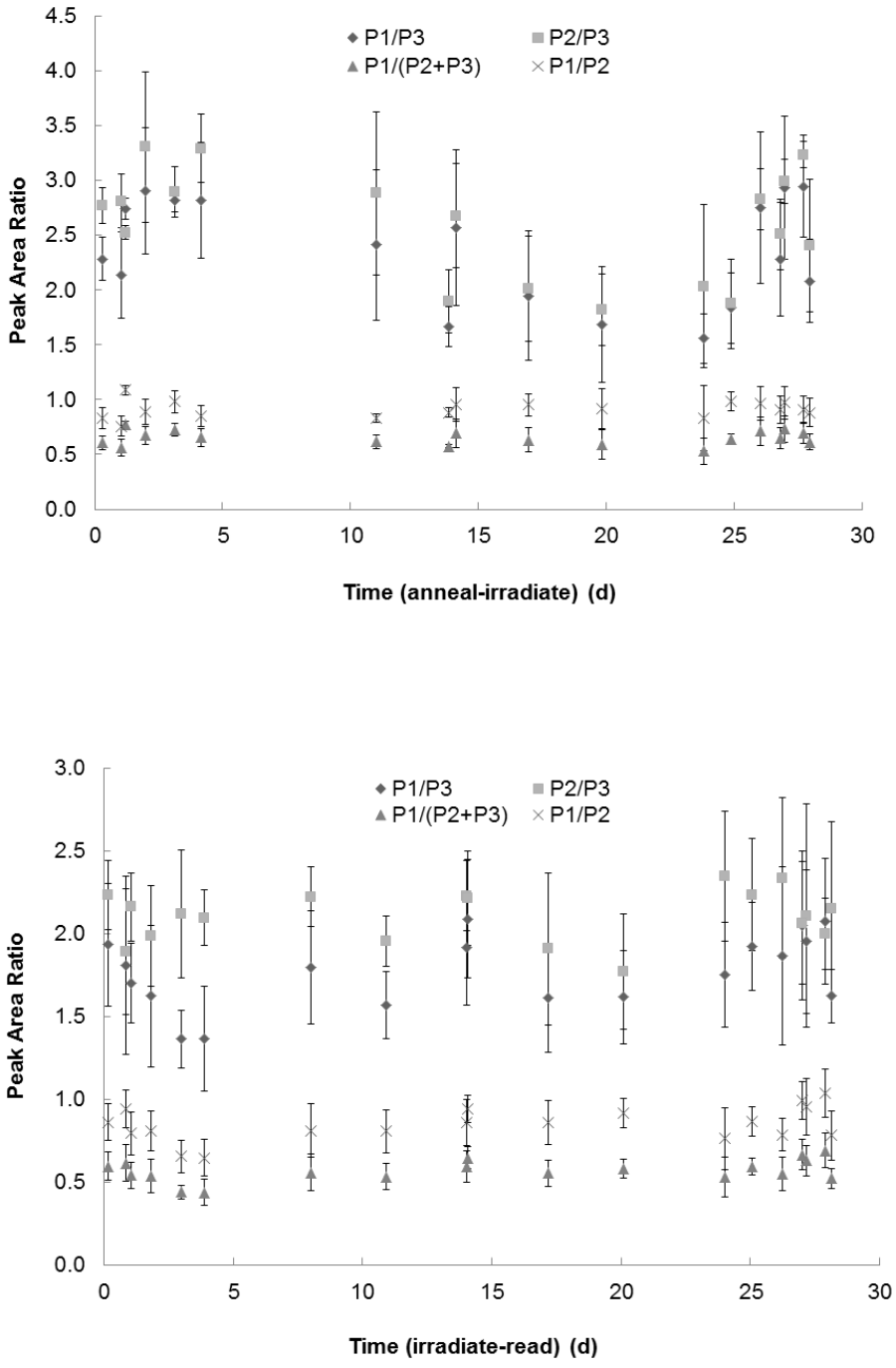

Fig 3.13. (a) Pre-irradiation and (b) post-irradiation fading of the peak area ratios of CaF_2:Mn. Error bars represent one standard deviation.

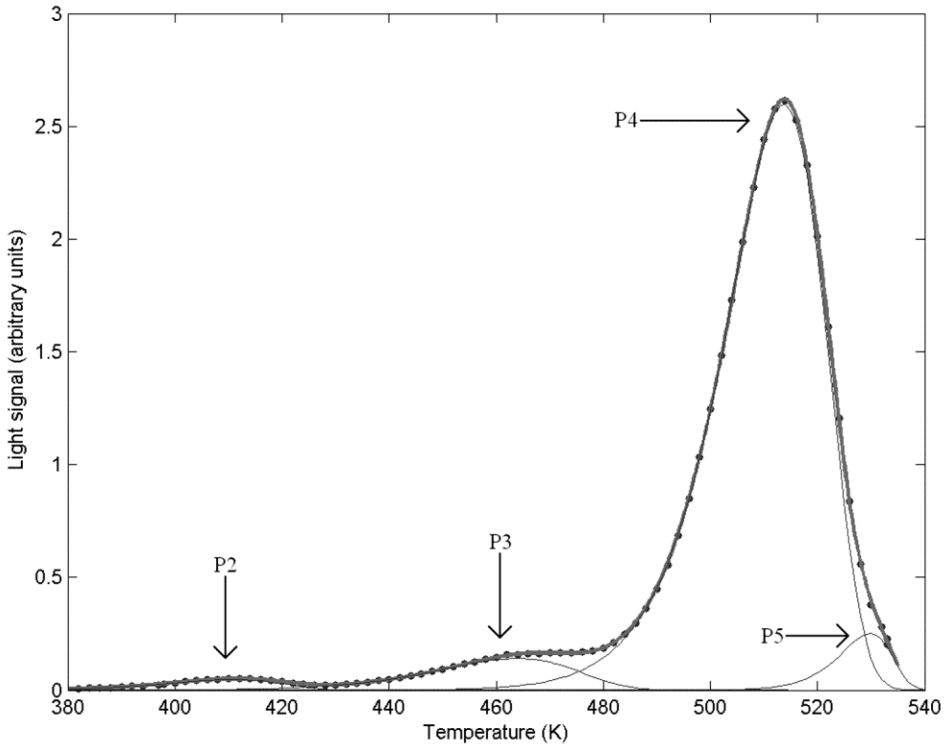

Fig 3.14. A typical glow curve of LiF:Mg,Cu,P and its separation into four glow peaks.

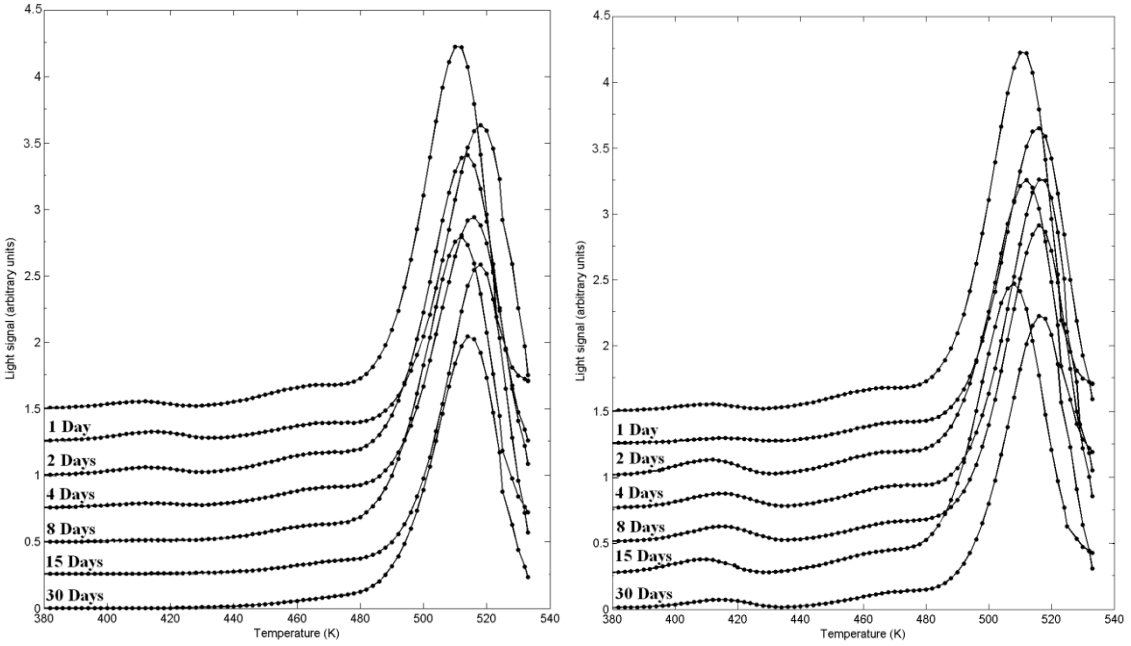

Fig 3.15. (a) Pre-irradiation fading and (b) post-irradiation fading of LiF:Mg,Cu,P. Each curve is displaced by 0.25 arbitrary units for clarity.

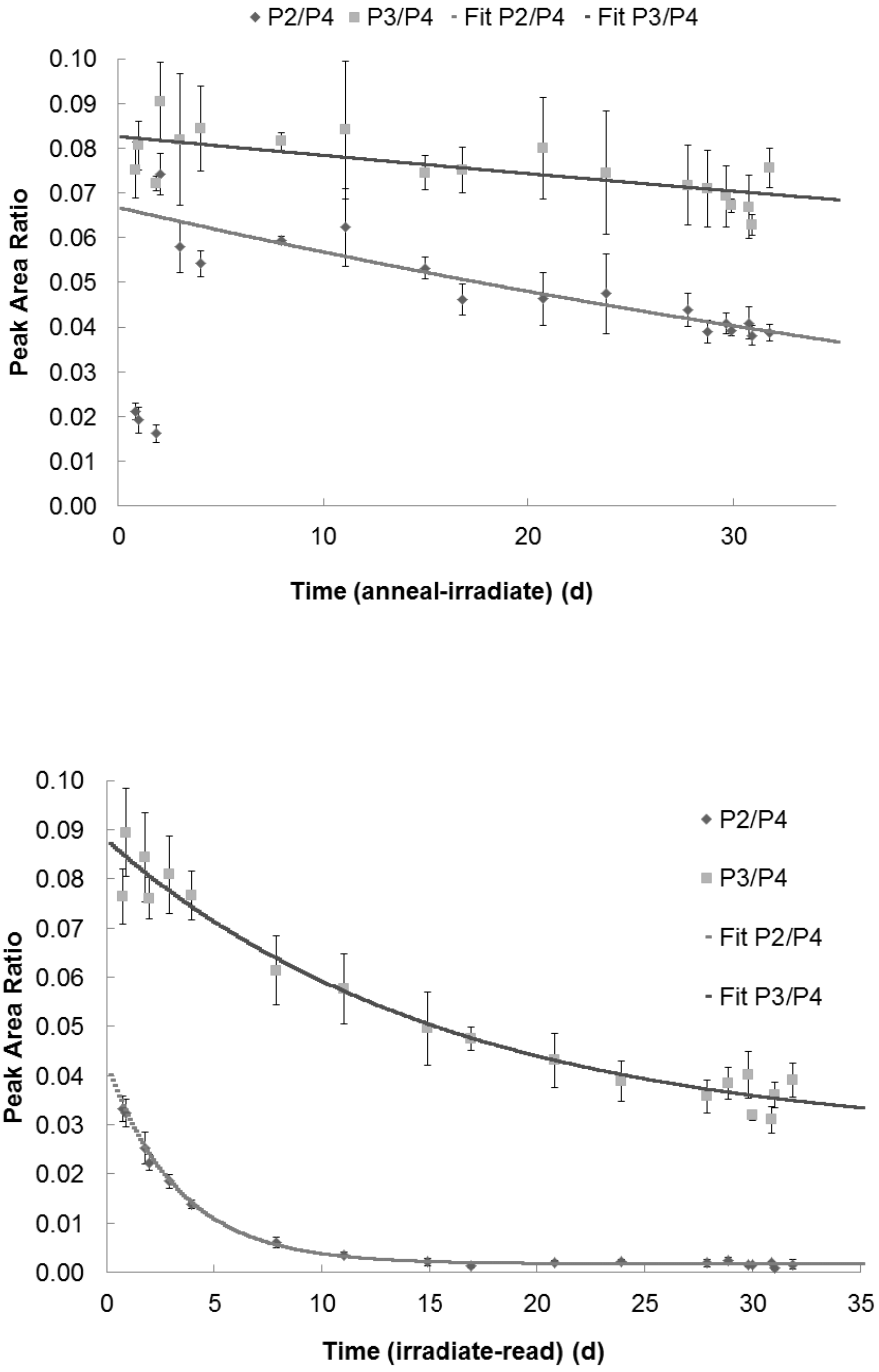

Fig 3.16. (a) Pre-irradiation and (b) post-irradiation fading of the peak area ratios of CaF_2:Mn. Error bars represent one standard deviation.

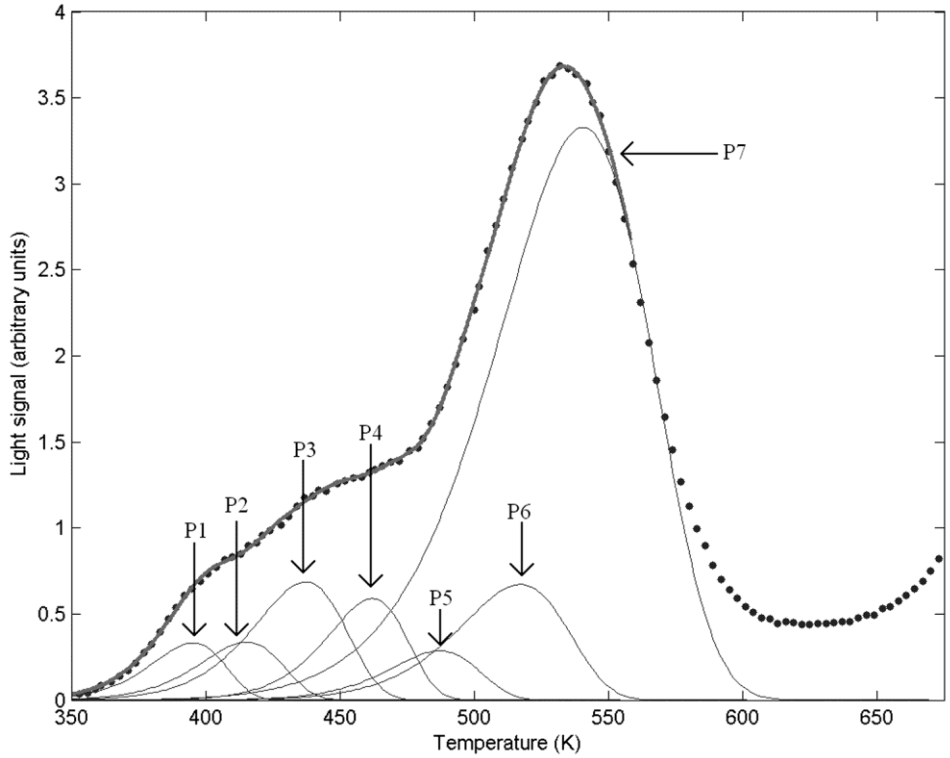

Fig 3.17. A typical glow curve of $CaSO_4$:Dy and its separation into seven glow peaks.

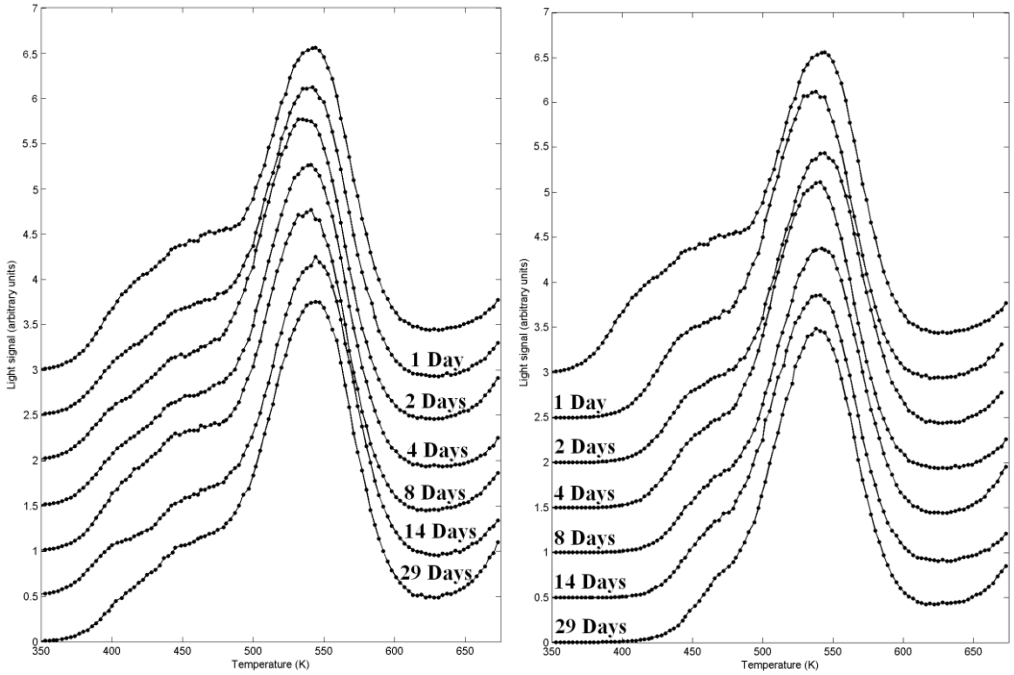

Fig 3.18. (a) Pre-irradiation fading and (b) post-irradiation fading of $CaSO_4$:Dy. Each curve is displaced by 0.5 arbitrary units for clarity.

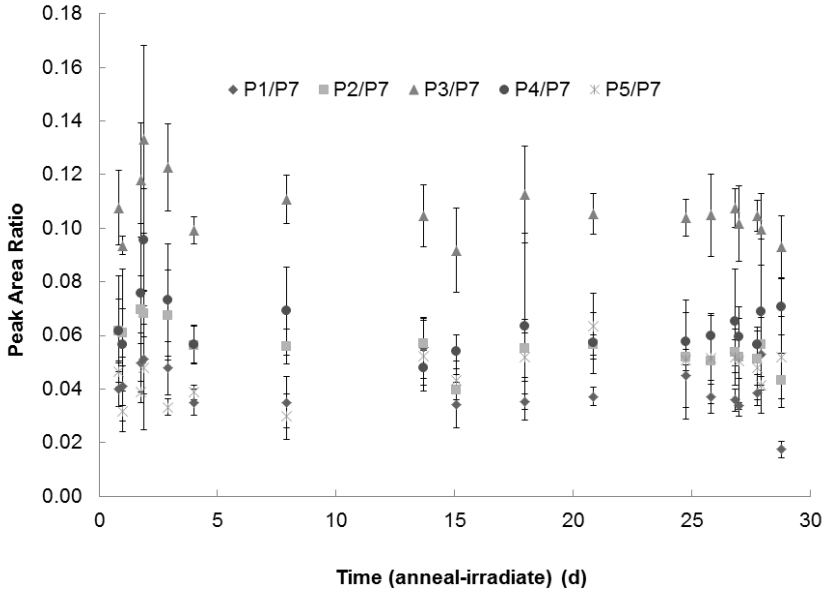

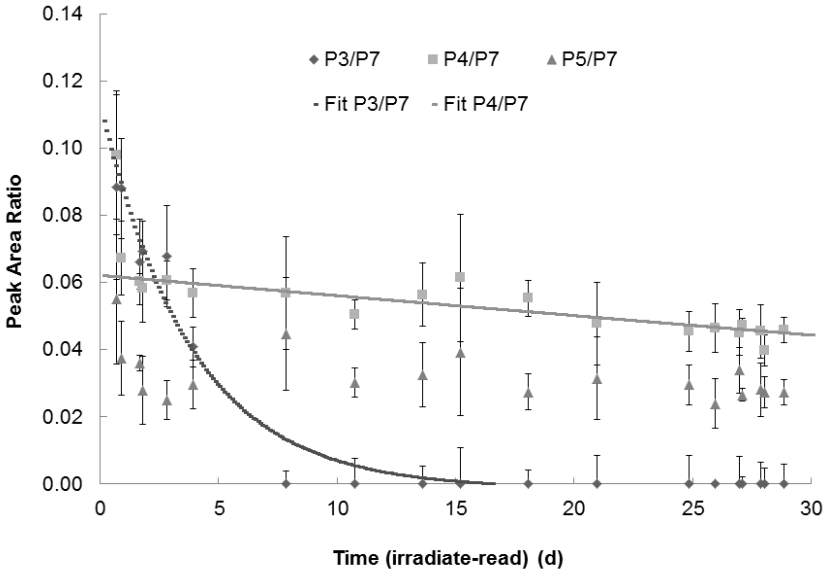

Fig 3.19. (a) Pre-irradiation and (b) post-irradiation fading of the peak area ratios of CaF_2:Mn. Error bars represent one standard deviation.

Table 3.1. Important TLD dimensions, characteristics, and manufacturer recommended time-temperature profiles.

Material	*Type*	*Size*	*Preheat Temp. (°C)*	*Preheat Time (s)*	*Acq. Rate ($°C \cdot s^{-1}$)*	*Acq. Time (s)*	*Anneal Temp. (°C)*	*Anneal Time (s)*
LiF:Mg,Ti (TLD-100)	Chip	0.3175 cm × 0.3175 cm × 0.0889 cm	50	0	10	33.3	300	0
CaF_2:Dy (TLD-200)	Chip	0.3175 cm × 0.3175 cm × 0.0889 cm	50	0	15	20	300	15
CaF_2:Tm (TLD-300)	Chip	0.3175 cm × 0.3175 cm × 0.0889 cm	50	0	15	23.3	300	10
CaF_2:Mn (TLD-400)	Chip	0.3175 cm × 0.3175 cm × 0.0889 cm	50	0	25	20	400	5
LiF:Mg,Cu,P (TLD-700H)[a]	Disk	Diameter 0.36 cm, thickness 0.038 cm	50	0	10	30	240	10
$CaSO_4$:Dy (TLD-900)	Chip	0.3175 cm × 0.3175 cm × 0.0889 cm	50	0	20	20	N/A	0

[a] It was discovered during the experiment that the incorrect TTP was used for the TLD-700H chips. The TTP used was intended for 0.3175 cm × 0.3175 cm × 0.0889 cm chips. See the TLD-700H Results and Discussion section for more information.

Table 3.2. Experimental averages and limits for glow peak parameters *E* and T_{max}.

Material	*Peak*	T_{max} *lower limit (K)*	T_{max} *upper limit (K)*	T_{max} *experiment average (K)*	*E lower limit (eV)*	*E upper limit (eV)*	*E experiment average (eV)*
LiF:Mg,Ti (TLD-100)	2	405	437	416	1.4	1.7	1.56
	3	443	473	456	1.4	1.9	1.67
	4	472	497	484	1.4	1.9	1.69
	5	495	526	510	1.7	2.4	2.04
CaF_2:Dy (TLD-200)	1	375	390	380	1.4	1.8	1.70
	2	387	402	394	1.1	1.4	1.35
	3	413	427	422	0.7	1.5	1.13
	4	440	454	445	0.8	1.3	1.01
	5	445	465	454	1.3	1.7	1.53
	6	460	474	466	0.8	1.2	1.00
	7	500	512	503	0.8	1.1	0.93
	8	520	534	525	1.1	1.6	1.38
	9	546	562	552	1.2	1.7	1.41
CaF_2:Tm (TLD-300)	1	360	377	367	1.0	1.5	1.45
	2	380	393	385	0.9	1.2	1.17
	3	395	414	406	0.7	1.7	1.30
	4	420	440	434	0.7	1.5	1.09
	5	450	470	461	1.0	1.5	1.31
	6	485	495	489	1.2	1.5	1.26
	7	525	550	538	1.0	1.7	1.43
	8	555	575	562	1.0	1.7	1.31
CaF_2:Mn (TLD-400)	1	565	578	570	1.2	1.6	1.42
	2	590	606	597	1.1	1.6	1.32
	3	617	631	623	1.2	1.6	1.36
LiF:Mg,Cu,P (TLD-700H)	2	405	425	417	1.2	1.5	1.30
	3	460	475	468	1.3	1.7	1.48
	4	510	527	516	2.1	2.7	2.45
	5	523	535	530	5.0	5.5	5.30
$CaSO_4$:Dy (TLD-900)	1	390	410	396	0.9	1.1	1.02
	2	415	430	423	0.8	1.0	0.96
	3	400	447	435	0.8	1.1	1.05
	4	450	473	462	1.2	1.6	1.40
	5	470	487	479	1.2	1.6	1.42
	6	517	530	519	0.9	1.1	0.96
	7	535	575	546	0.8	1.1	0.88

Table 3.3. Fit parameters for the pre-irradiation and post-irradiation fading of the peak area ratios P_2 to P_4 and P_3 to P_4 to Equation 3.3 for LiF:Mg,Ti.

	Ratio	**A**	**B**	**C**	**D**	**E**	**R^2**
Pre-Irradiation	P_2/P_4	0.4659	0.1721	0.1556	N/A	N/A	0.9179
	P_3/P_4	3.583	0.002063	-2.914	N/A	N/A	0.939
Post-Irradiation	P_2/P_4	0.4496	1.381	0.1734	0.2425	0.9997	0.9906
	P_3/P_4	0.5327	0.03631	0.1271	N/A	N/A	0.983

Table 3.4. Fit parameters for the pre-irradiation and post-irradiation fading of the peak area ratios P_3 to P_5 and P_4 to P_5 to Equation 3.4 for LiF:Mg,Ti.

	Ratio	**A**	**B**	**C**	**D**	**E**	**R^2**
Pre-Irradiation	P_3/P_5	0.3402	0.01878	0.3752	0.3767	0.2906	0.995
	P_4/P_5	0.4715	0.003138	0.5197	0.5227	0.2737	0.9717
Post-Irradiation	P_3/P_5	0.2737	0.01594	0.3434	0.4007	0.1801	0.9936
	P_4/P_5	0.5513	0	0.5289	0.5765	0.2963	0.8277

Table 3.5. Fit parameters for the post-irradiation fading of the peak area ratio of P_3 to P_4 to Equation 3.2 for CaF_2:Dy.

	Ratio	**A**	**B**	**C**	**R^2**
Post-Irradiation	P_3/P_4	0.5353	0.04755	0.08064	0.912

Table 3.6. Fit parameters for the post-irradiation fading of the peak area ratios P_3 to P_5 and P_4 to P_5 to Equation 3.2 for CaF_2:Tm.

	Ratio	**A**	**B**	**C**	**R^2**
Post-Irradiation	P_3/P_5	0.1588	0.3307	-0.00029	0.9994
	P_4/P_5	0.2121	0.09037	0.07887	0.9696

Table 3.7. Fit parameters for the pre-irradiation and post-irradiation fading of the peak area ratios of P_2 to P_4 and P_3 to P_4 to Equation 3.2 for LiF:Mg,Cu,P.

	Ratio	**A**	**B**	**C**	**R^2**
Pre-Irradiation	P_2/P_4	0.08239	0.0129	-0.01577	0.8289
	P_3/P_4	0.1102	0.003917	-0.02765	0.518
Post-Irradiation	P_2/P_4	0.03968	0.2997	0.001746	0.9982
	P_3/P_4	0.0606	0.06356	0.02688	0.9683

Table 3.8. Fit parameters for the post-irradiation fading of the peak area ratios of P_3 to P_7 and P_4 to P_7 to Equation 3.2 for $CaSO_4$:Dy.

	Ratio	**A**	**B**	**C**	**R^2**
Post-Irradiation	P_3/P_7	0.1124	0.2626	-0.001499	0.9767
	P_4/P_7	0.2943	0.002075	-0.2323	0.7813

REFERENCES

Al-Ghorabie F.H.H., 2005. Measurements of indoor gamma radiation dose in At-Taif City, Saudi Arabia using $CaSO_4$:Dy (TLD-900). Radiat. Prot. Dosim. 113:178-84.

Allen P., McKeever S.W.S., 1990. Studies of PTTL and OSL in TLD-400. Radiat. Prot. Dosim. 33:19-22.

Alves J.G., Muñiz J.L., Gómez-Ros J.M., Delgado A., 1999. A comparative study on the thermal stability of LiF:Mg,Ti, and LiF:Mg,Cu,P detectors for environmental monitoring. Radiat. Prot. Dosim. 85:253-257.

Bacci C., Furetta C., Rispoli B., Roubaud G., Tuyu J.W.N., 1988. The effect of storage temperature on the thermoluminescence response of some phosphors. Radiat. Prot. Dosim. 25:43-48.

Biderman S., Horowitz Y.S., Oster L., Einav Y., Dubi Y., 2002. Glow curve analysis of composite peak 5 in LiF:Mg,Ti (TLD-100) using optical bleaching, thermal annealing and computerised glow curve deconvolution. Radiat. Prot. Dosim. 101:69-72.

Biderman S., Oster L., Horowitz Y.S., 2006. Modeling the dose response of peaks 4, 5 and 5b, in TLD-100, as a function of recombination temperature. Radiat. Prot. Dosim. 119:285-288.

Binder W., Cameron J.R., 1969. Dosimetric properties of CaF_2:Dy. Health Phys. 17:613-618.

Bos A.J.J., Dielhof J.B., 1991. The analysis of thermoluminescent glow peaks in CaF_2:Tm (TLD-300). Radiat. Prot. Dosim. 37:231-239.

Brandan M., Angeles O., Mercado-Uribe H., 2006. Phenomenological study of the ionization density-dependence of TLD-100 peak 5a. Radiat. Prot. Dosim. 119:29-32.

Budzanowski M., Sáez-Vergara J.C., Ryba E., Bilski P., Olko P., Waligórski M.P.R., 1999. Estimation of the time elapsed between exposure and readout using peak ratios of LiF:Mg,Cu,P (MCP-N, GR200A). Radiat. Prot. Dosim. 85:149-152.

Cassata J.R., Moscovitch M., Rotunda J.E., Velbeck K.J., 2002. A new paradigm in personal dosimetry using LiF:Mg,Cu,P. Radiat. Prot. Dosim. 101:27-42.

Delgado A., Gómez-Ros J.M., Muñiz J.L., Bos A.J.J., Piters T.M., 1993. Confirmation of the evolution of TLD-100 glow peaks 4 and 5 during storage at ambient temperatures. Radiat. Prot. Dosim. 47:231-234.

DeWerd L.A., Cameron J.R., Papini T., Das I.J., 1984. Characteristics of a new dosimeter material LiF(Mg,Cu,P). Radiat. Prot. Dosim. 6:350-352.

Drazic G., Trontelj M., 1983. Properties of sintered $CaSO_4$:Dy TL dosimeters. Int. J. Appl. Radiat. Isot. 34:1633-1637.

Duggan L., Kron T., 1999. Glow curve analysis of long-term stability of LiF:Mg,Cu,P as compared to LiF:Mg,Ti. Radiat. Prot. Dosim. 85:213-216.

Fairchild R.G., Mattern P.L., Lengweiler P.W., 1978. Thermoluminescence of LiF TLD-100: Emission-spectra measurements. J. Appl. Phys. 49:4512-4522.

Furetta C., Lee Y.K., 1983. Annealing and fading properties of CaF_2:Tm (TLD-300). Radiat. Prot. Dosim. 5:57-63.

Furetta C, Weng P., 1998. Operational Thermoluminescence Dosimetry. Singapore: World Scientific Publishing Co.

Guelev M.G., Mishev I.T., Burgkhardt B., Piesch E., 1994. A two-element $CaSO_4$:Dy dosimeter for environmental monitoring. Radiat. Prot. Dosim. 51:35-40.

Hasan F., Charalambous S., 1983. The thermoluminescence behavior of CaF_2:Dy (TLD-200) for low up to high doses. J. Phys. C: Solid State Phys. 16:5921-5928.

Horowitz A., Horowitz Y.S., 1990. Optimization of LiF:Cu,Mg,P for Radiat. Prot. Dosim.. Radiat. Prot. Dosim. 33:267-270.

Horowitz A., Horowitz Y., 1993. Elimination of the high temperature glow peak in LiF:Cu,Mg,P. Radiat. Prot. Dosim. 47:69-72.

Horowitz Y., 1990. New thermoluminescent materials. Radiat. Prot. Dosim. 30(2):75-76.

Horowitz Y., 1990. Editorial: Fading in LiF:Mg,TI. Radiat. Prot. Dosim. 32:147.

Horowitz Y.S., 1993. LiF:Mg,Ti versus LiF:Mg,Cu,P: The competition heats up. Radiat. Prot. Dosim. 47:135-141.

Horowitz Y.S., Satinger D., Brandan M.E., Avila O., Rodriguez-Villafuerte, M., 2002. Supralinearity of peaks 5a, 5 and 5b in TLD-100 following 6.8 MeV and 2.6 MeV He ion irradiation: The extended track interaction model. Radiat. Prot. Dosim. 100:95-98.

Horowitz Y.S., Oster L., Satinger D., Biderman, S., 2002. The composite structure of peak 5 in the glow curve of LiF:Mg,Ti (TLD-100): Confirmation of peak 5a arising from a locally trapped electron-hole configuration. Radiat. Prot. Dosim. 100:123-126.

Horowitz Y.S., Satinger D., Avila O., 2006. Track structure approach to the calculation of peak 5a to peak 5 (TLD-100) relative intensities following heavy charged particle irradiation. Radiat. Prot. Dosim. 119:45-48.

Hosseini-Pooya M., Jafarizadeh M., 2004. Effect of reader and oven annealing on the glow curve structure and fading of a LiF:Mg,Cu,P TL dosimeter. J. Radiol. Prot. 24:173-178.

Hsu P.C., Weng P.S., 1995. Influence of ultraviolet radiation on CaF_2:Tm thermoluminescence dosimeters. Radiat. Prot. Dosim. 48:297-300.

Izak-Biran T., Malchi S., Shamai Y., Alfassi Z.B., 1996. Low pre- and post-irradiation fading of LiF:Mg,Ti (TLD-100, TLD-600, TLD-700) using a preheat technique. Radiat. Prot. Dosim. 64:269-274.

Jafarizadeh M., Sohrabi M., Nazeri F., 1999. Analysis of glow curve kinetics of CaF_2:Tm (TLD-300) based on a general order model. Radiat. Prot. Dosim. 84:119-122.

Jones L.A., Stokes R.P., 2007. Pre-irradiation and post-irradiation fading of the Harshaw 8841 TLD in different environmental conditions. Radiat. Prot. Dosim. 125:241-246.

Li S.H., Hsu P.C., 1990. The role of annealing: Effect on $CaSO_4$:Dy phosphor with manganese and sodium impurities. Radiat. Prot. Dosim., 33:147-150.

McKeever S.W.S., Moscovitch M., Townsend P.D., 1995. Thermoluminescence Dosimetry Materials: Properties and Uses. Nuclear Technology Publishing, Ashford.

McMasters D.W., Jassemnejad B., McKeever S.W.S., 1987. Some observations regarding the effects of background rare-earth impurities on the thermoluminescence and optical absorption of CaF_2:Mn. J. Phys. D: Appl. Phys. 20:1182-1190.

Moscovitch M., 1986. Automatic method for evaluating elapsed time between irradiation and readout in LiF-TLD. Radiat. Prot. Dosim. 17:165-169.

Moscovitch M., Szalanczy A., Bruml W.W., Velbeck K.J., Tawil R.A., 1990. A TLD system based on gas heating with linear time-temperature profile. Radiat. Prot. Dosim. 34:361-364.

Moscovitch M., 1999. Personnel dosimetry using LiF:Mg,Cu,P. Radiat. Prot. Dosim. 85:49-56.

Nambi K.S.V., Bapat V.N., Ganguly A.K., 1974. Thermoluminescence of $CaSO_4$ doped with rare earths. J. Phys. C: Solid State Phys. 7:4403-4415.

Pradhan A.S., 1993. Emission spectra and influence of sunlight on thermoluminescence of dysprosium doped $CaSO_4$ and CaF_2. Radiat. Prot. Dosim. 47:151-154.

Sáez-Vergara J.C., Budzanowski M., Gómez-Ros J.M., Romero A.M., 1999. Thermally induced fading of individual glow peaks in LiF:Mg,Cu,P at different storage temperatures. Radiat. Prot. Dosim., 85:269-272.

Shachar B.B., Horowitz Y.S., 1988. Dosimetric characterisation of the high temperature peaks of LiF:Mg,Ti and CaF_2:Tm using computerised glow curve deconvolution. Radiat. Prot. Dosim. 22:87-96.

Shachar B.B., Horowitz Y.S., 1991. Anomalous thermally induced fading of annealed and unannealed LiF:Mg,Ti (TLD-100, Harshaw) using computerized glow curve deconvolution. J. Phys. D: Appl. Phys. 24:1649-1657.

Shachar B.B., Horowitz Y.S., 1993. Long-term fading of peak 5 in TLD-100 using computerised glow curve deconvolution (CGCD) and thermal peak isolation techniques. Radiat. Prot. Dosim. 47:181-185.

Skopec M., Loew M., Price J.L., Guardala, N., Moscovitch, M., 2006. Discrimination of photon from proton irradiation using glow curve feature extraction and vector analysis. Radiat. Prot. Dosim. 120:268-272.

Souza J.H., Rosa L.A.R.D., Mauricio C.L.P., 1993. On the thermoluminescence glow curve of $CaSO_4$:Dy. Radiat. Prot. Dosim. 47:103-106.

Studenski M.T., Haverland N.P., Kearfott K.J., 1997. Simulation, design, and construction of a ^{137}Cs irradiation facility, Health Phys. 92:S78-S86.

Velbeck K.J., Luo L.Z., Ramlo M.J., Rotunda J.E., 2006. The dose-response of Harshaw TLD-700H. Radiat. Prot. Dosim. 119:255-258.

Wang T.K., Hsu P.C., Weng P.S., 1986. Application of TLD-200 dosimeters to the discrimination of α, β, and γ radiation. Radiat. Prot. Dosim. 16:225-230.

Wang T.K., Hsu P.C., Weng P.S., 1987. Feasibility study of using $CaSO_4$:Dy phosphor for simultaneous estimation of exposure and time elapsed post-exposure. Radiat. Prot. Dosim. 18:157-161.

Weinstein M., German U., Dubinsky S., 2003. On the determination of the post-irradiation time from the glow curve of TLD-100. Radiat. Prot. Dosim. 106:121-130.

Yazici A.N., Chen R., Solak S., Yagingil Z., 2002. The analysis of thermoluminescent glow peaks of CaF_2:Dy (TLD-200) after β-irradiation. J. Phys. D: Appl. Phys. 35:2526-2535.

Chapter IV

Reproducibility of Glow Peak Fading Characteristics of Thermoluminescent Dosimeters

ABSTRACT

This study examines the reproducibility of LiF:Mg,Ti pre-irradiation and post-irradiation fading rates. To test post-irradiation fading, 99 calibrated 3.2 × 3.2 × 0.9 mm^3 LiF:Mg,Ti thermoluminescent dosimeters (TLDs) of dimensions were first annealed. The set was then irradiated to an average of 4.4 mGy using a 3.2×10^{11} Bq ^{137}Cs source. The irradiated TLDs were allowed to fade at room temperature for 0.5, 1, 2, 3, 4, 8, or 17 d. The TLDs were then read out over a 3.5 h time period using a standard commercial hot planchet TLD reader with nitrogen gas to prevent chemiluminescence. The experiment was then repeated for the other fading times. To test pre-irradiation fading, the TLDs were annealed, then placed in storage for 0.5, 1.6, 3, 4, 8, 18, 27, or 43 d. After that time, the TLDs were irradiated and read out. A computerized glow curve analysis program was used to fit the glow curve data to a four-peak first-order Gaussian kinetics model. The areas of peaks 2, 3, 4, and 5 were retrieved in order to be studied alone, as well as normalized to other peaks. The peak areas and peak area ratios were then fit to two or three term exponential decay equations that allowed the determination of the fading rate by calculating their parameters. These parameters were then compared for different TLDs in order to determine if their values followed a Gaussian distribution. Then, a group mean and standard deviation could be used for each value for all TLDs for later use instead of calculating an individual mean for each TLD.

INTRODUCTION

The study of fading in thermoluminescent dosimeter (TLD) signals has advanced from determining a correction in order to accurately determine dose based on length of deployment time (Fowler et al. 1965) to use in determination of time passed since irradiation (Weinstein et al. 2003). In addition to the effect of TL signal degradation over time after irradiation, called post-irradiation fading, TLD sensitivity after annealing but prior to irradiation, called pre-irradiation fading, can be taken into account. Both of these effects have been characterized in previous studies for LiF:Mg,Ti (Harvey et al. 2010).

Typically, fading properties of each TLD are determined separately for each element by experiment, similar to the determination of calibration factors (Plato and Miklos 1985; Simpkins and Kearfott 1997). TLD-to-TLD calibration factor variability may be quite large, resulting in large errors in the performance of mixed field dosimetry algorithms (Kearfott et al. 1990; Kearfott et al. 1995). Substantial variability in glow curve parameters may also arise as a result of variability in heating processes, as demonstrated for a detailed analysis of planchet heating (Samei et al. 1994). The goal of this study was to determine if fading properties of individual TLD elements need to be characterized individually, or if empirical fading functions can be used for a larger group. If this can be done, later experiments can then be performed which do not require every TLD in a set to be individually characterized; merely that an acceptable range be established for each fading parameter.

The most common characterization of the LiF:Mg,Ti glow curve when exposed to a low dose is the summation of four peaks using first-order kinetics, numbered peaks 2 through 5, appearing between 325 and 575 K (Horowitz et al. 2006). Although more peaks may be characterized at higher doses, high dose dosimetry is beyond the scope of this work, as are the measurements of actual fading rates, which have been characterized previously (Harvey et al. 2010).

MATERIALS AND METHODS

The TLDs used in this experiment were LiF:Mg,Ti chips (BICRON/Harshaw, 6801 Cochran Road, Solon, OH 44139, USA) of dimensions 3.175 × 3.175 × 0.889 mm^3. While being irradiated or in storage, the TLDs were kept in a 40 × 40 × 0.6 cm^3 polymethyl methacrylate (PMMA) plate with one hundred wells of depth 3 mm, which was designed to facilitate experiments of this type (Parker et al. 2011). A 40 × 40 × 0.25 cm^3 PMMA sheet was placed over this storage plate and the two were fastened together with four acrylic screws. During irradiation in a dedicated facility (Studenski et al. 2007), the plate was mounted to a 40 × 40 × 15 cm^3 custom manufactured PMMA phantom 60 cm above ground level and 150 cm from a 320 GBq ^{137}Cs source (Model 28-8A Irradiator, J.L. Shepherd and Associates, 1010 Arroyo Avenue, San Fernando, CA 91340-8122), in a custom designed facility (Studenski et al. 2007, Parker et al. 2011).

The TLDs were read out using a standard TLD reader (Model 4500 TLD Reader, BICRON/Harshaw, 6801 Cochran Road, Solon, OH 44139, USA) in hot planchet mode. During readout, the chamber was supplied with nitrogen gas (Prepurified compressed nitrogen cylinder 300, Metro Welding Supply Corporation, 12620 Southfield Road, Detroit, MI 48223) in order to limit the contributions of chemiluminescence, triboluminescence, infrared, and other undesired high temperature effects. When not in use, the TLD plate was stored on a wooden rack under controlled temperature and humidity conditions and covered with a black drape to limit optical fading.

The TLDs were first calibrated to 4.4 mGy three times, previously shown to give the best balance between precision and efficiency (Harvey et al. 2011). To study post-irradiation fading, the 99 TLDs were first annealed in the TLD reader using a standard manufacturer recommended readout cycle. The preheat temperature was 50°C, with a heating rate of 10°C s^{-1} for 25 s to a maximum temperature of 300°C, and the anneal was held at 300°C for 8.33 s. The chips were then given a dose of 4.4 mGy over an exposure time of approximately 20 min and stored until readout. The post-irradiation times studied were 0.5, 1, 2, 3,

4, 8, and 17 d. All 99 TLDs were read out, irradiated again, and the process repeated until all post-irradiation fading experiments were complete. All irradiations occurred within 24 h of annealing in order to minimize the effect of pre-irradiation fading.

To study pre-irradiation fading, the TLDs were first annealed in the TLD reader, then put back into storage. After 0.5, 1.6, 3, 4, 8, 18, 27, or 43 d, the TLDs were irradiated to 4.4 mGy and read out. All readouts occurred within 30 min of irradiation, in order to minimize the effect of post-irradiation fading.

A computerized glow curve analysis (GCA) program in a standard commercially available mathematics package format (MATLAB R2008b with Curve Fitting Toolbox, The MathWorks Inc., 3 Apple Hill Drive, Natick, MA 01760) was used to separate the glow curve data into four glow peaks using the first-order kinetics model, plus an exponential high temperature background signal term. Chauvenet's criterion was applied once to individual peak areas in order to reject significant outliers before any additional analysis was done (Chauvenet 1871).

The signal for each peak and peak ratio was fit using a least-squares method to the following empirically determined equations:

$$S_i = Ae^{-k_1 t} + Be^{-k_2 t} \tag{4.1}$$

for single peaks, and

$$S_i / S_j = Ae^{-k_1 t} - Ae^{-k_2 t} + Ce^{-k_3 t} \tag{4.2}$$

for peak ratios. Fading parameters k_i were determined by fitting each TLD's peak or peak ratio individually. Each fading component was sequentially numbered, with k_1 corresponding to the first component of fading, k_2 to the second and so on. However, due to the nature of the fitting method, a numbered fading parameter for one fit is not necessarily comparable to any other. The additional exponential decay terms were added later in the process in order to fit the initial rise in the fading functions for small *t.*

Then, data from all TLDs were used to determine fading functions for each peak and peak ratio. In order to determine the correlation between each individual TLD and the group fading function for each peak and peak ratio, the percent deviation from the fading function for each data point was determined using

$$\% \text{ Deviation} = \frac{\left|P_m - P_f(t)\right|}{P_f(t)} \cdot 100, \tag{4.3}$$

where P_m is the measured peak area or peak area ratio at time t, and $P_f(t)$ is the value of the fading function at time t. The percent deviations for each time point were then averaged for each TLD to give an average percent deviation for that TLD for each peak and peak ratio.

For comparison to previous studies, peak ratios 2/3, 2/4, 2/5, 3/4, 3/5, and 4/5 were also fit to a single exponential decay equation,

$$\frac{P_i}{P_j} = Ae^{-kt}. \tag{4.4}$$

Gaussian distribution curves were fit to histograms of the k values using a statistics package (SPSS 17.0, SPSS Inc., 233 S. Wacker Drive, 11th floor, Chicago, IL 60606). The Kolmogorov-Smirnov test for goodness of fit was used to determine if the data fit the distribution well (Massey 1951).

RESULTS AND DISCUSSION

Figs. 4.1 through 4.4 show the pre-irradiation and post-irradiation fading rates for Peaks 2 through 5, with fading parameters given in Table 4.1. All peaks showed measureable fading over the time period of interest with the exception of Peak 5 for post-irradiation fading. The fading functions for Peaks 3, 4, and 5 also show an initial rise for small *t.* As these were initially fit using a single exponential decay equation, empirically determined additional terms were necessary in order to obtain a more accurate fit for each equation. Though capturing this initial rise in each fit was not always possible, such as post-irradiation fading for Peaks 3 and 4, the fit was much improved in those cases where it was successful. Also of

note was the pre-irradiation fading rate of Peak 5, which was negative, indicating an increase in signal over the time period of interest.

As shown in Table 4.2, 99% of all TLD peak area values were within 35% of the group fading functions for pre-irradiation fading. For post-irradiation fading, the group fading function for P_2 produced a poorer correlation for large *t*, leading to deviations of up to 100% between the group fading function and actual peak areas, shown in Table 4.3. However, peak areas for P_3 to P_5 peaks were much closer to their group fading functions, with 98% of all TLDs within 25% of the value of the group fading function at that point, shown in Table 4.4.

The peak ratio fading functions shown in Figs. 4.5 through 4.10 show similar agreement between the individual data points and the fit functions for ratios P_3/P_4, P_3/P_5, and P_4/P_5. However, due to the rapid fading exhibited by P_2 for large *t*, group fading functions for ratios involving P_2 appear inaccurate, often not falling within one standard deviation of the group mean for $t > 8$ d.

Despite this, when ratio fading functions are individually fit for each TLD for ratios P_2/P_3, P_2/P_4, and P_2/P_5 to a single exponential decay equation (Eq. 4.4), the resultant fading constants *k* fall in Gaussian distributions, shown in Figs. 4.11 to 4.13. A ratio fading function suitable for the entire group could then easily be determined using the mean of the *k* values obtained, if the additional fitting accuracy gained by using the additional terms present in Eq. 4.2 is not required.

CONCLUSIONS

Signals from each individual peak in LiF:Mg,Ti TLDs subject to pre-irradiation fading, when fit to a group fading function using 99 elements, 98 fall within 35% of the group fading function. For post-irradiation fading, signals from each individual peak fit to the group fading function all fall within 25% of the group fading function for P_3 to P_5, but differ by as much as 100% for P_2.

When individual single exponential decay functions were fit to peak ratio data for each chip, the decay constants *k* were found to have a Gaussian distribution, showing that fading functions can be characterized using a single group function with a decay constant equal to the mean of the individual decay constants found for each TLD. Peak area ratio fading functions can also be

characterized similarly to the peak area fading functions described above, using more complicated empirically determined fading functions.

These results show that, unlike element correction factors, , fading functions can be determined for groups of chips, with actual values falling within 35% of the fit line for pre-irradiation fading, and 25% of the fit line for P_3 to P_5 for post-irradiation fading. However, rapid post-irradiation fading in P_2 makes a group fading function problematic. Post-irradiation fading in P_2 may have to be determined individually for each chip if a high degree of accuracy is required, due to the uncertainty in the measurement in the fading constant for P_2.

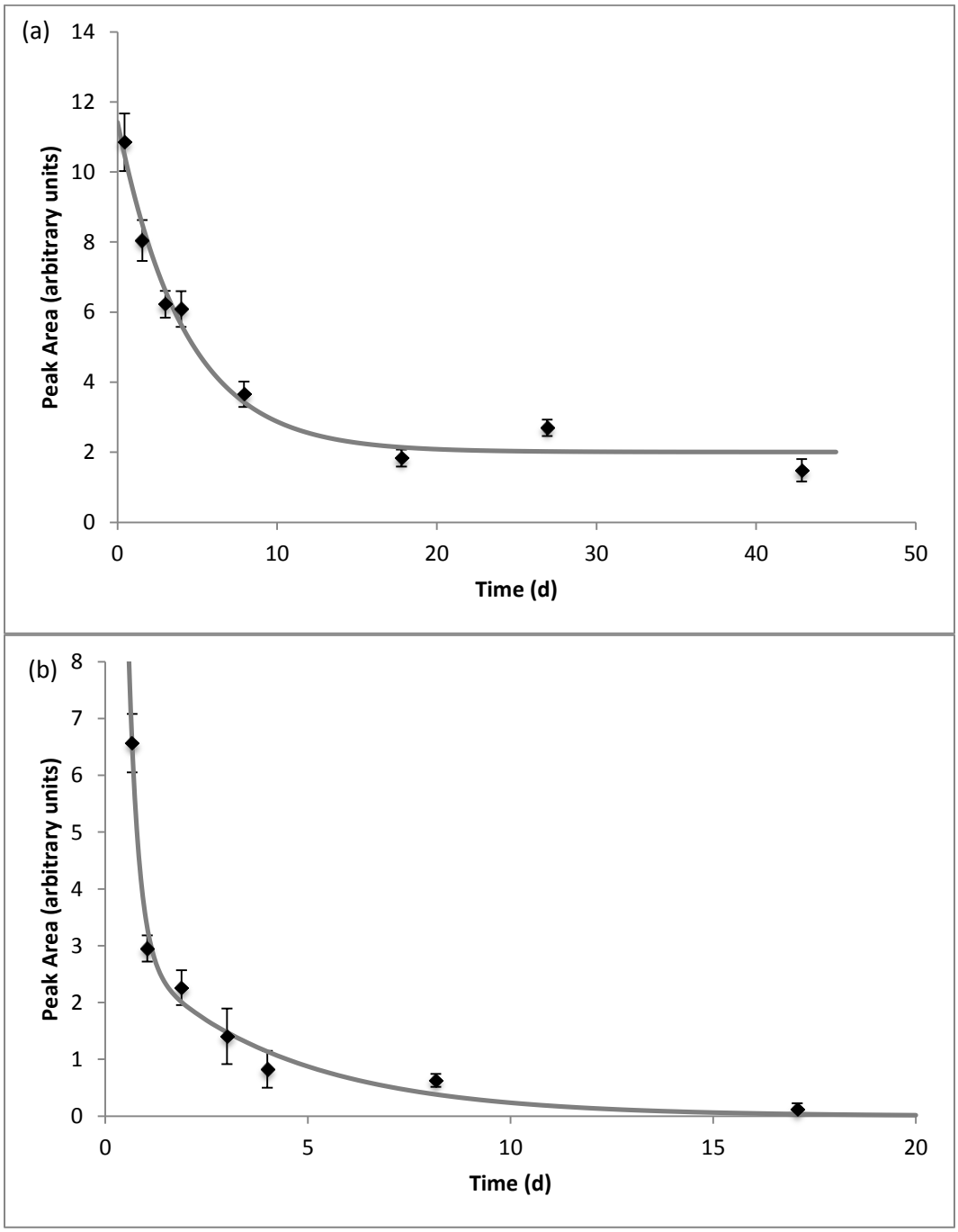

Fig 4.1. Signal arising from Peak 2 in LiF:Mg,Ti after being subject to (a) pre-irradiation fading (R^2 = 0.96) and (b) post-irradiation fading (R^2 = 0.96).

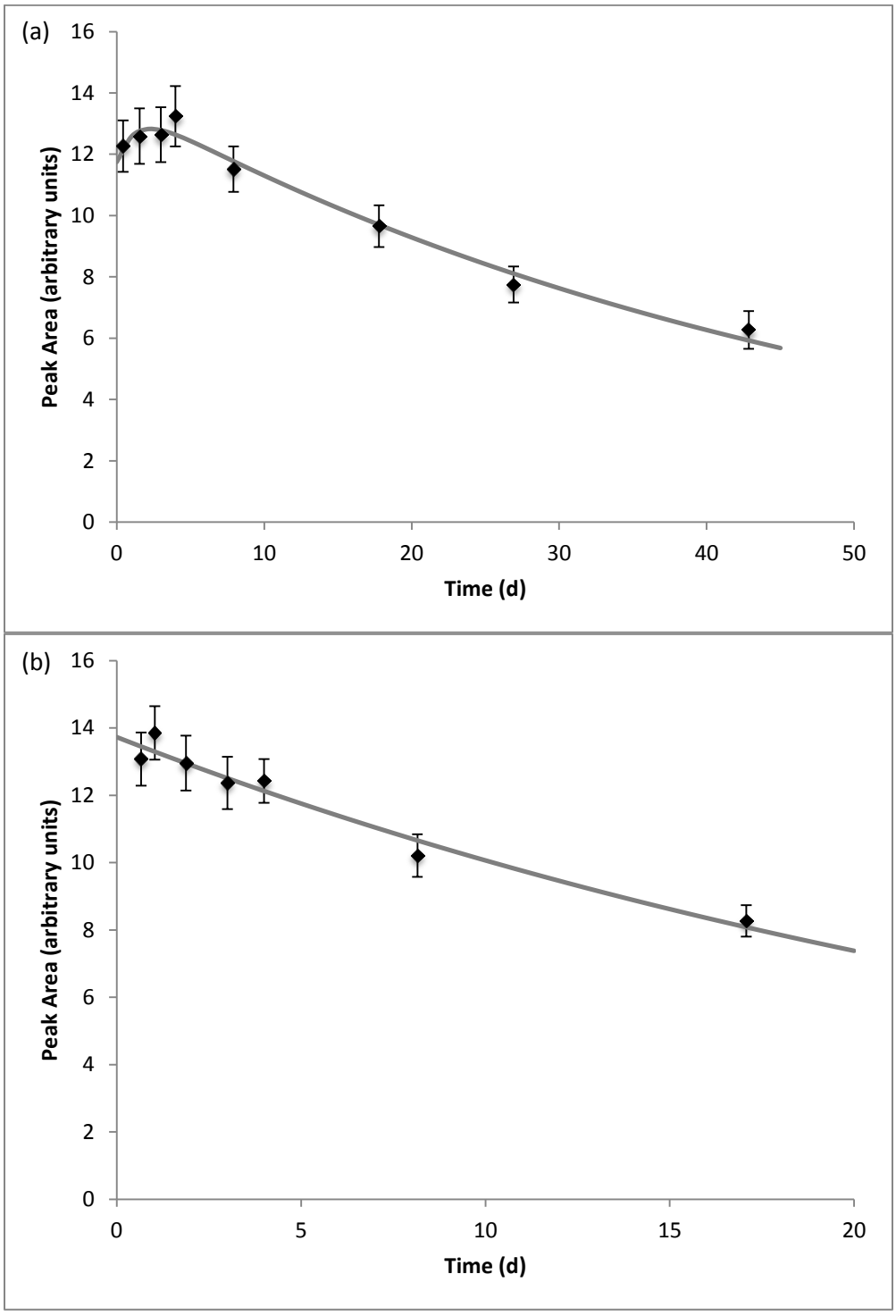

Fig 4.2. Signal arising from Peak 3 in LiF:Mg,Ti after being subject to (a) pre-irradiation fading (R^2 = 0.98) and (b) post-irradiation fading (R^2 = 0.97).

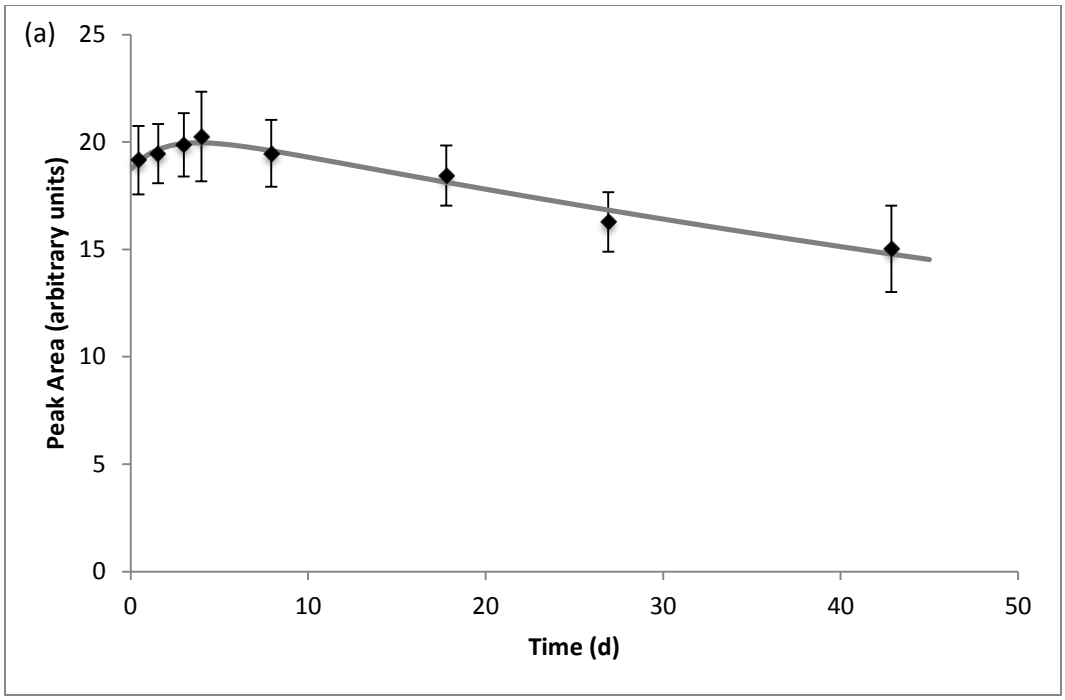

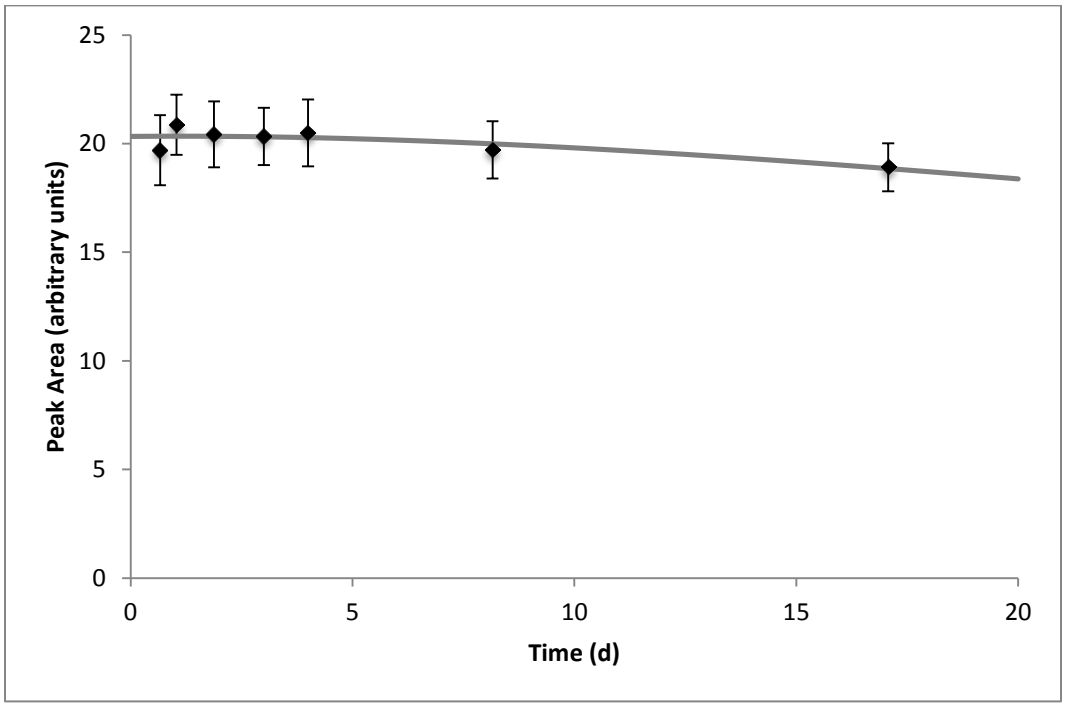

Fig 4.3. Signal arising from Peak 4 in LiF:Mg,Ti after being subject to (a) pre-irradiation fading (R^2 = 0.98) and (b) post-irradiation fading (R^2 = 0.68).

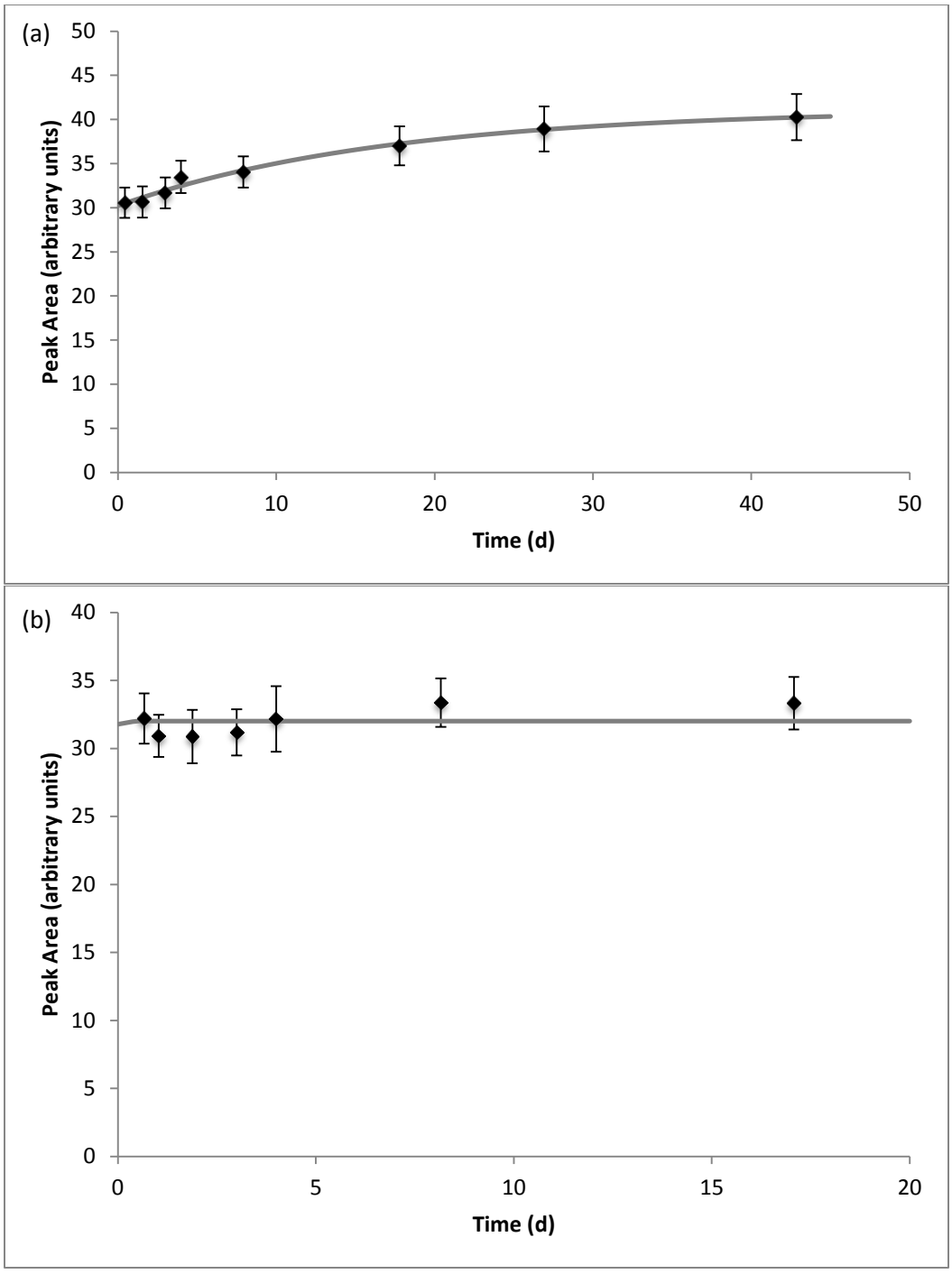

Fig 4.4. Signal arising from Peak 5 in LiF:Mg,Ti after being subject to (a) pre-irradiation fading (R^2 = 0.99) and (b) post-irradiation fading (R^2 = 0.00; no appreciable fading during time period).

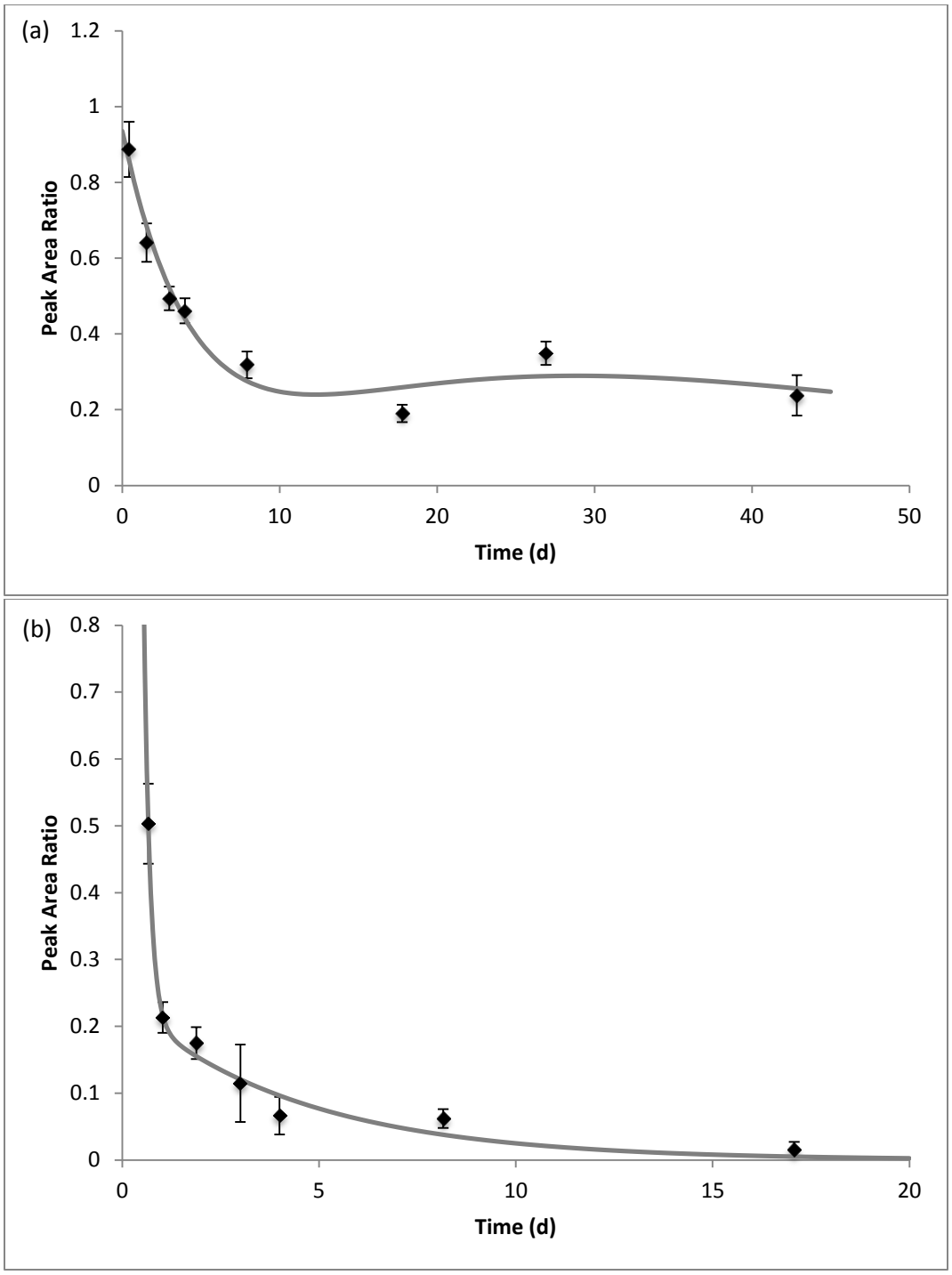

Fig 4.5. Ratio of signal from Peak 2 to signal of Peak 3 in LiF:Mg,Ti after being subject to (a) pre-irradiation fading (R^2 = 0.96) and (b) post-irradiation fading (R^2 = 0.99).

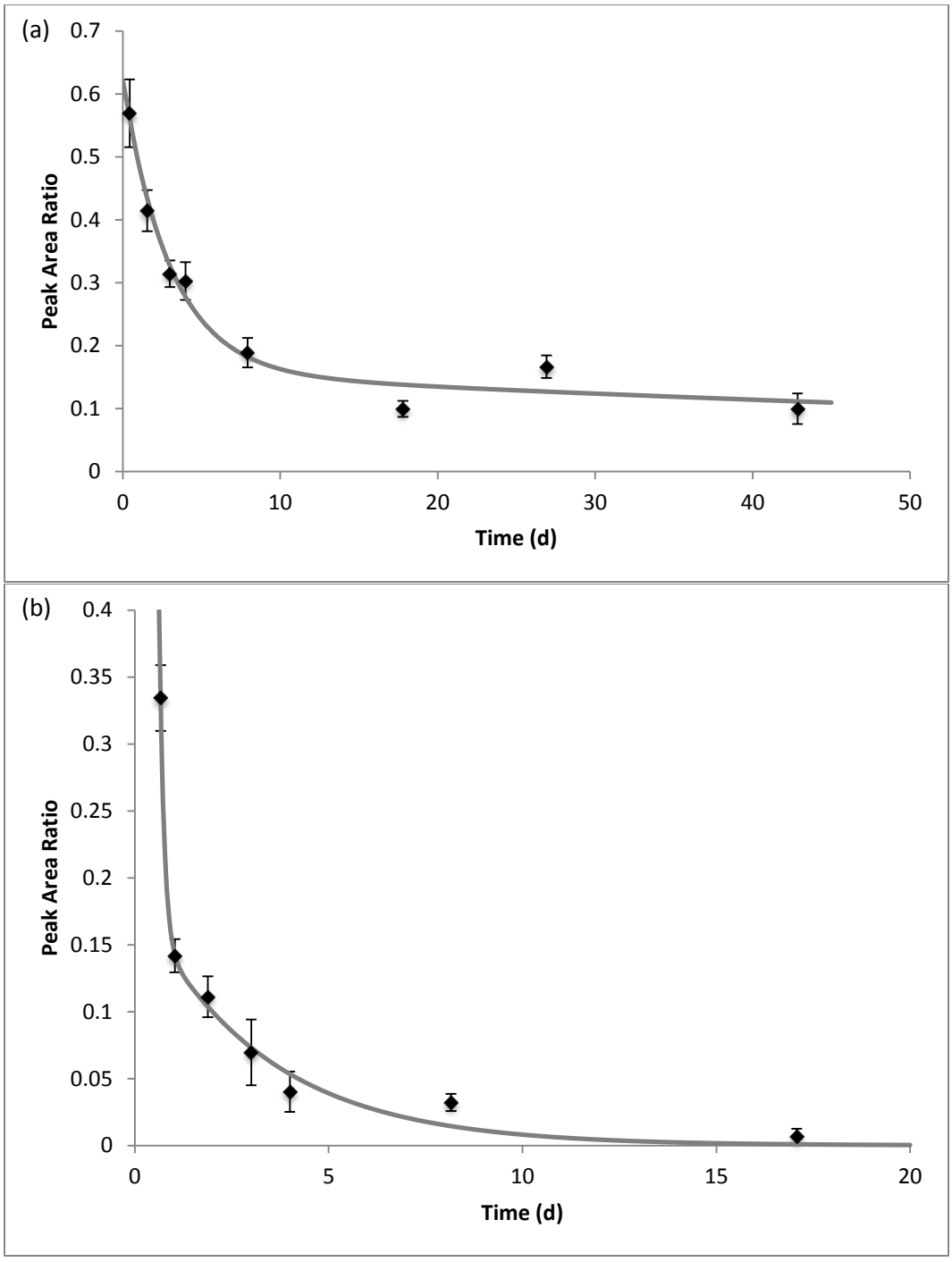

Fig 4.6. Ratio of signal from Peak 2 to signal of Peak 4 in LiF:Mg,Ti after being subject to (a) pre-irradiation fading (R^2 = 0.98) and (b) post-irradiation fading (R^2 = 0.992).

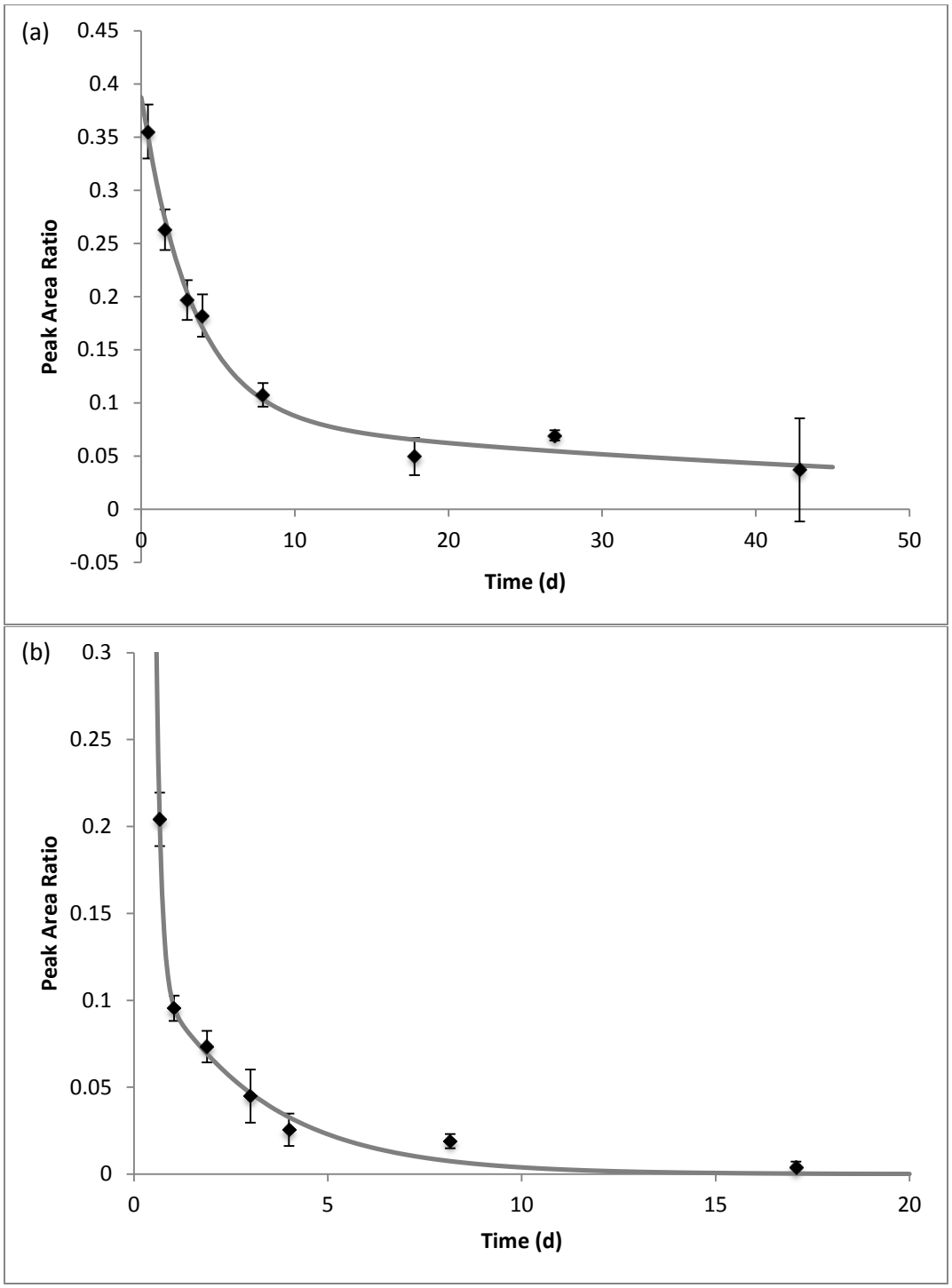

Fig 4.7. Ratio of signal from Peak 2 to signal of Peak 5 in LiF:Mg,Ti after being subject to (a) pre-irradiation fading (R^2 = 0.991) and (b) post-irradiation fading (R^2 = 0.992).

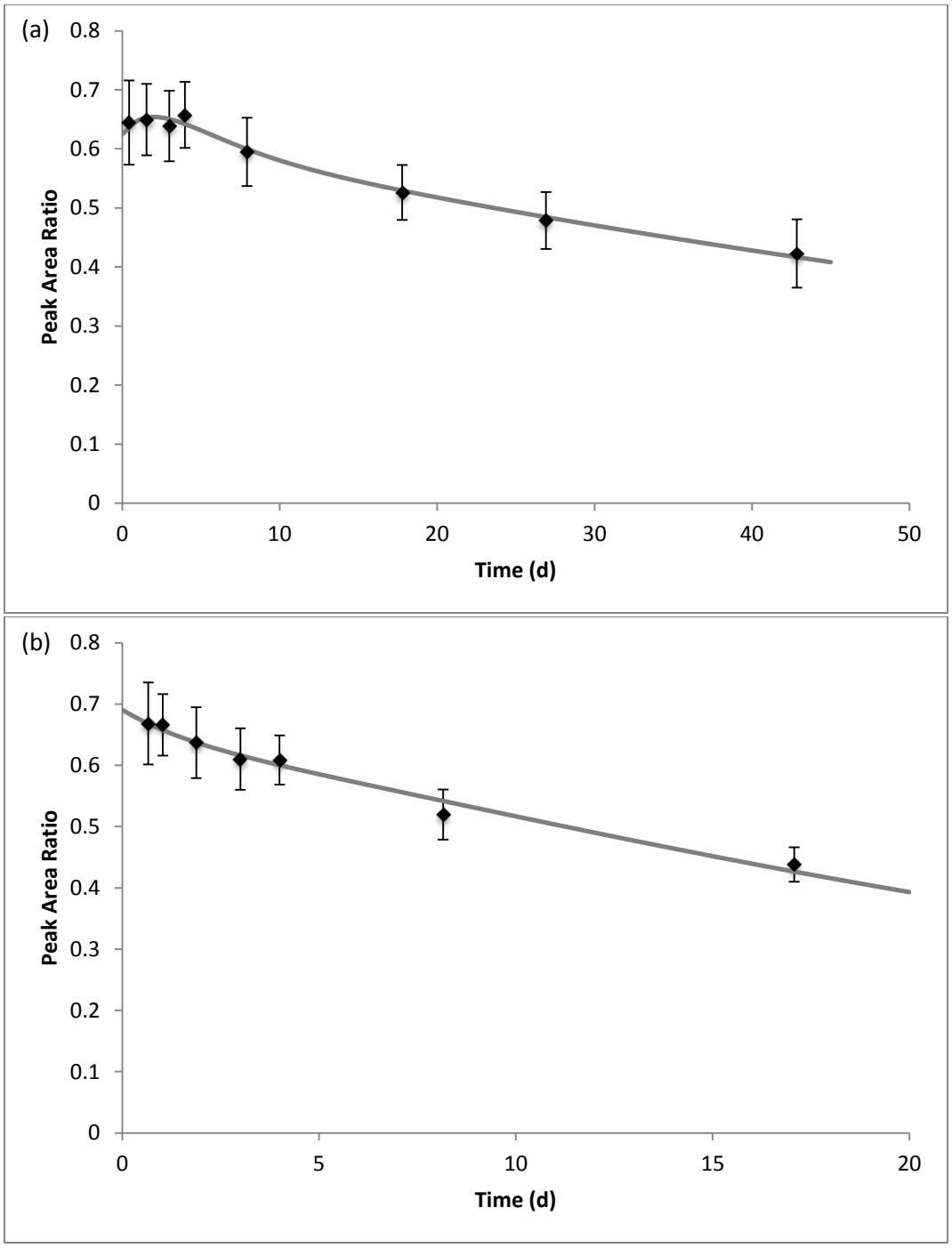

Fig 4.8. Ratio of signal from Peak 3 to signal of Peak 4 in LiF:Mg,Ti after being subject to (a) pre-irradiation fading (R^2 = 0.991) and (b) post-irradiation fading (R^2 = 0.98).

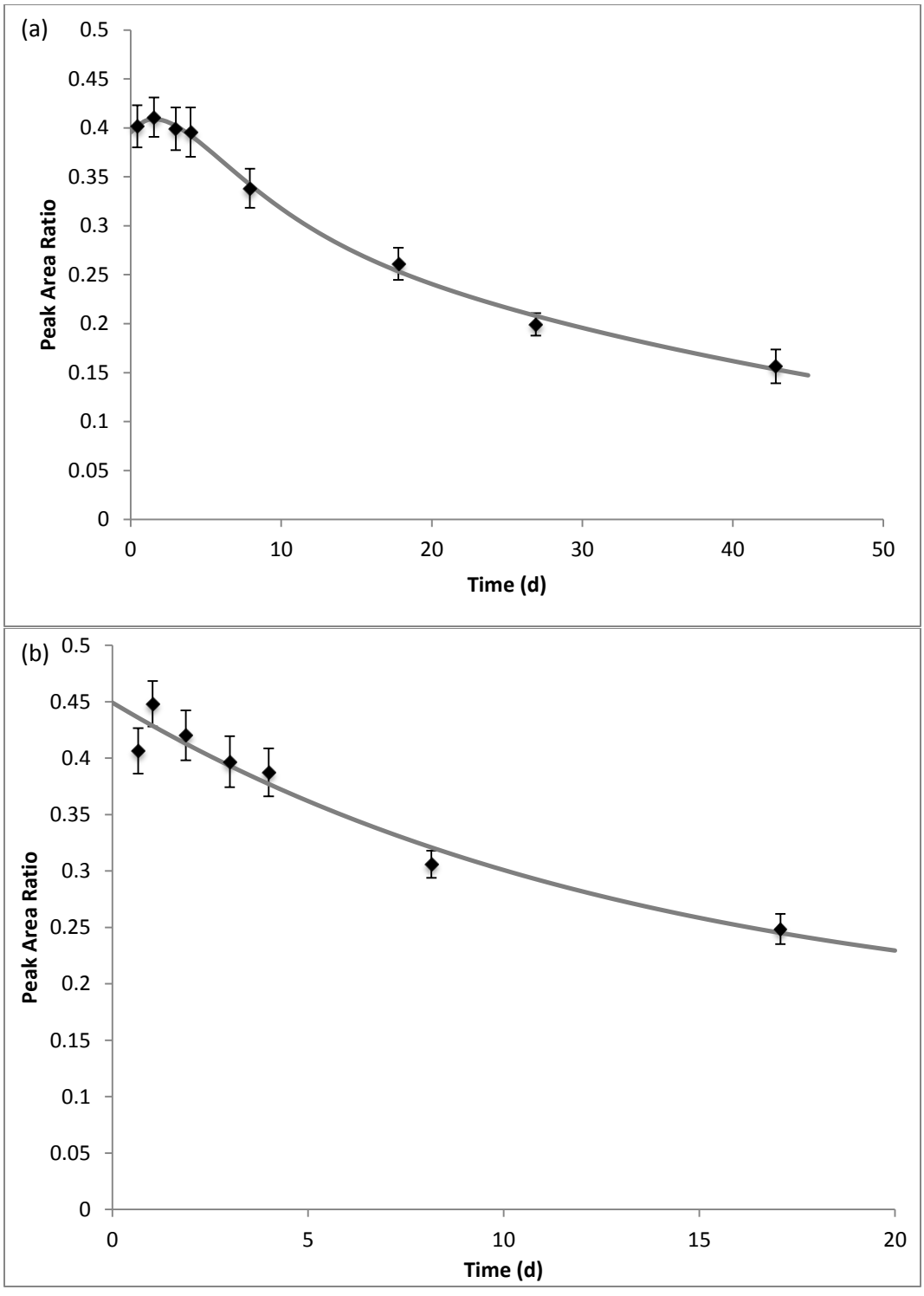

Fig 4.9. Ratio of signal from Peak 3 to signal of Peak 5 in LiF:Mg,Ti after being subject to (a) pre-irradiation fading (R^2 = 0.997) and (b) post-irradiation fading (R^2 = 0.94).

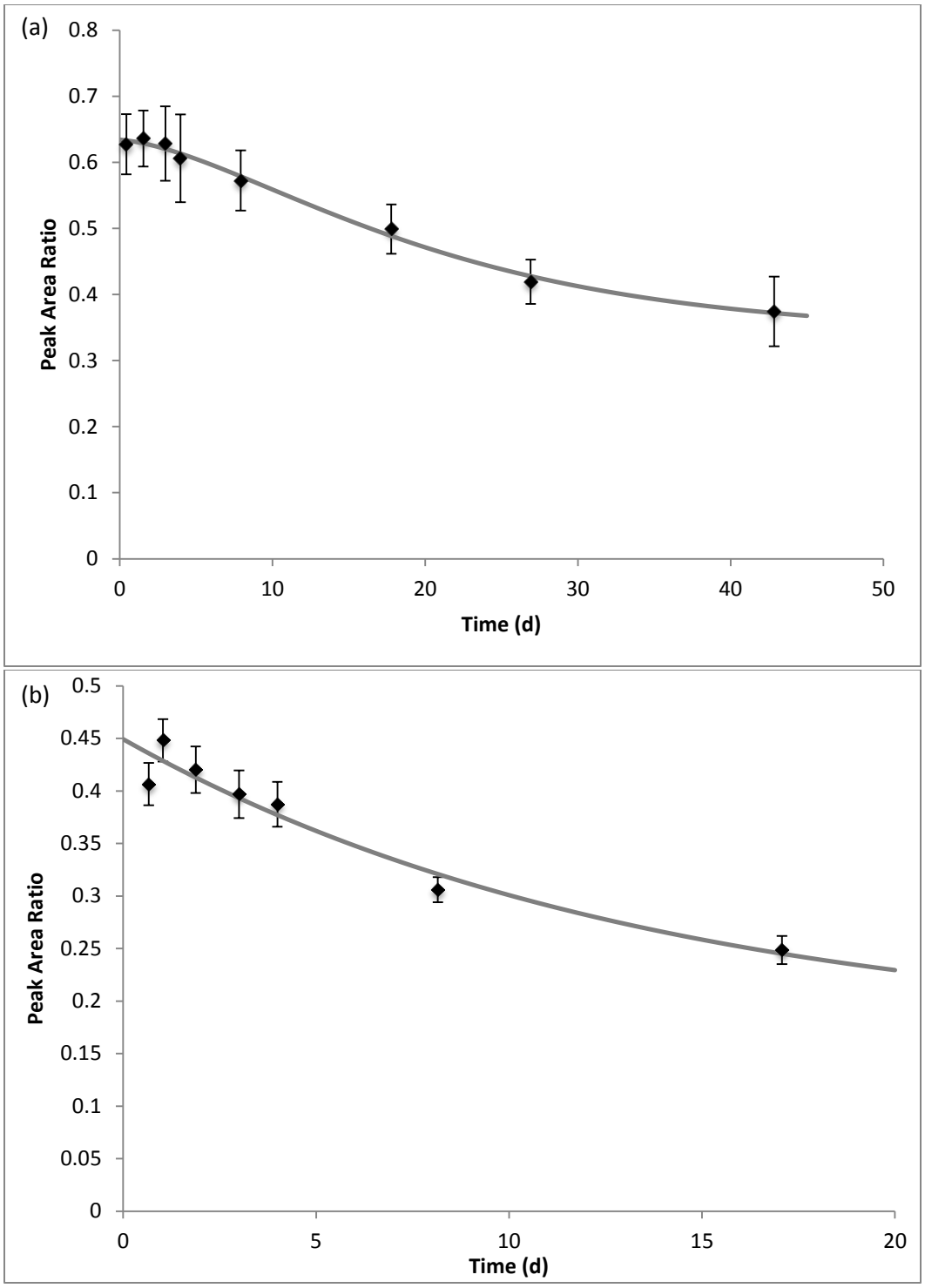

Fig 4.10. Ratio of signal from Peak 4 to signal of Peak 5 in LiF:Mg,Ti after being subject to (a) pre-irradiation fading (R2 = 0.994) and (b) post-irradiation fading (R^2 = 0.98).

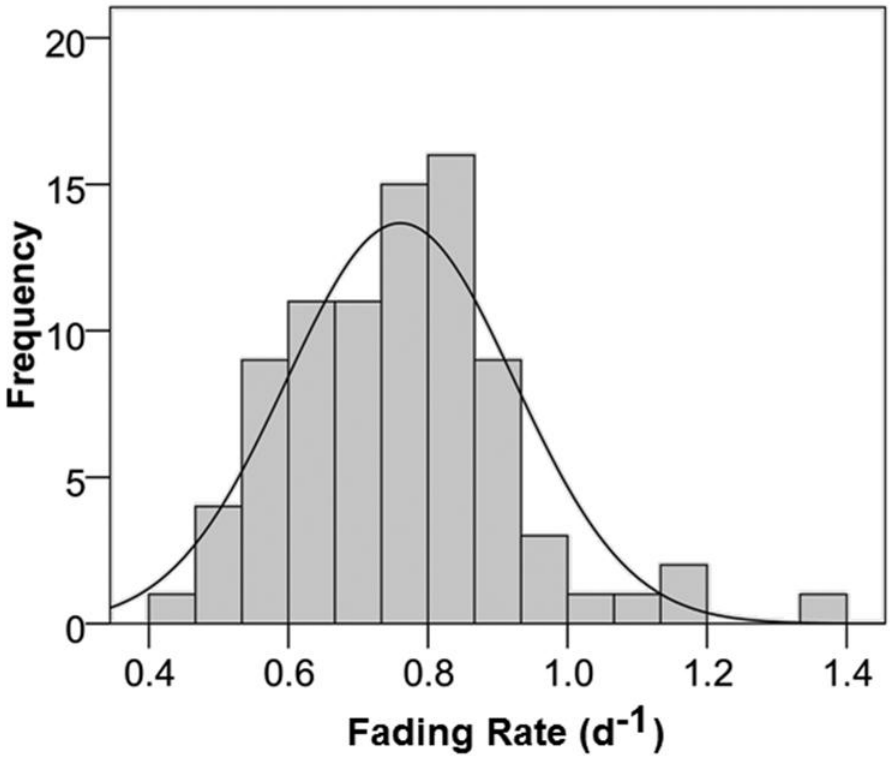

Fig 4.11. Histogram of individual LiF:Mg,Ti pre-irradiation fading rates *k* for P_2 normalized to P_5 using equation 4.4.

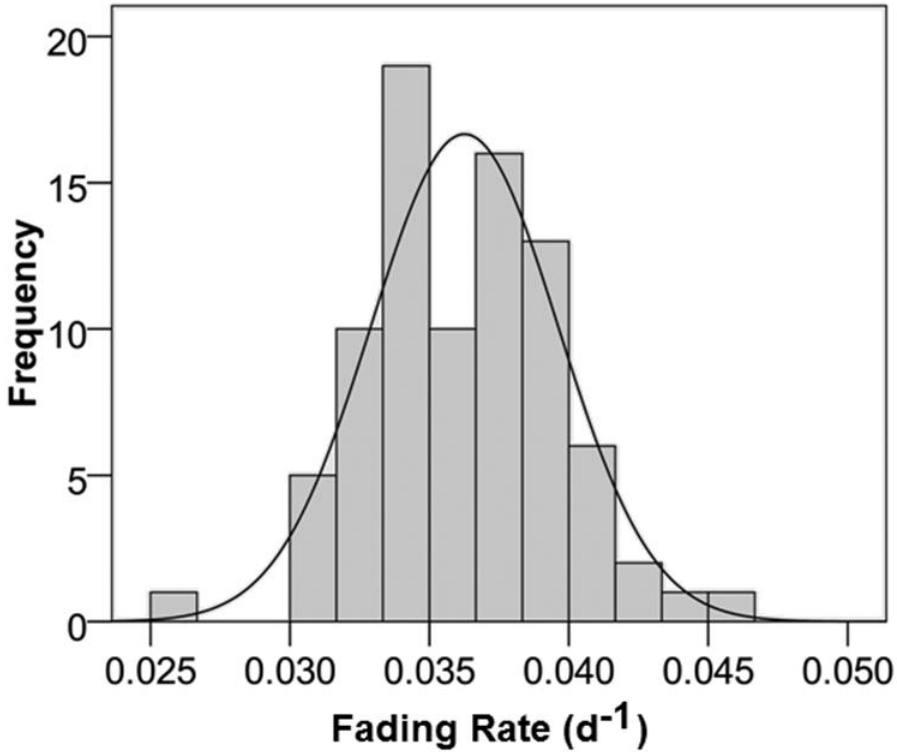

Fig 4.12. Histogram of individual LiF:Mg,Ti pre-irradiation fading rates *k* for P_3 normalized to P_5 using equation 4.4.

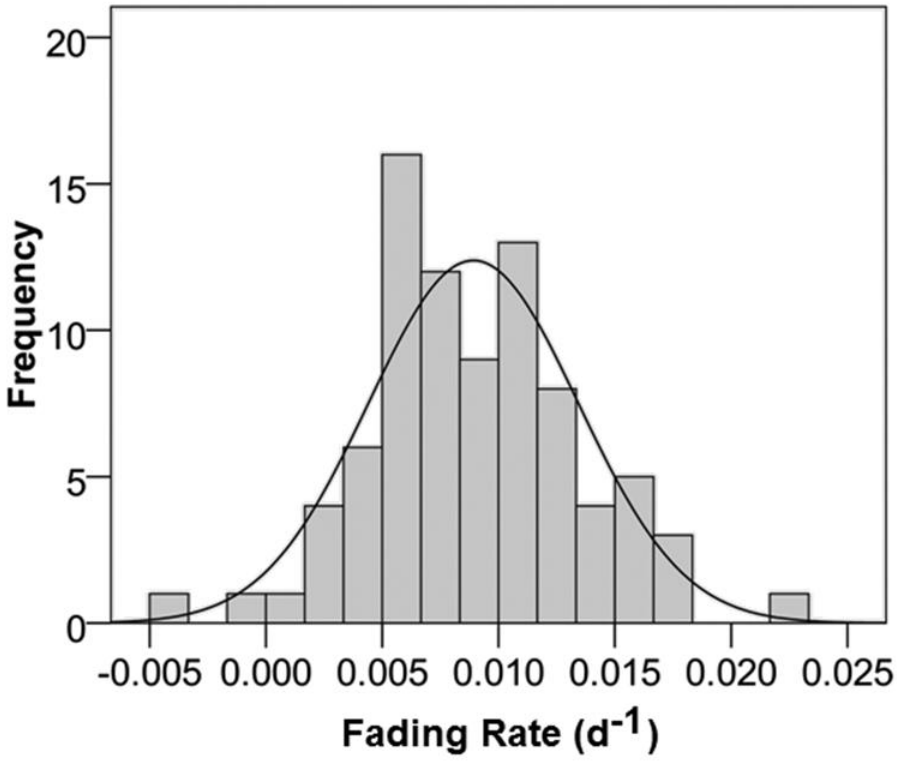

Fig 4.13. Histogram of individual LiF:Mg,Ti pre-irradiation fading rates *k* for P_4 normalized to P_5 using equation 4.4.

Table 4.1. Fit parameters for areas of peaks P_2 through P_5 fit to $A \cdot \exp(-k_1) + B \cdot \exp(-k_2)$.

	Peak	A	B	k_1	k_2	R^2
Pre-Irradiation	P_2	9.41×10^5	2.01×10^5	0.239	0	0.9551
	P_3	1.38×10^6	-2.01×10^5	0.020	0.786	0.9842
	P_4	2.09×10^6	-2.21×10^5	0.008	0.486	0.9753
	P_5	4.11×10^6	-1.09×10^6	0	0.058	0[a]
Post-Irradiation	P_2	5.47×10^6	3.24×10^5	4.029	0.262	0.9592
	P_3	1.42×10^6	-5.00×10^4	0.031	0.031	0.9650
	P_4	2.95×10^6	-9.13×10^5	0.016	0.052	0.6834
	P_5	3.20×10^6	-2.28×10^4	0	45.03	0.9851

[a] No appreciable post-irradiation fading occurred during the time period studied.

Table 4.2. Distribution of averaged deviations from fit pre-irradiation fading functions for each TLD for P_2 to P_5.

	Peak 2	Peak 3	Peak 4	Peak 5
Average Deviation from Fit Line	*Frequency*	*Frequency*	*Frequency*	*Frequency*
0-5%	0	34	32	63
5-10%	31	49	51	23
10-15%	37	5	3	3
15-20%	18	6	8	9
20-25%	8	4	5	1
25-30%	2	1	0	0
30-35%	3	0	0	0
> 35%	1	1	1	1

Table 4.3. Distribution of averaged deviations from fit post-irradiation fading functions for each TLD for P_2.

Average Deviation from Fit Line	*Frequency*	*Average Deviation from Fit Line*	*Frequency*
20-30%	10	70-80%	6
30-40%	23	80-90%	7
40-50%	19	90-100%	3
50-60%	20	>100%	5
60-70%	7		

Table 4.4. Distribution of averaged deviations from fit post-irradiation fading functions for each TLD for P_3 to P_5.

	Peak 3	Peak 4	Peak 5
Average Deviation from Fit Line	*Frequency*	*Frequency*	*Frequency*
0-5%	46	41	45
5-10%	38	40	39
10-15%	2	5	2
15-20%	13	12	12
20-25%	1	2	2

REFERENCES

Chauvenet W., 1971. A Manual of Spherical and Practical Astronomy, Volume II. J.B. Lippincott Company, Philadelphia.

Fowler J.F., Shuttleworth E., Svarcer V., White J.T., Karzmark C.J., 1965. Fading in Thermoluminescent Lithium Fluoride used for Radiation Dosimetry. Nature 207:997-998.

Harvey J.A., Haverland N.P., Kearfott K.J., 2010. Characterization of the glow-peak fading properties of six common thermoluminescent materials. Appl. Radiat. Isot. 68(10):1988-2000.

Harvey J.A., Thomas E.M., Kearfott K.J., 2011. Quantification of various factors influencing the precision of thermoluminescent detector calibrations for new and used chip sets. Health Phys. In press.

Horowitz Y.S., Satinger D., Avila O., 2006. Track structure approach to the calculation of peak 5a to peak 5 (TLD-100) relative intensities following heavy charged particle irradiation. Radiat. Prot. Dosim. 119:45-48.

Kearfott K.J., Han S., McMahan K.L., Samei E., 1995. Sensitivity of a mixed field dosimetry algorithm to uncertainties in thermoluminescent element readings. Health Phys. 68: 340-349.

Kearfott K.J., Nabelssi B.K., Rucker R.H., Klingler G.W., 1990. Evaluation of two thermoluminescent detection systems for medical imaging environments. Health Phys. 59:827-836.

Massey F.J., 1951. The Kolmogorov-Smirnov Test for Goodness of Fit. J. Am. Stat. Assoc. 46:68-78.

Parker L. W., Harvey J. A., Kearfott K. J., 2011. An integrated system for the beta, gamma and neutron calibration and storage of thermoluminescent dosimeters for a research laboratory. Health Phys. 100(2):S43-S49.

Plato P., Miklos J., 1985. Production of element correction factors for thermoluminescent dosimeters. Health Phys. 49:873-881.

Samei E., Kearfott K.J., Wang C.-K., Han S., 1994. Impact of variations in physical parameters on glow curves for planchet heating of TL dosimeters. Nucl. Instrum. Methods Phys. Res. A 353:415-419.

Simpkins R.W., Kearfott K.J., 1997. The minimum number of observations necessary to develop an average thermoluminescent dosimeter element correction factor. Radiation Protection Management 13:55-61.

Studenski M.T., Haverland N.P., Kearfott K.J., 2007. Simulation, design, and construction of a ^{137}Cs irradiation facility. Health Phys. 92:S78-S86.

Weinstein M., German U., Dubinsky S., Alfassi Z.B., 2003. On the determination of the post-irradiation time from the glow curve of TLD-100. Radiat. Prot. Dosimetry 106:121-130.

Chapter V

Effects of High Ambient Temperature on Glow Peak Fading Properties of LiF:Mg,Ti Thermoluminescent Dosimeters

ABSTRACT

In this study, the effects of storage in a controlled high temperature environment on LiF:Mg,Ti thermoluminescent detectors (TLDs) are investigated. Two hundred TLDs were exposed to ambient temperatures of 30°C, 40°C, and 50°C, near the upper limit of temperatures common to environments on Earth. Both the effects of sensitivity changes before irradiation, typically called pre-irradiation fading, and signal loss after irradiation, called post-irradiation fading, were studied. Dosimeters were subjected to up to 33 d of storage before irradiation and up to 68 d of storage after irradiation. In general, results were similar for each temperature but accelerated as storage temperature increased. Of the main dosimetric peaks of LiF:Mg,Ti, for pre-irradiation fading peak 5 showed a signal increase of up to 30% after 20 d and peak 4 showed a similar 30% decrease in 20 d. The sum the areas of peaks 4 and 5, a common dosimetric measure, remained relatively constant even for long pre-irradiation fading times, although at 50°C losses in peak 5 signal were too significant to keep the sum of peaks 4 and 5 constant. Peaks 2 and 3 faded gradually pre-irradiation and sharply post-irradiation. Peak 3 was still detectable even at 50°C and the longest irradiation times, but peak 2 was very difficult to detect after 15 to 20 d, especially with post-irradiation fading.

INTRODUCTION

The thermoluminescent dosimeters (TLDs) intended for environmental dosimetry are subject to the vast range of temperatures present throughout the globe. Changes in the response of various common TLD types as a function of time have been extensively studied at room temperature (Harvey et al. 2010) for both sensitivity changes that occur following annealing and prior to irradiation, commonly called pre-irradiation fading, and signal loss after irradiation, called post-irradiation fading. At higher and lower ambient temperatures, fading rates for TLDs vary considerably, with fading rates increasing as ambient temperature increases. While post-irradiation fading is unambiguously attributed to thermal loss of signal in the material, pre-irradiation fading is due to the loss of high temperature trap equilibrium established during annealing that settles into a new equilibrium involving aggregation of defects and solid state precipitation following a prolonged storage period at a lower temperature (McKeever et al. 1995).

Several studies of LiF:Mg,Ti examine its dependence of fading rate on ambient temperature. An early study at -20°C, 20°C, and 50°C examined both pre- and post-irradiation fading, showing total TL to be highly dependent on the storage temperature (Julius and de Planque 1983). Delgado and Gomez Ros examined LiF:Mg,Ti fading at elevated temperatures extensively, finding significant increased fading of peak 4 at 25°C and 45°C (Delgado and Gomez Ros 1990) and later, even higher fading rates at 70°C (Delgado et al. 1992). Both studies showed an increase in the signal from peak 5 with time for each tested temperature, which has also been observed at room temperature (Harvey and Kearfott 2011). The sum of peaks 4 and 5 has also been shown to remain relatively constant at room temperature (Shachar and Horowitz 1992) and this holds true even for real-world ambient temperatures varying from lower than 10°C to over 40°C in a desert climate (Al-Haj and Lagarde 2006).

Previous work lacks an analysis of all of the peaks of the glow curve. If any information is to be obtained about the time of irradiation, the ratio of the area of peak 3 to the sum of the areas of peaks 4 and 5 is extremely helpful (Weinstein et al. 2003). Also, some of the previous studies analyzed fading for

only 7 to 10 d, much shorter than typical deployments. As ambient humidity can also alter fading rates (Julius and de Planque 1983), it was desired to perform a high ambient temperature experiment in an environment tightly controlled with respect to humidity as well as temperature and visible light.

MATERIALS AND METHODS

Two hundred LiF:Mg,Ti TLDs of dimensions 3.2 mm × 3.2 mm × 0.9 mm (TLD-100, BICRON/Harshaw, 6801 Cochran Road, Solon, OH 44139, USA) were employed in this experiment. These were stored in two custom designed polymethyl methacrylate (PMMA) plates with 100 individual wells mounted to a custom designed PMMA phantom with acrylic screws (Parker et al. 2010) for irradiation in a purpose-built ^{137}Cs irradiation facility (Studenski et al. 2007). A manual TLD reader with hot gas and hot planchet modes (Model 4500 TLD Reader, BICRON/Harshaw, 6801 Cochran Road, Solon, OH 44139, USA) was used for readout with the standard manufacturer recommended time temperature profile (TTP). Nitrogen gas (Prepurified compressed nitrogen cylinder 300, Metro Welding Supply Corporation, 12620 Southfield Road, Detroit, MI 48223) flowed to the reader at all times during readouts to suppress oxygen-induced light effects. The manufacturer recommended reader cycle was used to anneal the dosimeters, starting at 50°C with no preheat, increasing to 300°C at 10°C s^{-1}, and staying at 300°C until 33.3 s had passed since the beginning of the cycle.

All TLDs were initially calibrated three times, previously found to give adequate precision with high time efficiency (Simpkins and Kearfott 1997, Harvey et al. 2011b), to 4.4 mGy using a 320 GBq ^{137}Cs irradiator (Model 28-8A Irradiator, J.L. Shepherd and Associates, 1010 Arroyo Avenue, San Fernando, CA 91340-8122). After calibration, all TLDs were kept in a water-jacketed incubator (NuAire Model NU2700 Dual Chamber CO_2 Incubator, NuAire Inc., 2100 Fernbrook Lane N, Plymouth, MN 55447) when not in use. The two chambers of the incubator were kept at 30.0 ± 0.6^{o}C, 40.0 ± 0.6^{o}C, or 50.0 ± 0.6^{o}C. The plates were kept in the same or different chambers in accordance

with the experiment schedule. Both sets of 100 TLDs were used to study fading at all three temperatures. Both chambers also contained approximately 500 mL of anhydrous $CaSO_4$ as a desiccant to keep relative humidity at 12.4 $\pm$ 6.4%. Minimal ambient light reached the TLDs inside the incubator with the door closed.

To study post-irradiation fading at high ambient storage temperature, TLDs were kept in the incubator a maximum of 24 h between anneal or last readout and irradiation. After irradiation to 4.4 mGy, the TLDs were replaced in the incubator and left for storage times of 1 to 68 d. Groups of 20 TLDs were removed from the plate and read, with the rest left in the incubator for a longer fade duration. After readout for the post-irradiation fading portion of the study, the TLDs were replaced in the incubator and left to fade for another 1 to 34 d. They were then removed, irradiated to 4.4 mGy, and read within 24 h to collect the pre-irradiation fading data. This process was repeated for each of the three temperatures of interest. Storage durations for post-irradiation fading were 1, 2, 3, 6, 11, 19, and 67 d and 5, 12, 15, 22, 26, 29, and 34 d for pre-irradiation fading at 30°C. At 40°C and 50°C, storage durations were 6, 8, 11, 14, 19, 32, and 68 d for post-irradiation fading and 4, 6, 11, 15, 21, 25, 27, and 33 d for pre-irradiation fading.

Glow curve analysis was performed with a computerized glow curve analysis program (Harvey et al. 2011a) written in a mathematics package format (MATLAB R2010b with Curve Fitting Toolbox, The MathWorks Inc., 3 Apple Hill Drive, Natick, MA 01760). This program separates the glow curve into the four peaks typically seen for low dose irradiations of TLD-100, peaks 2 through 5, using the first-order kinetics model. The results were used to obtain fading functions by peak.

All single peak fading data were fit to double exponential decay functions when possible, of the following form:

$$I(t) = Ae^{-k_1 t} + Be^{-k_2 t} + C \tag{5.1}$$

where $I(t)$ is the glow peak area, t is the dosimeter storage time, and k_1, k_2, A, B, and C are empirical fitted parameters.

RESULTS AND DISCUSSION

Figs. 5.1 and 5.2 show the results from storage at 30°C. Stark differences can be seen between pre-irradiation and post-irradiation fading. The increase in peak 5 is much more apparent for pre-irradiation fading, with a 30% increase between 5 to 12 d. This increase is matched by a 28% decrease in peak 4, causing the sum of the areas of peaks 4 and 5 to be fairly constant, as seen in previous work (Shachar and Horowitz 1992).

The decrease in peaks 2 and 3 is much more gradual in pre-irradiation fading, with much faster drops from post-irradiation fading. For either fading type, peak 2 is negligible after 10 d. Peak 3 gradually decreases for both fading types but is still detectable after 34 d of pre-irradiation fading or 67 d of pre-irradiation fading.

Fading trends are similar for 40°C, as seen in Figs. 5.3 and 5.4. The increase in peak 5 and decrease in peak 4 are still readily apparent and of similar magnitude. However, after 20 d at 40°C, peaks 4 and 5 start to blend together, making them more difficult for the computer to distinguish. This leads to a much higher error in peak 4, as can be seen on the graphs.

Lower peaks are only limited sources of information at 40°C. Peak 2 signal is negligible after as few as 6 d and peak 3 signal is nearly gone after 20 d for both types of fading. Like at 30°C, fading is much more gradual in these peaks for pre-irradiation fading than post-irradiation fading. This implies that the predominant source of fading in low energy traps for dosimeters deployed for extended periods is signal loss after irradiation, not sensitivity change before irradiation.

At 50°C, signals from peaks 4 and 5 stay relatively constant for post-irradiation fading, as seen in Fig. 5.5. Where peak 3 had a 20% rise between 5 and 10 d intervals at 40°C, this is gone at 50°C. The signal still takes

approximately 20 d to largely disappear. For all tested intervals, peak 2 is negligible after 5 d of post-irradiation fading.

For pre-irradiation fading, seen in Fig. 5.6, peak 4 decreases more sharply and the increase in peak 5 manifesting after 10 d of pre-irradiation storage time is no longer enough to cancel out the decrease in peak 4, which begins to decline after a 30% increase after 10 d. As a result, the sum of peaks 4 and 5 is no longer constant and drops 15% after 20 d. A summary of all fading results fit to double exponential decay functions may be found in Table 5.1.

CONCLUSIONS

LiF:Mg,Ti TLDs suffer from accelerated fading at higher ambient temperatures, with these trends generally becoming more severe as temperature increases. However, the trends are quite different for pre-irradiation fading and post-irradiation fading, and so should not be taken to be interchangeable. When stored before irradiation, peak 5 increases by 30% in 20 d and peak 4 decreases by 30% in 20 d. When subject to post-irradiation fading, these peaks stay mostly constant over 68 d, with no increasing or decreasing signal trends discernable when measurement error is considered.

For both pre-irradiation and post-irradiation fading, peaks 2 and 3 both approach zero exponentially, but the decrease is much sharper in post-irradiation fading then pre-irradiation fading, in which peaks 2 and 3 fade much more gradually. Even at a storage temperature of 50°, peak 3 is still barely discernable after 30 d for both fading types. Peak 2 sensitivity declines slowly enough during the pre-irradiation time period that its presence after a long deployment, especially at high temperature, may imply that an acute irradiation is much closer to the end of the deployment period than the beginning. The same is true of peak 3, but to a lesser degree. It is likely that the primary mode of fading in these peaks is signal loss, not sensitivity change.--.

At the highest ambient temperature tested, 50°C, the sum of peaks 4 and 5 was observed to decline after 20 d. As this sum is routinely relied upon for

dosimetry, it should be noted that dose in this temperature range may be problematic in the long term. Few exterior environments are subject to such a high temperature, especially on a constant basis: the desert study done in Saudi Arabia by Al-Haj and Lagarde (Al-Haj and Lagarde 2006) experienced daily temperature ranges of at least 10 to 20°C even in the hottest areas.

High constant temperatures may be present in interior occupational environments not frequented by personnel, indicating that control badges left in these areas may require special handling so as not to underestimate their absorbed dose. High ambient temperature areas may also be found occupationally, such as boiling water reactor drywells, and rooms that are not typically air-conditioned, such as basements. Vehicles left in direct sunlight unattended can reach 43°C in 1 h with an ambient temperature of 22°C, or as high as 54°C in 1 h with an ambient temperature of 34°C (McLaren et al., 2005), which may cause problems for badges accidentally left within.

Though dose can be calculated using the sum of the Peak 4 and Peak 5 areas, that value may still decrease noticeably, causing an underestimate of dose, if ambient temperature is 50°C or higher. Corrections are made more difficult if the approximate time of irradiation is not known, as only storage before irradiation causes a significant effect, as well as if the approximate temperature is not known, as fading even in the sum of Peak 4 and Peak 5 areas occurs more noticeably at temperatures above 50°C. In as little as 7 to 14 d, signal decreases by 5 to 15% in a 50°C environment.

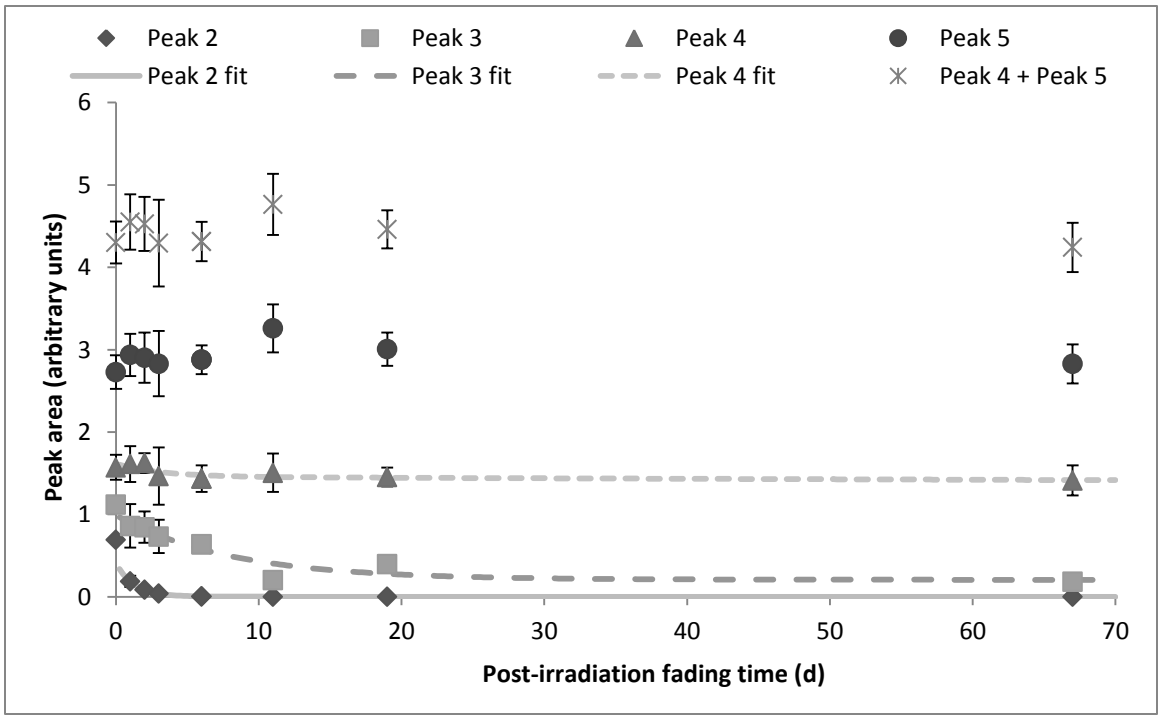

Fig 5.1. Evolution of the areas of peaks 2, 3, 4, and 5, and the sum of the areas of peaks 4 and 5, when subject to post-irradiation fading at 30°C.

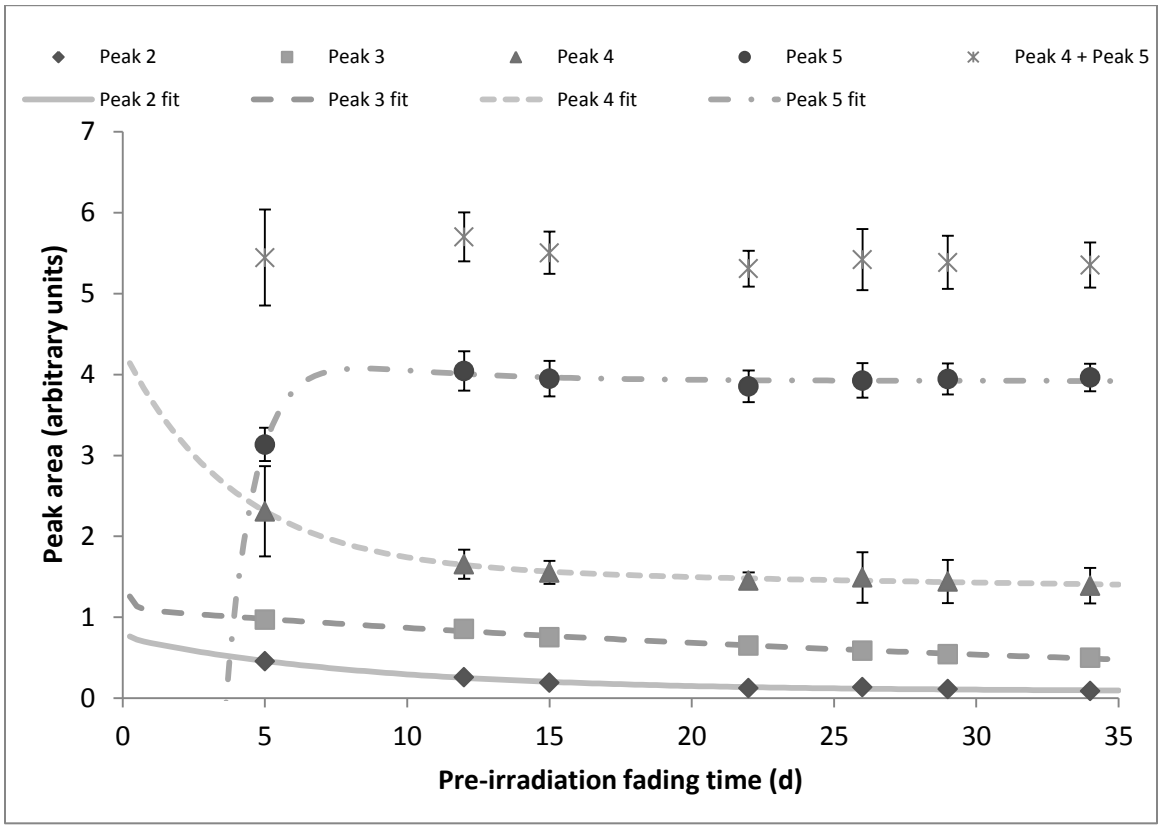

Fig 5.2. Evolution of the areas of peaks 2, 3, 4, and 5, and the sum of the areas of peaks 4 and 5, when subject to pre-irradiation fading at 30°C.

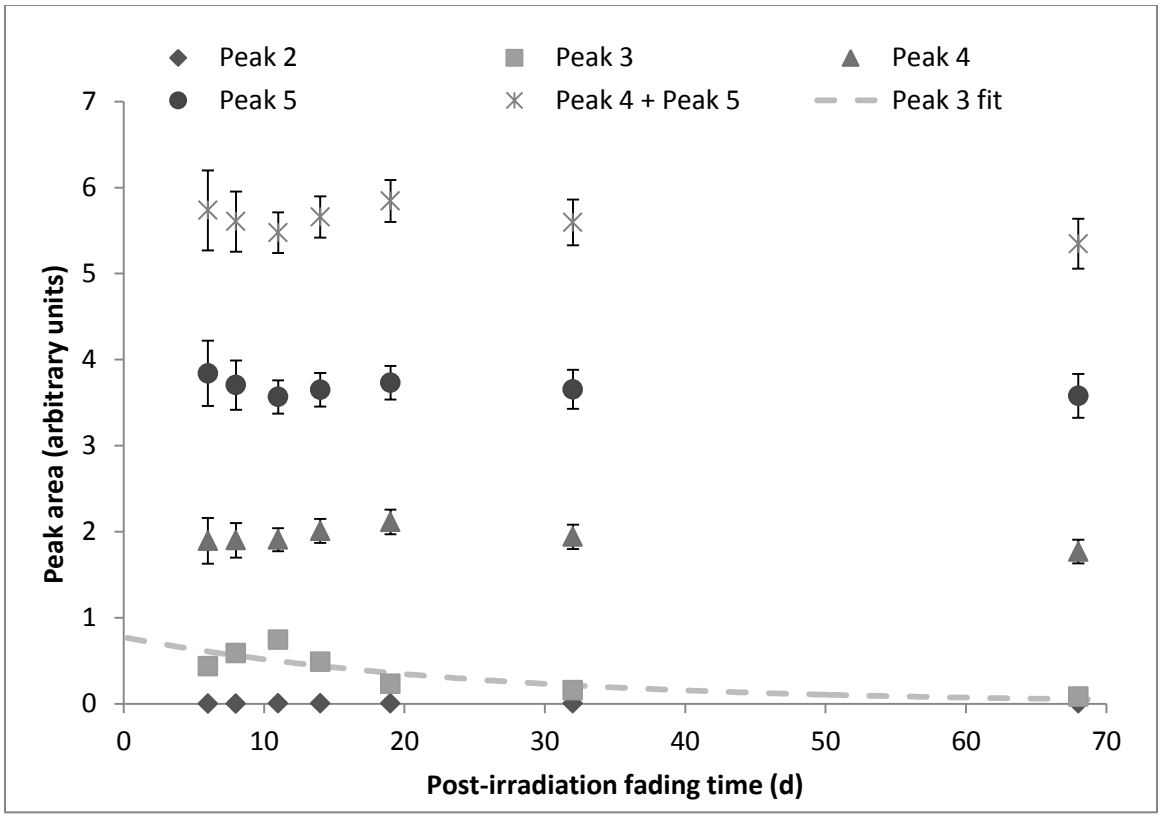

Fig 5.3. Evolution of the areas of peaks 2, 3, 4, and 5, and the sum of the areas of peaks 4 and 5, when subject to post-irradiation fading at 40°C.

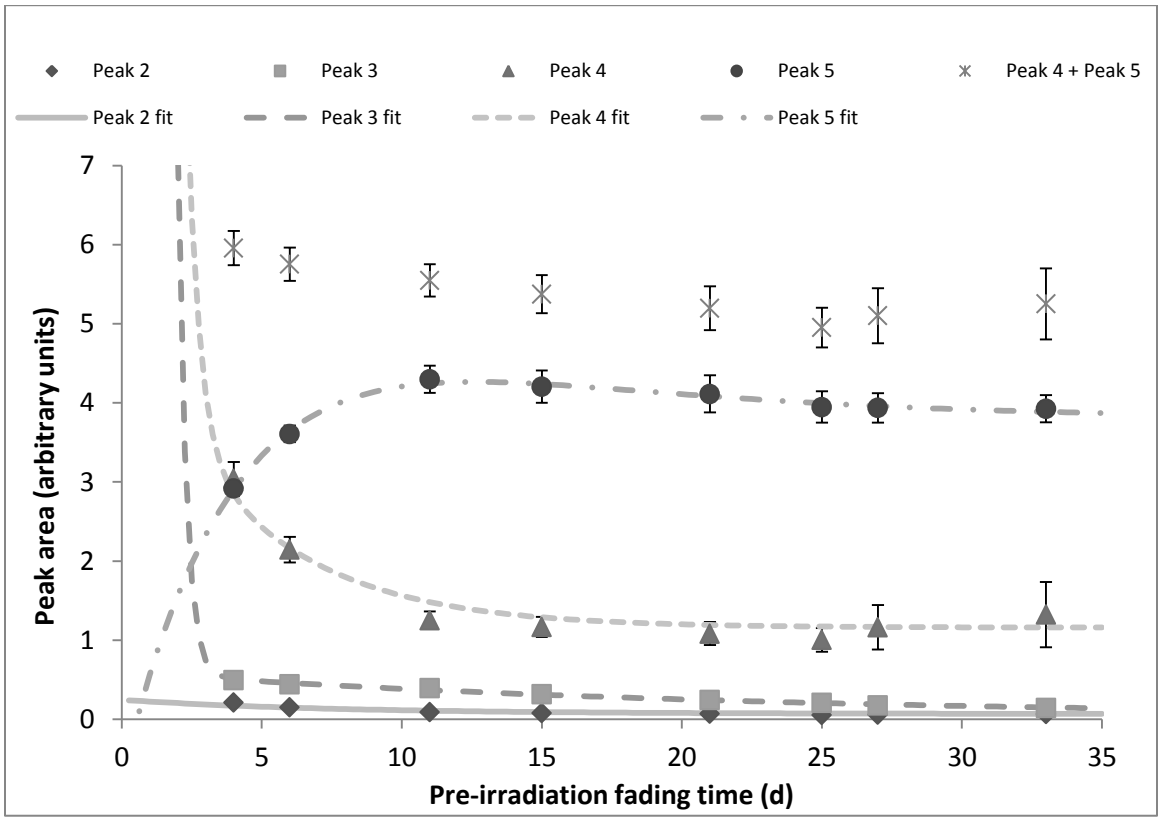

Fig 5.4. Evolution of the areas of peaks 2, 3, 4, and 5, and the sum of the areas of peaks 4 and 5, when subject to pre-irradiation fading at 40°C.

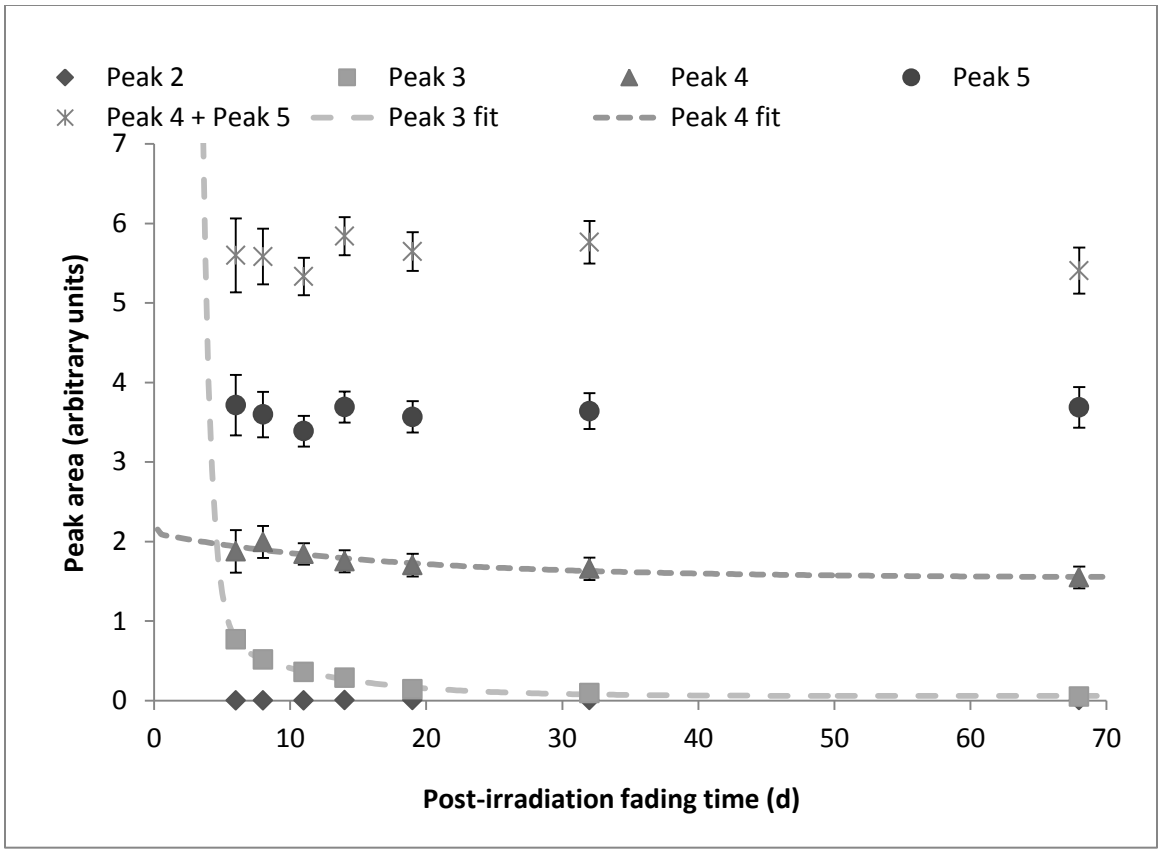

Fig 5.5. Evolution of the areas of peaks 2, 3, 4, and 5, and the sum of the areas of peaks 4 and 5, when subject to post-irradiation fading at 50°C.

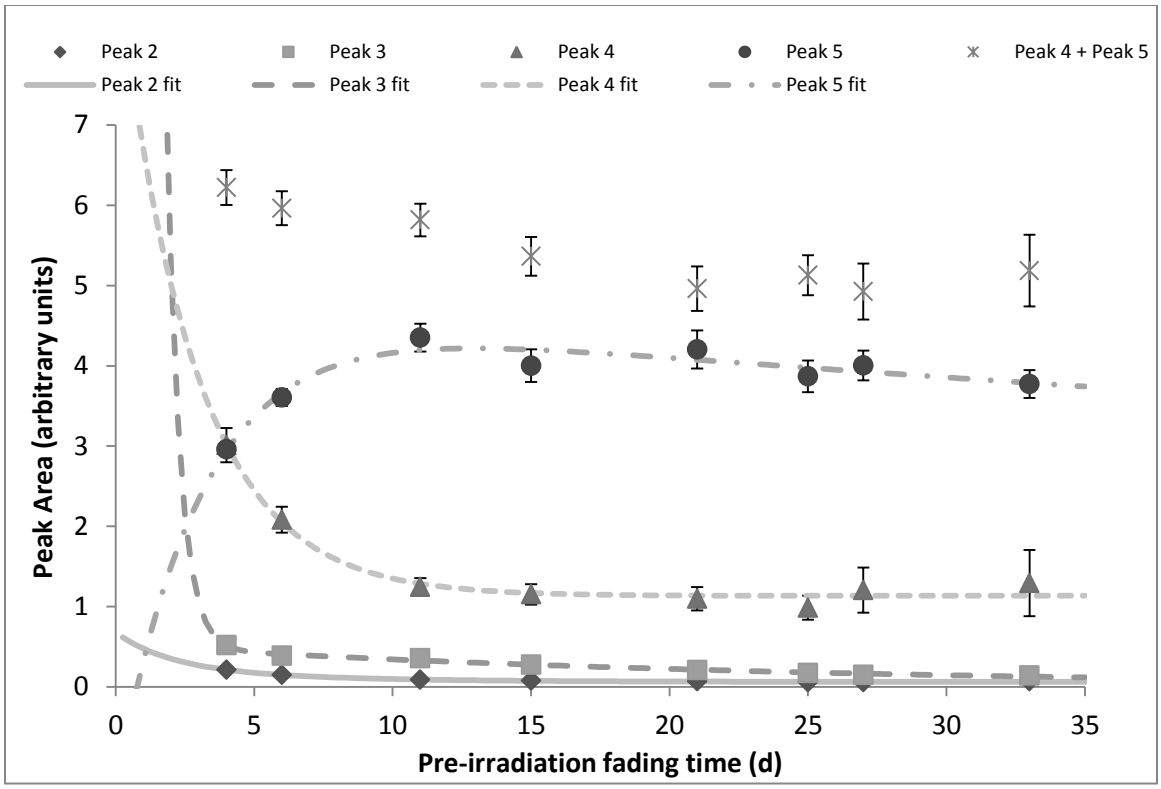

Fig 5.6. Evolution of the areas of peaks 2, 3, 4, and 5, and the sum of the areas of peaks 4 and 5, when subject to pre-irradiation fading at 50°C.

REFERENCES

Al-Haj A. N., Lagarde C. S., 2006. A study on the behaviour of TLD-100 glow peaks at extreme ambient temperatures in Riyadh, Saudi Arabia. Radiat. Prot. Dosim. 119(1-4):430-433.

Delgado A., Gomez Ros J. M., 1990. Modifications induced in the TLD-100 trap distribution during exposures at different ambient temperatures. Radiat. Prot. Dosim. 34(1-4):233-235.

Delgado A., Gomez Ros J. M., Muniz J. L., 1992. Temperature effects in LiF TLD-100 based environmental dosimetry. Radiat. Prot. Dosim. 45(1-4):101-105.

Harvey J. A., Haverland N. P., Kearfott K. J., 2010. Characterization of the glow-peak fading properties of six common thermoluminescent materials. Appl. Radiat. Isotopes 68:1988-2000.

Harvey J. A., Kearfott K. J., 2011. Reproducibility of glow peak fading characteristics of thermoluminescent dosimeters. Radiat. Meas. doi: 10.1016/j.radmeas.2011.01.005.

Harvey J. A., Rodrigues M. L., Kearfott K. J., 2011. A computerized glow curve analysis (GCA) method for WinREMS thermoluminescent dosimeter data using MATLAB. Appl. Radiat. Isotopes. In press.

Harvey J. A., Thomas E. M., Kearfott K. J., 2011. Quantification of various factors influencing the precision of thermoluminescent detector calibrations for new and used chip sets. Health Phys. In press.

Julius H. W., de Planque G., 1983. Influence of annealing and readout procedures on fading and sensitivity changes in LiF for temperatures and humidities typical for environmental and personnel dosimetry. Radiat. Prot. Dosim. 6(1-4):253-256.

McKeever S. W. S., Moscovitch M., Townsend P. D., 1995. Thermoluminescence Dosimetry Materials: Properties and Uses. Ashford, Kent, UK: Nuclear Technology Publishing.

McLaren C., Null J., Quinn J., 2005. Heat Stress from Enclosed Vehicles: Moderate Ambient Temperatures Cause Significant Temperature Rise in Enclosed Vehicles. Pediatrics 116:e109-e112.

Parker L. W., Harvey J. A., Kearfott K. J., 2011. An integrated system for the beta, gamma and neutron calibration and storage of thermoluminescent dosimeters for a research laboratory. Health Phys. 100(2):S43-S49.

Shachar B. B., Horowitz Y. S., 1992. Thermoluminescence in annealed and unannealed LiF:Mg,Ti (TLD-100, Harshaw) as a function of glow curve heating rate and using computerized glow curve deconvolution. J. Phys. D: Appl. Phys. 25:694-703.

Simpkins R. W., Kearfott K. J., 1997. The minimum number of observations necessary to develop an average thermoluminescent dosimeter element correction factor. Radiation Protection Management 13:55-61.

Studenski M. T., Haverland N. P., Kearfott K. J., 2007. Simulation, design, and construction of a 137Cs irradiation facility. Health Phys. 92:S78-S86.

Weinstein M. German U., Dubinsky S., Alfassi Z.B., 2003. On the determination of the post-irradiation time from the glow curve of TLD-100. Radiat. Prot. Dosim. 106:121-130.

Chapter VI

The Effects of High Ambient Radon on Thermoluminescent Dosimetry Readings

ABSTRACT

The effect of a high level of ambient ^{222}Rn gas on thermoluminescent dosimeters (TLDs) is examined. Groups of LiF:Mg,Ti and CaF_2:Dy TLDs were exposed to ^{222}Rn under controlled environmental conditions over approximately 7 d using a luminous ^{226}Ra aircraft dial. LiF:Mg,Ti TLDs were tested bare, and both types were tested mounted in cards used for environmental dosimetry and mounted in cards enclosed in plastic badges. A passive continuous radon monitor was used to measure the ^{222}Rn level in the small chamber during the experiments. The data were analyzed to determine the relationship between integrated ^{222}Rn level and TLD response. Although both LiF:Mg,Ti and CaF_2:Dy TLDs showed a strong response to ^{222}Rn, the badges prevented measurable radon detection by the TLDs within. The TLDs were not used to directly measure the radon concentration; rather, a correction for its influence was desired.

INTRODUCTION

Levels of indoor radon have been observed as high as 410 kBq m^{-3} in homes (Kearfott 1989), which can be enhanced through various unusual ventilation methods, such as underground air returns (Kearfott et al. 1992a, Kearfott et al. 1992b). Thermoluminescent dosimeters are used in a variety of workplace environments, including but not limited to subterranean or low-ventilation areas and locations near uranium mill tailings. Although these areas are more likely to contain ambient radon than those above ground level or with adequate ventilation, such as those found in homes, TLD readings are typically not examined nor corrected for the potentially elevated radon concentrations unrelated to occupational exposures. TLDs that show high signal may need to be adjusted for possible radon signal in order to determine the true dose from other external sources in high radon environments. This study is not intended to develop a novel method of radon detection, as superior inexpensive passive radon screening detection devices exist, such as activated charcoal (Lehnert and Kearfott 2010a, Zak et al. 2010). Rather, it is to establish that an existing dosimetry method may need to be corrected based on the presence of a high level of ambient radon.

Few previous studies of the effects of radon on TLDs exist. $CaSO_4$:Dy was found to function as a rudimentary radon detector when used as a thin foil as part of a specially designed apparatus for the measurement of near-surface soil gas (Ho and Weng 1981). CaF_2:Dy has also been found to respond to alpha and beta particles from radon progeny during short term exposures of less than 14 d (Brits and Van As 1984). TLDs are still used to measure background gamma radiation in experiments where another detector type, such as a track-etch detector, is used to measure radon (Anjos et al.2010). In cases such as these, TLDs may need to be corrected for the radon exposure as well. However, although attempts have been made to study the effects of ambient radon on direct reading pocket ionization chambers (Bergen et al. 2010), studies of signals produced by ambient radon on TLDs for the purposes of corrections to occupational readings are not readily available in the common literature.

The goal of this study was to determine if ^{222}Rn has a significant effect upon TLD types commonly used for personnel and environmental dosimetry, namely LiF:Mg,Ti (TLD-100) and CaF_2:Dy (TLD-200).

MATERIALS AND METHODS

Dosimeter types and calibration

TLD materials used in this experiment were 98 bare LiF:Mg,Ti dosimeter chips of dimensions 3.2 mm × 3.2 mm × 0.9 mm, and 60 dosimeter cards containing two LiF:Mg,Ti chips and two CaF_2:Dy chips of thickness 0.089 cm encased in 0.0076 cm thick polytetrafluoroethylene, held in an aluminum card. These cards are sold and intended to be used with a plastic badge, which shields all four dosimeters with 80 mg · cm^{-2} acrylonitrile butadiene styrene plastic and the CaF_2:Dy dosimeters shielded from the front and behind with an additional 0.025 cm of tantalum and 0.0051 cm of lead (Type 8807 Environmental Dosimeter, BICRON/Harshaw, 6801 Cochran Road, Solon, OH 44139, USA).

Before each experiment was performed, the TLDs to be used were calibrated to a dose of 4.4 mGy using a 320 GBq ^{137}Cs source (Model 28-8A Irradiator, J.L. Shepherd and Associates, 1010 Arroyo Avenue, San Fernando, CA 91340-8122, USA), in a specially designed facility (Studenski et al. 2007) while mounted to an appropriate calibration phantom (Parker et al. 2011), which also greatly facilitated handling of the bare chips. Three calibrations were performed for each TLD, a number previously determined to be adequate for similar systems (Simpkins and Kearfott 1997) and an optimal balance of precision and efficiency for TLDs of this type (Harvey et al. 2011).

After calibration, each of the TLDs or cards was subjected to an in-reader annealing procedure using a standard TLD reader with hot gas and hot planchet capabilities (Model 4500 TLD Reader, BICRON/Harshaw, 6801 Cochran Road, Solon, OH 44139, USA). Planchet heating mode was employed for the bare TLDs, and hot gas heating mode for the cards. Nitrogen gas (Pre-purified compressed nitrogen cylinder 300, Metro Welding Supply Corporation, 12620 Southfield Road, Detroit, MI 48223, USA) was kept flowing for the bare TLD planchet mode readouts to reduce oxygen induced light effects.

Experimental setup

Two small radon chambers were used in this experiment, made of converted 0.21 m^3 [55 U.S. gallon] steel drums (Lehnert and Kearfott 2010b), which had less leakage than prior small chamber designs (Moore and Kearfott 2005). These drums were mounted horizontally on a rack. In the bottom chamber, a luminous aircraft dial containing approximately 2.9 kBq of ^{226}Ra was placed on a purpose-built shelf held in the center of the chamber, surrounded by lead bricks so that radiation originating directly from the source, as opposed to the ^{222}Rn emitted, could be blocked and not contribute to signal in the TLDs. The top chamber was used as a control chamber, with no source other than radon found in the ambient laboratory air. Because radon is heavier than air, the migration of radon upwards from the experiment chamber was much less likely with such an arrangement. A shelf and lead bricks were also placed in this chamber to duplicate the conditions in the other, with the exception of the radium source. A passive continuous radon monitor (Model CRM-510LP, Femto-Tech Inc., P.O. Box 8257, 25 Eagle Court, Carlisle, OH 45005, USA) was placed in each chamber to measure the radon levels as functions of time as these were not in equilibrium throughout the experiment.

The set of 98 bare LiF:Mg,Ti TLDs was split into one group of 50, to be placed in the radon chamber, and one group of 48 for the control chamber. The set of 60 environmental dosimetry cards was first split into two equal groups, with 30 cards placed inside the badges and 30 for which badges were not used. These sets of 30 were then further subdivided into groups of 15, with one group of each placed in the radon chamber, and one group of each placed in the control chamber. The bare TLDs were stored in a ceramic holder with no lid, so that they could be directly exposed to any radon present, and placed on the bottom of the chamber. The cards and cards inside badges were placed directly on the bottom of the chamber, as was the continuous radon monitor. This was done to maximize radon exposure, as the radon was expected to sink to the bottom of the chamber immediately after emission from the radium source. Bare

cards were tested eight times, and bare TLD chips and cards inside badges were tested six times.

To ensure that the radiation background levels were similar in both chambers, a background radiation exposure test was conducted using a handheld survey meter containing a sodium iodide scintillator (Ludlum Model 19, Ludlum Measurements Inc., 501 Oak Street, Sweetwater, TX 79556 USA). After being run through a standard readout cycle, glow curves resulting from TLD readouts were integrated using the reader control software (WinREMS version PL-26732.8.0.0.0, BICRON/Harshaw, 6801 Cochran Road, Solon, OH 44139, USA). These data were then statistically analyzed using commercial spreadsheet software (Microsoft Excel 2010, Microsoft Corporation, One Microsoft Way, Redmond, WA 98052) and commercial statistical analysis software (SPSS 17.0, SPSS Inc., 233 S. Wacker Drive, 11th floor, Chicago, IL 60606).

RESULTS AND DISCUSSION

Bare LiF:Mg,Ti TLDs were significantly affected by a 7 d exposure to radon. Data from the radon chamber showed a clear increase in signal of 20% to 180% over the control chamber depending on trial, while the TLDs' signal from the radon chamber also exhibits a wider distribution, shown in Fig 6.1. As the radon level was not constant in the chambers, the hourly measurements of radon from the passive monitor were summed to obtain an integrated radon level for each experiment. These values were then compared to the signal obtained from the TLDs in the chambers. The radon level in the experimental chamber increased in a $1\text{-}e^{-kt}$ fashion during the experiments, reaching a maximum level of 5.6 to 9.3 kBq · m^{-3} at the end of 7 d. This level is significantly higher than those recommended as an action level by various agencies, which vary from 150 Bq · m^{-3} [4.0 pCi L^{-1}] to 200 Bq · m^{-3} for residential dwellings to as high as 400 Bq · m^{-3} to 1000 Bq · m^{-3} for the workplace (USEPA 2009, Denman 2008, ICRP 1994, IAEA 2003). Radon concentration in the control chamber was 40 Bq · m^{-3} on average for all experiments and did not increase or decrease significantly during the experiment periods.

Cards containing LiF:Mg,Ti and CaF_2:Dy also exhibited a significant signal increase when not contained in badges. LiF:Mg,Ti signal distributions show 20% to 40% separation between the radon and control chambers, as seen in Fig 6.2a. Due to the short deployment time of 7 d, the significantly higher sensitivity of CaF_2:Dy, from 15 to 30 times higher than LiF:Mg,Ti (Binder and Cameron 1969), and the lower response to environmental radiation due to its higher effective atomic number, this material shows an even greater difference, 50% to 80% separation and no overlap between the radon and control chamber data. Results of one of the eight experiments are shown in Fig 6.2b.

Cards contained in badges show no significant additional signal due to radon, if any. In fact, the CaF_2:Dy showed higher dose from the control chamber as opposed to the radon chamber. Although this was on average only 10% higher, a Student's *t*-test applied to the two data sets passes with $p = 0.45$, indicating no significant statistical difference between the two means. Fig 6.3 provides a visual comparison of the two groups' results.

The handheld survey meter gave a background radiation exposure rate value of $2.6 \cdot 10^{-9}$ C $\cdot$ kg$^{-1} \cdot$ h^{-1} in each chamber with a manufacturer stated uncertainty of 10%. Although the values in the two chambers were not significantly different, it should be noted that the radon chambers are located above the ^{137}Cs TLD calibration facility on a mezzanine that is part of a neutron generation facility (Studenski and Kearfott 2007). Background may have been present that could differed between the bottom and top chambers when either of the facilities were active, and the measurements were taken when neither the ^{137}Cs nor neutron facility were in use.

Although a 1% difference in the average sensitivities of the CaF_2:Dy elements in the two card sets used was noted, this was corrected for by calibration. However, there is inherent experimental error and variation contained in the calibration factors. A combination of these experimental uncertainties and systematic errors is believed to have caused possibly slight additional signal for the CaF_2:Dy elements in the cards encased in badges in the control chamber. It has been previously seen that even very small fluctuations in dose applied to a

TLD contained within a badge can cause significant effects on signal (Kearfott et al. 1995).

With the ability of LiF:Mg,Ti and CaF_2:Dy to detect radon established, this effect was then quantified by correlating the measured TLD signal with the integrated radon level over each 7 d test period. It is noted that several high signal outliers exist throughout the data, namely:

(1) two in the control group and one in the radon group for bare TLD chips;

(2) four in the radon group for LiF:Mg,Ti elements in bare cards;

(3) one in the control group for CaF_2:Dy elements in bare cards;

(4) one in the control group and two in the radon group for LiF:Mg,Ti elements in cards encased in badges;

(5) one in the control group for CaF_2:Dy elements in cards encased in badges.

These data points were eliminated from the radon concentration to dose correlation calculations using Chauvenet's criterion (Chauvenet 1871). In addition, all data from one LiF:Mg,Ti TLD in one card encased in a badge were discarded due to abnormally high signal observed during calibration. Although LiF:Mg,Ti did show a small correlation with integrated radon, the added dose of 31.6 μGy per MBq · m^{-3} · h of integrated radon concentration was slight compared to the average standard deviation of 5.0 to 12 μGy per MBq · m^{-3} · h in each group. This resulted in low correlation coefficients of $R^2 = 0.57$ for bare chips and $R^2 = 0.47$ for bare cards. CaF_2:Dy showed a much higher correlation of $R^2 = 0.87$ inside uncovered cards, with an added dose of 7.3 μGy per MBq · m^{-3} · h. These results are shown visually in Figs. 6.4 and 6.5. As no signal increase was seen with radon level for the cards encased in badges, no effort was made to correlate those data, shown in Fig 6.6.

Although each TLD element in a card was exposed to the same radon level, a significant difference in the dose calculated using a calibration to ^{137}Cs was observed. This discrepancy was likely due to the different gamma ray energies observed from ^{137}Cs, ^{222}Rn, and the progeny of ^{222}Rn, as well as the different gamma ray interaction properties of the two TLD materials studied.

Several gamma rays present in the ^{222}Rn decay chain, notably those emitted from the decay of ^{214}Pb at 242, 295, and 352 keV, are considerably lower in energy than ^{137}Cs at 662 keV. CaF_2, with its much higher effective atomic number, will more readily absorb the lower energy gamma rays from ^{214}Pb than LiF, causing an under-estimate of the dose from ^{222}Rn when a calibration to ^{137}Cs is used. Therefore, the doses calculated using the calibration to ^{137}Cs should not be considered absolute. For a true dose, a calibration to ^{222}Rn and its progeny would be required, preferably using a large, high concentration equilibrium radon chamber for which radon levels are well characterized.

Each experiment was performed over 7 d, enough to cause a small but significant amount of pre-irradiation and post-irradiation fading in both TLD types used, especially CaF_2:Dy (Harvey et al. 2010). Determining radon dose using TLDs alone would have to be adjusted for practical applications in which longer deployment times are used. For the radon concentrations seen here, peaking at 5.6 to 9.3 kBq · m^{-3} over 7 d, it was assumed that that fading affects the TLDs in both chambers similarly. In addition, since the radon concentration started at a low level and then increased, most of the imparted signal is at the end of the irradiation period, allowing less time for post-irradiation fading to occur before readout. Emphasis was placed on the difference between the control and radon chamber measurements, not the absolute dose received. Therefore, fading was disregarded and it will not be discussed further here.

The influence of radon on TLD cards cannot be due to alpha particles originating outside the cards. While both bare and card-encased TLDs were affected, the PTFE holding the TLDs in the cards has a density thickness of 16.8 mg · cm^{-2}. The most energetic alpha particle in the ^{222}Rn decay chain, that of ^{214}Po at 7.7 MeV, has an approximate range of 12 mg · cm^{-2} in silicon based on a figure from a reference text (Knoll 2010). This was then converted to an approximate range in PTFE using the Bragg-Kleeman Rule (Knoll 2010):

$$\frac{R_1}{R_0} \cong \frac{\rho_0 \sqrt{A_1}}{\rho_1 \sqrt{A_0}} \tag{6.1}$$

where R is the alpha particle range in cm, ρ represents the material density of 2.3 $g \cdot cm^{-3}$ for silicon and 2.2 $g \cdot cm^{-3}$ for PTFE, and A represents the effective atomic number of 14 for silicon and 9 for PTFE. Though the actual effective atomic number of PTFE will be between that of the constituent atoms carbon and fluorine, the higher value for fluorine is used as a conservative estimate. These values give an approximate range in PTFE of 10 $mg \cdot cm^{-3}$, less than the thickness of the material.

Therefore, it is much more likely that gamma rays or beta particles were responsible for the additional signal. However, it is possible that radon could have penetrated the PTFE, leading to alpha doses imparted on the TLDs directly. Radon progeny settling on the TLDs may have caused the high readings otherwise excluded using Chauvenet's criterion, as no high readings occurred during calibration in the ^{137}Cs facility.

Many institutions use a control badge in order to correct worker badges for radiation background. Subtracting its measurement from the worker badges would also correct for radon exposure, but only if the control badge is kept in a location with a similar radon level. That would require the control badge to be located in an area with similar ventilation and wall composition as well as at a similar height off the ground to the worker badges. In a facility with many different worker areas, especially those in which the rate of ventilation varies, it would be very difficult to ensure a uniform radon level through the facility. Multiple control badges could also be used, though that would require that workers do not often move throughout areas of the facility.

Special care should be taken in situations where TLDs are left unprotected, such as the usage of bare TLDs in medical facilities or the storage of cards. In these situations, any TLDs to be used should be annealed before deployment. Even when kept in an area shielded from background radiation, radon may easily penetrate inside and cause unintended exposure.

CONCLUSIONS

Results from the bare TLDs and uncovered TLD cards indicate that some care should be used when deploying TLDs in a high-radon environment. Bare or

sparsely shielded LiF:Mg,Ti TLDs exposed to integrated radon levels of 0.5 to 1.3 MBq · m^{-3} · h were shown to experience an increase in signal of 50% or higher and the more sensitive CaF_2:Dy TLDs experienced increases in signal of 75% or higher compared to a control chamber, with integrated radon 6.7 kBq · m^{-3} · h on average. It is noted, however, that these results are valid only for the card and badge enclosures tested, both of which are capable of blocking alpha particles and preventing the entrance of radon. It is recommended that institutions seeking to make corrections to their dosimetry protocols test their specific card and badge types individually in order to quantify the mitigation effect they may have on radon, if any.

Using the estimate generated by a calibration to ^{137}Cs, a LiF:Mg,Ti TLD over a typical deployment period of 30 d at a radon concentration equal to an action level of 200 Bq · m^{-3} would result in an additional dose of 2.2 μGy for chips in environmental cards and 4.6 μGy for bare chips. CaF_2:Dy chips in environmental cards would show an additional 1.1 μGy. Although the specific type of badge tested was found to be capable of resisting TLD signal influence from radon over a 7 d period, there are additional problems with assuming that radon will not affect badges as they are commonly used. The 7 d experimental period was fairly short compared to typical 30 to 90 d dosimetry deployments, and inert radon gas will eventually penetrate into anything not completely hermetically sealed, which is not typical of dosimetry badges.

It is recommended that TLDs showing abnormally high readings in areas not otherwise screened for radon that a radon test be performed, as high ambient radon may be the cause of a high TLD signal that could not be explained by an accidental exposure. It is vital that radon dose on the badge be distinguished from other dose, so that a high dose could be properly attributed to its source and the appropriate mitigation measures can be taken.

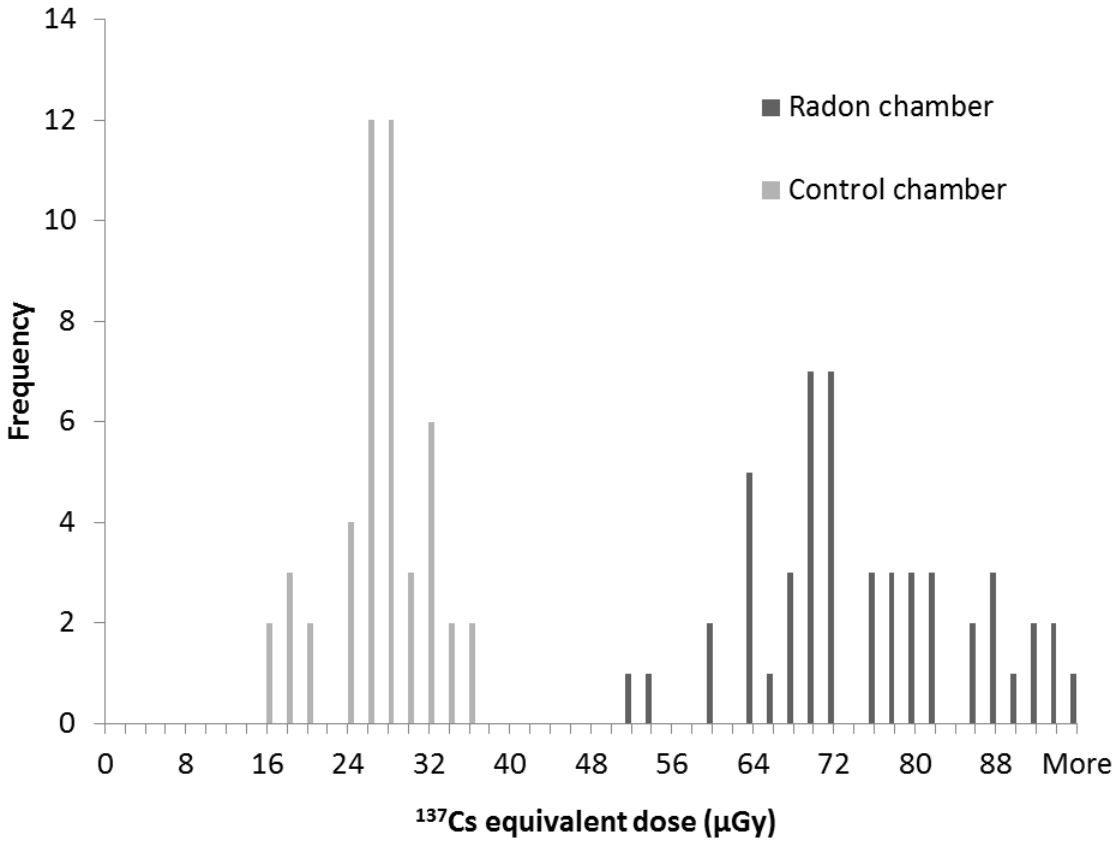

Fig 6.1. Histogram showing the results of one of six experiments comparing the absorbed dose, calculated using a calibration to ^{137}Cs, arising from bare LiF:Mg,Ti samples exposed to artificially high ambient radon and a normal, low radon level.

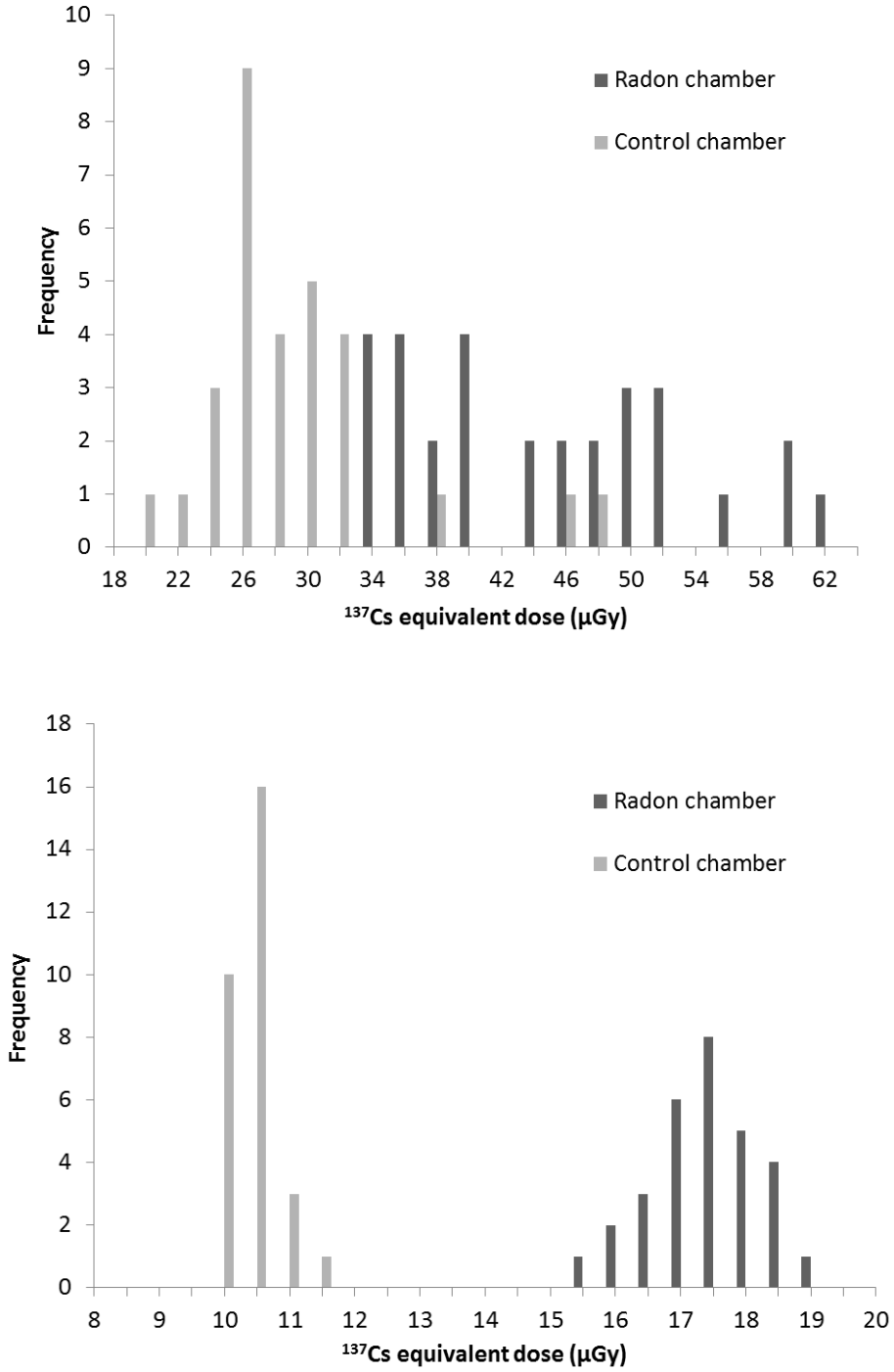

Fig 6.2. Histograms showing the results of one of eight experiments comparing the absorbed dose, calculated using a calibration to ^{137}Cs, arising from the (a) LiF:Mg,Ti and (b) CaF_2:Dy elements present in four-element cards exposed to artificially high ambient radon and a normal, low radon level.

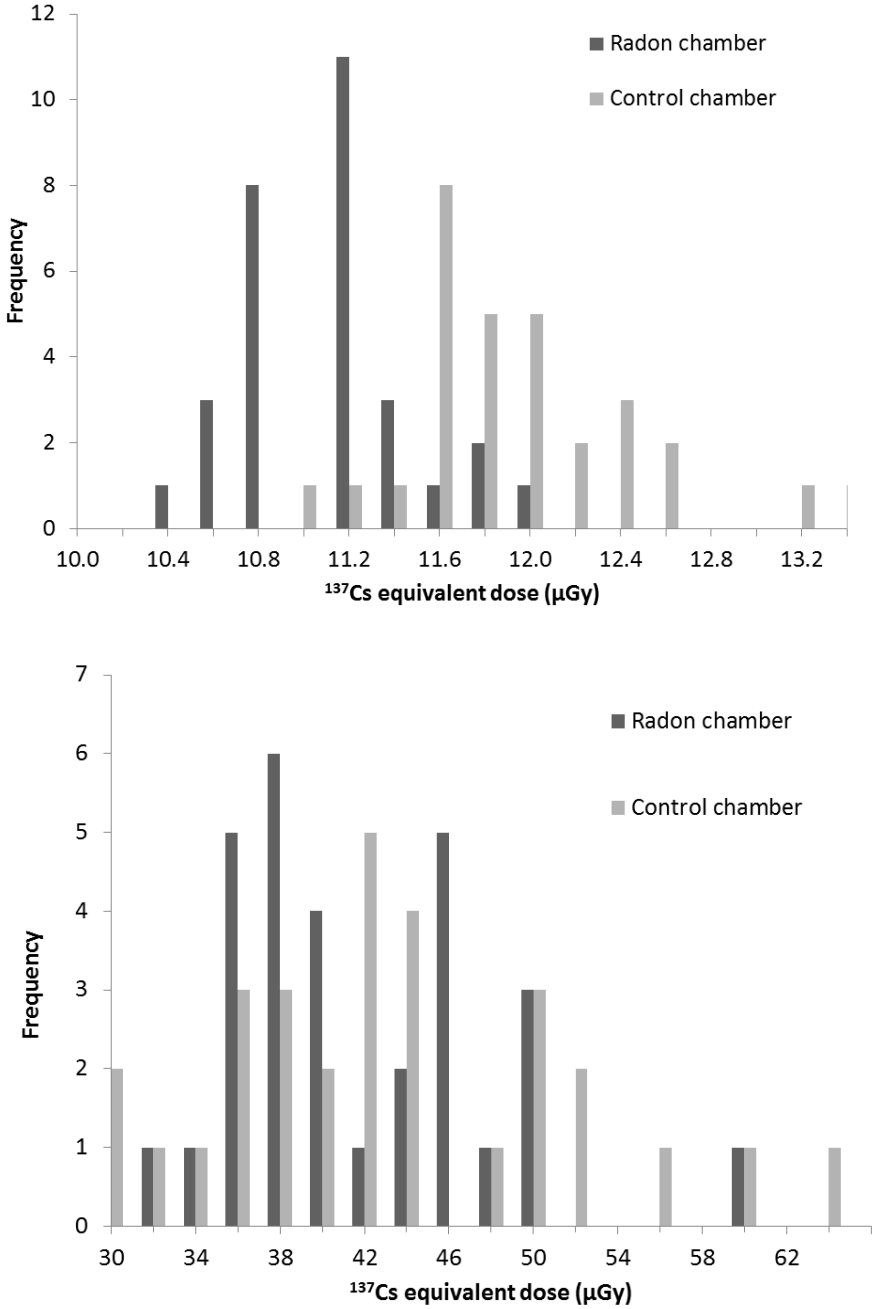

Fig 6.3. Histograms showing the results of one of six experiments comparing the absorbed dose, calculated using a calibration to ^{137}Cs, arising from the (a) LiF:Mg,Ti and (b) CaF_2:Dy elements present in four-element cards contained in plastic badges exposed to artificially high ambient radon and a normal, low radon level.

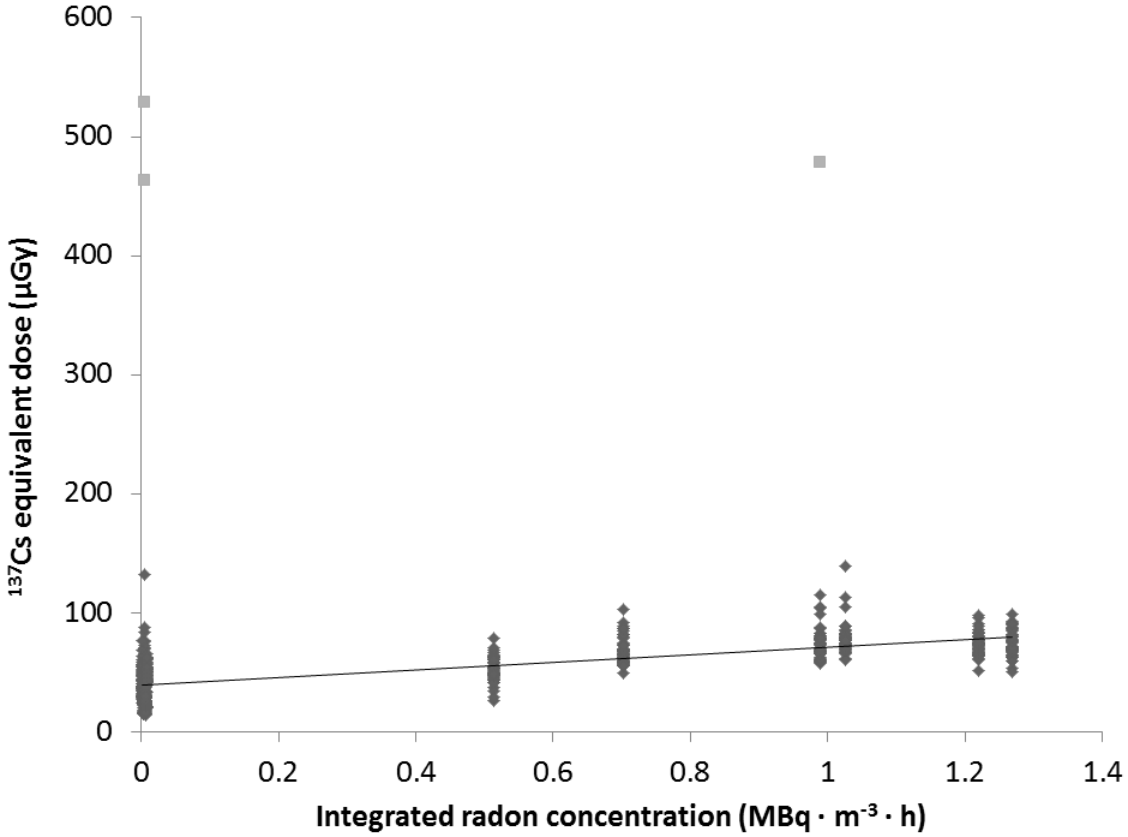

Fig 6.4. Correlation of the absorbed dose, calculated using a calibration to ^{137}Cs, arising from bare LiF:Mg,Ti samples exposed to various high levels of ambient radon and normal radon over a 7 d period. ^{137}Cs equivalent dose (D) was found to be related to integrated radon concentration (C) by the equation D [µGy] = 2.16 C [MBq · m^{-3} · h] + 2.86 with R^2 = 0.54.

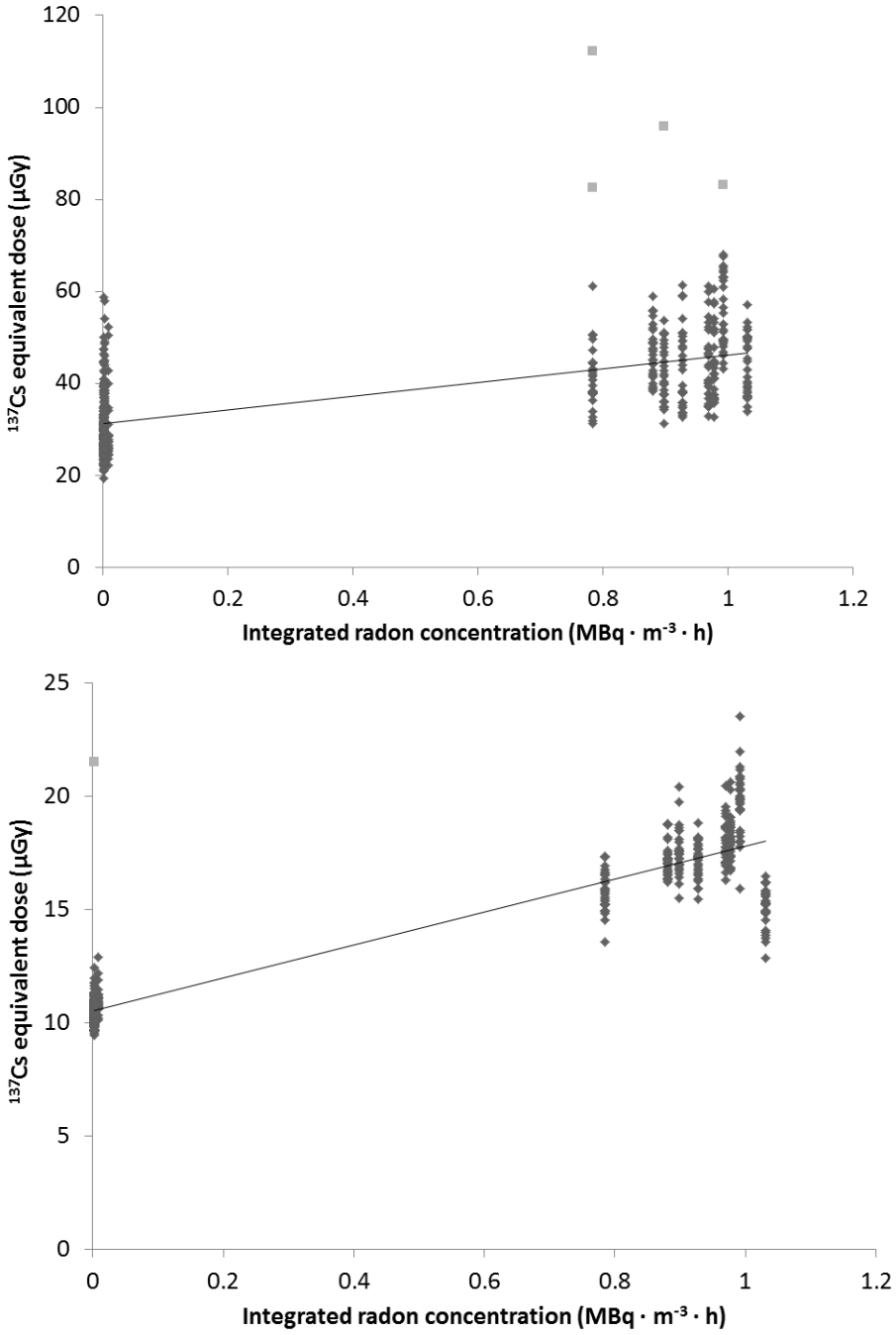

Fig 6.5. Correlation of the absorbed dose, calculated using a calibration to ^{137}Cs, arising from (a) LiF:Mg,Ti and (b) CaF_2:Dy samples present in four-element cards exposed to various high levels of ambient radon and normal radon over a 7 d period. ^{137}Cs equivalent dose (D) was found to be related to integrated radon concentration (C) by the equation D [µGy] = 14.9 C [MBq · m^{-3} · h] + 31.2 with R^2 = 0.45 for LiF:Mg,Ti and D [µGy] = 7.30 C [MBq · m^{-3} · h] + 10.5 with R^2 = 0.88 for CaF_2:Dy.

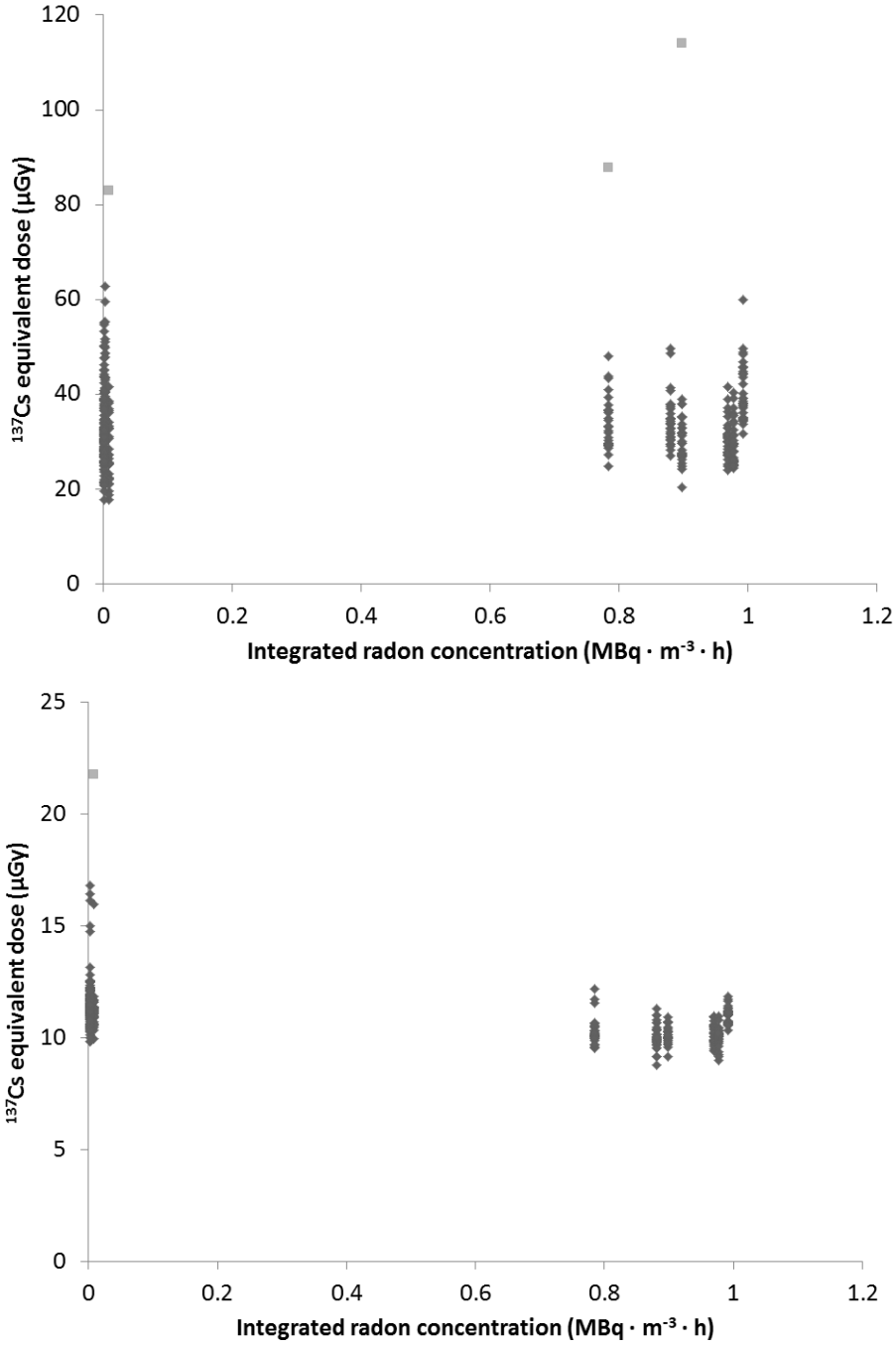

Fig 6.6. Correlation of the absorbed dose, calculated using a calibration to ^{137}Cs, arising from (a) LiF:Mg,Ti and (b) CaF_2:Dy samples present in four-element cards contained in plastic badges exposed to various high levels of ambient radon and normal radon over a 7 d period.

REFERENCES

Anjos R. M., Umisedo N., da Silva A. A. R., Estellita L., Rizzotto M., Yoshimura E. M., Velasco H., Santos A. M. A., 2010. Occupational exposure to radon and natural gamma radiation in the La Carolina, a former gold mine in San Luis Province, Argentina. J. Environ. Radioact. 101:153-158.

Bergen R. J., Harvey J. A., Kearfott K. J., 2010. Performance of vintage direct reading pocket ionization chambers. Health Phys. 98:S56-S62.

Binder W., Cameron J. R., 1969. Dosimetric properties of CaF2:Dy. Health Phys. 17:613-618.

Brits R. J. N., Van As D., 1984. Methodology for the measurement of radon with passive instruments. Radiat. Prot. Dosim. 2:219-221.

Chauvenet W., 1871. A manual of spherical and practical astronomy, volume II. Philadelphia: J.B. Lippincott Company. ISBN 1 103 929488.

Denman A. R., 2008. Applying the ionising radiation regulations to radon in the UK workplace. Rad. Prot. Dosim. 130:38-42.

Harvey J. A., Haverland N. P., Kearfott K. J., 2010. Characterization of the glow-peak fading properties of six common thermoluminescent materials. Appl. Radiat. Isotopes 68:1988-2000.

Harvey J. A., Thomas E. M., Kearfott K. J., 2011. Quantification of various factors influencing the precision of thermoluminescent detector calibrations for new and used chip sets. Health Phys. In press.

Ho W., Weng P.-S., 1981. Measurement of radon emanation rate in soil with thermoluminescent dosimeters. Int. J. Appl. Radiat. Isot. 32:521-523.

International Atomic Energy Agency, 2003. Radiation protection in workplaces other than mines. Safety Report Series No. 33. (Vienna: IAEA).

International Commission on Radiological Protection, 1994. Protection against radon-222 at home and at work. ICRP 65. Oxford: Pergamon Press.

Kearfott K. J., Han S., McMahan K. L., Samei E., 1995. Sensitivity of a mixed field dosimetry algorithm to uncertainties in thermoluminescent element readings. Health Phys. 68:340-349.

Kearfott K. J., Metzger R. L., Kraft K. R., Holbert K. E., 1992. Mitigation of elevated indoor radon gas resulting from underground air return usage. Health Phys. 63:674-680.

Kearfott K. J., Metzger R. L., Kraft K. R., Holbert K. E., 1992. Underground air returns as active transportation pathways for radon gas entry into homes", Health Phys. 63:665-673.

Kearfott K. J., 1989. Preliminary experiences with Rn-222 in Arizona homes. Health Phys. 56:169-179.

Knoll G. F., 2010. Radiation interactions. In: Radiation Detection and Measurement, 4th ed. New York: John Wiley & Sons.

Lehnert A. L., Kearfott K. J, 2010. An equilibrium-based model for measuring environmental radon using charcoal canisters. Health Phys. 99:S154-S163.

Lehnert A. L., Kearfott K. J., 2011. Application of an equilibrium-based model for diffusion barrier charcoal canisters in a small volume non-steady state radon chamber. Health Phys. 100(2):138-147.

Moore J. A., Kearfott K. J., 2005. A radon chamber for educational purposes. Health Phys. 89:S78-S84.

Parker L. W., Harvey J. A., Kearfott K. J., 2011. An integrated system for the beta, gamma and neutron calibration and storage of thermoluminescent dosimeters for a research laboratory. Health Phys. 100(2):S43-S49.

Simpkins R. W., Kearfott K. J., 1997. The minimum number of observations necessary to develop an average thermoluminescent dosimeter element correction factor. Radiation Protection Management 13:55-61.

Studenski M. T., Haverland N. P., Kearfott K. J., 2007. Simulation, design, and construction of a 137Cs irradiation facility. Health Phys. 92:S78-S86.

Studenski M. T., Kearfott K. J., 2007. Design and simulation of a neutron facility. Health Phys. 92:S37-S44.

United States Environmental Protection Agency, 2009. A citizen's guide to radon. EPA 402/K-09/001. Washington: United States Environmental Protection Agency.

Zak T., Thompson K. H., Ambers S. D., Fetterley J. A., Kearfott K. J., 2011. An intercomparison study of simultaneous radon measurements using two separate radon screening tests under as-deployed conditions. Health Phys. 100(2):S13-S20.

Chapter VII

A Computerized Glow Curve Analysis (GCA) Method for WinREMS Thermoluminescent Dosimeter Data Using MATLAB

ABSTRACT

A computerized glow curve analysis (GCA) program for handling of thermoluminescence data originating from WinREMS is presented. The MATLAB program fits the glow peaks using the first-order kinetics model. Tested materials are LiF:Mg,Ti, CaF_2:Dy, CaF_2:Tm, CaF_2:Mn, LiF:Mg,Cu,P, and $CaSO_4$:Dy, with most having an average figure of merit (FOM) of 1.3% or less, with $CaSO_4$:Dy 2.2% or less. Output is a list of fit parameters, peak areas, and graphs for each fit, evaluating each glow curve in 1.5 s or less.

Note: All MATLAB code referred to by this chapter may be found in the Appendix to this dissertation.

INTRODUCTION

The analysis of thermoluminescence data greatly benefits from the separation of a glow curve into individual glow peaks. This technique is especially useful if fading is to be studied. Glow curve analysis methods have been has been common for at least 30 years, with more recent versions aided by computerized implementations, commonly known as computerized glow curve analysis (GCA). Though previously, pure and modified Gaussian expressions were used for fitting glow peaks (Bos et al. 1993; Lang and Deme, 1997), the glow peak functions proposed by Kitis et al. (Kitis et al. 1998) much increased the accuracy of GCA programs by providing simple functions for first-order, second-order, and general order kinetics.

The main task performed by a GCA program, the separation of a glow curve into individual peaks, is the one that benefits most from a computer-aided methodology. The first-order kinetics model was chosen for its advantages of simplicity and fast convergence while still having high accuracy. The program was also intended to fit many glow curves consecutively, routinely 100 or more, so the ability to do batch processing was deemed highly important.

The present work aims to present a new GCA implementation using a standard commercially available mathematics package format (MATLAB R2008b with Curve Fitting Toolbox, The MathWorks Inc., 3 Apple Hill Drive, Natick, MA 01760), with input that can be obtained from the reader control software included with Harshaw thermoluminescence dosimeter (TLD) readers (WinREMS version PL-26732.8.0.0.0, BICRON/Harshaw, 6801 Cochran Road, Solon, OH 44139, USA). Previous GCA implementations have used programming languages that are efficient, but difficult to learn, edit, and use on computers with different operating systems (Chung et al., 2005). As this code does not need to be compiled, it is portable across a wide range of computers and easily modified by end users for their specific purposes.

METHODS

Model and fit method

A fitting equation describing a glow peak using first-order kinetics was described by Kitis et al. in 1998 as:

$$I(T) = I_m \exp\left[1 + \frac{E}{kT}\frac{T - T_m}{T_m} - \frac{T^2}{T_m^2} \times \exp\left(\frac{E}{kT}\frac{T - T_m}{T_m}\right)(1 - \Delta) - \Delta_m\right] \quad (7.1)$$

where *I(T)* is the peak intensity *I* at temperature *T* in K, I_m is the intensity at the peak maximum, *E* is the activation energy in eV, *k* is the Boltzmann constant in eV K^{-1}, T_m is the temperature at the peak maximum in K, Δ is $2kT(E)^{-1}$ and Δ_m is $2kT_m(E)^{-1}$. The GCA program fits the glow curve data to a sum of functions similar to equation 1, with different terms *E, T,* T_m and I_m for each peak, using a least-squares method for non-linear functions and the Levenberg-Marquardt algorithm for minimization.

Levenberg-Marquardt was chosen for its robustness over the Gauss-Newton method also available to MATLAB, despite its lower convergence rate (Salas-Gonzalez et al. 2008). Although first-order kinetics is only valid when using a linear time-temperature profile (TTP), WinREMS cannot use nonlinear TTPs and hence the code can be used for separation of any glow curve arising from WinREMS data. Although robustness was not tested with respect to serious variations in reader performance that impact shapes of glow curves, the program was devised to handle reasonable variations such as those defined in the literature (Samei et al. 1994, Harvey et al. 2011).

By varying the number of peaks and initial fitting parameters, multiple types of glow GCA programs were constructed, for LiF:Mg,Ti, CaF_2:Dy, CaF_2:Tm, CaF_2:Mn, LiF:Mg,Cu,P, and $CaSO_4$:Dy (TLD-100, TLD-200, TLD-300, TLD-400, TLD-700H, TLD-900 respectively; BICRON/Harshaw, 6801 Cochran Road, Solon, OH 44139, USA). The number of peaks and fitting parameters T_m and *E* were determined for each TLD type through trial and error using sources from the literature as starting points until the best possible fits were obtained. MATLAB functions were written, one for each TLD type, called by the main GCA program

when necessary. When these fitting functions are called, a graph of the original glow curve data, total fit function, and individual peak functions are shown for visual analysis by the user as well as saved for later reference. The horizontal axis of the graph shows the temperature of the planchet or hot gas, unlike WinREMS, which displays the horizontal axis as signal collected over time from the light collection device, with the temperature on a second vertical axis. This was necessary to properly fit the kinetics equation, which is with respect to temperature, and is done by plotting the glow curve data directly against the TTP data.

Goodness of fit

The "goodness of fit" is judged objectively using the figure of merit (FOM) approach. This was first used to describe fits to gamma ray spectral peaks (Balian and Eddy 1976), but has since been commonly used to compare GCA programs (Bos et al. 1994). The FOM in percent is defined as

$$FOM = \sum_{j_{start}}^{j_{stop}} \frac{\left| y_j - y\left(x_j\right) \right|}{A} \times 100 \tag{7.2}$$

where j_{start} is initial temperature in the fit region, j_{stop} is the ending temperature in the fit region, y_j is the photomultiplier tube (PMT) current at temperature j, $y(x_j)$ is the value of the fit function at channel j, and A is the area under the peak, i.e., the integral of the fit function between j_{start} and j_{stop}. The original authors of the FOM equation considered a good fit to have an FOM of less than 2.5% (Balian and Eddy 1976), and a value on the order of a few percent has been suggested to indicate an accurate fit for GCA programs (Horowitz and Yossian 1995), though for this program a more rigorous goal of 2.0% was used. This was not an unreasonable goal, as a comparison study of GCA programs by Bos et al. found 11 out of the 13 tested to have FOM values of 1.75% or less (Bos et al. 1994).

Data input/output and batch processing

A main GCA program was written to handle processing of input files, multiple glow curve fits, and the appropriate output to data files. On execution, the user is prompted for TLD type and approximate dose, after which the input data files are read and an output file in comma separated variable (CSV) format is opened. The fitting function appropriate to the TLD type is called and a loop started over all TLDs if chips were used, or two loops started with cards, then chips, if cards were used. Then, the fitting program appropriate to the TLD type is called, with dosimeter number, dose entered by the user, glow curve data, and TTP data passed to it. A flow chart of the main program and one such fitting function is shown in Fig. 1.

The glow curve and TTP data were obtained from WinREMS by exporting it using two modified configuration files, which output the data in two files as follows, one line per TLD element:

"Dosimeter_ID", YYYYMMDD, HHMMSS, *A*

where *A* is a sequence of comma-separated values A_i over all TLD chips *i* representing the PMT current in nA for each channel, for all channels. The TTP data are represented similarly, where A_i is instead a sequence of comma-separated values representing the temperature of the heating element or heated nitrogen gas present while the corresponding channel was read. These two files were then named "MM_DD_YYYY_S_g1.asc" and "MM_DD_YYYY_S_h1.asc" for the glow curve and TTP data respectively, where S is a sequence number which may be used to differentiate multiple readouts performed on the same day. Though these data files are generated in Microsoft Windows (Microsoft Windows XP with Service Pack 3, One Microsoft Way, Redmond, WA 98052, YSA), they are formatted in plain text and can be used by MATLAB executed on Linux (Red Hat Enterprise Linux 5.5, Red Hat Inc., 1801 Varsity Drive, Raleigh, NC 27606, USA) and Mac OS (Mac OS 10.6.4, Apple Inc., 1 Infinite Loop, Cupertino, CA 95014, USA) platforms.

Output from the fitting function includes a screenshot of the graph as a JPG image file, and the fit parameters and peak areas passed back to the original program, which are written in the CSV file. The CSV file is in a format that can be read by a standard spreadsheet program as follows:

seq_num, tal, chip_num, date, time, FOM, {E}, {I}, {T}, {A}

Where “seq_num” is the dosimeter ID; “tal” is the order in which the dosimeter was read by the code, starting with 1; “date” is the date read in YYYYMMDD format; and “time” is the time in HHMMSS format. These are followed by the sequences E, I, T, and A, which are lists of the eccentricity parameters, height (intensity) parameters, temperature parameters, and peak areas respectively. Each set of parameters is given first as the lower bound used to fit, then the upper bound used to fit, then the actual fit value. Peak areas are calculated by summing the area under the fit curve, and are in arbitrary units. The fit values for the exponential background curve are also included for LiF:Mg,Ti.

Experimental testing

The GCA program was then tested on six sets of 20 TLD elements, one set of each type that can be processed by the program. All TLDs were 0.3175 cm × 0.3175 cm × 0.0889 cm chips, except for LiF:Mg,Cu,P, which were disks of diameter 0.36 cm and thickness 0.038 cm. With a maximum of 24 h of pre-irradiation and 1 h of post-irradiation fading, irradiations were done with a beta-shielded 320 GBq ^{137}Cs source to 44 µGy, 88 µGy, 0.13 mGy, 0.18 mGy, 0.22 mGy, 0.44 mGy, 0.66 mGy, 0.88 mGy, 2.2 mGy, 4.4 mGy, 6.6 mGy, and 8.8 mGy. Irradiations were also done to 4.4 mGy with significant pre-irradiation and post-irradiation fading, with the results published previously (Harvey et al. 2010, Harvey and Kearfott 2011). All irradiations were done in a specially designed facility (Studenski et al. 2007) with TLDs mounted to a custom designed phantom (Parker et al. 2011). Readout was performed with a standard TLD reader with hot gas and hot planchet capabilities (Model 4500 TLD Reader, BICRON/Harshaw,

6801 Cochran Road, Solon, OH 44139, USA) using manufacturer recommended TTPs, except for LiF:Mg,Cu,P, where an incorrect TTP was used. This TTP started at 50°C with no preheat with an acquisition rate of 10°C s^{-1} up to 240°C, and annealed at 240°C for 10 s.

RESULTS

Three of the materials were found to fit well to the number of peaks described in literature sources. These were LiF:Mg,Ti with four peaks (Horowitz et al., 2006), CaF_2:Dy with nine peaks (Yazici et al., 2002), and CaF_2:Tm with eight peaks (Skopec et al., 2006).

The three other materials required more extensive trial and error in order to produce acceptable fits. LiF:Mg,Cu,P has been described as having three main peaks (Horowitz, 1993), however, the addition of a fourth high temperature peak above the main dosimetric peak P_4 was necessary to obtain a good fit. CaF_2:Mn similarly required one more peak than the two previously observed (Allen and McKeever, 1990), resulting in three peaks that were closely spaced but discrete. $CaSO_4$:Dy was the most problematic to fit, as an additional two peaks were necessary in the low temperature region to adequately fit the curve, augmenting the four described in the literature (Souza et al., 1994). These six low temperature peaks in addition to the main dosimetric peak gives a total of seven peaks needed to describe $CaSO_4$:Dy for low dose irradiations. A more detailed account of the process of obtaining the number of peaks for each dosimeter type, as well as a table of fitting parameters, may be found in a previously published work (Harvey et al. 2010).

FOM varied somewhat for each TLD type, with five of six types under the 2.0% goal. The average FOM with 100 chips irradiated to 4.4 mGy was 1.3% for LiF:Mg,Ti; 0.99% for CaF_2:Dy; 0.84% for CaF_2:Tm; 0.82% for CaF_2:Mn; 0.46% for LiF:Mg,Cu,P; and 2.2% for $CaSO_4$:Dy. Other FOM statistics are found in Table 1.

$CaSO_4$:Dy exhibited significant darkening during readout, despite using the manufacturer recommended TTP. A high temperature tail was also observed, leading to the poor FOM value for that material. This may have been due to

blackbody radiation. Figs. 7.2 through 7.7 show example fits for the six tested TLD types and are normalized to the same arbitrary units.

Calculation time required for each curve was mostly consistent for each TLD type, averaging 0.5 to 1.5 s per graph generated. Although the program has a relatively long run time compared to other programs of this type, the ease of modification and operating system portability afforded by MATLAB is judged to offset the lengthier computation time of a program that is not compiled before execution. The code was tested successfully on various platforms, including Microsoft Windows XP, Windows Vista, Windows 7, Red Hat Enterprise Linux, and Apple Mac OS X, under a wide range of processor specifications ranging from an Intel Pentium III at 933 MHz to an Intel Core 2 Duo at 2.26 GHz.

CONCLUSIONS

Separation of glow curves from various thermoluminescent materials was performed efficiently and effectively in MATLAB for WinREMS data. The code can be used in any computing environment that MATLAB itself supports. Several dosimeter types were tested to show that the fitting method is valid for nearly any type of TLD, provided that the user knows or is able to determine the initial variable constraints for that TLD type. Closely overlapping glow peaks could be determined accurately, allowing even complex glow curves to be fit properly.

Over a wide range of irradiation doses, FOM values were below 2.0% for nearly all glow curve fits except for $CaSO_4$:Dy due to abnormal darkening of those chips during readout. Despite this, FOM values for $CaSO_4$:Dy was still 2.2% on average. When fading was present, initial variable constraints for some peaks needed to be adjusted manually in order for the observed data to fit well. Other than for that reason, the code does not typically need to be changed by the user. As such, new users unfamiliar with TLDs, WinREMS, and even MATLAB could be trained to use the code effectively by a skilled user in less than 1 h.

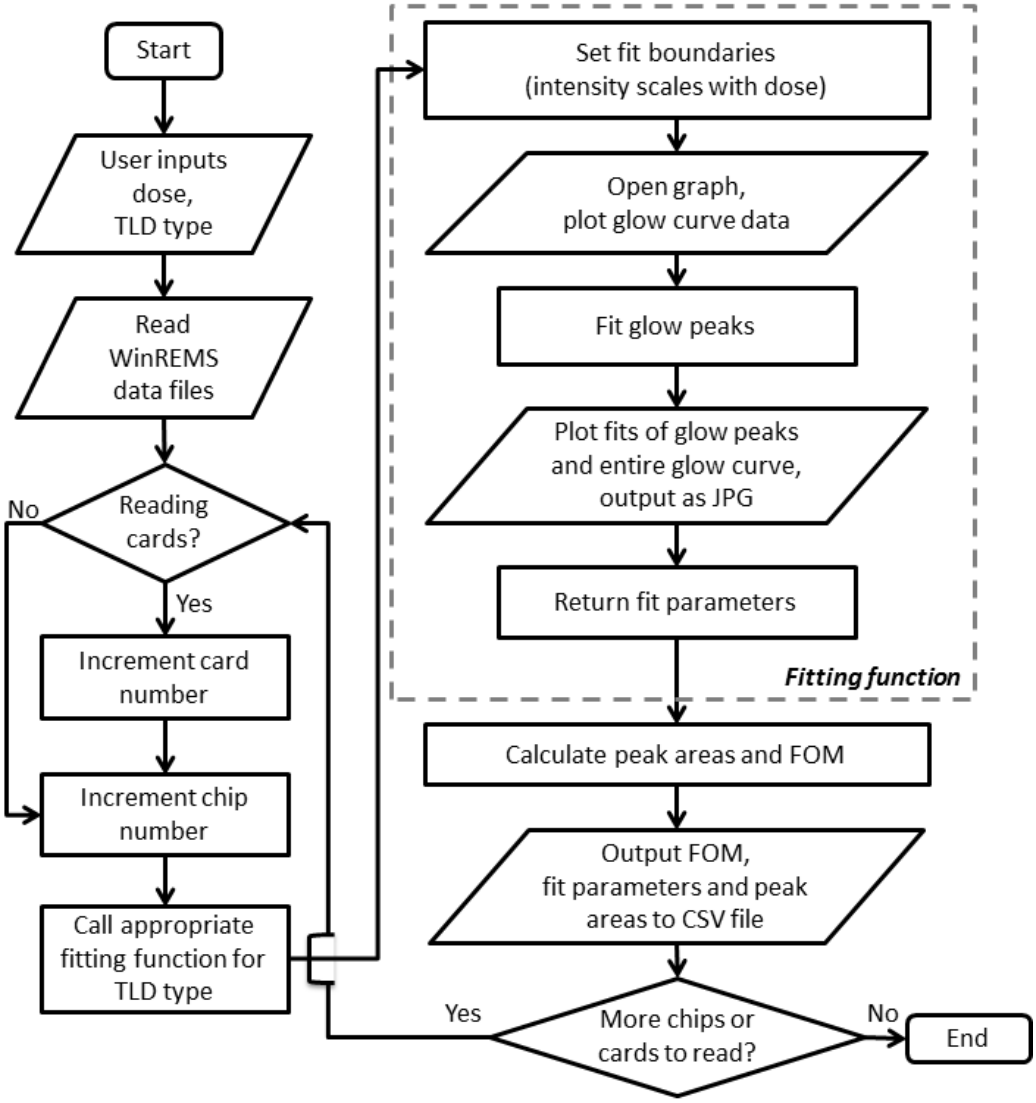

Fig 7.1. Flow chart of entire computerized glow curve analysis program. The fitting function called by the main code is given in the dashed box.

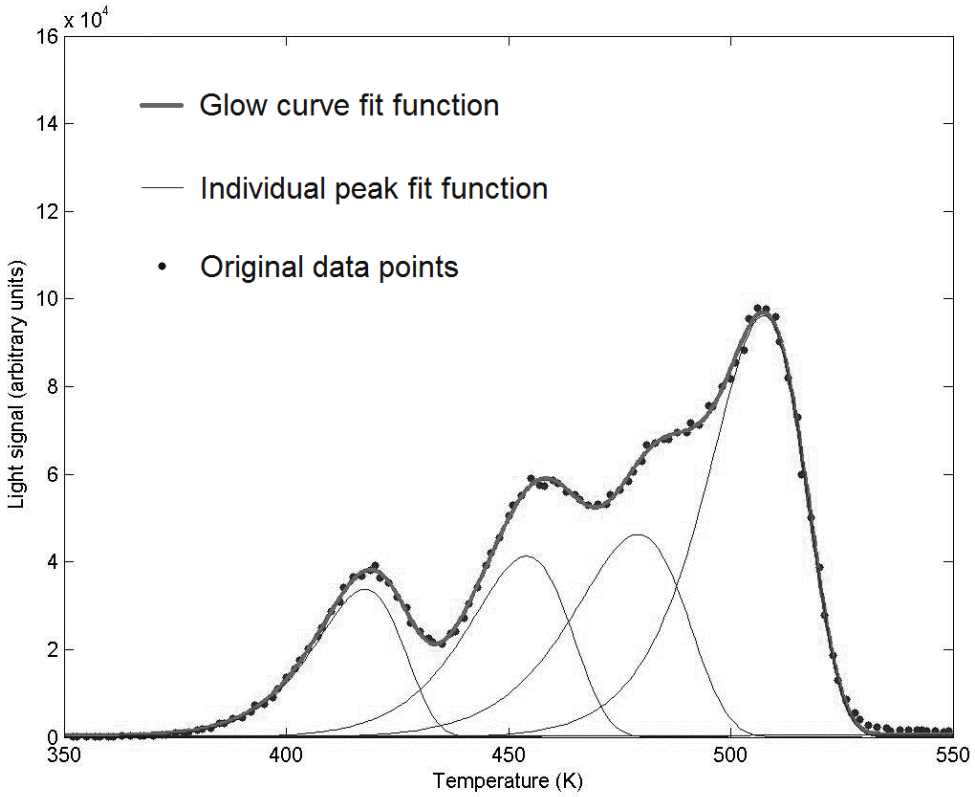

Fig 7.2. Output of computerized glow curve analysis program for LiF:Mg,Ti irradiated to 4.4 mGy with 662 keV gamma rays from 137Cs. The figure of merit is 1.4%.

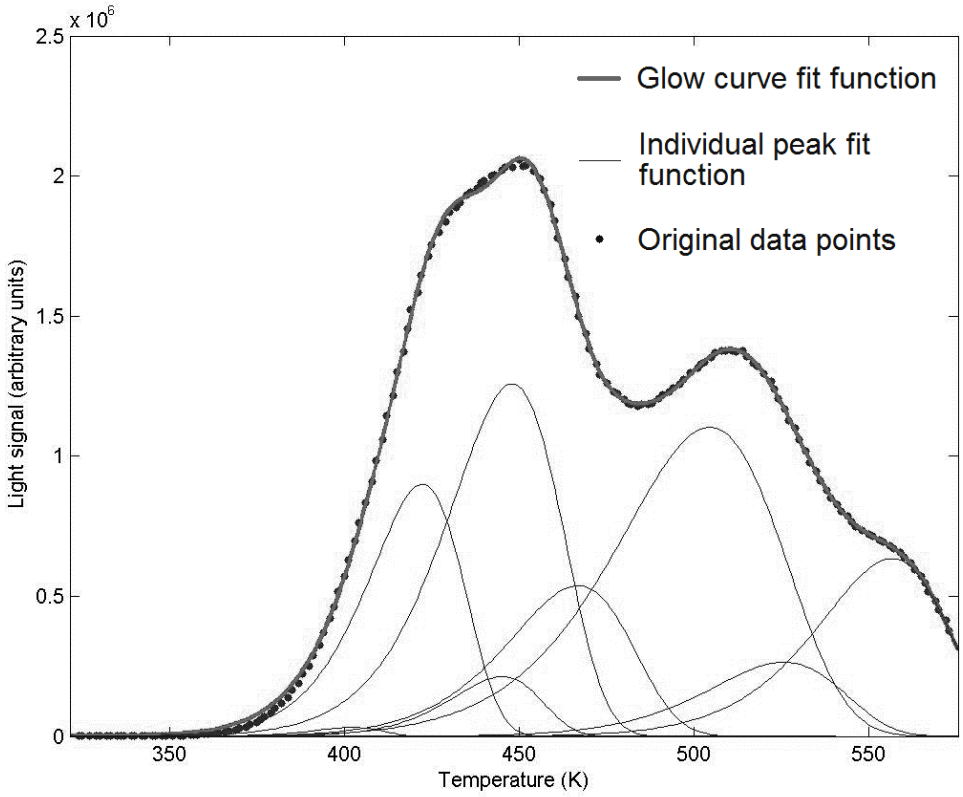

Fig 7.3. Output of computerized glow curve analysis program for CaF_2:Dy irradiated to 4.4 mGy with 662 keV gamma rays from ^{137}Cs. The figure of merit is 0.68%.

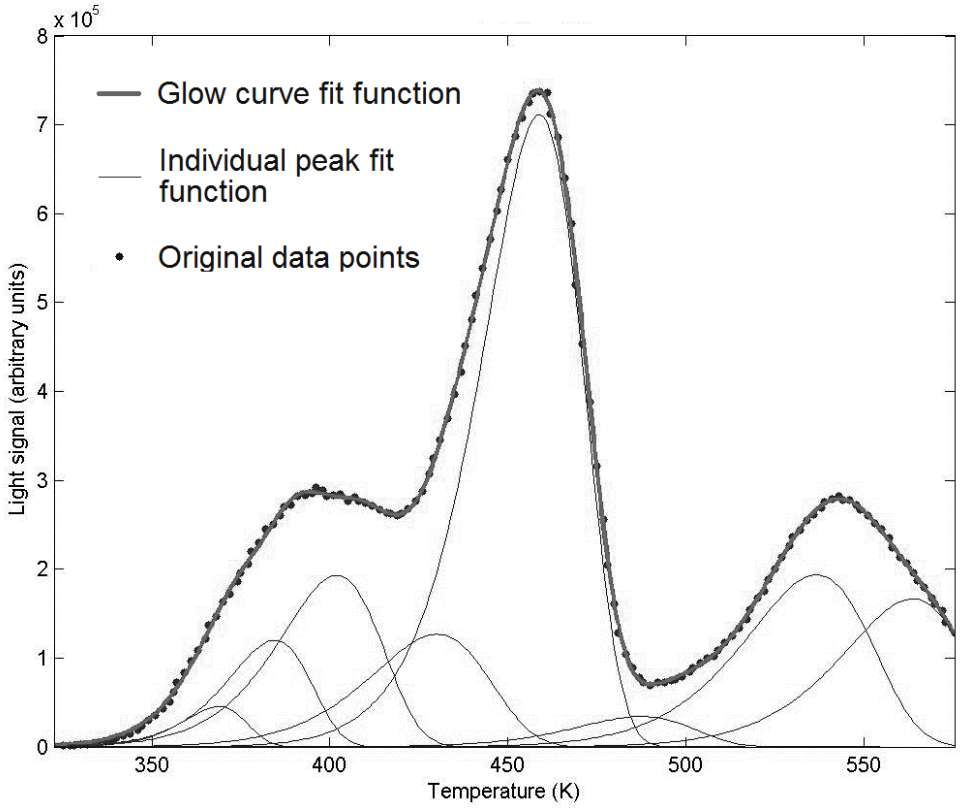

Fig 7.4. Output of computerized glow curve analysis program for CaF_2:Tm irradiated to 4.4 mGy with 662 keV gamma rays from ^{137}Cs. The figure of merit is 0.65%.

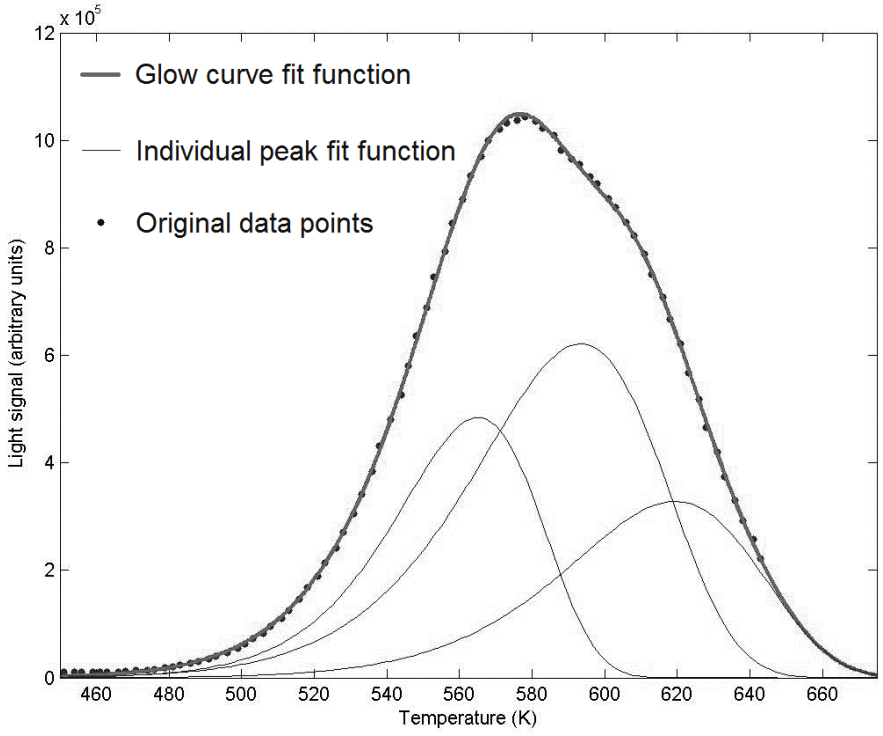

Fig 7.5. Output of computerized glow curve analysis program for CaF_2:Mn irradiated to 4.4 mGy with 662 keV gamma rays from ^{137}Cs. The figure of merit is 0.93%.

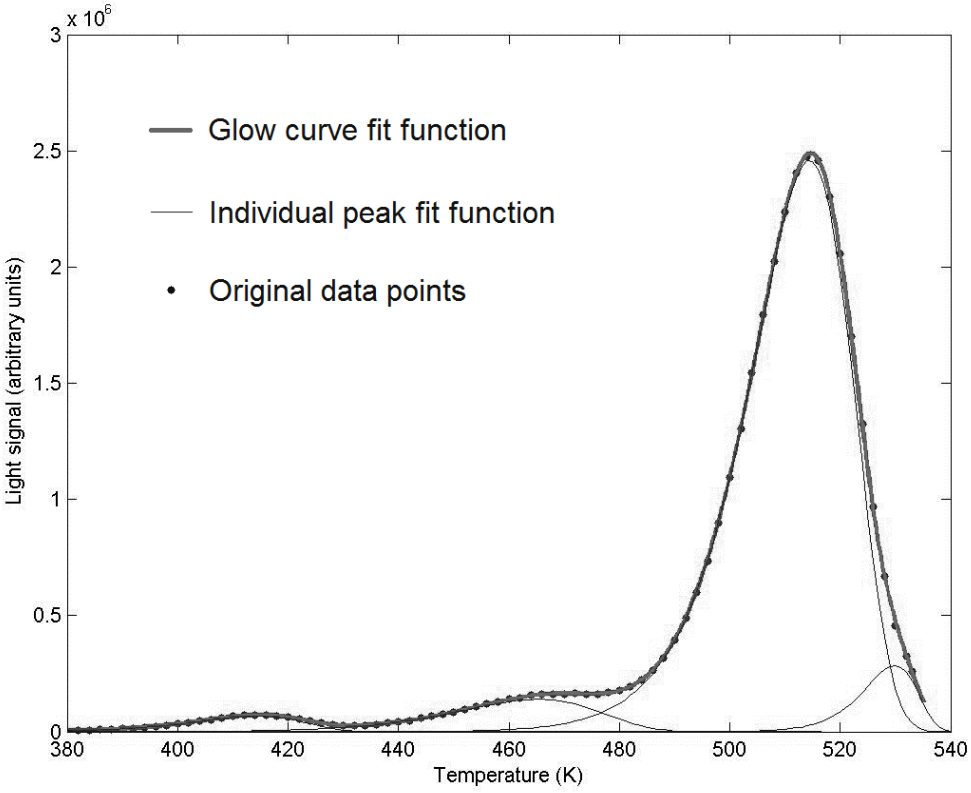

Fig 7.6. Output of computerized glow curve analysis program for LiF:Mg,Cu,P irradiated to 4.4 mGy with 662 keV gamma rays from ^{137}Cs. The figure of merit is 0.29%.

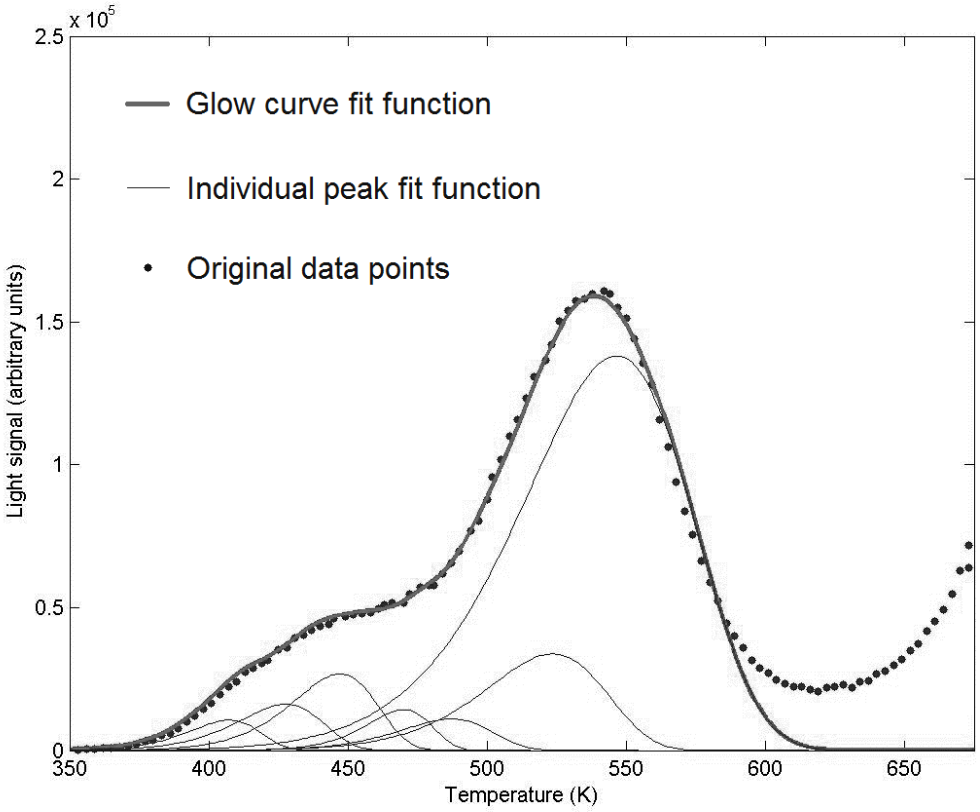

Fig 7.7. Output of computerized glow curve analysis program for $CaSO_4$:Dy irradiated to 4.4 mGy with 662 keV gamma rays from ^{137}Cs. The figure of merit is 2.8%.

Table 7.1. Number of peaks fit and figure of merit statistics for thermoluminescent dosimeter types tested with computerized glow curve analysis program using 20 elements of each type.

Material	***Peaks***	***FOM average (%) ± 1 standard deviation***	***FOM minimum (%)***	***FOM maximum (%)***
LiF:Mg,Ti	4	1.34 ± 0.102	1.11	1.48
CaF_2:Dy	9	0.993 ± 0.183	0.692	1.25
CaF_2:Tm	8	0.841 ± 0.377	0.642	2.05
CaF_2:Mn	3	0.820 ± 0.0809	0.718	0.933
LiF:Mg,Cu,P	4	0.459 ± 0.289	0.263	1.144
$CaSO_4$:Dy	7	2.15 ± 0.604	0.944	3.29

REFERENCES

Allen P., McKeever S.W.S., 1990. Studies of PTTL and OSL in TLD-400. Radiat. Prot. Dosim. 33:19-22.

Balian H. G., Eddy N. W., 1977. Figure-of-merit (FOM), an improved criterion over the normalized chi-squared test for assessing goodness-of fit of gamma-ray spectra peaks. Nucl. Instrum. Methods 145:389-395.

Bos A. J. J., Piters T. M., Gomez Ros, J. M., Delgado A., 1993. An intercomparison of glow curve analysis computer programs: I. Synthetic glow curves. Radiat. Prot. Dosim. 47(1-4):483-487.

Bos A. J. J., Piters T. M., Gomez Ros J. M., Delgado A., 1994. An intercomparison of glow curve analysis computer programs: II. Measured glow curves. Radiat. Prot. Dosim. 51(4):257-264.

Chung K. S., Choe H. S., Lee J. I., Kim J. L., Chang S. Y., 2005. A computer program for the deconvolution of thermoluminescence glow curves. Rad. Prot. Dosim. 115(1-4):345-349.

Harvey J. A., Haverland N. P., Kearfott K. J., 2010. Characterization of the glow-peak fading properties of six common thermoluminescent materials. Appl. Radiat. Isotopes 68, 1988-2000.

Harvey J. A., Kearfott K. J., 2011. Reproducibility of glow peak fading characteristics of thermoluminescent dosimeters. Radiat. Meas. doi: 10.1016/j.radmeas.2011.01.005.

Harvey J. A., Thomas E. M., Kearfott K. J., 2011. Quantification of various factors influencing the precision of thermoluminescent detector calibrations for new and used chip sets. Health Phys. In press.

Horowitz Y. S., Yossian D., 1995. Computerised glow curve deconvolution: application to thermoluminescence dosimetry. Radiat. Prot. Dosim. 60(1).

Horowitz Y.S., 1993. LiF:Mg,Ti versus LiF:Mg,Cu,P: The competition heats up. Radiat. Prot. Dosim. 47:135-141.

Horowitz Y.S., Satinger D., Avila O., 2006. Track structure approach to the calculation of peak 5a to peak 5 (TLD-100) relative intensities following heavy charged particle irradiation. Radiat. Prot. Dosim. 119:45-48.

Kitis G., Gomez-Ros J. M., Tuyn J. W. N., 1998. Thermoluminescence glow-curve deconvolution functions for first, second and general orders of kinetics. J. Phys. D: Appl. Phys. 31:2636-2641.

Lang E., Deme S., 1997. A glow curve fitting method for portable TLD readers using $CaSO_4$:Dy detectors. Radiat. Prot. Dosim. 74(1-2):93-96.

Parker L.W., Harvey J.A., Kearfott K.J., 2011. An integrated system for the beta, gamma and neutron calibration and storage of thermoluminescent dosimeters for a research laboratory. Health Phys. 100(2):S43-S49.

Samei E., Kearfott K. J., Wang C.-K., Han S., 1994. Impact of variations in physical parameters on glow curves for planchet heating of TL dosimeters. Nucl. Instrum. Meth. A, 353(1-3):415-419.

Skopec M., Loew M., Price J.L., Guardala N., Moscovitch, M., 2006. Discrimination of photon from proton irradiation using glow curve feature extraction and vector analysis. Radiat. Prot. Dosim. 120:268-272.

Salas-Gonzalez D., Gorriz J. M., Ramirez J., Lassl A., Puntonet C. G., 2008. Improved Gauss-Newton optimisation methods in affine registration of SPECT brain images. Electron. Lett. 44(22):1291-1292.

Souza J. H., Rosa L. A. R. D., Mauricio C. L. P., 1993. On the thermoluminescence glow curve of $CaSO_4$:Dy. Radiat. Prot. Dosim. 47:103-106.

Studenski M. T., Haverland N. P., Kearfott K. J, 2007. Simulation, Design, and Construction of a ^{137}Cs Irradiation Facility. Health Phys. 92:S78-S86.

Yazici A.N., Chen R., Solak S., Yagingil Z., 2002. The analysis of thermoluminescent glow peaks of CaF_2:Dy (TLD-200) after β-irradiation. J. Phys. D: Appl. Phys. 35:2526-2535.

Chapter VIII

Dose Response Linearity and Practical Factors Influencing Minimum Detectable Dose for Various Thermoluminescent Detector Types

ABSTRACT

The minimum detectable dose limit was examined in four different ways for groups of LiF:Mg,Ti thermoluminescent dosimeters (TLDs), and two ways for CaF_2:Dy, CaF_2:Tm, CaF_2:Mn, and $CaSO_4$:Dy dosimeters. All five dosimeter types were irradiated at doses ranging from 6.6 mGy to 8.8 μGy to determine if the linear dose-response relationship would be lost at very low doses. Linearity was never lost for any dose tested, indicating that loss of linearity is below the common minimum detectable dose. As an ideal minimum detectable dose, the dark current inherent to the TLD reader's light sensor, a photomultiplier tube, was compared to the signal arising from true doses for comparison, resulting in equivalent doses of 0.04 to 0.1 μGy. The effect of high ambient radon exposure on the minimum detectable dose was examined for LiF:Mg,Ti using previously derived detection and determination limits for TLDs. Pre-irradiation and post-irradiation fading functions were also compared to detection and determination limits to determine the fading time required for the signal from various prompt doses to fall below the detection and determination limits.

INTRODUCTION

Different detector types can be compared through their ability to determine a minimum amount of radioactive material. This is dependent on the background radiation level, absolute detection efficiency, radiation source properties, and time of deployment, the last of which being the only one fully under the control of the user. All radiation detector types benefit from a longer deployment time in order to determine if a minimum detectable amount exists. A general treatment of the lower limits of any measurement process involving radiation defines the detection limit L_D and determination limit L_Q (Currie 1968). These were defined in that work as "true" net signal level which may be expected to lead to detection, and the level at which the measurement precision will be satisfactory for quantitative detection respectively. The detection limit for any detector was given by Currie as

$$L_D = k_\alpha \sigma_b + k_\beta \sigma_D \tag{8.1}$$

where α and β are the false positive and false negative probabilities, respectively, and k_α and k_β come from the standard normal distribution and correspond to one-sided confidence levels of 1 – α and 1 – β.

For a TLD, however, which quantifies radiation in terms of delivered dose rather than detected counts, further work was required to determine the detection and determination limits, derived by Hirning (Hirning 1992). Hirning reworked Currie's equation for the detection limit L_D for a TLD as follows:

$$L_D = \frac{2(t_n s_b + t_m^2 s_\mu^2 \bar{K}_b)}{1 - t_m^2 s_\mu^2} \tag{8.2}$$

where t_m, t_n are Student *t*-factors for sample sizes of *n* and *m* dosimeters at the required confidence level, s_b is the sample standard deviation of *n* background dosimeters, s_μ is the relative standard deviation of *m* high kerma (where high kerma means significantly higher than background) dosimeters, and $\bar{K}_b$ is the measured background air kerma. However, the detection limit is only the boundary at which a TLD can be determined to have had any non-background exposure at all. To specify the minimum air kerma that can be measured with a given precision, the determination limit L_Q can be used (Hirning 1992):

$$L_Q = \frac{k_Q^2 s_\mu^2 \bar{K}_b + \left[k_Q^4 s_\mu^4 \bar{K}_b^2 + k_Q^2 s_b^2 (1 - k_Q^2 s_\mu^2)\right]^{1/2}}{(1 - k_Q^2 s_\mu^2)} \quad (8.3)$$

where s_b, s_μ, and $\bar{K}_b$ are as before, and k_Q is the inverse of the maximum relative standard deviation desired for the measurement.

Other minimum detectable dose limits inherent to the reader and dosimeters also exist in addition to the statistical limits given above. Even if background and fading were completely negligible, the dark current present in the reader's light collection device, such as a photomultiplier tube (PMT), would serve as a lower limit to any dose measurement, as no signal weaker than the dark current would appear on readout. This would serve as an ideal lower limit, if no other factors inherent to the dosimeters or the environment were significant.

Additionally, accurate measurement of dose is also reliant upon it falling within the dosimeters' linear dose-response region, in which the signal emitted upon heating is directly proportional to dose. Outside this region, accurate dose quantification is hindered by supralinearity, or over-response in proportion to dose, and sublinearity, or under-response in proportion to dose. Although deviations from linearity can be corrected for with detailed measurement protocols and additional in-depth calibration (Knoll 2010b), the breakdown of dose-response linearity at low doses is an important factor to consider when quoting a minimum detectable dose. If additional calibration is not possible or practical, the minimum value of the linear region would provide another minimum detectable dose limit. This value has been stated in the literature (Busuoli 1981) to be as high as 100 μGy for LiF:Mg,Ti, and as low as 1 μGy for CaF_2:Mn and 0.1 μGy for CaF_2:Dy.

Realistic TLD deployments last between 30 and 90 d, and as such deployment time needs to be considered. Additional deployment time can increase the minimum detectable dose limit, as longer deployments increase the background signal $\bar{K}_b$ in a linear fashion with time as well as the sample standard deviation of background dosimeters s_b in a square root fashion following the statistics of accumulation times (Traino et al. 1998).

In addition to accumulated background signal, however, long deployment times may cause the effect of fading to be significant. In the case of LiF:Mg,Ti over a typical deployment period of 30 to 90 d, the sum of peaks 4 and 5 do not fade significantly, even at high ambient temperatures up to 40°C (Harvey 2011). If peaks 2 and 3 are considered as well, their fading could cause the signal actually seen to drop below the minimum detectable signal level. Known fading rates could be used to augment a time-sensitive minimum detectable dose function with the time it takes for a certain prompt dose to fade below the limit.

Finally, at low doses, individual glow curve peaks may not be discernable by the computer if using a computerized glow curve analysis program. If such a program is necessary for the desired dosimetry application, such as for determination of post-irradiation time in LiF:Mg,Ti, which requires the measurement of the areas of peaks 3, 4, and 5 (Weinstein et al. 2003) and no other limit applies, some dosimetry applications may not be possible once the individual peaks in a glow curve are no longer separable by the computer.

MATERIALS AND METHODS

Dose-response linearity experiment

Twenty TLD chips each of LiF:Mg,Ti, CaF_2:Dy, CaF_2:Tm, CaF_2:Mn, and $CaSO_4$:Dy were used in an experiment to determine the minimum detectable dose for each type. All chips were of dimensions 3.2 mm × 3.2 mm × 0.9 mm. These were calibrated to a dose of 4.4 mGy using a 320 GBq ^{137}Cs source facility (Studenski et al., 2007) while mounted to a polytetrafluoroethylene calibration phantom (Parker et al., 2011).

Each TLD was calibrated three times, deemed adequate for characterization of individual chip sensitivities (Harvey et al. 2011, Simpkins and Kearfott 1997), then read out with a standard TLD reader with hot gas and hot planchet capabilities (Model 4500 TLD Reader, BICRON/Harshaw, 6801 Cochran Road, Solon, OH 44139, USA). Readout cycles were performed using nitrogen gas (Pre-purified compressed nitrogen cylinder 300, Metro Welding Supply Corporation, 12620 Southfield Road, Detroit, MI 48223, USA) flowing

through the chamber to suppress light effects that occur only with oxygen present, such as triboluminescence (McKeever et al. 1995). Annealing was performed using a standard readout cycle, during which the planchet was heated to 50°C, then heated to 300°C at a rate of 10°C s^{-1}. The planchet was held at 300°C until 33.3 s after the cycle started, then cooled to 50°C where the TLD chip could then be replaced.

After calibration, the TLDs were exposed to 6.6 mGy, a relatively high dose compared to the manufacturer's stated minimum detectable dose of 100 µGy. To see if dose response linearity failed at doses lower than the manufacturer's stated minimum detectable dose, the process was then repeated for incrementally lower doses of 2.2 mGy, 880 µGy, 660 µGy, 440 µGy, 220 µGy, 180 µGy, 130 µGy, 90 µGy, 40 µGy, and 8.8 µGy. Lower doses could not be tested due to the relatively high strength of the source.

A maximum of 24 h of pre-irradiation and 1 h of post-irradiation fading was allowed to occur in between annealing and readout. The glow curve data were obtained using the packaged TLD reader software (WinREMS version PL-26732.8.0.0.0, BICRON/Harshaw, 6801 Cochran Road, Solon, OH 44139, USA) and the glow curve separated into individual glow peaks using a computerized glow curve analysis (GCA) program (Harvey et al. 2011) for a numerical computing package (MATLAB R2010b, The MathWorks Inc., 3 Apple Hill Drive, Natick, MA 01760).

At the lowest dose levels, the dark current was observed and compared to the maximum glow peak height. An approximate dose was determined from the dark current signal, in order to determine the ideal minimum detectable dose were dark current the only contributor. Fading and background radiation dose was ignored for this experiment.

During all other experiments, the GCA program used was observed for analysis of low dose glow curves to determine if the computer had more difficulty with or was unable to perform the separation of individual glow peaks from the glow curve at low doses. This was order to determine if a lower dose limit applies

should GCA be necessary for desired dosimetry applications. Additionally, the figure of merit (FOM), a common metric

Detection and determination limits

In order to obtain detection and determination limits proposed by Hirning, equations 8.2 and 8.3, influences on the three main factors present in both equations were determined. These are sample standard deviation s_b, measured background air kerma $\overline{K}_b$, and relative standard deviation of high kerma dosimeters s_μ.

Several factors inherent to the reader, dosimeters, and calibration contribute to dosimeter signal precision, increasing s_μ. These include reader drift, TLD readout history, source and dosimeter positioning if calibrating multiple dosimeters at once. Though difficult to quantify separately, these can be corrected for to result in an s_μ of 10% or less for new or nearly new dosimeters. An increase in the number of calibrations beyond that which is normally necessary for dosimetry can decrease the statistical variance for high kerma dosimeters as well, reducing s_μ accordingly.

Factors not involving irradiation, such as reader drift, may contribute to s_b as well. However, previous work has shown s_b to be dominated by background signal, varying with time according to the statistics of accumulation times as background signal is accumulated (Traino et al. 1998).

Factors contributing to background signal, increasing $\overline{K}_b$, will cause s_b to increase as well as it is not a relative value. In addition to background radiation at the storage location, radon can also increase background signal for TLDs (Harvey and Kearfott 2011). For personnel dosimetry, movement through multiple areas may change background signal with time dramatically, though for simplicity this effect was ignored, with background signal assumed to be constant with time.

Data from a previous work (Harvey et al. 2011) was used to apply fading to a previous study (Traino et al. 1998) of the effect of deployment time on the detection and determination limits. Though fading did not significantly affect s_μ, s_b

or $\overline{K}_b$, it may cause the TLD signal to drop below the signal required for a minimum detectable dose with a prompt measurement. All of the above factors were manipulated individually in order to determine their practical effects on the detection and determination limits.

RESULTS AND DISCUSSION

Linearity was confirmed in all five tested TLD materials from 8.8 mGy to 8.8 μGy, as shown in Fig. 8.1. R^2 correlation values were 0.997 or greater over the entire dose range for all TLD materials tested, confirming dose-response linearity. Although linearity on the high range was expected, as TLD materials have been previously shown (Busuoli 1981) to exhibit dose-response linearity to at least 1 Gy, the dose response remained linear down to the lowest tested dose level, with R^2 values of 0.987 or greater over the low dose range 8.8 μGy to 0.88 mGy. Low dose results may be seen more clearly in Fig. 8.2.

Below 180 μGy, the individual glow peaks of LiF:Mg,Ti blended together, with the GCA program requiring as many as ten times more iterations to separate the glow curve accurately. Below 88 μGy, the GCA program became ineffective, unable to separate the glow peaks at all. An example of this peak blending seen at 44 μGy is shown in Fig. 8.3. Despite this, the total glow curve area remained linear with dose. Glow curves from all other TLD types could still be separated accurately down to 8.8 μGy, the lowest dose tested.

In addition, the simple use of a GCA program causes an increase in s_μ. As the fitted functions for sum of the individual glow peaks does not exactly match the original glow curve data, a small error is imparted when using peak areas computed by the program instead of the total glow peak area measured directly from the original TLD reader's light sensor data. A typical measure of the goodness of fit of a GCA program, the figure of merit (FOM), quantifies this effect (Bos et al. 1994):

$$FOM = \sum_{j_{start}}^{j_{stop}} \frac{\left| y_j - y(x_j) \right|}{A} \times 100 \qquad (7\text{-}2)$$

where A is area under the individual peak or the entire glow curve, j_{start} and j_{stop} are the starting and ending temperatures in the fit region respectively, y_j is light sensor current (in this case, a photomultiplier tube) at temperature j, and $y(x_j)$ is the value of the fit function at temperature j. A value of 1.75% or less is typical of GCA programs. The effect of a larger FOM on s_μ is difficult to quantify in general, as it depends on GCA program parameters, the number of peaks in the TLD material studied, and the high kerma dosimeter set size at a minimum. If the absolute minimization of dose limits is desired, a computerized glow curve analysis method should be avoided.

A thermoluminescent signal from a TLD can be obscured by background radiation or dark current. If background radiation is ignored, one way of defining the minimum detectable dose is that which is perceptible above the dark current level. For the TLD reader used for this study with LiF:Mg,Ti, the PMT dark current's equivalent dose level is stated to be less than 1 µGy by the manufacturer. This was verified by comparing values of the dark current level to the maximum of the tallest peak of the glow curve for each TLD material tested. Each was found to be less than 1 µGy, with results summarized in Table 8.1.

The presence or absence of radon, though previously found to affect background signal, and hence $\overline{K}_b$, in bare LiF:Mg,Ti TLDs, was not found to significantly affect s_b. Even in TLD groups not exposed to additional radon, s_b fluctuated by as much as 20% from group to group. Background signal showed an increase of 2.16 µGy for each MBq · m^{-3} · h of integrated radon. The effect of high radon concentrations up to 37 kBq · m^{-3} for a 7 d exposure, using a fixed radiation background air kerma rate of 0.131 µGy · h^{-1}, is shown in Fig. 8.4. Values used in Fig. 8.4 used in equations 8.2 and 8.3 were s_μ = 0.0519, s_b = 4.71, $\overline{K}_b$ = 14.7 µGy, and k_Q = 10.

As variance in $\overline{K}_b$ alone has little effect on the detection and determination limits, very large radon concentrations are required before a significant difference is seen. A radon concentration of 18.5 kBq · m^{-3} for 7 d is required to cause a 10% increase in the 71 µGy determination limit, and no significant difference was found in the detection limit. Compared to the United States Environmental

Protection Agency's action level of 148 Bq · m^{-3} (USEPA 2009), a very high radon concentration is required to have a significant effect on minimum detectable dose, though quantities as high as 410 kBq · m^{-3} have been measured in homes (Kearfott 1989). If extrapolated to this value, the determination limit becomes 230 µGy, a clearly non-trivial increase; the detection limit only increases from 16 to 18 µGy.

In order to determine the effect of deployment time on the minimum dose limits, modifications were made to equations 8.2 and 8.3 by Traino et al. to replace the background air kerma $\bar{K}_b$ and the sample standard deviation of dosimeters exposed to background s_b with parameters that account for the accumulation of background radiation dose with time. In so doing, the background air kerma was found to be $\bar{K}_b = \tau \cdot \langle \bar{k}_b \rangle$, where τ is measured in days and $\langle \bar{k}_b \rangle$ is the average daily background air kerma rate. The sample standard deviation of the background dosimeters was found to be $s_B = \sqrt{s_0^2 + \tau \cdot \alpha_b}$, where s_b is the sample standard deviation with no deployment time, and α_b is the statistical variance of the daily air kerma value, which varies with the square root of τ based on the statistics of accumulation times. Using data from a previous experiment and methodology from Traino et al., $\langle \bar{k}_b \rangle$ for this dosimetry system was found to be 2.10 µGy d^{-1}, s_0 to be 4.71 µGy and α_b to be 9.7×10^{-4} µGy^2 d^{-1}.

Though fading could not be introduced into the time-sensitive detection and determination limits, as fading does not significantly change any of the included parameters, fading data from a previous experiment were used to determine the storage time necessary before irradiations to known low doses fell below the detection and determination limits. The time value at which a limit curve and a fading curve intersect is the maximum storage time allowed before fading causes a signal to be undetectable.

Pre-irradiation and post-irradiation fading functions for the entire LiF:Mg,Ti glow curve were compared to the detection and determination limits for various prompt doses over a typical 90 d deployment period, using the same statistical values as before. Graphical results for a prompt dose of 100 µGy are shown in Fig. 8.5. The time axis value of the crossing point between a fading function and

a limit indicates the time necessary for fading to push the signal below a limit. For 100 µGy, approximately 12 d of post-irradiation fading are required for the signal to fall below the determination limit, while 32 d of pre-irradiation fading is required. The sharp drop in the post-irradiation fading function is due to the rapid fading of peaks 2 and 3. Excluding these peaks renders the effect of fading on minimum detectable dose trivial, however, as the fading of the sum of peaks 4 and 5 is negligible over 90 d. Additional results for other prompt dose levels are given in Table 8.2. Prompt doses of 25 µGy are detectable for at least 4 d even with fading, and surpass the determination limit at 75 µGy. At 200 µGy, fading does not cause signal loss below the determination limit for at least 52 days of deployment.

Previous work found s_μ to improve from 4.2% after a single calibration to 3.2% after three calibrations and 3.0% after five calibrations. The effectiveness of additional calibration drops sharply after three calibrations, with the effect on s_μ becoming insignificant after five calibrations. (Harvey et al. 2011) A reduction in s_μ from 5% to 4% has only a small effect on the detection limit, but a profound effect on the determination limit at high radiation background values. For example, at a background kerma of 200 µGy, the detection limit is reduced from 165 µGy to 110 µGy when s_μ is reduced from 5% to 4%.

CONCLUSIONS

Both dose and response continue a linear relationship for doses even as low as 8.8 µGy, much less than the manufacturer-stated minimum of 100 µGy for the five TLD materials studied. An ideal minimum detectable dose can be determined in comparison to the PMT dark current, which was found to range from an equivalent dose of 0.04 µGy in CaF_2:Dy to 0.1 µGy in CaF_2:Tm and $CaSO_4$:Dy. However, this holds true only with background radiation and fading neglected, an impractical assertion. Also, if a different TLD readout system is used that has a higher dark current level, such as a CCD or photodiode array, this value may become limiting instead of the detection and determination limits if the equivalent dose of the dark current signal is higher than the detection limit from the TLD material statistics alone.

If the a dosimetry application requires computerized glow curve analysis, blending of adjacent peaks in LiF:Mg,Ti at low doses causes difficultly for the computer below 180 μGy. At 88 μGy and below, the GCA program tested is unable to separate the glow curve. CaF_2:Dy, CaF_2:Tm, $CaSO_4$:Dy, and LiF:Mg,Cu,P could still be analyzed by the computer down to 8.8 μGy, however, and the peak blending seen in LiF:Mg,Ti could still be analyzed by an integrating region of interest method to confirm dose-response linearity at low doses.

Radon can affect the minimum detection and determination limits for LiF:Mg,Ti by increasing the background air kerma $\overline{K}_b$, though other statistical parameters are unaffected. A very high radon concentration of 18.5 kBq · m^{-3} for 7 d was required to increase the determination limit by 10% from an original value of 70 μGy. The detection limit remained nearly unaffected. Though a longer deployment time would increase the integrated radon level, it would increase the background air kerma $\overline{K}_b$ as well. Unless the radon concentration is very high, the dose attributed to it alone will be small compared to radiation background. Still, LiF:Mg,Ti dosimeters left in an area with a high radon concentration may experience a slightly increased minimum detectable dose as a result of radon exposure. Before making a correction, the planned badge enclosure should be tested for radon permeability, as at least one common environmental dosimeter badge has been shown to be impervious to radon over short time periods (Harvey and Kearfott 2011).

Although fading does not affect the standard deviation of background or high kerma dosimeter groups, fading functions can be used to determine the amount of time in storage required for the signal from various prompt doses to fall below the detection and determination limits. When using the entire integrated glow curve, it should be noted that peaks 2 and 3 in LiF:Mg,Ti fade very quickly post-irradiation, causing a must faster approach to the limits. This may be remedied by considering peaks 4 and 5 only, though this would cause problems with dosimetry applications requiring other peaks, such as the determination of post-irradiation fading time, which requires peak 3 (Weinstein et al. 2003). In general, over a 90 d deployment period, a prompt dose of below 75

µGy caused crossover with the detection limit within 90 d, while a prompt dose of above 75 µGy did not cross the detection limit but did cross the determination limit within 90 d. Fading data from other dosimeter types could be studied similarly in order to determine realistic detection and determination limits for more common materials.

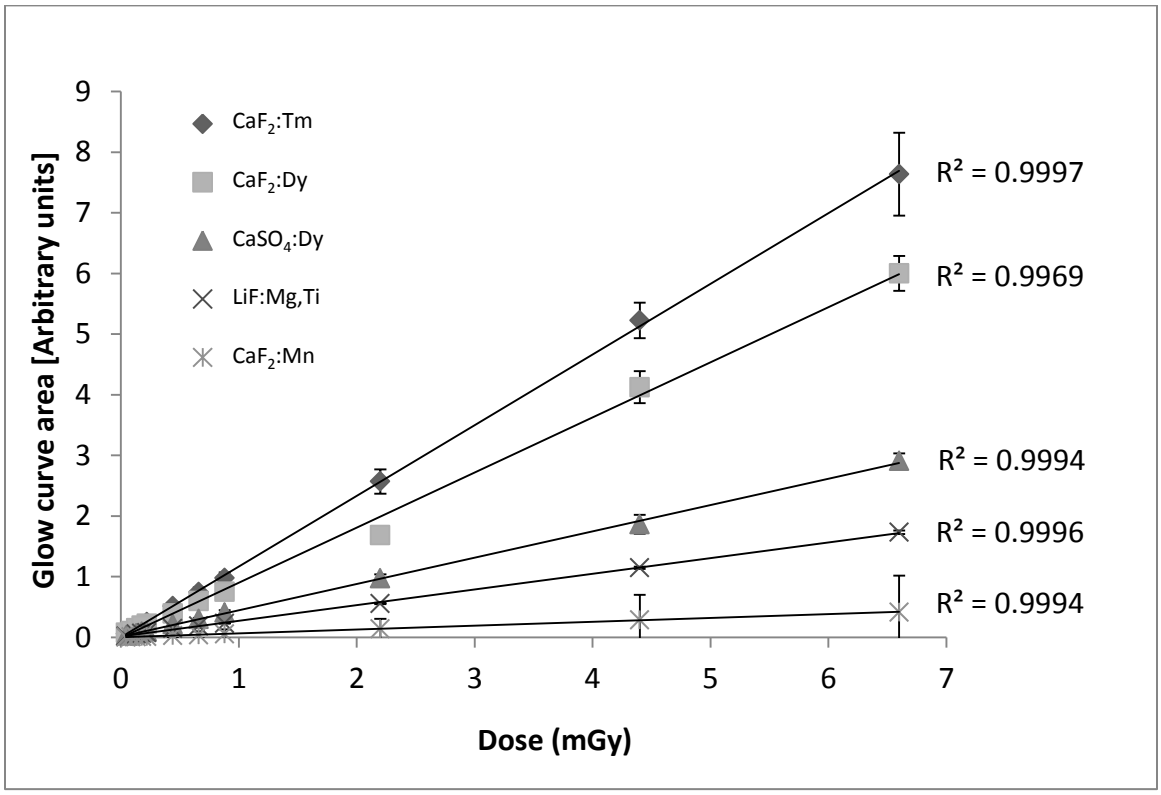

Fig 8.1. Dose response linearity for LiF:Mg,Ti (TLD-100), CaF_2:Dy (TLD-200), CaF_2:Tm (TLD-300), CaF_2:Mn (TLD-400), and $CaSO_4$:Dy (TLD-900) from 8.8 uGy to 6.6 mGy.

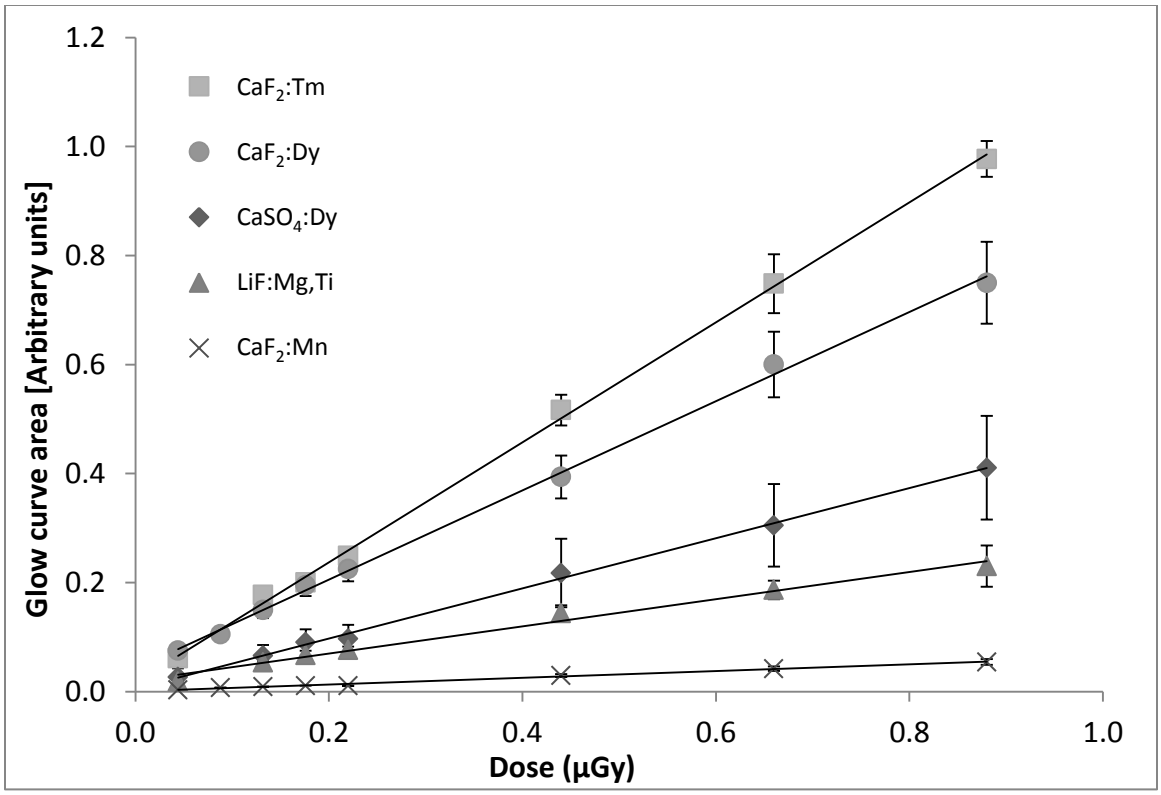

Fig 8.2. Dose response linearity for LiF:Mg,Ti (TLD-100), CaF_2:Dy (TLD-200), CaF_2:Tm (TLD-300), CaF_2:Mn (TLD-400), and $CaSO_4$:Dy (TLD-900) from 8.8 uGy to 0.88 mGy. R^2 values range from 0.987 (LiF:Mg,Ti) to 0.999 (CaF_2:Tm).

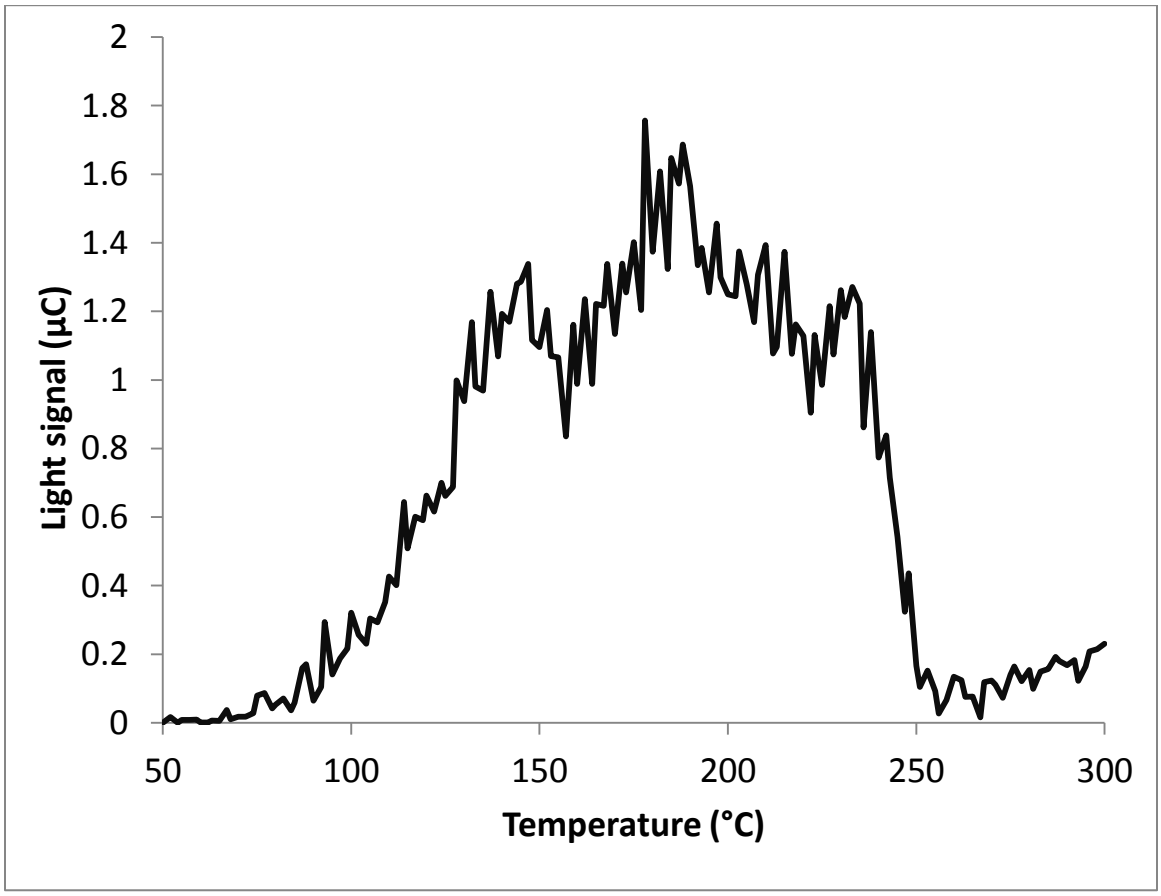

Fig. 8.3. Glow curve for LiF:Mg,Ti after 44 µGy of ^{137}Cs exposure, with individual peaks not discernable.

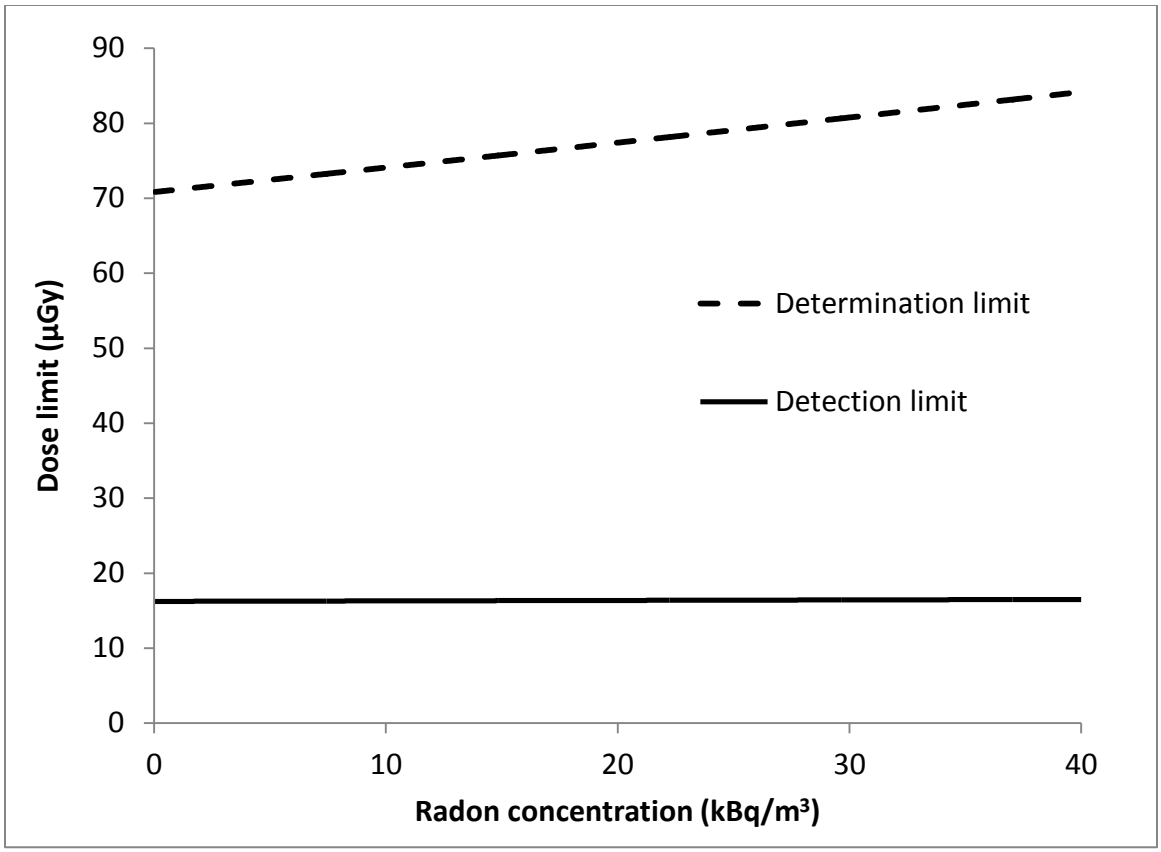

Fig. 8.4. Detection and determination limits for LiF:Mg,Ti dosimeters deployed for 7 d in a high radon environment using equations 8.2 and 8.3. The background air kerma rate was kept constant at 0.131 µGy h^{-1}.

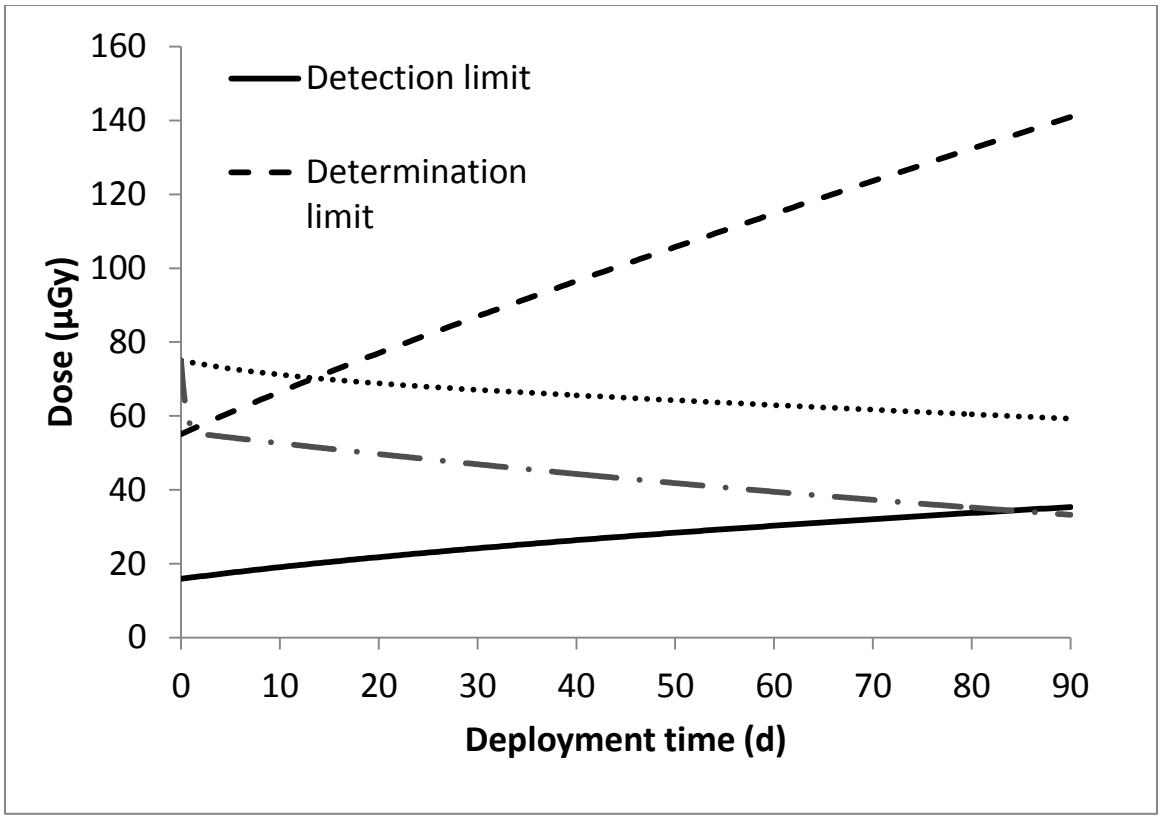

Fig. 8.5. Pre-irradiation and post-irradiation fading functions for LiF:Mg,Ti compared to the detection and determination limits for a prompt dose of 100 µGy. Crossing points between fading functions and limits denote time required for fading to push signal below a limit and are expanded upon for other prompt doses in Table 8.2.

Table 8.1. Measurements of the maximum point of the glow curve of each dosimeter type at an applied ^{137}Cs dose of 1 μGy compared to the dark current, with the two values used to determine the equivalent dose level were the dark current a thermoluminescent signal.

Material	***Glow curve maximum (nA)***	***Dark current maximum (nA)***	***Dark current equivalent dose (μGy)***
LiF:Mg,Ti	0.28 ± 0.08	0.1	0.4 ± 0.1
CaF_2:Dy	2.8 ± 0.8	0.1	0.04 ± 0.01
CaF_2:Tm	0.75 ± 0.15	0.1	0.1 ± 0.03
CaF_2:Mn	1.2 ± 0.2	0.1	0.08 ± 0.01
$CaSO_4$:Dy	0.85 ± 0.35	0.1	0.1 ± 0.05

Table 8.2. Pre-irradiation and post-irradiation fading time required for a LiF:Mg,Ti dose to fall below the detection limit L_D and determination limit L_Q for deployments of less than 90 d.

Prompt dose (μGy)	***Pre-irradiation fading time required (d)***		***Post-irradiation fading time required (d)***	
	L_D	L_Q	L_D	L_Q
25	22	Below limit	4	Below limit
50	> 90	Below limit	47	Below limit
75	> 90	12	83	1
100	> 90	32	> 90	12
150	> 90	69	> 90	33
200	> 90	> 90	> 90	52

REFERENCES

Bos A. J. J., Piters T. M., Gomez Ros J. M., Delgado A., 1994. An intercomparison of glow curve analysis computer programs: II. Measured glow curves. Radiat. Prot. Dosim. 51(4):257-264.

Busuoli G., 1981. *General Characteristics of TL Materials*. In: Oberhofer M, Scharmann A, eds. Applied Thermoluminescence Dosimetry. Bristol: Adam Hilger Ltd; 83-96.

Currie L.A., 1968. Limits for qualitative detection and quantitative determination: Application to radiochemistry. Anal. Chem. 40(3):586-593.

Harvey J.A., Kearfott K.J., 2010. The effects of high ambient radon on thermoluminescent dosimetry readings. Rad. Prot. Dosim. doi: 10.1093/rpd/ncq500.

Harvey J.A., 2011. *Effects of high ambient temperature on glow peak fading properties of thermoluminescent materials.* In: Performance of Thermoluminescent Dosimeters Under As-Deployed Conditions (Doctoral dissertation). Ann Arbor: ProQuest/UMI.

Harvey J. A., Kearfott K. J., 2011. Reproducibility of glow peak fading characteristics of thermoluminescent dosimeters. Radiat. Meas. doi: 10.1016/j.radmeas.2011.01.005.

Harvey J.A., Rodrigues M.L., Kearfott K.J., 2011. A computerized glow curve analysis (GCA) method for WinREMS thermoluminescent dosimeter data using MATLAB. Appl. Radiat. Isotopes. In press.

Harvey, J.A., Thomas, E.M., Kearfott, K.J., 2011. Quantification of various factors influencing the precision of thermoluminescent detector calibrations for new and used chip sets. Health Phys. In press.

Hirning, C.R., 1992. Detection and determination limits for thermoluminescence dosimetry. Health Phys. 62(3):223-227.

Julius H.W., 1981. *Instrumentation*. In: Oberhofer M, Scharmann A, eds. Applied Thermoluminescence Dosimetry. Bristol: Adam Hilger Ltd; 39-66.

Kearfott K. J., 1989. Preliminary experiences with Rn-222 in Arizona homes. Health Phys. 56:169-179.

Knoll, G.F. *Miscellaneous Detector Types*. In: Radiation Detection and Measurement, 4th ed. New York: John Wiley & Sons; 2010:733-778.

McKeever S.W.S., Moscovitch M., Townsend P.D., 1995. Thermoluminescence Dosimetry Materials: Properties and Uses. Nuclear Technology Publishing, Ashford.

Parker, L.W., Harvey, J.A., Kearfott, K.J., 2011. An integrated system for the beta, gamma and neutron calibration and storage of thermoluminescent dosimeters for a research laboratory. Health Phys. 100(2):S43-S49.

Simpkins RW, Kearfott KJ, 1997. The Minimum Number of Observations Necessary to Develop an Average Thermoluminescent Dosimeter Element Correction Factor. Radiation Protection Management 13:55-61.

Studenski M.T., Haverland N.P., Kearfott K.J., 2007. Simulation, Design, and Construction of a 137Cs Irradiation Facility. Health Physics 92:S78-S86.

Traino A.C., Perrone F., Luperini C., Tana L., Lazzeri M., d'Errico F., 1998. Influence of background exposure on TLD minimum dose detection and determination limits. Radiat. Prot. Dosim. 78(4):257-262.

Weinstein M., German U., Dubinsky S., Alfassi Z.B., 2003. On the determination of the post-irradiation time from the glow curve of TLD-100. Radiat. Prot. Dosim. 106:121-130.

United States Environmental Protection Agency, 2009. A citizen's guide to radon. EPA 402/K-09/001. Washington: United States Environmental Protection Agency.

Chapter IX

Potential Design for a Self-Reading Long-Term Radiation Detection System Based upon Integrating Dosimetric Materials

The previous chapters have analyzed a host of factors affecting TLD measurements. To summarize these factors, a simple, portable self-reading passive radiation detection and dosimetry system suitable for deployment in diverse environments is proposed. Such a system could run for multiple deployment cycles of 30 to 90 d or more without human intervention.

Passive dosimeters, including thermoluminescent (TL) and optically stimulated luminescent (OSL) dosimeters, are commonly used for personnel and environmental screening in various interior and exterior conditions. Passive and active detectors are rarely compared directly, as the situations in which they are generally considered to be useful are quite different. However, it is believed that passive dosimetry materials could be useful in situations for which active detectors have been historically used. Their main benefits of easy long-term deployment, robustness against physical damage (Harvey et al. 2011), low cost, and low power requirements justify using them in many diverse situations such as personnel monitoring, cargo container characterization (if deployed upon shipment over a long period, such as on an ocean freighter), and monitoring of infrequently occupied or hazardous areas.

Historically, portable TLD systems have been impractical. Only bulky photomultiplier tubes (PMTs) were feasible in TL dosimetry due to their high sensitivity (Julius 1981). More recently, high sensitivity charge coupled devices (CCDs) have been made available that can be used for TLD applications (Olko et al. 2008). A previous portable TLD system concept (Ikeya et al. 1990) was proposed which used a photodiode, but the system could read only relatively

high doses from 0.12 Gy to 50 Gy due to the comparatively low sensitivity of the photodiodes available at the time. An OSL-based system would also have this limitation, as highly efficient light collection is required to determine dose for both processes.

A TLD or OSL system capable of measuring low doses that could be read or annealed with no human intervention would no longer require nearly as frequent collection and redeployment, reducing the work hours necessary to run a dosimetry program. The low cost of TLD and OSL materials are also a motivating factor for such a system. Radiation energy discrimination could be provided through the creative use of filters in front of the dosimetry material, similar to what is done for the characterization of radiation type at the current time. Additional work is required, however, to optimize and characterize an enhanced energy-discrimination feature.

Prototype design

A portable self-reading radiation detection system based upon integrating dosimetric materials requires the following components:

- TLD or OSL material, either as one or more chips, a thin film, or a larger volume of material
- Physical filters, to cause an axial or otherwise positional encoding of radiation type and energy bias the dosimeters or dosimeter material
- A shielded badge casing, to ensure that the dosimeters cannot be exposed from any direction other than perpendicular to the above filters, precluding confounding factors for radiation type and energy determination
- A light sensor, for signal collection
- A method of heating TLDs, such as a contact heating surface (TLD only)

- A thermocouple, for TLD heating cycle quality control (TLD only)
- A light source, for OSL readout (OSL only)
- Optical filters, for shielding the light sensor from infrared light and signals not caused by the dosimetric materials during readout
- A data storage device, for retention of glow curve data (essential for TLDs, as they can only be read out once and glow curve information is useful for added data extraction and detecting difficulties such as dust incineration; necessary for OSL materials as they never completely clear signal from prior irradiation so subtractions from previous signals would be necessary)
- A microprocessor, as a control system for the readout, collection, and storage of dosimetry data
- A method of data transmission and reception, for communication of radiation detection system data and remote wakeup signals
- A compact, self-contained power source with characteristics sufficient for signal readout, retention, communications and longetivity for the desired application

A proposed physical arrangement of all of the above-mentioned components may be seen in Fig. 9.1 for TL and Fig. 9.2 for OSL. For this system to be feasible and advantageous compared to other detector types, it must be low cost, failure resistant, and able to function independently from a human operator for long periods. TL and OSL dosimeters themselves fill all of these requirements. Best of all, they are typically only $20 USD, or far less if bought in bulk. The price appears to be strongly dictated by the demand and re-usability of the materials for these materials. For example, one-use-only OSL dosimeters are provided in bulk to large institutions at costs far less than $10 a piece, including analysis and record keeping, while the same dosimeters may be sold to smaller

facilities for several hundred dollars apiece. Other components require more complex design considerations and difficult decisions.

The makeup and configuration of the physical filters for extracting information about radiation type and energy is relatively complicated. A variety of configurations of filter thicknesses and shapes (such as ramps) and materials could lead to an optimum design that encodes the desired information positionally across the one or more pieces of dosimetric material. For example, one portion of the dosimeter could be exposed to both low and high energy photons, while the other side is exposed only to higher energy radiation, with ramping or stepping of the response in between. The best design requires additional study and is beyond the scope of this work.

The badge casing may be made of any sufficiently dense material to block low energy gamma radiation, as well as alpha and beta particles and neutrons if appropriate. Very high energy gamma radiation need not be blocked, as it is much more likely to pass through the system without interacting with anything. Plastic, such as acrylonitrile butadiene styrene plastic commonly found in dosimeter badge casings (e.g. Type 8807 Environmental Dosimeter, BICRON/Harshaw, 6801 Cochran Road, Solon, OH 44139, USA), could be used. A high Z metal badge casing would cause the generation of secondary x-ray radiation if exposed to photons, but these could be absorbed by an additional layer of copper. An exterior badge casing of metal could then be in contact with the TLD heating surface to dissipate excess heat more quickly using a larger surface area in a manner similar to a heat sink.

An additional choice for the badge casing concerns its resistance to influx of radon, which has previously been shown (Harvey and Kearfott 2011) to cause additional background signal in TLDs. As every OSL dosimeter can also act as a TLD, and has similar solid state properties, it can be assumed that radon would affect them as well. As such, a badge casing that prevents the influx of radon is

desirable, if possible. If one is possible, a variant dosimeter system that does not interdict radon could be used as a crude measure of the ambient radon in the deployment area as well. If not possible, a measurement of radon using a different device would be desirable in order to correct for the measured signal by the dosimeter system.

For TL, the choices of heating and light collection are linked. With a filter system used to expose one axis of a TLD to both low and higher energy radiation and the other to high energy radiation, with a continuous linear ramp in between, there are two choices to obtain this energy sensitive information. If a single large TLD is used, it can be spot-heated on one end, then in the middle, then the other side as desired. If multiple TLD chips are used, they can be heated in sequence. Alternatively, the entire TLD or all TLDs can be heated at once and a position-sensitive light collection device used. Position-sensitive PMTs, CCDs, and photodiode arrays are all available. However, PMTs in general are expensive and delicate with high voltage requirements. Rectangular or linear CCDs or photodiode arrays, which were originally designed to produce images inexpensively and are continuously improving in sensitivity, appear to be the optimal choice. However, it should be noted that the light sensor's dark current level may the limiting factor in determining the lower limit of detectable dose for the system.

Contact heating is most practical for this system. Infrared heating with a high intensity photodiode is possible, though the heated air inside the badge could warm up the light sensor, causing an undesired increase in dark current. There is also no way to easily provide the steady supply of nitrogen required for gas heating at appropriate pressures in a portable system. As a result, unless the badge is hermetically sealed, oxygen will be present around the TLD. With oxygen present, high temperature noise resulting from chemiluminescence and triboluminescence may appear on the TLD glow curves (Harvey et al. 2010).

Tungsten is desired for the contact heater material, as it is inert, has favorable specific heat capacity, and compared to other high specific heat capacity materials, is not excessively malleable (lead), valuable (gold), or radioactive (uranium). It also possesses a much higher thermal conductivity than bismuth. Care should be taken to avoid an alloy of tungsten that exhibits incandescence when heated to 300°C, however, and the material should be handled carefully due to its toxicity. Positional heating could be achieved using an appropriate arrangement of wires on the back of a continuous TL material or wrapped around individual pieces of the detection material.

For OSL, high power LEDs are desired to read out the stored signal. A system of multiple colored LEDs (West 2011) is desirable to obtain information from different traps in the material, akin to TLD glow curve analysis. Luxeon Rebel LEDs (Philips Lumileds Lighting Company, 370 West Trimble Road, San Jose, CA 95131 USA) can be operated in pulsed mode to save power without loss of signal. To do this, an LED would be turned on for 0.1 s, then back off, and the OSL signal measured for 0.5 s. This cycle would be repeated for 10 to 20 s for each LED present. To save costs, a single high-power blue or royal blue LED could be used to free all traps simultaneously if analysis of the signals of various traps is not necessary for the desired application.

Optical filters are desired for both TL and OSL for different reasons. In TL, the TLD itself and any contact heater on which it rests may emit infrared light, which is generally undesirable for TL dosimetry. In OSL, filters may be used to ensure that the LED light does not reach the light collection device, even if operated in pulsed mode.

Once the TL or OSL signal data is collected, the signal should be stored immediately. This is particularly important in the case of TL, as the signal cannot be obtained again once read. Only a small amount of storage is required, as data from TL and OSL can be saved as plain text comma separated value lists on the

order of kilobytes in size. A small flash memory chip is desired for this purpose, as it is non-volatile, retaining the data even if power is removed. This is important for power-saving purposes.

A small microprocessor is necessary for use as a control system for the dosimeter. For TL, this would require analysis of the thermocouple data to monitor and control the contact heater's temperature. For OSL, this would require sequential triggering and pulse timing of the LED light sources and control over the light sensor's discontinuous operational periods as described above. Both cases require the microprocessor to receive and store the resulting light signal data. A pre-programmed cycle start time may be programmed into memory, in which case an internal clock is required, or the system may receive a remote signal as a trigger to begin a cycle necessitating the use of a wireless data transmitter and receiver.

Bluetooth was originally designed as a low-cost, low-power wireless data transmission protocol, and as such is optimal for this application. Depending on the expected distance between the dosimeter and a remote workstation, a Class 2 transceiver can be used for an approximate range of 10 meters, or a Class 3 transceiver for 100 meters (SIG Bluetooth 2010). Bluetooth is capable of transmitting wake signals, such that the microprocessor could remain off or in a low-power state until triggered to transmit stored data or begin a readout cycle remotely. If a longer range is desired, a cellular data link could be used, though for simplicity a short-range Bluetooth connection will be assumed.

The choice of battery is primarily dependent on the capacity required. In order to judge the capacity necessary, a power estimate is required for each of the components. This is summarized in Table 9.1. In order to calculate the power requirements of the tungsten grid, a short calculation was required. The tungsten grid must be heated from approximately 20°C to 300°C over a 60 second cycle. A tungsten grid of dimensions 10 mm × 10 mm × 0.32 mm, which allows for a

fairly large TLD film or four standard TLD chips, with wires consisting of 25% of its surface area (allowing 75% of light from the TLD to reach the CCD), is 8.0 mm^3 in area, and approximately 0.154 g in mass. With a specific heat capacity of 24.27 J g^{-1} K^{-1}, heating the grid by 280 K requires 5.8 J, which over a 60 s cycle produces an average of 97 mW. This was rounded up to 100 mW in the table, with a maximum of 200 mW to allow for some leeway in the exact dimensions of the grid. If the grid were spot-heated instead, this would reduce the amount of power necessary considerably, though reading out only some of the dosimeter material would reduce the amount of light received by the CCD, lowering the sensitivity of the system.

One considerable advantage of this system is that its components only need to be operational when a readout cycle is active, which takes approximately 60 s for TLD and 3.5 s for OSL, where each lamp emits a 0.1 s pulse and then the CCD activates for 0.5 s. A timer can wake up the system when needed, or a wireless wake up signal could be sent to the device, which would require only minimal power at all other times. A typical button cell battery has its capacity given in mAh, and range in capacity from 150 to 620 mAh depending on material. At approximately 1.5 V average voltage while discharging, this equates to 810 to 3300 J of energy. Even at the maximum power estimates listed in Table 9.1, a 150 mAh battery could run the TLD system for 23 cycles and the OSL system for 12 cycles.

Table 9.1 also shows cost estimates for each component, with the parts required for a TLD system prototype estimated at $130 and the parts required for an OSL prototype at $160. If manufactured with parts obtained in bulk, the costs would be far less. Some assumptions were made for parts, for example a simple $20 ARM processor for the microprocessor, similar to that found in a graphing calculator. Luxeon Rebel LEDs are approximately $5 each. TL and OSL dosimeters are typically $20 each if bought separately. The light sensor,

assumed to be a CCD, is estimated at $50 but considerable testing is required to determine the appropriate model. A photodiode array may also be used, which carries a similar cost. Thermocouples typically cost $3 to $5, and enough tungsten for a heating grid would be less than $1, perhaps more if not bought in quantity.

To compare, electronic personal dosimeters can cost $250 to $300, NaI systems $1,000 or more, and HPGe systems $15,000 or more. For a true cost comparison, the parts costs for the electronic personal dosimeters would need to be compared to the parts costs for the integrating dosimetric material-based systems.

The largest advantage of this system over active detector alternatives is in the cost and manpower savings. For what might turn out to be much lower costs than electronic personnel dosimeters, this system could provide automated dose monitoring with longer deployment times and no expenditures of human resources except during infrequent 30 to 90 d readouts which could be performed remotely. With no moving parts, components would only very rarely fail and need to be replaced. Still, for a system such as that proposed here to be competitive with NaI and HPGe radiation detection systems, which are by their nature tied to more restrictive power sources, systems of temporal dose and radiation energy determination should be devised to determine additional information which an active detector provides by default. Previous work has indicated that the determination of post-irradiation time in LiF:Mg,Ti is possible (Weinstein et al. 2003) and this could be extended to a more general system of temporal dose determination using the fading parameters of individual peaks. Perhaps the greatest application for an inexpensive self-reading portable radiation detection system based upon integrating dosimetric materials would be distributed networks of very large numbers of radiation detectors, either for

shipping containers, along borders, or for other areas of concern for homeland security and nuclear accident monitoring and response.

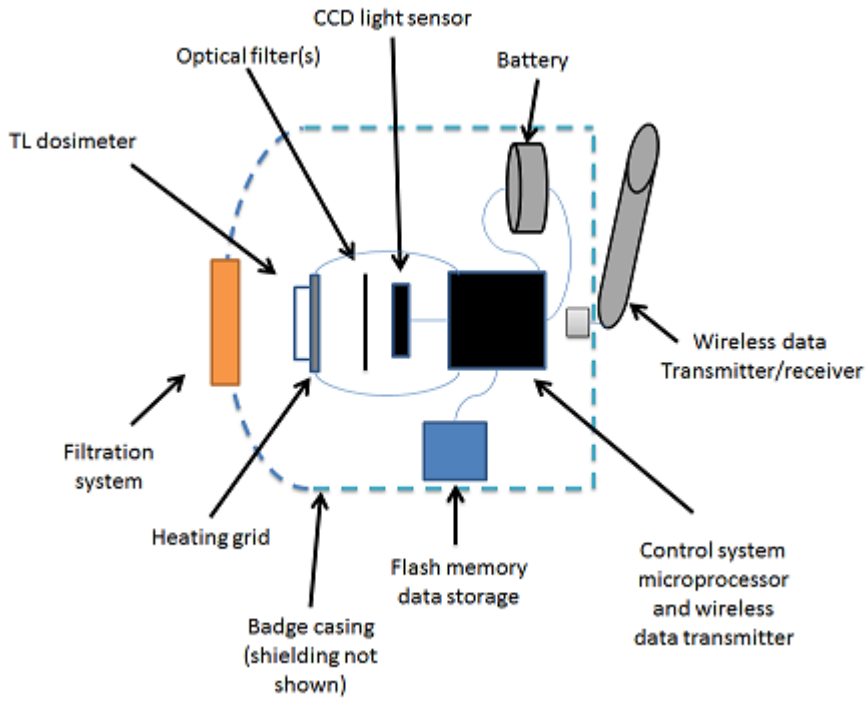

Fig. 9.1. Concept diagram of a self-reading portable TLD system, side view.

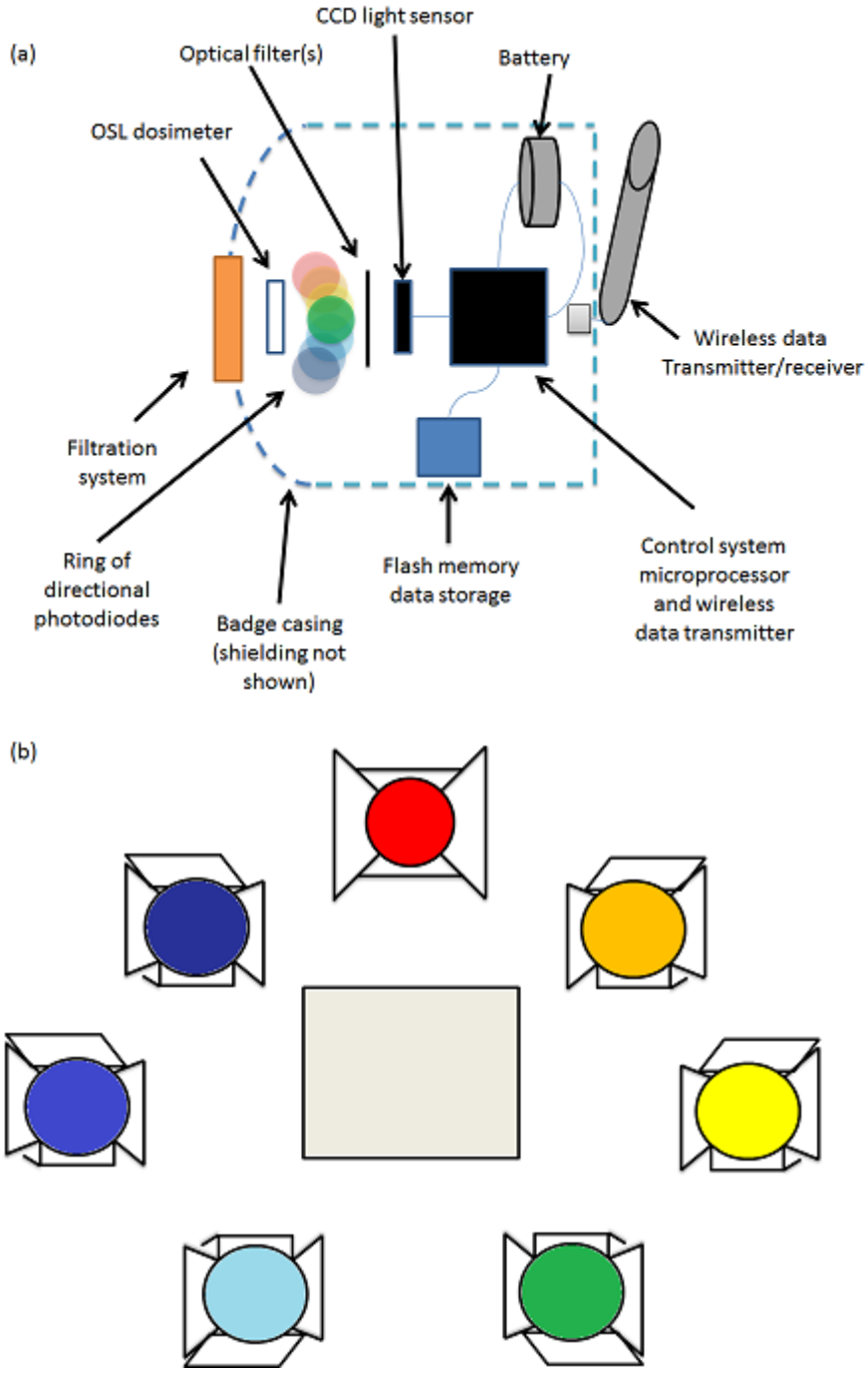

Fig. 9.2. Concept diagram of a self-reading portable OSL system. (a) Side view; (b) front view of OSL material with surrounding ring of colored light sources.

Table 9.1. Cost estimates and power requirements with minimum and maximum bounds for the components of a portable dosimetry system.

Component	*Estimated cost (USD)*	*Power consumption (mW)*	*Operation time per readout (s)*	*Energy required (J)*
CCD	$50	5 to 65	60 (TL)	0.3 to 3.9 (TL)
			70 (OSL)	0.36 to 5.6 (OSL)
Tungsten heating element (TL only)	$5	100 to 200	60	6.0 to 12
LED lamps (OSL only)	$35	1790 to 2460[a] 1620 to 2460[b]	14	24 to 34
Flash memory	$5	50 to 75	60 (TL)	3.0 to 3.5 (TL)
			14 (OSL)	3.6 to 5.2 (OSL)
Microprocessor	$20	2 to 250	60 (TL)	0.12 to 15 (TL)
			14 (OSL)	0.14 to 17.6 (OSL)
Bluetooth transmitter	$25	2.5 to 100	1 to 10	0.0025 to 1
TLD material	$20	--	--	--
OSL material	$20	--	--	--
Battery	$5	--	--	--
Total (TL)	$130			6.5 to 35
Total (OSL)	$160			28 to 63

[a]Green, cyan, blue, royal blue

[b]Red, red-orange, amber

REFERENCES

Harvey, J.A., Haverland, N. P., Kearfott, K. J., 2010. Characterization of the glow-peak fading properties of six common thermoluminescent materials. Appl. Radiat. Isotopes 68, 1988-2000.

Harvey J.A., Kearfott K.J., 2010. The effects of high ambient radon on thermoluminescent dosimetry readings. Rad. Prot. Dosim. doi: 10.1093/rpd/ncq500.

Harvey, J.A., Thomas, E.M., Kearfott, K.J., 2011. Quantification of various factors influencing the precision of thermoluminescent detector calibrations for new and used chip sets. Health Phys. In press.

Ikeya M., Katakuse I., Ichihara T. Portable thermoluminescence reader for dosimetry and dating in fields. J. Nucl. Sci. Technol. 27(2):188-190, 1990.

Julius H.W. *Instrumentation*. In: Oberhofer M, Scharmann A, eds. Applied Thermoluminescence Dosimetry. Bristol: Adam Hilger Ltd; 1981: 3966.

Olko P., Czopyk L., Klosowski M., Waligorski M.P.R., 2008. Thermoluminescence dosimetry using TL-readers equipped with CCD cameras. Radiat. Meas. 43:864-869.

SIG Bluetooth. Bluetooth Core Specification v4.0 [online]. Available at: http://www.bluetooth.com/English/Technology/Building/Pages/Specification.aspx. Accessed 21 January 2011.

West W.G., 2011. *An Affordable Optically Stimulated Luminescent Dosimeter Reader Utilizing Multiple Excitation Wavelengths*. In: *Investigations into the Optically Stimulated Luminescence Response of Various Materials* (Doctoral dissertation). Ann Arbor: ProQuest/UMI.

Chapter X

Conclusion

This dissertation had as its main objective the examination of the practical performance of TLDs under a variety of longer-term, as-deployed conditions. Existing research on various aspects of performance was systematically amplified, gaps in data filled, and the results brought together to generally characterize performance limitations. In addition, a new concept of using time-integrating dosimetric materials, such as TLDs, was presented taking into account the findings of the dissertation.

In Chapter II, any link between visible physical damage, discoloration, and slight variance in mass with sensitivity, which have been observed to occur over extended usage of TLDs in practical circumstances, was disproved for LiF:Mg,Ti. Thus minor scratching and damage which could occur for TLDs while deployed should not radically influence their calibrations relative to other members in a set.

Irradiation history, however, was found to be a highly significant variable influencing TLD performance. This implies that TLDs deployed in conditions varying from their cohorts in a group might require careful attention and recalibration over time. If, for example, a TLD has received a very high dose, it may require re-calibration relative to its cohorts.

Calibrations were shown to be much more effective in determining a TLD's desirability for deployment than a physical inspection. A technical basis for the standard practice of using three calibrations to determine a TLD's sensitivity, absent from both the academic and commercial literature, was rigorously developed in this dissertation. Using calibrations, a method was devised for selecting desirable TLDs from otherwise undesirable sets. To improve the precision of TLD calibrations, corrections were made for variances in source-

detector positioning across an irradiation target and the drift of TLD reader performance over time. The dissertation thus places the standard practice of TLD calibration on firmer ground while suggesting some enhancements to it. In addition, a method was suggested using calibrations for selecting desirable TLDs from otherwise undesirable sets, extending the utility of sets of TLDs for which it is not desirable to track individual chip sensitivities.

Chapter III presented a detailed study of sensitivity changes occurring during storage before irradiation and signal loss during storage after irradiation, commonly called pre-irradiation and post-irradiation fading respectively. This work represents the first comprehensive treatment of this topic, including detailed empirical fits, for different materials and fading traps. LiF:Mg,Ti, CaF_2:Dy, CaF_2:Tm, LiF:Mg,Cu,P, and $CaSO_4$:Dy all experienced significant post-irradiation fading, while CaF_2:Mn did not. The lithium fluoride dosimeters, LiF:Mg,Ti and LiF:Mg,Cu,P, also experienced significant pre-irradiation fading. In general, peak ratios involving lower temperature peaks faded more quickly.

The pre-irradiation and post-irradiation fading rates were found to be reproducible for groups of LiF:Mg,Ti dosimeters in Chapter IV, which quantitatively answered the previously unexplored question as to how variable TLD post-annealing and post-irradiation signal changes are from chip-to-chip in a group of TLDs. Such information is critical in assessing the performance of any applications or methods which may require corrections for these effects. Such methods may include the extraction of temporal information or corrections that would improve quantitation over long deployment periods.

Decay constants calculated for single glow peaks for individual dosimeters were found to fall within a Gaussian distribution. The mean of this distribution could then be used to characterize that glow peak for the entire group. Of 99 TLDs, 98 fell within 35% of the group fading functions for each peak for pre-irradiation fading. For post-irradiation fading, all dosimeters fell within 25% of the fading functions for peaks 3 to 5, but differed by as much as 100% for peak 2. As such, post-irradiation fading in peak 2 may have to be determined individually for each chip if high accuracy is required.

Because long-term deployments environmental monitoring could involve conditions that are higher than those routinely encountered by personnel, and exploration of the effects of such higher temperatures on TLD fading was indicated. The high ambient temperature study of Chapter V determined that LiF:Mg,Ti TLDs suffer from accelerated pre-irradiation and post-irradiation fading at 30°C, 40°C and 50°C compared to room temperature. In general, fading functions were similar for each temperature but accelerated with increasing temperature. An important dosimetric quantity, the areas under peaks 4 and 5, remained fairly constant for pre- and post-irradiation fading for 30°C and 40°C. Only for pre-irradiation fading was there a significant increase in peak 5 signal, but it was balanced by the loss in peak 4 signal. At 50°C, accelerated fading in peak 4 led to the sum of the peak 4 and 5 areas no longer remaining constant after approximately 20 d. Peak 3 remained detectable for all temperatures and time period tested, but peak 2 was difficult to detect after 15 to 20 d at all temperatures, especially post-irradiation fading. The experiments in the dissertation thus provide a sound basis for both analyzing signals from and correcting for signals from TLDs deployed in higher temperature environments.

Radon gas is a common source of background that may be elevated in confined spaces where certain work may be performed or environmental monitoring desired. The effects of high ambient radon examined in Chapter VI showed that LiF:Mg,Ti TLDs are affected by radon in bare chip form and when contained in dosimeter cards. CaF_2:Dy chips in dosimeter cards are even more profoundly affected owing to their higher sensitivity. A relationship between radon concentration and a ^{137}Cs equivalent dose was determined. Over a 7 d deployment, however, dosimeter cards encased in acrylonitrile butadiene styrene plastic badges showed no radon effect. Regardless, this work showed that TLD enclosures should be tested over their desired deployment time in high radon environments to determine if they are susceptible, especially if deployment in such an environment is expected.

The computerized glow curve analysis program devised for Chapter VII was used for many of the other experiments. It was capable of deconstructing

glow curves from LiF:Mg,Ti, CaF_2:Dy, CaF_2:Tm, LiF:Mg,Cu,P, and CaF_2:Mn using the first-order kinetics model with a figure of merit of 1.3% or less, and $CaSO_4$:Dy with a figure of merit of 2.2% or less. This is comparable to 1.75% in most other common glow curve analysis systems. The program, written in a common mathematics parser, is readily implementable on any computer and easily modifiable to analyze data from any TLD analysis system.

Many of the prior chapters in the dissertation explored the factors which play a role in determining the minimum detectable dose, a primary performance parameter of interest for detection systems. In Chapter VIII, the minimum detectable dose of a TLD was determined rigorously using results from the previous chapters. Limits were found based on TLD reader light sensor dark current, accumulation of radiation and radon background, and inability of the glow curve analysis program to function. Dose-response linearity was also tested and proven, but linearity was not lost for any of LiF:Mg,Ti, CaF_2:Dy, CaF_2:Tm, $CaSO_4$:Dy, and CaF_2:Mn down to 8.8 μGy, the lowest dose tested. The detection limit for a typical system was found to be approximately 20 μGy and the determination limit found to be 70 μGy in a typical LiF:Mg,Ti system, steadily increasing with time due to additional accumulation of background. This was found to increase with additional radon and the use of a glow curve analysis program, which imparts error into its peak area calculations compared to a simple region of interest method. Fading was also found to cause LiF:Mg,Ti TLD signal to dip below the minimum detectable signal over a typical 90 d deployment, but only if peaks 2 and 3 are required for consideration. With peaks 4 and 5 alone, the effect of fading on minimum detectable dose over 90 d is negligible.

Chapter IX presented a future work concept design for a thermoluminescent and optically stimulated luminescent radiation detection system. Capable of long-term autonomous deployment and the ability for self-readout, these systems were shown to have low cost and power usage potential, with the ability to perform ten or more readout cycles and store or transmit data wirelessly on a single battery charge. This appears to represent a

previously unexplored application for integrating dosimetric materials. This dissertation answered many questions that had to be addressed, such as minimum detectable dose and signal sensitivity changes with time, to assess viability of such a system.

Overall, these studies presented in this dissertation can be used to improve the precision, utility, and efficiency of many currently deployed TLD systems in a wide range of interior and exterior environments. Future work into temporal dose and energy discrimination could further improve the TLD's standing as a valuable, cost-effective radiation detection tool.

Appendix: MATLAB files

CurveFitting2.m
(Main GCA program for MATLAB; see Chapter VII)

```
%%%%%%%%%%%%%%%%%%%%%%%%%%%%%%%%%%%%%%%%%%%%%%%%%%%%%%%%%%%%%%%%
% This function reads the heat and glow curve files under the name
% file_name_h and file_name_g and fits them.
%
% For use with TLD-100, 200, 300, 400, 700H, 900
%
%
% Authors: Miesher Rodrigues, Nathan Haverland, John Harvey, Douglas Kripke
%
% This software is the property of the University of Michigan per the
% Bylaws of the Regents of the University of Michigan, section 3.10.
%
% Copyright 2005-2010 University of Michigan
%
%%%%%%%%%%%%%%%%%%%%%%%%%%%%%%%%%%%%%%%%%%%%%%%%%%%%%%%%%%%%%%%%

Dose = input('Enter the Cs-137 exposure in mR: ');
if(Dose <= 0)
   disp('Dose must be positive and non-zero.');
   return
end
Type = input('Enter the TLD type: ','s');
disp(strcat('The TLD type is: TLD-',Type));
disp(strcat('and the Cs-137 exposure is: ',num2str(Dose),' mR'));
file_name = '03_09_2007_5';

% Initialize some variables to be used throghout
num_shift = 0;
tal = 0;
file_size=0;
seq_num=0;

% File name format must be in the form 'MM_DD_YYYY_#'
file_month = strcat(file_name(1),file_name(2));
file_day = strcat(file_name(4),file_name(5));
file_year = strcat(file_name(7),file_name(8),file_name(9),file_name(10));
```

```
file_order = file_name(12);

% Open file to write results
output_filename = strcat('CF2output',file_name,'.txt');
fid = fopen(output_filename,'w');

start_peak = 1; % Assume first peak is peak 1 unless otherwise specified
withBG = 0; % Assume background is not fit unless otherwise specified
switch Type
   case '100'
      num_peaks = 4; % Number of peaks for this TLD type
      withBG = 1; % Pads answer vectors to include BG data
      start_peak = 2; % Start on peak 2
      max_temp = [550 550];

fprintf(fid,'%s,%s,%s,%s,%s,%s,%s,%s,%s,%s,%s,%s,%s,%s,%s,%s,%s,%s,%s
,%s,%s,%s,%s,%s,%s,%s,%s,%s,%s,%s,%s,%s,%s,%s,%s,%s,%s,%s,%s,%s,
%s,%s,%s,%s,%s,%s,%s,%s,%s,%s,%s,%s,%s,%s,%s,%s,%s,\n','DATA','seq(s
eq_num)','tal','j','''gdata.data(i,1)''','''gdata.data(i,2)''','FOM','ee2','ee2_low','ee2_hig
h','ee3','ee3_low','ee3_high','ee4','ee4_low','ee4_high','ee5','ee5_low','ee5_high','i
i2','ii2_low','ii2_high','ii3','ii3_low','ii3_high','ii4','ii4_low','ii4_high','ii5','ii5_low','ii5_hi
gh','tt2','tt2_low','tt2_high','tt3','tt3_low','tt3_high','tt4','tt4_low','tt4_high','tt5','tt5_lo
w','tt5_high','yy0','yy0_low','yy0_high','aa','aa_low','aa_high','tt0','tt0_low','tt0_high'
,'areabg','area2','area3','area4','area5');

   case '200'
      num_peaks = 9;
      max_temp = [680 680];

fprintf(fid,'%s,%s,%s,%s,%s,%s,%s,%s,%s,%s,%s,%s,%s,%s,%s,%s,%s,%s,%s
,%s,%s,%s,%s,%s,%s,%s,%s,%s,%s,%s,%s,%s,%s,%s,%s,%s,%s,%s,%s,%s,
%s,%s,%s,%s,%s,%s,%s,%s,%s,%s,%s,%s,%s,%s,%s,%s,%s,%s,%s,%s,%s,%
s,%s,%s,%s,%s,%s,%s,%s,%s,%s,%s,%s,%s,%s,%s,%s,%s,%s,%s,%s,%s,%s,
%s,%s,%s,%s,%s,%s,%s,%s,%s,%s,%s,%s,%s,%s,\n','DATA','seq(seq_num)','t
al','j','gdata.data(i,1)','gdata.data(i,2)','FOM','ee1','ee1_low','ee1_high','ee2','ee2_l
ow','ee2_high','ee3','ee3_low','ee3_high','ee4','ee4_low','ee4_high','ee5','ee5_low'
,'ee5_high','ee6','ee6_low','ee6_high','ee7','ee7_low','ee7_high','ee8','ee8_low','e
e8_high','ee9','ee9_low','ee9_high','ii1','ii1_low','ii1_high','ii2','ii2_low','ii2_high','ii3'
,'ii3_low','ii3_high','ii4','ii4_low','ii4_high','ii5','ii5_low','ii5_high','ii6','ii6_low','ii6_hig
h','ii7','ii7_low','ii7_high','ii8','ii8_low','ii8_high','ii9','ii9_low','ii9_high','tt1','tt1_low','tt
1_high','tt2','tt2_low','tt2_high','tt3','tt3_low','tt3_high','tt4','tt4_low','tt4_high','tt5','tt5
_low','tt5_high','tt6','tt6_low','tt6_high','tt7','tt7_low','tt7_high','tt8','tt8_low','tt8_high'
,'tt9','tt9_low','tt9_high','area1','area2','area3','area4','area5','area6','area7','area8',
'area9');
```

```
    case '300'
        num_peaks = 8;
        max_temp = [700 680];
        fprintf(fid,'%s %s %s %s %s %s %s %s %s %s %s %s %s %s %s %s %s
%s %s %s %s %s %s %s %s %s %s %s %s %s %s %s %s %s %s %s %s %s
%s %s %s %s %s %s %s %s %s %s %s %s %s %s %s %s %s %s %s %s %s
%s %s %s %s %s %s %s %s %s %s %s %s %s %s %s %s %s %s %s %s %s
%s %s %s %s %s %s %s %s %s
\n','DATA','tot','A','seq(seq_num)','tal','j','gdata.data(i,1)','gdata.data(i,2)','FOM','ee
(1)','ee_low(1)','ee_high(1)','ee(2)','ee_low(2)','ee_high(2)','ee(3)','ee_low(3)','ee_
high(3)','ee(4)','ee_low(4)','ee_high(4)','ee(5)','ee_low(5)','ee_high(5)','ee(6)','ee_l
ow(6)','ee_high(6)','ee(7)','ee_low(7)','ee_high(7)','ee(8)','ee_low(8)','ee_high(8)','i
i(1)','ii_low(1)','ii_high(1)','ii(2)','ii_low(2)','ii_high(2)','ii(3)','ii_low(3)','ii_high(3)','ii(4)
','ii_low(4)','ii_high(4)','ii(5)','ii_low(5)','ii_high(5)','ii(6)','ii_low(6)','ii_high(6)','ii(7)','ii
_low(7)','ii_high(7)','ii(8)','ii_low(8)','ii_high(8)','tt(1)','tt_low(1)','tt_high(1)','tt(2)','tt_l
ow(2)','tt_high(2)','tt(3)','tt_low(3)','tt_high(3)','tt(4)','tt_low(4)','tt_high(4)','tt(5)','tt_l
ow(5)','tt_high(5)','tt(6)','tt_low(6)','tt_high(6)','tt(7)','tt_low(7)','tt_high(7)','tt(8)','tt_l
ow(8)','tt_high(8)','area(1)','area(2)','area(3)','area(4)','area(5)','area(6)','area(7)','a
rea(8)');

    case '400'
        num_peaks = 3;
        start_peak = 2;
        max_temp = [600 700];

fprintf(fid,'%s,%s,%s,%s,%s,%s,%s,%s,%s,%s,%s,%s,%s,%s,%s,%s,%s,%s,%s
,%s,%s,%s,%s,%s,%s,%s,%s,%s,%s,%s,%s,%s,%s,%s,%s,%s,%s,\n','DATA','s
eq(seq_num)','tal','j','gdata.data(i,1)','gdata.data(i,2)','FOM','ee2','ee2_low','ee2_hi
gh','ee3','ee3_low','ee3_high','ee4','ee4_low','ee4_high','ii2','ii2_low','ii2_high','ii3','
ii3_low','ii3_high','ii4','ii4_low','ii4_high','tt2','tt2_low','tt2_high','tt3','tt3_low','tt3_hig
h','tt4','tt4_low','tt4_high','area2','area3','area4');

    case '700'
        num_peaks = 4;
        start_peak = 2;
        max_temp = [700 680];

fprintf(fid,'%s,%s,%s,%s,%s,%s,%s,%s,%s,%s,%s,%s,%s,%s,%s,%s,%s,%s,%s
,%s,%s,%s,%s,%s,%s,%s,%s,%s,%s,%s,%s,%s,%s,%s,%s,%s,%s,%s,%s,
%s,%s,%s,%s,%s,%s,%s,\n','DATA','seq(seq_num)','tal','j','gdata.data(i,1)','gdata
.data(i,2)','FOM','ee2','ee2_low','ee2_high','ee3','ee3_low','ee3_high','ee4','ee4_lo
w','ee4_high','ee5','ee5_low','ee5_high','ii2','ii2_low','ii2_high','ii3','ii3_low','ii3_high
','ii4','ii4_low','ii4_high','ii5','ii5_low','ii5_high','tt2','tt2_low','tt2_high','tt3','tt3_low','tt
3_high','tt4','tt4_low','tt4_high','tt5','tt5_low','tt5_high','area2','area3','area4','area5'
);
```

```
   case '900'
      num_peaks = 7;
      max_temp = [600 600];

fprintf(fid,'%s,%s,%s,%s,%s,%s,%s,%s,%s,%s,%s,%s,%s,%s,%s,%s,%s,%s,%s
,%s,%s,%s,%s,%s,%s,%s,%s,%s,%s,%s,%s,%s,%s,%s,%s,%s,%s,%s,%s,%s,
%s,%s,%s,%s,%s,%s,%s,%s,%s,%s,%s,%s,%s,%s,%s,%s,%s,%s,%s,%s,%s,%
s,%s,%s,%s,%s,%s,%s,%s,%s,%s,%s,%s,%s,%s,%s,%s,\n','DATA','seq(seq_nu
m)','tal','j','gdata.data(i,1)','gdata.data(i,2)','FOF','ee1','ee1_low','ee1_high','ee2','e
e2_low','ee2_high','ee3','ee3_low','ee3_high','ee4','ee4_low','ee4_high','ee5','ee5
_low','ee5_high','ee6','ee6_low','ee6_high','ee7','ee7_low','ee7_high','ii1','ii1_low','
ii1_high','ii2','ii2_low','ii2_high','ii3','ii3_low','ii3_high','ii4','ii4_low','ii4_high','ii5','ii5_l
ow','ii5_high','ii6','ii6_low','ii6_high','ii7','ii7_low','ii7_high','tt1','tt1_low','tt1_high','tt2
','tt2_low','tt2_high','tt3','tt3_low','tt3_high','tt4','tt4_low','tt4_high','tt5','tt5_low','tt5_
high','tt6','tt6_low','tt6_high','tt7','tt7_low','tt7_high','area1','area2','area3','area4','ar
ea5','area6','area7');

   otherwise
      disp('Unknown TLD type entered.')
      return;
end

%determines the number of cards to be read
test_file_name = strcat(file_name,'_g1.asc');
hdata_test=importdata(test_file_name,','); %imports heat curve data placing ',' in
between data
[rows,cols]=size(hdata_test.data);
skip_list=ones(rows,1);%creates a vector of 1's of length rows

%Remove PMT noise/reference light data
PMT = 'PMT Noise       ';
RL = 'Reference Light ';
for r=1:rows
   ans1 = strcmp(hdata_test.textdata(r,1),PMT); %compare first object in row to
string PMT   1=same 0=different
   ans2 = strcmp(hdata_test.textdata(r,1),RL); %compare first object in row to
string RL
   if ((ans1 == 0) && (ans2 == 0))  %if it is not PMT noise or RL, increments
counter and puts card number in seq
      file_size = file_size + 1;

      %determines card number and puts into seq
      card_number = '';
      char_string = char(hdata_test.textdata(r,1));
      for L=2:8 %for L=1:4
         card_number = strcat(card_number,char_string(L));
```

```
            %string_name = string_name + char_string(L);
        end
        %seq(file_size)= str2num(card_number);  Bug?
        seq(file_size)= str2double(card_number);
        else  %must be pmt noise or RL, puts row number on skip list
            skip_list(r,1)=0;
    end;
end

% This i for loop goes through and fits each card-each line(i) being a card
for i=1:rows
    % Determines the sequence number
    if skip_list(i,1)~=0  %if shouldn't skip this line, increment seq_num
        seq_num = seq_num + 1;
    end

    % This j for loop goes through each chip on a card
    for j=1:1 % for cards use j=1:4 , for chips use j=1:1
        tal = tal + 1; %increments tally

        fileg_name=strcat(file_name,'_g',num2str(j,'%01.0f'),'.asc'); %Determines
name of glow curve file to open
        fileh_name=strcat(file_name,'_h',num2str(j,'%01.0f'),'.asc'); %Determines
name of heat curve file to open

        hdata=importdata(fileh_name,','); %imports heat curve data placing ',' in
between data
        gdata=importdata(fileg_name,','); %imports glow curve data placing ',' in
between data

        % Exports only data from gdata and hdata into files ydata and xdata
        if skip_list(i,1)==0  %if should skip this line for PMT/RL
            num_shift = num_shift + 1;
            break; %line should not be read
        else %if should keep this line
            for l=3:202   %i is row number, l is column number
                hdata.data(i,l)=hdata.data(i,l)+273; %convert deg C to K
                xdata(l-2)=hdata.data(i,l);  %puts hdata.data into xdata getting rid of
date and time from hdata.data
                ydata(l-2)=gdata.data(i,l);  %puts gdata.data into ydata getting rid of
date and time from gdata.data
            end
        end

        % Determines number of repeating values (z) in xdata
        z=0;
```

```
w=1;
while(xdata(end-w-1)==xdata(end-z))
   while(xdata(end-w)==xdata(end-z))
      z=z+1;
      w=w+1;
   end
   if (xdata(end-w-1)==xdata(end-z))
      z=z+2;
      w=w+2;
   end
end

% Removes z number of elements from the end of xdata and ydata
for v=1:z
   xdata(end)=[];
   ydata(end)=[];
end


name=strcat('CF2_',file_name,'_',num2str(seq_num,'%01.0f'),'_',num2str(j,'%01.0
f')');

answer = zeros((num_peaks*3+withBG*3),1); %answer = [0 0 0 0 0 0 0 0 0
0 0 0 0 0 0];
ci = zeros(2,(num_peaks*3+withBG*3)); %ci =
[0,0,0,0,0,0,0,0,0,0,0,0,0,0,0;0,0,0,0,0,0,0,0,0,0,0,0,0,0,0];

% Calculate fitting parameters
vector_answer = [];
ci_answer = [];

switch Type % Call fitting program
   case '100'
      [vector_answer, ci_answer] =
fitglow100(seq_num,seq,name,xdata,ydata,Dose);
   case '200'
      [vector_answer, ci_answer] =
fitglow200(seq_num,seq,name,xdata,ydata,Dose);
   case '300'
      [vector_answer, ci_answer] =
fitglow300(seq_num,seq,name,xdata,ydata,Dose);
   case '400'
      [vector_answer, ci_answer] =
fitglow400(seq_num,seq,name,xdata,ydata,Dose);
   case '700'
```

```
            [vector_answer, ci_answer] =
fitglow700(seq_num,seq,name,xdata,ydata,Dose);
        case '900'
            [vector_answer, ci_answer] =
fitglow900(seq_num,seq,name,xdata,ydata,Dose);
    end

    answer=vector_answer;
    ci=ci_answer;

    end_peak=start_peak+num_peaks-1; % Ex. TLD-100: End peak is peak 5,
2+4-1 = 5
    area=zeros(end_peak,1);
    ee=zeros(end_peak,1);
    ii=zeros(end_peak,1);
    tt=zeros(end_peak,1);
    ee_low=zeros(end_peak,1);
    ii_low=zeros(end_peak,1);
    tt_low=zeros(end_peak,1);
    ee_high=zeros(end_peak,1);
    ii_high=zeros(end_peak,1);
    tt_high=zeros(end_peak,1);

    for k = 1:length(answer) % Format of answer vector: ee(start_peak), ... ,
ee(end_peak), ii(start_peak), ... , ii(end_peak), tt(start_peak), ... , tt(end_peak)(,
yy0, aa, tt0 if BG present)
        if(ceil(k/num_peaks) == 1)
            ee(k+start_peak-1) = answer(k);
            ee_low(k+start_peak-1) = ci(1,k);
            ee_high(k+start_peak-1) = ci(2,k);
        elseif(ceil(k/num_peaks) == 2)
            ii(k+start_peak-1-num_peaks) = answer(k);
            ii_low(k+start_peak-1-num_peaks) = ci(1,k);
            ii_high(k+start_peak-1-num_peaks) = ci(2,k);
        elseif(ceil(k/num_peaks) == 3)
            tt(k+start_peak-1-num_peaks*2) = answer(k);
            tt_low(k+start_peak-1-num_peaks*2) = ci(1,k);
            tt_high(k+start_peak-1-num_peaks*2) = ci(2,k);
        end
    end

    bg='0';
    area = zeros(end_peak,1);
    areabg = 0;
```

```
        if(withBG == 1) % Extract background function parameters (last three values
in answer vector)
            yy0 = answer(length(answer)-2);
            yy0_low = ci(1,length(answer)-2);
            yy0_high = ci(2,length(answer)-2);
            aa = answer(length(answer)-1);
            aa_low=ci(1,length(answer)-1);
            aa_high=ci(2,length(answer)-1);
            tt0 = answer(length(answer));
            tt0_low=ci(1,length(answer));
            tt0_high=ci(2,length(answer));
            bg='yy0+aa*exp(x/tt0)';
        end

        %peak=zeros(end_peak,1); % Deconvoluted functions
        peak = cellstr(num2str(zeros(end_peak,1)));
        all=''; % Sum of all peaks

        for m = start_peak:end_peak

peak(m)=cellstr(strcat('ii(',num2str(m),')*exp(1+ee(',num2str(m),')/8.617385e-5/x*
(x-tt(',num2str(m),'))/tt(',num2str(m),')-x*x/tt(',num2str(m),')/tt(',num2str(m),')*exp(
ee(',num2str(m),')/8.617385e-5/x*(x-tt(',num2str(m),'))/tt(',num2str(m),'))*(1-2*8.6
17385e-5*x/ee(',num2str(m),'))))'); %kept "8.617385e-5" instead of k, since
"num2str(k)" is nearly as long
%
peak(m)=cellstr(strcat('ii(',num2str(m),')*exp(1+ee(',num2str(m),')/8.617385e-5/x*
(x-tt(',num2str(m),'))/tt(',num2str(m),')-x*x/tt(',num2str(m),')/tt(',num2str(m),')*exp(
ee(',num2str(m),')/8.617385e-5/x*(x-tt(',num2str(m),'))/tt(',num2str(m),'))*(1-(',num
2str(m),')*8.617385e-5*x/ee(',num2str(m),'))-((',num2str(m),')*8.617385e-5*tt(',nu
m2str(m),')/ee(',num2str(m),')))'); %kept "8.617385e-5" instead of k, since
"num2str(k)" is nearly as long
            all=strcat(all, peak(m), '+');
            for x=300:max_temp(1) % Temperature range
                area(m)=area(m)+eval(char(peak(m))); % Calculate peak areas
                areabg=areabg+eval(bg);
            end
        end
        all=char(strcat(all,bg));

        % Calculate Figure of Merit (FOM)
        A=sum(area)+areabg;
        tot=0;
        for x=300:max_temp(2)
            intensity=0;
            %Loop through data to find x data of this point
```

```
            for p=1:(200-z)
                if xdata(1,p)==x
                    intensity=ydata(1,p);
                end
            end
            if (intensity ~= 0) && (isnan(intensity) == 0)
                abc=intensity-eval(all);
                tot=tot+abs(abc);
            end
        end
        FOM=tot*100/A;

         switch Type % write data into CSV file
            case '100'
                fprintf(fid,'"
",%4.0f,%2.0f,%1.0f,%8.0f,%6.0f,%5.3f,%5.3f,%5.3f,%5.3f,%5.3f,%5.3f,%5.3f,%
5.3f,%5.3f,%5.3f,%5.3f,%5.3f,%5.3f,%9.3f,%9.3f,%9.3f,%9.3f,%9.3f,%9.3f,%9.3f,
%9.3f,%9.3f,%9.3f,%9.3f,%9.3f,%6.2f,%6.2f,%6.2f,%6.2f,%6.2f,%6.2f,%6.2f,%6.
2f,%6.2f,%6.2f,%6.2f,%6.2f,%7.1f,%7.1f,%7.1f,%7.5f,%7.5f,%7.5f,%7.5f,%7.5f,
%7.5f,%10.3f,%10.3f,%10.3f,%10.3f,%10.3f\n',seq(seq_num),tal,j,gdata.data(i,1)
,gdata.data(i,2),FOM,ee(2),ee_low(2),ee_high(2),ee(3),ee_low(3),ee_high(3),ee(
4),ee_low(4),ee_high(4),ee(5),ee_low(5),ee_high(5),ii(2),ii_low(2),ii_high(2),ii(3),ii
_low(3),ii_high(3),ii(4),ii_low(4),ii_high(4),ii(5),ii_low(5),ii_high(5),tt(2),tt_low(2),tt_
high(2),tt(3),tt_low(3),tt_high(3),tt(4),tt_low(4),tt_high(4),tt(5),tt_low(5),tt_high(5),y
y0,yy0_low,yy0_high,aa,aa_low,aa_high,tt0,tt0_low,tt0_high,areabg,area(2),area
(3),area(4),area(5));
            case '200'
                fprintf(fid,'"
",%4.0f,%2.0f,%1.0f,%8.0f,%6.0f,%5.3f,%5.3f,%5.3f,%5.3f,%5.3f,%5.3f,%5.3f,%
5.3f,%5.3f,%5.3f,%5.3f,%5.3f,%5.3f,%5.3f,%5.3f,%5.3f,%5.3f,%5.3f,%5.3f,%5.3f,
%5.3f,%5.3f,%5.3f,%5.3f,%5.3f,%5.3f,%5.3f,%9.3f,%9.3f,%9.3f,%9.3f,%9.
3f,%9.3f,%9.3f,%9.3f,%9.3f,%9.3f,%9.3f,%9.3f,%9.3f,%9.3f,%9.3f,%9.3f,%9.3f,
%9.3f,%9.3f,%9.3f,%9.3f,%9.3f,%9.3f,%9.3f,%9.3f,%9.3f,%6.2f,%6.2f,%6.
2f,%6.2f,%6.2f,%6.2f,%6.2f,%6.2f,%6.2f,%6.2f,%6.2f,%6.2f,%6.2f,%6.2f,%6.2f,
%6.2f,%6.2f,%6.2f,%6.2f,%6.2f,%6.2f,%6.2f,%6.2f,%6.2f,%6.2f,%6.2f,%10
0.3f,%10.3f,%10.3f,%10.3f,%10.3f,%10.3f,%10.3f,%10.3f,\n',seq(seq_nu
m),tal,j,gdata.data(i,1),gdata.data(i,2),FOM,ee(1),ee_low(1),ee_high(1),ee(2),ee_
low(2),ee_high(2),ee(3),ee_low(3),ee_high(3),ee(4),ee_low(4),ee_high(4),ee(5),e
e_low(5),ee_high(5),ee(6),ee_low(6),ee_high(6),ee(7),ee_low(7),ee_high(7),ee(8
),ee_low(8),ee_high(8),ee(9),ee_low(9),ee_high(9),ii(1),ii_low(1),ii_high(1),ii(2),ii_
low(2),ii_high(2),ii(3),ii_low(3),ii_high(3),ii(4),ii_low(4),ii_high(4),ii(5),ii_low(5),ii_hi
gh(5),ii(6),ii_low(6),ii_high(6),ii(7),ii_low(7),ii_high(7),ii(8),ii_low(8),ii_high(8),ii(9),i
i_low(9),ii_high(9),tt(1),tt_low(1),tt_high(1),tt(2),tt_low(2),tt_high(2),tt(3),tt_low(3),t
t_high(3),tt(4),tt_low(4),tt_high(4),tt(5),tt_low(5),tt_high(5),tt(6),tt_low(6),tt_high(6)
,tt(7),tt_low(7),tt_high(7),tt(8),tt_low(8),tt_high(8),tt(9),tt_low(9),tt_high(9),area(1),
area(2),area(3),area(4),area(5),area(6),area(7),area(8),area(9));
```

```
        case '300'
            fprintf(fid,'" " %5.3f %5.3f %4.0f %2.0f %1.0f %8.0f %6.0f %5.3f %5.3f
%5.3f %5.3f %5.3f %5.3f %5.3f %5.3f %5.3f %5.3f %5.3f %5.3f %5.3f %5.3f %5.3f %5.3f
%5.3f %5.3f %5.3f %5.3f %5.3f %5.3f %5.3f %5.3f %5.3f %5.3f %5.3f %9.3f
%9.3f %9.3f %9.3f %9.3f %9.3f %9.3f %9.3f %9.3f %9.3f %9.3f %9.3f %9.3f
%9.3f %9.3f %9.3f %9.3f %9.3f %9.3f %9.3f %9.3f %9.3f %9.3f %9.3f %6.2f
%6.2f %6.2f %6.2f %6.2f %6.2f %6.2f %6.2f %6.2f %6.2f %6.2f %6.2f %6.2f
%6.2f %6.2f %6.2f %6.2f %6.2f %6.2f %6.2f %6.2f %6.2f %6.2f %6.2f %10.3f
%10.3f %10.3f %10.3f %10.3f %10.3f %10.3f %10.3f %10.3f
\n',tot,A,seq(seq_num),tal,j,gdata.data(i,1),gdata.data(i,2),FOM,ee(1),ee_low(1),e
e_high(1),ee(2),ee_low(2),ee_high(2),ee(3),ee_low(3),ee_high(3),ee(4),ee_low(4
),ee_high(4),ee(5),ee_low(5),ee_high(5),ee(6),ee_low(6),ee_high(6),ee(7),ee_lo
w(7),ee_high(7),ee(8),ee_low(8),ee_high(8),ii(1),ii_low(1),ii_high(1),ii(2),ii_low(2),
ii_high(2),ii(3),ii_low(3),ii_high(3),ii(4),ii_low(4),ii_high(4),ii(5),ii_low(5),ii_high(5),ii
(6),ii_low(6),ii_high(6),ii(7),ii_low(7),ii_high(7),ii(8),ii_low(8),ii_high(8),tt(1),tt_low(
1),tt_high(1),tt(2),tt_low(2),tt_high(2),tt(3),tt_low(3),tt_high(3),tt(4),tt_low(4),tt_hig
h(4),tt(5),tt_low(5),tt_high(5),tt(6),tt_low(6),tt_high(6),tt(7),tt_low(7),tt_high(7),tt(8)
,tt_low(8),tt_high(8),area(1),area(2),area(3),area(4),area(5),area(6),area(7),area(
8));
        case '400'
            fprintf(fid,'"
",%4.0f,%2.0f,%1.0f,%8.0f,%6.0f,%5.3f,%5.3f,%5.3f,%5.3f,%5.3f,%5.3f,%5.3f,%
5.3f,%5.3f,%5.3f,%9.3f,%9.3f,%9.3f,%9.3f,%9.3f,%9.3f,%9.3f,%9.3f,%9.3f,%6.2f,
%6.2f,%6.2f,%6.2f,%6.2f,%6.2f,%6.2f,%6.2f,%6.2f,%10.3f,%10.3f,%10.3f\n',seq(
seq_num),tal,j,gdata.data(i,1),gdata.data(i,2),FOM,ee(2),ee_low(2),ee_high(2),ee
(3),ee_low(3),ee_high(3),ee(4),ee_low(4),ee_high(4),ii(2),ii_low(2),ii_high(2),ii(3),
ii_low(3),ii_high(3),ii(4),ii_low(4),ii_high(4),tt(2),tt_low(2),tt_high(2),tt(3),tt_low(3),t
t_high(3),tt(4),tt_low(4),tt_high(4),area(2),area(3),area(4));
        case '700'
            fprintf(fid,'"
",%4.0f,%2.0f,%1.0f,%8.0f,%6.0f,%5.3f,%5.3f,%5.3f,%5.3f,%5.3f,%5.3f,%5.3f,%
5.3f,%5.3f,%5.3f,%5.3f,%5.3f,%5.3f,%9.3f,%9.3f,%9.3f,%9.3f,%9.3f,%9.3f,%9.3f,
%9.3f,%9.3f,%9.3f,%9.3f,%9.3f,%6.2f,%6.2f,%6.2f,%6.2f,%6.2f,%6.2f,%6.2f,%6.
2f,%6.2f,%6.2f,%6.2f,%6.2f,%10.3f,%10.3f,%10.3f,%10.3f\n',seq(seq_num),tal,j,
gdata.data(i,1),gdata.data(i,2),FOM,ee(2),ee_low(2),ee_high(2),ee(3),ee_low(3),
ee_high(3),ee(4),ee_low(4),ee_high(4),ee(5),ee_low(5),ee_high(5),ii(2),ii_low(2),i
i_high(2),ii(3),ii_low(3),ii_high(3),ii(4),ii_low(4),ii_high(4),ii(5),ii_low(5),ii_high(5),tt
(2),tt_low(2),tt_high(2),tt(3),tt_low(3),tt_high(3),tt(4),tt_low(4),tt_high(4),tt(5),tt_lo
w(5),tt_high(5),area(2),area(3),area(4),area(5));
        case '900'
            fprintf(fid,'"
",%4.0f,%2.0f,%1.0f,%8.0f,%6.0f,%5.3f,%5.3f,%5.3f,%5.3f,%5.3f,%5.3f,%5.3f,%
5.3f,%5.3f,%5.3f,%5.3f,%5.3f,%5.3f,%5.3f,%5.3f,%5.3f,%5.3f,%5.3f,%5.3f,%5.3f,
%5.3f,%5.3f,%9.3f,%9.3f,%9.3f,%9.3f,%9.3f,%9.3f,%9.3f,%9.3f,%9.3f,%9.3f,%9.
3f,%9.3f,%9.3f,%9.3f,%9.3f,%9.3f,%9.3f,%9.3f,%9.3f,%9.3f,%6.2f,%6.2f,
%6.2f,%6.2f,%6.2f,%6.2f,%6.2f,%6.2f,%6.2f,%6.2f,%6.2f,%6.2f,%6.2f,%6.2f,%6.
```

```
2f,%6.2f,%6.2f,%6.2f,%6.2f,%6.2f,%6.2f,%10.3f,%10.3f,%10.3f,%10.3f,%10.3f,%
10.3f,%10.3f,\n',seq(seq_num),tal,j,gdata.data(i,1),gdata.data(i,2),FOM,ee(1),ee_
low(1),ee_high(1),ee(2),ee_low(2),ee_high(2),ee(3),ee_low(3),ee_high(3),ee(4),e
e_low(4),ee_high(4),ee(5),ee_low(5),ee_high(5),ee(6),ee_low(6),ee_high(6),ee(7
),ee_low(7),ee_high(7),ii(1),ii_low(1),ii_high(1),ii(2),ii_low(2),ii_high(2),ii(3),ii_low(
3),ii_high(3),ii(4),ii_low(4),ii_high(4),ii(5),ii_low(5),ii_high(5),ii(6),ii_low(6),ii_high(6
),ii(7),ii_low(7),ii_high(7),tt(1),tt_low(1),tt_high(1),tt(2),tt_low(2),tt_high(2),tt(3),tt_l
ow(3),tt_high(3),tt(4),tt_low(4),tt_high(4),tt(5),tt_low(5),tt_high(5),tt(6),tt_low(6),tt_
high(6),tt(7),tt_low(7),tt_high(7),area(1),area(2),area(3),area(4),area(5),area(6),ar
ea(7));
        end
    end %ends j for loop
end %ends i for loop

% Close output file
fclose(fid);
```

Fitglow100.m
(MATLAB fitting code for Harshaw TLD-100 LiF:Mg,Ti dosimeters)

```
function [vector_answer, ci_answer] =
fitglow100(seq_num,seq,name,xdata,ydata,dose)
%FITGLOW100 Fit thermoluminescent glow curve data for LiF:Mg,Ti.
% This function determines the best fitting parameters for the curve.
% Takes as input the TLD chip identifiers, glow curve data, and dose in mR.
% Outputs FOUR peaks plus background.
%
% FITGLOW100 is only intended to be called from CURVEFITTING, which
% provides those values.
%
% This software is the property of the University of Michigan per the
% Bylaws of the Regents of the University of Michigan, section 3.10.
%
% Copyright 2005-2010 University of Michigan
%
% Authors: Miesher Rodrigues, Nathan Haverland, John Harvey, Samba Danfa

% Set up figure to receive datasets and fits
f_ = clf;  %returns image handles
figure(f_); %makes image visible
set(f_,'Units','Pixels','Position',[318 115 680 484]);
legh_ = []; legt_ = {}; % handles and legend: {}=cell array []=normal array
xlim_ = [Inf -Inf]; % limits of x axis
ax_ = axes; %return handle of axes
set(ax_,'Units','normalized','OuterPosition',[0 0 1 1]);
set(ax_,'Box','on');
axes(ax_);
hold on;

% Plot data originally in dataset "ydata (glow) vs. xdata (heat)"
xdata = xdata(:);
ydata = ydata(:);
h_ = line(xdata,ydata,'Parent',ax_,'Color',[0.333333 0 0.666667],...
     'LineStyle','none', 'LineWidth',1,...
     'Marker','.', 'MarkerSize',12);
xlim_(1) = min(xlim_(1),min(xdata));
xlim_(2) = max(xlim_(2),max(xdata));
legh_(end+1) = h_;
legt_{end+1} = 'ydata vs. xdata';

% Nudge axis limits beyond data limits
if all(isfinite(xlim_))
   xlim_ = xlim_ + [-1 1] * 0.01 * diff(xlim_);
```

```
   set(ax_,'XLim',xlim_)
end

% Set scaling factor (depends on dose)
X=dose/500 * 0.9; % Verified

%Set initial fitting values
energ2 = 1.52;
energ3 = 1.562;
energ4 = 1.44;
energ5 = 1.9;
amp2 = 1;%i2 = 58181.79;
amp3 = 50000;
amp4 = 600000;
amp5 = 125000;
temp2 = 419;
temp3 = 445;
temp4 = 476;
temp5 = 507;
y0 = -100;
a = 3.191;
t0 = 43.1;

%set fit limits - change here if necessary
e2_low=1.4;  e2_high=1.7;
e3_low=1.4;  e3_high=1.9;
e4_low=1.4;  e4_high=1.9;
e5_low=1.7;  e5_high=2.4;

i2_low=0.5*X;  i2_high=70000*X;
i3_low=10000*X;  i3_high=92000*X;
i4_low=30000*X;  i4_high=100000*X;
i5_low=100000*X;  i5_high=200000*X;

t2_low=405;  t2_high=437;
t3_low=443; t3_high=473;
t4_low=472;  t4_high=497;
t5_low=495;  t5_high=526;

y0_low=-700;   y0_high=1000;
a_low=.0001;     a_high=5.001;
tt0_low=1;   tt0_high=75;

% Create fit "fit 1"
fo_ = fitoptions('method','NonlinearLeastSquares','Lower',[e2_low e3_low e4_low
e5_low i2_low i3_low i4_low i5_low t2_low t3_low t4_low t5_low y0_low a_low
```

```
tt0_low],'Upper',[e2_high e3_high e4_high e5_high i2_high i3_high i4_high
i5_high t2_high t3_high t4_high t5_high y0_high a_high tt0_high]);
ok_ = ~(isnan(xdata) | isnan(ydata));
st_ = [energ2 energ3 energ4 energ5 amp2 amp3 amp4 amp5 temp2 temp3
temp4 temp5 y0 a t0];
set(fo_,'Startpoint',st_);
ft_ =
fittype('amp2*exp(1+energ2/8.617385e-5/x*(x-temp2)/temp2-x*x/temp2/temp2*ex
p(energ2/8.617385e-5/x*(x-temp2)/temp2)*(1-2*8.617385e-5*x/energ2))+amp3*e
xp(1+energ3/8.617385e-5/x*(x-temp3)/temp3-x*x/temp3/temp3*exp(energ3/8.61
7385e-5/x*(x-temp3)/temp3)*(1-2*8.617385e-5*x/energ3))+amp4*exp(1+energ4/
8.617385e-5/x*(x-temp4)/temp4-x*x/temp4/temp4*exp(energ4/8.617385e-5/x*(x-t
emp4)/temp4)*(1-2*8.617385e-5*x/energ4))+amp5*exp(1+energ5/8.617385e-5/x
*(x-temp5)/temp5-x*x/temp5/temp5*exp(energ5/8.617385e-5/x*(x-temp5)/temp5)
*(1-2*8.617385e-5*x/energ5))+y0+a*exp(x/t0)' ,...
    'dependent',{'y'},'independent',{'x'},...
    'coefficients',{'energ2', 'energ3', 'energ4', 'energ5', 'amp2', 'amp3', 'amp4',
'amp5', 'temp2', 'temp3', 'temp4', 'temp5', 'y0', 'a', 't0'});

% Fit this model using new data: fit(xdata,ydata,fittype,fitoptions)
cf_ = fit(xdata(ok_),ydata(ok_),ft_ ,fo_);
vector_answer=coeffvalues(cf_);
ci_answer = confint(cf_,0.95);

% Plot this fit
h_ = plot(cf_,'fit',0.95);
legend off;  % turn off legend from plot method call
set(h_(1),'Color',[1 0 0],...
    'LineStyle','-', 'LineWidth',2,...
    'Marker','none', 'MarkerSize',6);
legh_(end+1) = h_(1);
legt_{end+1} = 'fit 1';
xlabel('Temperature (K)');
ylabel('Light signal (arbitrary units)');
name=strcat('f',num2str(seq(seq_num),'%05.0f'),'_',name);
title(regexprep(name,'_','-')); % Underscores in titles produce subscript

% Plot individual Peaks
x=300:1:600;
% Return fit parameters to curvefitting.m
ee2=vector_answer(1);ii2=vector_answer(5);tt2=vector_answer(9);
ee3=vector_answer(2);ii3=vector_answer(6);tt3=vector_answer(10);
ee4=vector_answer(3);ii4=vector_answer(7);tt4=vector_answer(11);
ee5=vector_answer(4);ii5=vector_answer(8);tt5=vector_answer(12);
yy0=vector_answer(13);aa=vector_answer(14);tt0=vector_answer(15);
% fit equation (corresponds to Kitis et al., Thermoluminescence glow-curve
```

```
% deconvolution functions for first, second and general orders of kinetics.
% J. Phys. D: Appl. Phys. 31, 1998, equation 14)
k = 8.617385e-5; %Boltzmann constant in eV/K
peak2=ii2.*exp(1+ee2/k./x.*(x-tt2)/tt2-x.*x./tt2./tt2.*exp(ee2/k./x.*(x-tt2)/tt2).*(1-2*
k.*x./ee2));
peak3=ii3.*exp(1+ee3/k./x.*(x-tt3)/tt3-x.*x./tt3./tt3.*exp(ee3/k./x.*(x-tt3)/tt3).*(1-2*
k.*x./ee3));
peak4=ii4.*exp(1+ee4/k./x.*(x-tt4)/tt4-x.*x./tt4./tt4.*exp(ee4/k./x.*(x-tt4)/tt4).*(1-2*
k.*x./ee4));
peak5=ii5.*exp(1+ee5/k./x.*(x-tt5)/tt5-x.*x./tt5./tt5.*exp(ee5/k./x.*(x-tt5)/tt5).*(1-2*
k.*x./ee5));
%peak2=ii2.*exp(1+ee2/k./x.*(x-tt2)/tt2-x.*x./tt2./tt2.*exp(ee2/k./x.*(x-tt2)/tt2).*(1-
2*k.*x./ee2)-(2*k*tt2./ee2));
%peak3=ii3.*exp(1+ee3/k./x.*(x-tt3)/tt3-x.*x./tt3./tt3.*exp(ee3/k./x.*(x-tt3)/tt3).*(1-
2*k.*x./ee3)-(2*k*tt3./ee3));
%peak4=ii4.*exp(1+ee4/k./x.*(x-tt4)/tt4-x.*x./tt4./tt4.*exp(ee4/k./x.*(x-tt4)/tt4).*(1-
2*k.*x./ee4)-(2*k*tt4./ee4));
%peak5=ii5.*exp(1+ee5/k./x.*(x-tt5)/tt5-x.*x./tt5./tt5.*exp(ee5/k./x.*(x-tt5)/tt5).*(1-
2*k.*x./ee5)-(2*k*tt5./ee5));
bg=yy0+aa*exp(x/tt0);  % background
plot(x,peak2)
plot(x,peak3)
plot(x,peak4)
plot(x,peak5)
plot(x,bg)

%end;

% Done plotting data and fits.  Now finish up loose ends.
hold off;
name=strcat(name,'.jpg');
saveas(gcf,name);
xlabel(ax_,'');             % remove x label
ylabel(ax_,'');             % remove y label
```

Fitglow200.m
(MATLAB fitting code for Harshaw TLD-200 CaF_2:Dy dosimeters)

```
function [vector_answer, ci_answer] =
fitglow200(seq_num,seq,name,xdata,ydata,dose)
%FITGLOW200 Fit thermoluminescent glow curve data for CaF2:Dy.
% This function determines the best fitting parameters for the curve.
% Takes as input the TLD chip identifiers, glow curve data, and dose in mR.
% Outputs NINE peaks.
%
% FITGLOW200 is only intended to be called from CURVEFITTING, which
% provides those values.
%
% This software is the property of the University of Michigan per the
% Bylaws of the Regents of the University of Michigan, section 3.10.
%
% Copyright 2005-2010 University of Michigan
%
% Authors: Miesher Rodrigues, Nathan Haverland, John Harvey, Samba Danfa

% Set up figure to receive datasets and fits
f_ = clf;  %returns image handles
figure(f_); %makes image visible
set(f_,'Units','Pixels','Position',[318 115 680 484]);
legh_ = []; legt_ = {};   % handles and text for legend      %{}=cell array []=normal
array
xlim_ = [Inf -Inf];       % limits of x axis
ax_ = axes; %return hangle of axes
set(ax_,'Units','normalized','OuterPosition',[0 0 1 1]);
set(ax_,'Box','on');
axes(ax_);
hold on;

% Plot data originally in dataset "ydata vs. xdata"
xdata = xdata(:);
ydata = ydata(:);
h_ = line(xdata,ydata,'Parent',ax_,'Color',[0.333333 0 0.666667],...
    'LineStyle','none', 'LineWidth',1,...
    'Marker','.', 'MarkerSize',12);
xlim_(1) = min(xlim_(1),min(xdata));
%xlim_(2) = 675;
xlim_(2) = max(xlim_(2),max(xdata));
legh_(end+1) = h_;
legt_{end+1} = 'ydata vs. xdata';

% Nudge axis limits beyond data limits
```

```
if all(isfinite(xlim_))
   xlim_ = xlim_ + [-1 1] * 0.01 * diff(xlim_);
   set(ax_,'XLim',xlim_)
end

% Set scaling factor (depends on dose)
X = dose/500 * 0.65; % Verified
 % set initial fitting values
energ1 = 1.6;
energ2= 1.25;
energ3= 0.9;
energ4= 0.95;
energ5 = 1.5;
energ6 = 1.0;
energ7 = 0.95;
energ8 = 1.35;
energ9 = 1.45;
 amp1 = 151000;
 amp2 = 500000;
 amp3 = 1000000;
 amp4 = 200000;
 amp5 = 250000;
 amp6 = 600000;
 amp7 = 1400000;
 amp8 = 500000;
 amp9 = 600000;
 temp1 = 380;
 temp2 = 392;
 temp3 = 420;
 temp4 = 447;
 temp5 = 457;
 temp6 = 468;
 temp7 = 506;
 temp8 = 527;
 temp9  = 554;

%set boundaries-Change here if need be
e1_low=1.4;  e1_high=1.8;
e2_low=1.1;  e2_high=1.4;
e3_low=0.7;  e3_high=1.1;
e4_low=0.8;  e4_high=1.1;
e5_low=1.3;  e5_high=1.7;
e6_low=0.8;  e6_high=1.2;
e7_low=0.8;  e7_high=1.1;
e8_low=1.1;  e8_high=1.6;
e9_low=1.2;  e9_high=1.7;
```

```
i1_low=1*X; i1_high=310000*X;%i1_high=210000*X;
i2_low=250*X; i2_high=700000*X;%i2_high=380000*X;
i3_low=8000*X; i3_high=2000000*X;%i3_high=1000000*X;
i4_low=10000*X;  i4_high=4000000*X;%i4_high=1500000*X;
i5_low=200000*X; i5_high=300000*X; %i5_high=320000*X;
i6_low=400000*X;  i6_high=800000*X;%i6_high=600000*X;
i7_low=800000*X;  i7_high=2000000*X;%i7_high=1100000*X;
i8_low=200000*X;   i8_high=800000*X;%i8_high=400000*X;
i9_low=200000*X;  i9_high=1000000*X;%i9_high=600000*X;

t1_low=375;  t1_high=388;
t2_low=387;  t2_high=402;
t3_low=413;  t3_high=427;
t4_low=440;  t4_high=454;
t5_low=445;  t5_high=461;
t6_low=460;  t6_high=474;
t7_low=500;  t7_high=512;
t8_low=520;  t8_high=534;
t9_low=546;  t9_high=562;

% Create fit "fit 1"
fo_ = fitoptions('method','NonlinearLeastSquares','Lower',[e1_low e2_low e3_low
e4_low e5_low e6_low e7_low e8_low e9_low i1_low i2_low i3_low i4_low i5_low
i6_low i7_low i8_low i9_low t1_low t2_low t3_low t4_low t5_low t6_low t7_low
t8_low t9_low],'Upper',[e1_high e2_high e3_high e4_high e5_high e6_high
e7_high e8_high e9_high i1_high i2_high i3_high i4_high i5_high i6_high i7_high
i8_high i9_high t1_high t2_high t3_high t4_high t5_high t6_high t7_high t8_high
t9_high]);
ok_ = ~(isnan(xdata) | isnan(ydata));
st_ = [energ1 energ2 energ3 energ4 energ5 energ6 energ7 energ8 energ9 amp1
amp2 amp3 amp4 amp5 amp6 amp7 amp8 amp9 temp1 temp2 temp3 temp4
temp5 temp6 temp7 temp8 temp9];
set(fo_,'Startpoint',st_);
ft_ =
fittype('amp1*exp(1+energ1/8.617385e-5/x*(x-temp1)/temp1-x*x/temp1/temp1*ex
p(energ1/8.617385e-5/x*(x-temp1)/temp1)*(1-2*8.617385e-5*x/energ1))+amp2*e
xp(1+energ2/8.617385e-5/x*(x-temp2)/temp2-x*x/temp2/temp2*exp(energ2/8.61
7385e-5/x*(x-temp2)/temp2)*(1-2*8.617385e-5*x/energ2))+amp3*exp(1+energ3/
8.617385e-5/x*(x-temp3)/temp3-x*x/temp3/temp3*exp(energ3/8.617385e-5/x*(x-t
emp3)/temp3)*(1-2*8.617385e-5*x/energ3))+amp4*exp(1+energ4/8.617385e-5/x
*(x-temp4)/temp4-x*x/temp4/temp4*exp(energ4/8.617385e-5/x*(x-temp4)/temp4)
*(1-2*8.617385e-5*x/energ4))+amp5*exp(1+energ5/8.617385e-5/x*(x-temp5)/te
mp5-x*x/temp5/temp5*exp(energ5/8.617385e-5/x*(x-temp5)/temp5)*(1-2*8.6173
85e-5*x/energ5))+amp6*exp(1+energ6/8.617385e-5/x*(x-temp6)/temp6-x*x/temp
6/temp6*exp(energ6/8.617385e-5/x*(x-temp6)/temp6)*(1-2*8.617385e-5*x/energ
```

```
6))+amp7*exp(1+energ7/8.617385e-5/x*(x-temp7)/temp7-x*x/temp7/temp7*exp(
energ7/8.617385e-5/x*(x-temp7)/temp7)*(1-2*8.617385e-5*x/energ7))+amp8*ex
p(1+energ8/8.617385e-5/x*(x-temp8)/temp8-x*x/temp8/temp8*exp(energ8/8.617
385e-5/x*(x-temp8)/temp8)*(1-2*8.617385e-5*x/energ8))+amp9*exp(1+energ9/8.
617385e-5/x*(x-temp9)/temp9-x*x/temp9/temp9*exp(energ9/8.617385e-5/x*(x-te
mp9)/temp9)*(1-2*8.617385e-5*x/energ9))' ,...
    'dependent',{'y'},'independent',{'x'},...
    'coefficients',{'energ1', 'energ2', 'energ3', 'energ4', 'energ5', 'energ6', 'energ7',
'energ8', 'energ9','amp1', 'amp2', 'amp3', 'amp4', 'amp5', 'amp6', 'amp7', 'amp8',
'amp9', 'temp1', 'temp2', 'temp3', 'temp4', 'temp5', 'temp6',
'temp7','temp8','temp9'});

% Fit this model using new data
cf_ = fit(xdata(ok_),ydata(ok_),ft_ ,fo_);  %fit(xdata,ydata,fittype,fitoptions)
vector_answer=coeffvalues(cf_);
ci_answer = confint(cf_,0.95);

% Plot this fit
h_ = plot(cf_,'fit',0.95);
legend off;  % turn off legend from plot method call
set(h_(1),'Color',[1 0 0],...
    'LineStyle','-', 'LineWidth',2,...
    'Marker','none', 'MarkerSize',6);
legh_(end+1) = h_(1);
legt_{end+1} = 'fit 1';
xlabel('Temperature (K)');
ylabel('Light signal (arbitrary units)');
name=strcat('f',num2str(seq(seq_num),'%05.0f'),'_',name);
title(regexprep(name,'_','-')); % Replaces underscores with hyphens, since an
underscore in a plot title produces subscript

% Plot individual Peaks
x=300:1:675;
ee1=vector_answer(1);ii1=vector_answer(10);tt1=vector_answer(19);
ee2=vector_answer(2);ii2=vector_answer(11);tt2=vector_answer(20);
ee3=vector_answer(3);ii3=vector_answer(12);tt3=vector_answer(21);
ee4=vector_answer(4);ii4=vector_answer(13);tt4=vector_answer(22);
ee5=vector_answer(5);ii5=vector_answer(14);tt5=vector_answer(23);
ee6=vector_answer(6);ii6=vector_answer(15);tt6=vector_answer(24);
ee7=vector_answer(7);ii7=vector_answer(16);tt7=vector_answer(25);
ee8=vector_answer(8);ii8=vector_answer(17);tt8=vector_answer(26);
ee9=vector_answer(9);ii9=vector_answer(18);tt9=vector_answer(27);
peak1=ii1.*exp(1+ee1/8.617385e-5./x.*(x-tt1)/tt1-x.*x./tt1./tt1.*exp(ee1/8.617385e
-5./x.*(x-tt1)/tt1).*(1-2*8.617385e-5.*x./ee1));
peak2=ii2.*exp(1+ee2/8.617385e-5./x.*(x-tt2)/tt2-x.*x./tt2./tt2.*exp(ee2/8.617385e
-5./x.*(x-tt2)/tt2).*(1-2*8.617385e-5.*x./ee2));
```

```
peak3=ii3.*exp(1+ee3/8.617385e-5./x.*(x-tt3)/tt3-x.*x./tt3./tt3.*exp(ee3/8.617385e
-5./x.*(x-tt3)/tt3).*(1-2*8.617385e-5.*x./ee3));
peak4=ii4.*exp(1+ee4/8.617385e-5./x.*(x-tt4)/tt4-x.*x./tt4./tt4.*exp(ee4/8.617385e
-5./x.*(x-tt4)/tt4).*(1-2*8.617385e-5.*x./ee4));
peak5=ii5.*exp(1+ee5/8.617385e-5./x.*(x-tt5)/tt5-x.*x./tt5./tt5.*exp(ee5/8.617385e
-5./x.*(x-tt5)/tt5).*(1-2*8.617385e-5.*x./ee5));
peak6=ii6.*exp(1+ee6/8.617385e-5./x.*(x-tt6)/tt6-x.*x./tt6./tt6.*exp(ee6/8.617385e
-5./x.*(x-tt6)/tt6).*(1-2*8.617385e-5.*x./ee6));
peak7=ii7.*exp(1+ee7/8.617385e-5./x.*(x-tt7)/tt7-x.*x./tt7./tt7.*exp(ee7/8.617385e
-5./x.*(x-tt7)/tt7).*(1-2*8.617385e-5.*x./ee7));
peak8=ii8.*exp(1+ee8/8.617385e-5./x.*(x-tt8)/tt8-x.*x./tt8./tt8.*exp(ee8/8.617385e
-5./x.*(x-tt8)/tt8).*(1-2*8.617385e-5.*x./ee8));
peak9=ii9.*exp(1+ee9/8.617385e-5./x.*(x-tt9)/tt9-x.*x./tt9./tt9.*exp(ee9/8.617385e
-5./x.*(x-tt9)/tt9).*(1-2*8.617385e-5.*x./ee9));
plot(x,peak1)
plot(x,peak2)
plot(x,peak3)
plot(x,peak4)
plot(x,peak5)
plot(x,peak6)
plot(x,peak7)
plot(x,peak8)
plot(x,peak9)

% Done plotting data and fits.  Now finish up loose ends.
hold off;
name=strcat(name,'.jpg');
saveas(gcf,name);
%h_ = legend(ax_,legh_,legt_); % create and reposition legend
%set(h_,'Units','normalized');
%t_ = get(h_,'Position');
%t_(1:2) = [0.223627,0.716792];
%set(h_,'Interpreter','none','Position',t_);
xlabel(ax_,'');             % remove x label
ylabel(ax_,'');             % remove y label
```

Fitglow300.m
(MATLAB fitting code for Harshaw TLD-300 CaF_2:Tm dosimeters)

```
function [vector_answer, ci_answer] =
fitglow300(seq_num,seq,name,xdata,ydata,dose)
%FITGLOW300 Fit thermoluminescent glow curve data for CaF2:Tm.
% This function determines the best fitting parameters for the curve.
% Takes as input the TLD chip identifiers, glow curve data, and dose in mR.
% Outputs EIGHT peaks.
%
% FITGLOW300 is only intended to be called from CURVEFITTING, which
% provides those values.
%
% This software is the property of the University of Michigan per the
% Bylaws of the Regents of the University of Michigan, section 3.10.
%
% Copyright 2005-2010 University of Michigan
%
% Authors: Miesher Rodrigues, Nathan Haverland, John Harvey, Samba Danfa

% Set up figure to receive datasets and fits
f_ = clf;  %returns image handles
figure(f_); %makes image visible
set(f_,'Units','Pixels','Position',[318 115 680 484]);
legh_ = []; legt_ = {};   % handles and text for legend      %{}=cell array []=normal
array
xlim_ = [Inf -Inf];       % limits of x axis
ax_ = axes; %return hangle of axes
set(ax_,'Units','normalized','OuterPosition',[0 0 1 1]);
set(ax_,'Box','on');
axes(ax_);
hold on;

% Plot data originally in dataset "ydata vs. xdata"
xdata = xdata(:);
ydata = ydata(:);
h_ = line(xdata,ydata,'Parent',ax_,'Color',[0.333333 0 0.666667],...
    'LineStyle','none', 'LineWidth',1,...
    'Marker','.', 'MarkerSize',12);
xlim_(1) = min(xlim_(1),min(xdata));
xlim_(2) = max(xlim_(2),max(xdata));
legh_(end+1) = h_;
legt_{end+1} = 'ydata vs. xdata';

% Nudge axis limits beyond data limits
if all(isfinite(xlim_))
```

```
   xlim_ = xlim_ + [-1 1] * 0.01 * diff(xlim_);
   set(ax_,'XLim',xlim_)
end
% Set scaling factor
X= dose/500 * 0.62;
% set intial fitting values

energ1=1.25;
energ2 = 1.1;
energ3 = 1.2;
energ4 = 0.95;
energ5 = 1.25;
energ6 = 1.35;
energ7 = 1.35;
energ8 = 1.35;
amp1 = 90000;
amp2 = 160000;
amp3 = 180000;
amp4 = 180000;
amp5 = 700000;
amp6 = 320000;
amp7 = 160000;
amp8 = 180000;
temp1 = 368.5;
temp2 = 386.5;
temp3 = 404.4;
temp4 = 430;
temp5 = 460;
temp6 = 490;
temp7 = 530;
temp8 = 565;

%set boundaries-Change here if need be
e1_low=1.0;  e1_high=1.5;
e2_low=0.9;  e2_high=1.2;
e3_low=0.7;  e3_high=1.7;
e4_low=0.7;  e4_high=1.5;
e5_low=1.0;  e5_high=1.5;
e6_low=1.2;  e6_high=1.5;
e7_low=1.0;  e7_high=1.7;
e8_low=1.0;  e8_high=1.7;

i1_low=1*X;   i1_high=100000*X;
i2_low=1*X;  i2_high=200000*X;
i3_low=100000*X;  i3_high=300000*X;
i4_low=10000*X;  i4_high=300000*X;
```

```
i5_low=100000*X;  i5_high=1000000*X;
i6_low=30000*X;  i6_high=400000*X;
i7_low=100000*X;  i7_high=200000*X;
i8_low=100000*X;  i8_high=300000*X;

t1_low=360;  t1_high=377;
t2_low=380;  t2_high=393;
t3_low=395;  t3_high=414;
t4_low=420;  t4_high=440;
t5_low=450;  t5_high=470;
t6_low=485;  t6_high=495;
t7_low=525;  t7_high=550;
t8_low=555;  t8_high=575;

% Create fit "fit 1"
fo_ = fitoptions('method','NonlinearLeastSquares','Lower',[e1_low e2_low e3_low
e4_low e5_low e6_low e7_low e8_low i1_low i2_low i3_low i4_low i5_low i6_low
i7_low i8_low t1_low t2_low t3_low t4_low t5_low t6_low t7_low
t8_low],'Upper',[e1_high e2_high e3_high e4_high e5_high e6_high e7_high
e8_high i1_high i2_high i3_high i4_high i5_high i6_high i7_high i8_high t1_high
t2_high t3_high t4_high t5_high t6_high t7_high t8_high]);
ok_ = ~(isnan(xdata) | isnan(ydata));
st_ = [energ1 energ2 energ3 energ4 energ5 energ6 energ7 energ8 amp1 amp2
amp3 amp4 amp5 amp6 amp7 amp8 temp1 temp2 temp3 temp4 temp5 temp6
temp7 temp8];
set(fo_,'Startpoint',st_);
ft_ =
fittype('amp1*exp(1+energ1/8.617385e-5/x*(x-temp1)/temp1-x*x/temp1/temp1*ex
p(energ1/8.617385e-5/x*(x-temp1)/temp1)*(1-2*8.617385e-5*x/energ1))+amp2*e
xp(1+energ2/8.617385e-5/x*(x-temp2)/temp2-x*x/temp2/temp2*exp(energ2/8.61
7385e-5/x*(x-temp2)/temp2)*(1-2*8.617385e-5*x/energ2))+amp3*exp(1+energ3/
8.617385e-5/x*(x-temp3)/temp3-x*x/temp3/temp3*exp(energ3/8.617385e-5/x*(x-t
emp3)/temp3)*(1-2*8.617385e-5*x/energ3))+amp4*exp(1+energ4/8.617385e-5/x
*(x-temp4)/temp4-x*x/temp4/temp4*exp(energ4/8.617385e-5/x*(x-temp4)/temp4)
*(1-2*8.617385e-5*x/energ4))+amp5*exp(1+energ5/8.617385e-5/x*(x-temp5)/te
mp5-x*x/temp5/temp5*exp(energ5/8.617385e-5/x*(x-temp5)/temp5)*(1-2*8.6173
85e-5*x/energ5))+amp6*exp(1+energ6/8.617385e-5/x*(x-temp6)/temp6-x*x/temp
6/temp6*exp(energ6/8.617385e-5/x*(x-temp6)/temp6)*(1-2*8.617385e-5*x/energ
6))+amp7*exp(1+energ7/8.617385e-5/x*(x-temp7)/temp7-x*x/temp7/temp7*exp(
energ7/8.617385e-5/x*(x-temp7)/temp7)*(1-2*8.617385e-5*x/energ7))+amp8*ex
p(1+energ8/8.617385e-5/x*(x-temp8)/temp8-x*x/temp8/temp8*exp(energ8/8.617
385e-5/x*(x-temp8)/temp8)*(1-2*8.617385e-5*x/energ8))' ,...
    'dependent',{'y'},'independent',{'x'},...
    'coefficients',{'energ1', 'energ2', 'energ3', 'energ4', 'energ5', 'energ6', 'energ7',
'energ8','amp1', 'amp2', 'amp3', 'amp4', 'amp5', 'amp6', 'amp7', 'amp8', 'temp1',
'temp2', 'temp3', 'temp4', 'temp5', 'temp6', 'temp7', 'temp8'});
```

```
% Fit this model using new data
cf_ = fit(xdata(ok_),ydata(ok_),ft_ ,fo_);  %fit(xdata,ydata,fittype,fitoptions)
vector_answer=coeffvalues(cf_);
ci_answer = confint(cf_,0.95);

% Plot this fit
h_ = plot(cf_,'fit',0.95);
%axis ([325 575 0 800000]); %Set axis limits [xmin xmax ymin ymax]
legend off;  % turn off legend from plot method call
set(h_(1),'Color',[1 0 0],...
    'LineStyle','-', 'LineWidth',2,...
    'Marker','none', 'MarkerSize',6);
legh_(end+1) = h_(1);
legt_{end+1} = 'fit 1';
xlabel('Temperature (K)');
ylabel('Light signal (arbitrary units)');
name=strcat('f',num2str(seq(seq_num),'%05.0f'),'_',name);
title(regexprep(name,'_','-')); % Replaces underscores with hyphens, since an
underscore in a plot title produces subscript

% Plot individual Peaks
x=300:1:600;
ee1=vector_answer(1);ii1=vector_answer(9);tt1=vector_answer(17);
ee2=vector_answer(2);ii2=vector_answer(10);tt2=vector_answer(18);
ee3=vector_answer(3);ii3=vector_answer(11);tt3=vector_answer(19);
ee4=vector_answer(4);ii4=vector_answer(12);tt4=vector_answer(20);
ee5=vector_answer(5);ii5=vector_answer(13);tt5=vector_answer(21);
ee6=vector_answer(6);ii6=vector_answer(14);tt6=vector_answer(22);
ee7=vector_answer(7);ii7=vector_answer(15);tt7=vector_answer(23);
ee8=vector_answer(8);ii8=vector_answer(16);tt8=vector_answer(24);
peak1=ii1.*exp(1+ee1/8.617385e-5./x.*(x-tt1)/tt1-x.*x./tt1./tt1.*exp(ee1/8.617385e
-5./x.*(x-tt1)/tt1).*(1-2*8.617385e-5.*x./ee1));
peak2=ii2.*exp(1+ee2/8.617385e-5./x.*(x-tt2)/tt2-x.*x./tt2./tt2.*exp(ee2/8.617385e
-5./x.*(x-tt2)/tt2).*(1-2*8.617385e-5.*x./ee2));
peak3=ii3.*exp(1+ee3/8.617385e-5./x.*(x-tt3)/tt3-x.*x./tt3./tt3.*exp(ee3/8.617385e
-5./x.*(x-tt3)/tt3).*(1-2*8.617385e-5.*x./ee3));
peak4=ii4.*exp(1+ee4/8.617385e-5./x.*(x-tt4)/tt4-x.*x./tt4./tt4.*exp(ee4/8.617385e
-5./x.*(x-tt4)/tt4).*(1-2*8.617385e-5.*x./ee4));
peak5=ii5.*exp(1+ee5/8.617385e-5./x.*(x-tt5)/tt5-x.*x./tt5./tt5.*exp(ee5/8.617385e
-5./x.*(x-tt5)/tt5).*(1-2*8.617385e-5.*x./ee5));
peak6=ii6.*exp(1+ee6/8.617385e-5./x.*(x-tt6)/tt6-x.*x./tt6./tt6.*exp(ee6/8.617385e
-5./x.*(x-tt6)/tt6).*(1-2*8.617385e-5.*x./ee6));
peak7=ii7.*exp(1+ee7/8.617385e-5./x.*(x-tt7)/tt7-x.*x./tt7./tt7.*exp(ee7/8.617385e
-5./x.*(x-tt7)/tt7).*(1-2*8.617385e-5.*x./ee7));
```

```
peak8=ii8.*exp(1+ee8/8.617385e-5./x.*(x-tt8)/tt8-x.*x./tt8./tt8.*exp(ee8/8.617385e
-5./x.*(x-tt8)/tt8).*(1-2*8.617385e-5.*x./ee8));
plot(x,peak1)
plot(x,peak2)
plot(x,peak3)
plot(x,peak4)
plot(x,peak5)
plot(x,peak6)
plot(x,peak7)
plot(x,peak8)

% Done plotting data and fits.  Now finish up loose ends.
hold off;
name=strcat(name,'.jpg');
saveas(gcf,name);
%h_ = legend(ax_,legh_,legt_); % create and reposition legend
%set(h_,'Units','normalized');
%t_ = get(h_,'Position');
%t_(1:2) = [0.223627,0.716792];
%set(h_,'Interpreter','none','Position',t_);
xlabel(ax_,'');             % remove x label
ylabel(ax_,'');             % remove y label
```

Fitglow400.m
(MATLAB fitting code for Harshaw TLD-400 CaF_2:Mn dosimeters)

```
function [vector_answer, ci_answer] =
fitglow400(seq_num,seq,name,xdata,ydata,dose)
%FITGLOW400 Fit thermoluminescent glow curve data for CaF2:Mn.
% This function determines the best fitting parameters for the curve.
% Takes as input the TLD chip identifiers, glow curve data, and dose in mR.
% Outputs THREE peaks.
%
% FITGLOW400 is only intended to be called from CURVEFITTING, which
% provides those values.
%
% This software is the property of the University of Michigan per the
% Bylaws of the Regents of the University of Michigan, section 3.10.
%
% Copyright 2005-2010 University of Michigan
%
% Authors: Miesher Rodrigues, Nathan Haverland, John Harvey, Samba Danfa

% Set up figure to receive datasets and fits
f_ = clf;  %returns image handles
figure(f_); %makes image visible
set(f_,'Units','Pixels','Position',[318 115 680 484]);
legh_ = []; legt_ = {};   % handles and text for legend      %{}=cell array []=normal
array
xlim_ = [Inf -Inf];       % limits of x axis
ax_ = axes; %return hangle of axes
set(ax_,'Units','normalized','OuterPosition',[0 0 1 1]);
set(ax_,'Box','on');
axes(ax_);
hold on;

% Plot data originally in dataset "ydata vs. xdata"
xdata = xdata(:);
ydata = ydata(:);
h_ = line(xdata,ydata,'Parent',ax_,'Color',[0.333333 0 0.666667],...
    'LineStyle','none', 'LineWidth',1,...
    'Marker','.', 'MarkerSize',12);
xlim_(1) = min(xlim_(1),min(xdata));
xlim_(2) = 675;
%xlim_(2) = max(xlim_(2),max(xdata));
legh_(end+1) = h_;
legt_{end+1} = 'ydata vs. xdata';

% Nudge axis limits beyond data limits
```

```
if all(isfinite(xlim_))
   xlim_ = xlim_ + [-1 1] * 0.01 * diff(xlim_);
   set(ax_,'XLim',xlim_)
end

X= dose/500 * 0.75;

%Set initial fitting values
energ2 = 1.35;
energ3 = 1.75;
energ4 = 1.3;
amp2 = 59000;
amp3 = 80000;
amp4 = 50000;
temp2 = 568;
temp3 = 595;
temp4 = 620;

%set boundaries-Change here if need be
e2_low=1.3;  e2_high=1.4;
e3_low=1.1;  e3_high=1.25;
e4_low=1.2;  e4_high=1.4;

i2_low=350000/4*X;  i2_high=420000/4*X;
i3_low=500000/4*X;  i3_high=600000/4*X;
i4_low=380000/4*X;  i4_high=480000/4*X;

t2_low=565;  t2_high=572;
t3_low=590; t3_high=600;
t4_low=617;  t4_high=625;

%e2_low=1.35;  e2_high=1.55;
%e3_low=1.35;  e3_high=1.5;
%e4_low=1.4;  e4_high=1.55;
%i2_low=100000; i2_high=150000;
%i3_low=210000; i3_high=280000;
%i4_low=250000; i4_high=300000;
%t2_low=565;  t2_high=580;
%t3_low=595; t3_high=606;
%t4_low=620;  t4_high=635;

% Create fit "fit 1"
fo_ = fitoptions('method','NonlinearLeastSquares','Lower',[e2_low e3_low e4_low
i2_low i3_low i4_low t2_low t3_low t4_low],'Upper',[e2_high e3_high e4_high
i2_high i3_high i4_high t2_high t3_high t4_high]);
ok_ = ~(isnan(xdata) | isnan(ydata));
```

```
st_ = [energ2 energ3 energ4 amp2 amp3 amp4 temp2 temp3 temp4];
set(fo_,'Startpoint',st_);
ft_ =
fittype('amp2*exp(1+energ2/8.617385e-5/x*(x-temp2)/temp2-x*x/temp2/temp2*ex
p(energ2/8.617385e-5/x*(x-temp2)/temp2)*(1-2*8.617385e-5*x/energ2))+amp3*e
xp(1+energ3/8.617385e-5/x*(x-temp3)/temp3-x*x/temp3/temp3*exp(energ3/8.61
7385e-5/x*(x-temp3)/temp3)*(1-2*8.617385e-5*x/energ3))+amp4*exp(1+energ4/
8.617385e-5/x*(x-temp4)/temp4-x*x/temp4/temp4*exp(energ4/8.617385e-5/x*(x-t
emp4)/temp4)*(1-2*8.617385e-5*x/energ4))' ,...
    'dependent',{'y'},'independent',{'x'},...
    'coefficients',{'energ2', 'energ3', 'energ4', 'amp2', 'amp3', 'amp4', 'temp2',
'temp3', 'temp4'});

% Fit this model using new data
cf_ = fit(xdata(ok_),ydata(ok_),ft_ ,fo_);  %fit(xdata,ydata,fittype,fitoptions)
vector_answer=coeffvalues(cf_);
ci_answer = confint(cf_,0.95);

% Plot this fit
h_ = plot(cf_,'fit',0.95);
legend off;  % turn off legend from plot method call
set(h_(1),'Color',[1 0 0],...
    'LineStyle','-', 'LineWidth',2,...
    'Marker','none', 'MarkerSize',6);
legh_(end+1) = h_(1);
legt_{end+1} = 'fit 1';
xlabel('Temperature (K)');
ylabel('Light signal (arbitrary units)');
name=strcat('f',num2str(seq(seq_num),'%05.0f'),'_',name);
title(regexprep(name,'_','-')); % Replaces underscores with hyphens, since an
underscore in a plot title produces subscript
axis([450 675 0 400000]);

% Plot individual Peaks
x=300:1:675;
ee2=vector_answer(1);ii2=vector_answer(4);tt2=vector_answer(7);
ee3=vector_answer(2);ii3=vector_answer(5);tt3=vector_answer(8);
ee4=vector_answer(3);ii4=vector_answer(6);tt4=vector_answer(9);
peak2=ii2.*exp(1+ee2/8.617385e-5./x.*(x-tt2)/tt2-x.*x./tt2./tt2.*exp(ee2/8.617385e
-5./x.*(x-tt2)/tt2).*(1-2*8.617385e-5.*x./ee2));
peak3=ii3.*exp(1+ee3/8.617385e-5./x.*(x-tt3)/tt3-x.*x./tt3./tt3.*exp(ee3/8.617385e
-5./x.*(x-tt3)/tt3).*(1-2*8.617385e-5.*x./ee3));
peak4=ii4.*exp(1+ee4/8.617385e-5./x.*(x-tt4)/tt4-x.*x./tt4./tt4.*exp(ee4/8.617385e
-5./x.*(x-tt4)/tt4).*(1-2*8.617385e-5.*x./ee4));
plot(x,peak2)
plot(x,peak3)
```

```
plot(x,peak4)

% Done plotting data and fits.  Now finish up loose ends.
hold off;
name=strcat(name,'.jpg');
saveas(gcf,name);
%h_ = legend(ax_,legh_,legt_); % create and reposition legend
%set(h_,'Units','normalized');
%t_ = get(h_,'Position');
%t_(1:2) = [0.223627,0.716792];
%set(h_,'Interpreter','none','Position',t_);
xlabel(ax_,'');             % remove x label
ylabel(ax_,'');             % remove y label
```

Fitglow700.m
(MATLAB fitting code for Harshaw TLD-700H LiF:Mg,Cu,P dosimeters)

```
function [vector_answer, ci_answer] =
fitglow700(seq_num,seq,name,xdata,ydata,dose)
%FITGLOW700 Fit thermoluminescent glow curve data for LiF:Mg,Cu,P.
% This function determines the best fitting parameters for the curve.
% Takes as input the TLD chip identifiers, glow curve data, and dose in mR.
% Outputs FOUR peaks.
%
% FITGLOW700 is only intended to be called from CURVEFITTING, which
% provides those values.
%
% This software is the property of the University of Michigan per the
% Bylaws of the Regents of the University of Michigan, section 3.10.
%
% Copyright 2005-2010 University of Michigan
%
% Authors: Miesher Rodrigues, Nathan Haverland, John Harvey, Samba Danfa

% Set up figure to receive datasets and fits
f_ = clf;  %returns image handles
figure(f_); %makes image visible
set(f_,'Units','Pixels','Position',[318 115 680 484]);
legh_ = []; legt_ = {};   % handles and text for legend      %{}=cell array []=normal
array
xlim_ = [Inf -Inf];       % limits of x axis
ax_ = axes; %return hangle of axes
set(ax_,'Units','normalized','OuterPosition',[0 0 1 1]);
set(ax_,'Box','on');
axes(ax_);
hold on;

% Plot data originally in dataset "ydata vs. xdata"
xdata = xdata(:);
ydata = ydata(:);
h_ = line(xdata,ydata,'Parent',ax_,'Color',[0.333333 0 0.666667],...
    'LineStyle','none', 'LineWidth',1,...
    'Marker','.', 'MarkerSize',12);
xlim_(1) = min(xlim_(1),min(xdata));
%xlim_(2) = 675;
xlim_(2) = max(xlim_(2),max(xdata));
legh_(end+1) = h_;
legt_{end+1} = 'ydata vs. xdata';

% Nudge axis limits beyond data limits
```

```
if all(isfinite(xlim_))
   xlim_ = xlim_ + [-1 1] * 0.01 * diff(xlim_);
   set(ax_,'XLim',xlim_)
end

% Set scaling factor (depends on the dose)

X= dose/500*0.5;

% Set initial fitting values
energ2 = 1.4;
energ3 = 1.5;
energ4 = 2.4;
energ5  = 5.25;
amp2 = 100000;
amp3 = 100000;
amp4 = 2000000;
amp5 = 270000;
temp2 = 415;
temp3 = 467;
temp4 = 518;
temp5 = 528;

%set boundaries-Change here if need be
e2_low=1.2;  e2_high=1.6;
e3_low=1.3;  e3_high=1.7;
e4_low=2.1;  e4_high=2.7;
e5_low=5.0;  e5_high=5.5;

i2_low=1*X;  i2_high=200000*X;
i3_low=1*X;  i3_high=200000*X;
i4_low=1000000*X;  i4_high=3000000*X;
i5_low=200000*X;  i5_high=350000*X;

t2_low=405;  t2_high=425;%t2_high=420;
t3_low=460; t3_high=475;
t4_low=510;  t4_high=527;%t4_high=522;
t5_low=523;  t5_high=535;

% Create fit "fit 1"
fo_ = fitoptions('method','NonlinearLeastSquares','Lower',[e2_low e3_low e4_low
e5_low i2_low i3_low i4_low i5_low t2_low t3_low t4_low
t5_low],'Upper',[e2_high e3_high e4_high e5_high i2_high i3_high i4_high
i5_high t2_high t3_high t4_high t5_high]);
ok_ = ~(isnan(xdata) | isnan(ydata));
```

```
st_ = [energ2 energ3 energ4 energ5 amp2 amp3 amp4 amp5 temp2 temp3
temp4 temp5];
set(fo_,'Startpoint',st_);
ft_ =
fittype('amp2*exp(1+energ2/8.617385e-5/x*(x-temp2)/temp2-x*x/temp2/temp2*ex
p(energ2/8.617385e-5/x*(x-temp2)/temp2)*(1-2*8.617385e-5*x/energ2))+amp3*e
xp(1+energ3/8.617385e-5/x*(x-temp3)/temp3-x*x/temp3/temp3*exp(energ3/8.61
7385e-5/x*(x-temp3)/temp3)*(1-2*8.617385e-5*x/energ3))+amp4*exp(1+energ4/
8.617385e-5/x*(x-temp4)/temp4-x*x/temp4/temp4*exp(energ4/8.617385e-5/x*(x-t
emp4)/temp4)*(1-2*8.617385e-5*x/energ4))+amp5*exp(1+energ5/8.617385e-5/x
*(x-temp5)/temp5-x*x/temp5/temp5*exp(energ5/8.617385e-5/x*(x-temp5)/temp5)
*(1-2*8.617385e-5*x/energ5))' ,...
    'dependent',{'y'},'independent',{'x'},...
    'coefficients',{'energ2', 'energ3', 'energ4', 'energ5', 'amp2', 'amp3', 'amp4',
'amp5', 'temp2', 'temp3', 'temp4', 'temp5'});

% Fit this model using new data
cf_ = fit(xdata(ok_),ydata(ok_),ft_ ,fo_);  %fit(xdata,ydata,fittype,fitoptions)
vector_answer=coeffvalues(cf_);
ci_answer = confint(cf_,0.95);

% Plot this fit
h_ = plot(cf_,'fit',0.95);
legend off;  % turn off legend from plot method call
set(h_(1),'Color',[1 0 0],...
    'LineStyle','-', 'LineWidth',2,...
    'Marker','none', 'MarkerSize',6);
legh_(end+1) = h_(1);
legt_{end+1} = 'fit 1';
xlabel('Temperature (K)');
ylabel('Light signal (arbitrary units)');
name=strcat('f',num2str(seq(seq_num),'%05.0f'),'_',name);
title(regexprep(name,'_','-')); % Replaces underscores with hyphens, since an
underscore in a plot title produces subscript

% Plot individual Peaks
x=300:1:675;
ee2=vector_answer(1);ii2=vector_answer(5);tt2=vector_answer(9);
ee3=vector_answer(2);ii3=vector_answer(6);tt3=vector_answer(10);
ee4=vector_answer(3);ii4=vector_answer(7);tt4=vector_answer(11);
ee5=vector_answer(4);ii5=vector_answer(8);tt5=vector_answer(12);
peak2=ii2.*exp(1+ee2/8.617385e-5./x.*(x-tt2)/tt2-x.*x./tt2./tt2.*exp(ee2/8.617385e
-5./x.*(x-tt2)/tt2).*(1-2*8.617385e-5.*x./ee2));
peak3=ii3.*exp(1+ee3/8.617385e-5./x.*(x-tt3)/tt3-x.*x./tt3./tt3.*exp(ee3/8.617385e
-5./x.*(x-tt3)/tt3).*(1-2*8.617385e-5.*x./ee3));
```

```
peak4=ii4.*exp(1+ee4/8.617385e-5./x.*(x-tt4)/tt4-x.*x./tt4./tt4.*exp(ee4/8.617385e
-5./x.*(x-tt4)/tt4).*(1-2*8.617385e-5.*x./ee4));
peak5=ii5.*exp(1+ee5/8.617385e-5./x.*(x-tt5)/tt5-x.*x./tt5./tt5.*exp(ee5/8.617385e
-5./x.*(x-tt5)/tt5).*(1-2*8.617385e-5.*x./ee5));
plot(x,peak2)
plot(x,peak3)
plot(x,peak4)
plot(x,peak5)
axis([380 540 0 3000000]);

% Done plotting data and fits.  Now finish up loose ends.
hold off;
name=strcat(name,'.jpg');
saveas(gcf,name);
%h_ = legend(ax_,legh_,legt_); % create and reposition legend
%set(h_,'Units','normalized');
%t_ = get(h_,'Position');
%t_(1:2) = [0.223627,0.716792];
%set(h_,'Interpreter','none','Position',t_);
xlabel(ax_,'');             % remove x label
ylabel(ax_,'');             % remove y label
```

Fitglow900.m
(MATLAB fitting code for Harshaw TLD-900 $CaSO_4$:Dy dosimeters)

```
function [vector_answer, ci_answer] =
fitglow900(seq_num,seq,name,xdata,ydata,dose)
%FITGLOW900 Fit thermoluminescent glow curve data for CaSO4:Dy.
% This function determines the best fitting parameters for the curve.
% Takes as input the TLD chip identifiers, glow curve data, and dose in mR.
% Outputs SEVEN peaks.
%
% FITGLOW900 is only intended to be called from CURVEFITTING, which
% provides those values.
%
% This software is the property of the University of Michigan per the
% Bylaws of the Regents of the University of Michigan, section 3.10.
%
% Copyright 2005-2010 University of Michigan
%
% Authors: Miesher Rodrigues, Nathan Haverland, John Harvey, Samba Danfa

% Set up figure to receive datasets and fits
f_ = clf;  %returns image handles
figure(f_); %makes image visible
set(f_,'Units','Pixels','Position',[318 115 680 484]);
legh_ = []; legt_ = {};   % handles and text for legend      %{}=cell array []=normal
array
xlim_ = [Inf -Inf];       % limits of x axis
ax_ = axes; %return hangle of axes
set(ax_,'Units','normalized','OuterPosition',[0 0 1 1]);
set(ax_,'Box','on');
axes(ax_);
hold on;

% Plot data originally in dataset "ydata vs. xdata"
xdata = xdata(:);
ydata = ydata(:);
h_ = line(xdata,ydata,'Parent',ax_,'Color',[0.333333 0 0.666667],...
    'LineStyle','none', 'LineWidth',1,...
    'Marker','.', 'MarkerSize',12);
xlim_(1) = min(xlim_(1),min(xdata));
xlim_(2) = max(xlim_(2),max(xdata));
legh_(end+1) = h_;
legt_{end+1} = 'ydata vs. xdata';

% Nudge axis limits beyond data limits
if all(isfinite(xlim_))
```

```
   xlim_ = xlim_ + [-1 1] * 0.01 * diff(xlim_);
   set(ax_,'XLim',xlim_)
end

%set scaling factors
X= dose/500 * 0.75;

%Initial fitting values
  energ1 = 1.0;
 energ2 = 0.95;
 energ3 = 0.95;
 energ4 = 1.4;
 energ5 = 1.4;
 energ6 = 1.0;
 energ7 = 0.98;
 amp1 = 32000;
 amp2 = 400000;
 amp3 = 65000;
 amp4 = 80000;
 amp5 = 45000;
 amp6 = 51000;
 amp7 = 250000;
 temp1 = 400;
 temp2 = 427;
 temp3 = 423.5;
 temp4 = 461.5;
 temp5 = 479;
 temp6 = 424;
 temp7 = 457;

%set boundaries-Change here if need be
e1_low=0.9;  e1_high=1.1;
e2_low=0.8; e2_high=1.0;
e3_low=0.8;  e3_high=1.1;
e4_low=1.2;  e4_high=1.6;
e5_low=1.2;  e5_high=1.6;
e6_low=0.9;  e6_high=1.1;
e7_low=0.8;  e7_high=1.1;

i1_low=20000*X;   i1_high=50000*X;
i2_low=30000*X;  i2_high=50000*X;
i3_low=50000*X;  i3_high=80000*X;
i4_low=16000*X;  i4_high=100000*X;
i5_low=10000*X;  i5_high=80000*X;
i6_low=40000*X;  i6_high=62000*X;
i7_low=200000*X;  i7_high=300000*X;
```

```
t1_low=390;  t1_high=410;
t2_low=415;  t2_high=430;
t3_low=400;  t3_high=447;
t4_low=450;  t4_high=473;
t5_low=470;  t5_high=487;
t6_low=517;  t6_high=530;
t7_low=540;  t7_high=575;

% Create fit "fit 1"
fo_ = fitoptions('method','NonlinearLeastSquares','Lower',[e1_low e2_low e3_low
e4_low e5_low e6_low e7_low i1_low i2_low i3_low i4_low i5_low i6_low i7_low
t1_low t2_low t3_low t4_low t5_low t6_low t7_low],'Upper',[e1_high e2_high
e3_high e4_high e5_high e6_high e7_high i1_high i2_high i3_high i4_high
i5_high i6_high i7_high t1_high t2_high t3_high t4_high t5_high t6_high
t7_high]);
ok_ = ~(isnan(xdata) | isnan(ydata));
st_ = [energ1 energ2 energ3 energ4 energ5 energ6 energ7 amp1 amp2 amp3
amp4 amp5 amp6 amp7 temp1 temp2 temp3 temp4 temp5 temp6 temp7];
set(fo_,'Startpoint',st_);
ft_ =
fittype('amp1*exp(1+energ1/8.617385e-5/x*(x-temp1)/temp1-x*x/temp1/temp1*ex
p(energ1/8.617385e-5/x*(x-temp1)/temp1)*(1-2*8.617385e-5*x/energ1))+amp2*e
xp(1+energ2/8.617385e-5/x*(x-temp2)/temp2-x*x/temp2/temp2*exp(energ2/8.61
7385e-5/x*(x-temp2)/temp2)*(1-2*8.617385e-5*x/energ2))+amp3*exp(1+energ3/
8.617385e-5/x*(x-temp3)/temp3-x*x/temp3/temp3*exp(energ3/8.617385e-5/x*(x-t
emp3)/temp3)*(1-2*8.617385e-5*x/energ3))+amp4*exp(1+energ4/8.617385e-5/x
*(x-temp4)/temp4-x*x/temp4/temp4*exp(energ4/8.617385e-5/x*(x-temp4)/temp4)
*(1-2*8.617385e-5*x/energ4))+amp5*exp(1+energ5/8.617385e-5/x*(x-temp5)/te
mp5-x*x/temp5/temp5*exp(energ5/8.617385e-5/x*(x-temp5)/temp5)*(1-2*8.6173
85e-5*x/energ5))+amp6*exp(1+energ6/8.617385e-5/x*(x-temp6)/temp6-x*x/temp
6/temp6*exp(energ6/8.617385e-5/x*(x-temp6)/temp6)*(1-2*8.617385e-5*x/energ
6))+amp7*exp(1+energ7/8.617385e-5/x*(x-temp7)/temp7-x*x/temp7/temp7*exp(
energ7/8.617385e-5/x*(x-temp7)/temp7)*(1-2*8.617385e-5*x/energ7))' ,...
    'dependent',{'y'},'independent',{'x'},...
    'coefficients',{'energ1', 'energ2', 'energ3', 'energ4', 'energ5', 'energ6', 'energ7',
'amp1', 'amp2', 'amp3', 'amp4', 'amp5', 'amp6', 'amp7', 'temp1', 'temp2', 'temp3',
'temp4', 'temp5', 'temp6', 'temp7'});

% Fit this model using new data
cf_ = fit(xdata(ok_),ydata(ok_),ft_ ,fo_);  %fit(xdata,ydata,fittype,fitoptions)
vector_answer=coeffvalues(cf_);
ci_answer = confint(cf_,0.95);

% Plot this fit
h_ = plot(cf_,'fit',0.95);
```

```
legend off;  % turn off legend from plot method call
set(h_(1),'Color',[1 0 0],...
    'LineStyle','-', 'LineWidth',2,...
    'Marker','none', 'MarkerSize',6);
legh_(end+1) = h_(1);
legt_{end+1} = 'fit 1';
xlabel('Temperature (K)');
ylabel('Light signal (arbitrary units)');
name=strcat('f',num2str(seq(seq_num),'%05.0f'),'_',name);
title(regexprep(name,'_','-')); % Replaces underscores with hyphens, since an
underscore in a plot title produces subscript
axis([350 675 0 400000]);

% Plot individual Peaks
x=300:1:675;
ee1=vector_answer(1);ii1=vector_answer(8);tt1=vector_answer(15);
ee2=vector_answer(2);ii2=vector_answer(9);tt2=vector_answer(16);
ee3=vector_answer(3);ii3=vector_answer(10);tt3=vector_answer(17);
ee4=vector_answer(4);ii4=vector_answer(11);tt4=vector_answer(18);
ee5=vector_answer(5);ii5=vector_answer(12);tt5=vector_answer(19);
ee6=vector_answer(6);ii6=vector_answer(13);tt6=vector_answer(20);
ee7=vector_answer(7);ii7=vector_answer(14);tt7=vector_answer(21);
peak1=ii1.*exp(1+ee1/8.617385e-5./x.*(x-tt1)/tt1-x.*x./tt1./tt1.*exp(ee1/8.617385e
-5./x.*(x-tt1)/tt1).*(1-2*8.617385e-5.*x./ee1));
peak2=ii2.*exp(1+ee2/8.617385e-5./x.*(x-tt2)/tt2-x.*x./tt2./tt2.*exp(ee2/8.617385e
-5./x.*(x-tt2)/tt2).*(1-2*8.617385e-5.*x./ee2));
peak3=ii3.*exp(1+ee3/8.617385e-5./x.*(x-tt3)/tt3-x.*x./tt3./tt3.*exp(ee3/8.617385e
-5./x.*(x-tt3)/tt3).*(1-2*8.617385e-5.*x./ee3));
peak4=ii4.*exp(1+ee4/8.617385e-5./x.*(x-tt4)/tt4-x.*x./tt4./tt4.*exp(ee4/8.617385e
-5./x.*(x-tt4)/tt4).*(1-2*8.617385e-5.*x./ee4));
peak5=ii5.*exp(1+ee5/8.617385e-5./x.*(x-tt5)/tt5-x.*x./tt5./tt5.*exp(ee5/8.617385e
-5./x.*(x-tt5)/tt5).*(1-2*8.617385e-5.*x./ee5));
peak6=ii6.*exp(1+ee6/8.617385e-5./x.*(x-tt6)/tt6-x.*x./tt6./tt6.*exp(ee6/8.617385e
-5./x.*(x-tt6)/tt6).*(1-2*8.617385e-5.*x./ee6));
peak7=ii7.*exp(1+ee7/8.617385e-5./x.*(x-tt7)/tt7-x.*x./tt7./tt7.*exp(ee7/8.617385e
-5./x.*(x-tt7)/tt7).*(1-2*8.617385e-5.*x./ee7));
plot(x,peak1)
plot(x,peak2)
plot(x,peak3)
plot(x,peak4)
plot(x,peak5)
plot(x,peak6)
plot(x,peak7)

% Done plotting data and fits.  Now finish up loose ends.
hold off;
```

```
name=strcat(name,'.jpg');
saveas(gcf,name);
%h_ = legend(ax_,legh_,legt_); % create and reposition legend
%set(h_,'Units','normalized');
%t_ = get(h_,'Position');
%t_(1:2) = [0.223627,0.716792];
%set(h_,'Interpreter','none','Position',t_);
xlabel(ax_,'');             % remove x label
ylabel(ax_,'');             % remove y label
```